European Space Agency

Abstract Book

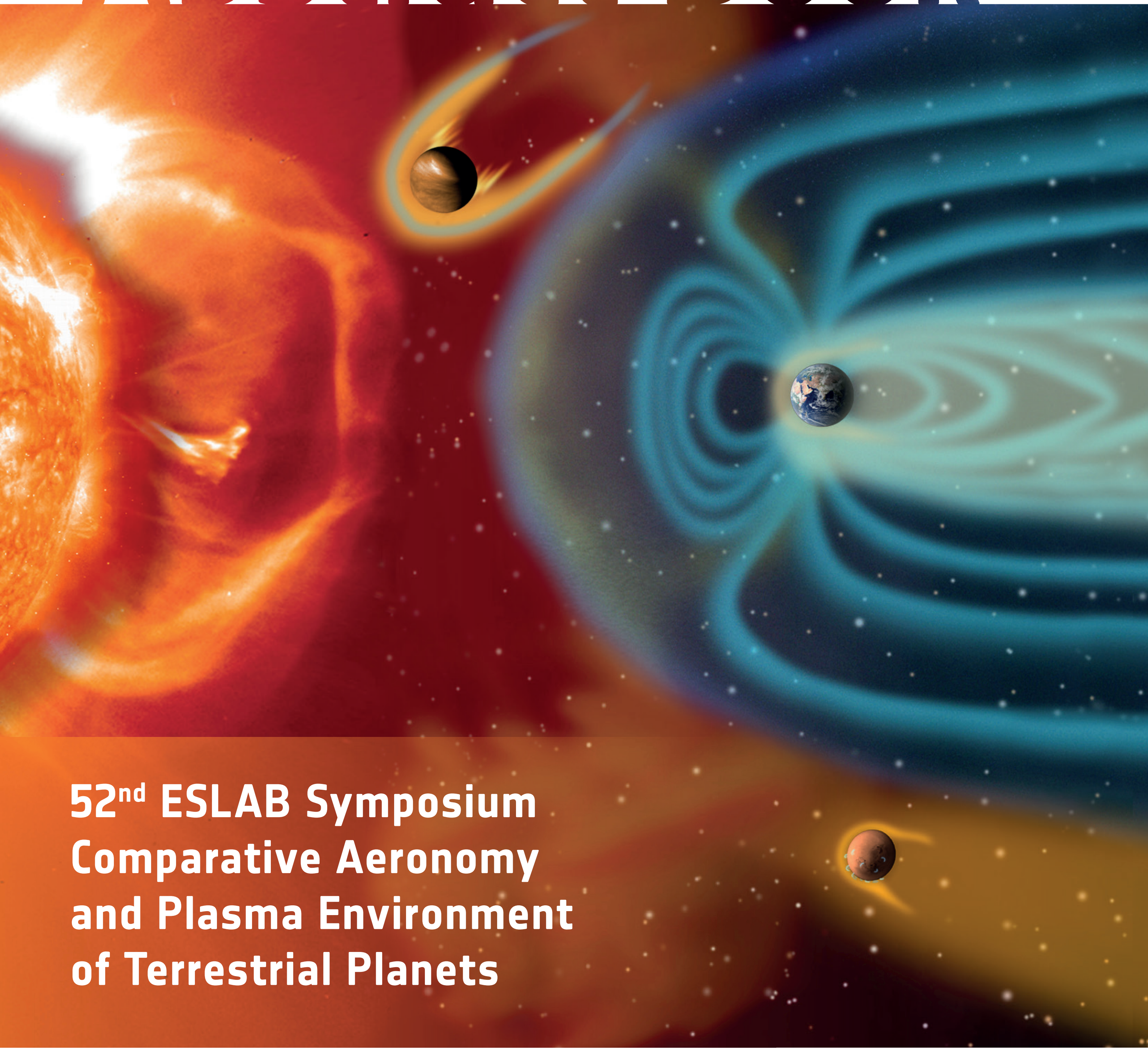

52nd ESLAB Symposium Comparative Aeronomy and Plasma Environment of Terrestrial Planets

14 – 18 May 2018
ESA-ESTEC, Noordwijk, The Netherlands

Table of Contents

Scientific Organizing Committee

Convenors

D. Titov
B. Jakosky

Members

A. Bhardwaj
G. DiBraccio
S. Bougher
J. Cui
P. Escoubet
A. Fedorova
F. González-Galindo
M. Holmström
J. Luhmann
R. Modolo
A. Nagy
A. Ocampo
C. Russell
B. Sanchez-Cano
K. Seki
O. Witasse

General Information

Organised Bus transfers

Please check the information panel next to the Registration Desk and/or the conference website for the scheduled 52nd ESLAB bus transfers.

Regular hotel shuttle

There is also a regular shuttle bus service between ESTEC and the Noordwijk hotels. For more information and timetables, please contact the ESA Conference Bureau at the Registration Desk, or the ESTEC Reception.

Taxi / Getting to the airport

In order to reserve a taxi, please consult the ESTEC Reception or send your request by email: Estec.Reception@esa.int

If you wish to reserve the Airport Shuttle, please bear in mind to reserve a seat one day in advance. Purchase a ticket at the ESTEC reception located in the A building. The costs for a one-way voucher are €15.00

Schedule ESTEC - Schiphol, Monday to Friday

- 14:30 hrs
- 15:00 hrs
- 15:30 hrs
- 16:00 hrs
- 16:30 hrs
- 17:00 hrs
- 17:30 hrs
- 18:00 hrs
- 18:30 hrs

Local Bus to Leiden

The local bus line 30 to Leiden has a bus stop just outside the gate, approximately 100 m from the gatehouse. Travel time to Leiden Central Station is approximately 20-25 min.
Further information can be found on www.arriva.nl or www.9292.nl/en

Wireless Internet

All pre-registered participants have received their login details by email, sent by the ESA ServDesk. A copy of your login details is also available at the back of your badge.

Map of ESTEC

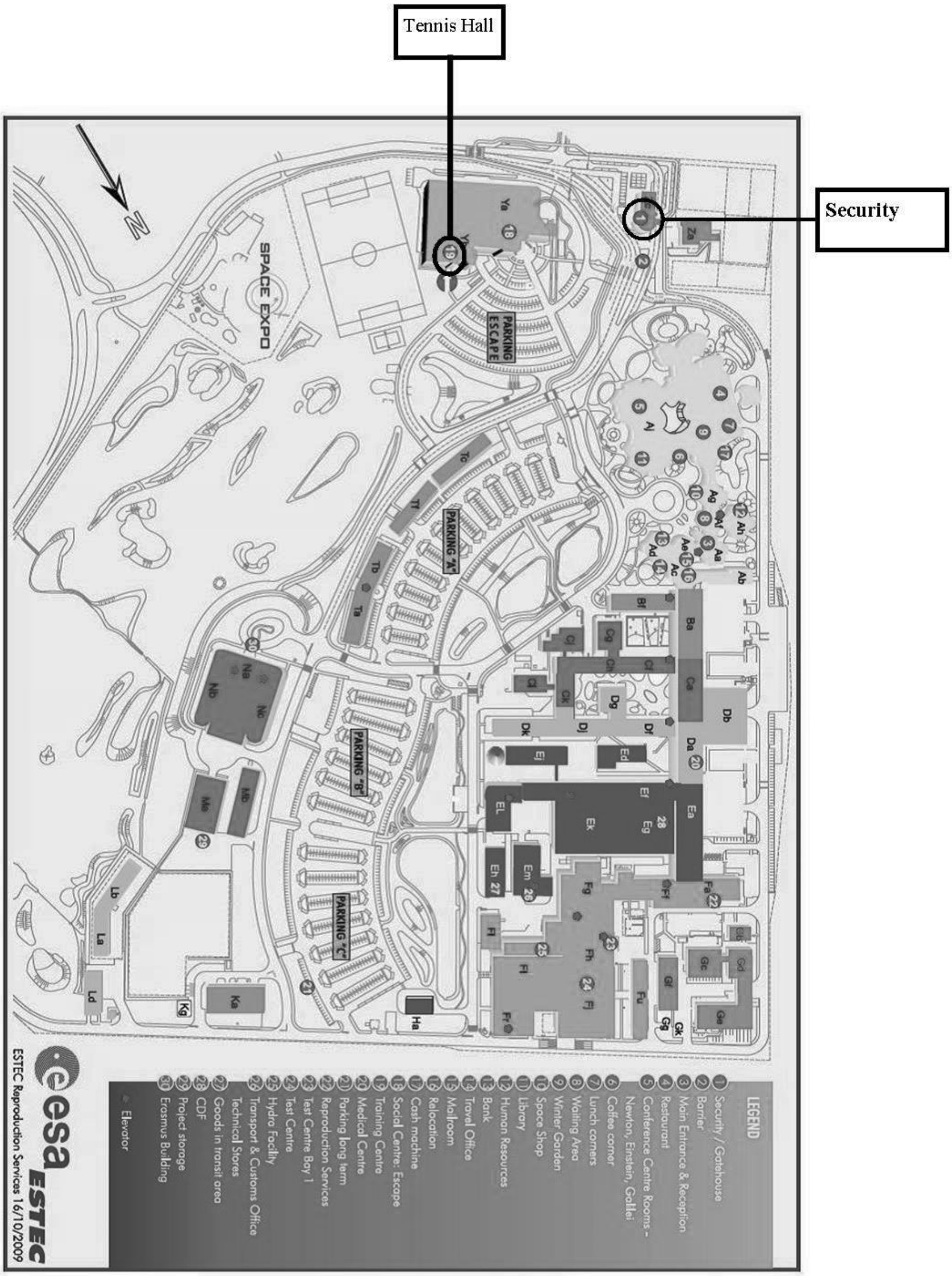
Tennis Hall
Security
SPACE EXPO
PARKING ESCAPE
PARKING "A"
PARKING "B"
PARKING "C"
LEGEND
Security / Gatehouse
Barrier
Main Entrance & Reception
Restaurant
Conference Centre Rooms - Newton, Einstein, Galilei
Coffee corner
Lunch corners
Waiting Area
Winter Garden
Space Shop
Library
Human Resources
Bank
Travel Office
Mailroom
Relocation
Cash machine
Social Centre: Escape
Training Centre
Medical Centre
Parking long term
Reproduction Services
Test Centre Bay 1
Test Centre
Hydro Facility
Transport & Customs Office
Technical Stores
Goods in transit area
CDF
Project storage
Erasmus Building
Elevator
esa ESTEC
ESTEC Reproduction Services 16/10/2009

Programme

Monday 14 May 2018

08:30 Registration of the participants

10:00 Opening of ESLAB 52
Welcome by A. Parmar, Head of Science Support Office

Keynote Lectures
Chair: D. Titov

10:15 History of Planetary Aeronomy (keynote)
Nagy A
University of Michigan, USA

10:45 Thermospheres of Terrestrial Planets including Coupling with the Lower Atmosphere (keynote)
Bougher S
University of Michigan, USA

11:15 Coffee break

11:45 Magnetospheres of Planets in the Inner Solar System.
Sixty Years of the Space Age - Lessons Learned (keynote)
Zelenyi L
Space Research Institute Russian Academy of Science, Russia

12:15 Living with the Sun (keynote)
Luhmann J
University of California, Berkeley, USA

12:45 *Lunch*

Upper Atmospheres
Chair: S. Stone and F. Gonzalez-Galindo

14:00 Mars Dayglow, Nightglow and Aurora observed by MAVEN's Imaging UltraViolet Spectrograph
Crismani M
LASP, University of Colorado, USA

14:20 Variability of UV dayglow in the Martian thermosphere from measurements by SPICAM/Mars Express and global simulations
Gonzalez-Galindo F
Instituto de Astrofísica de Andalucía-CSIC, Spain

14:40 Metastable oxygen O(1S) Martian airglow: observations and model
Gérard J-C
LPAP, Université de Liège, Belgium,

15:00 Complex Molecules in Titan's Upper Atmosphere (invited)
Lavvas P
GSMA/CNRS, France

15:20 Coffee break

15:50 Parameterizing Gravity Waves and Understanding their Impacts on Venus' Upper Atmosphere
Brecht A
NASA Ames Research Center, USA

16:10 MAVEN/IUVS Observations of Martian Mesospheric Clouds in 2017:

A Persistent Longitudinal Asymmetry at Southern Mid-Latitudes
Stevens M
Naval Research Laboratory, USA

16:30 September 10-11, 2017 Solar Flare Event: Rapid Enhancement of the Martian Neutral Exosphere from the X-class flare as observed by MAVEN
Elrod M
NASA Goddard Space Flight Center, USA

16:50 Protonated Ions and the Seasonal Variation of Hydrogen Observed by the MAVEN Neutral Gas and Ion Mass Spectrometer
Stone S
Lunar and Planetary Laboratory, University of Arizona, USA

17:30 Icebreaking reception (Wintergarden at ESTEC restaurant)

19:00 End of day 1

Tuesday 15 May 2018

Ionospheres
Chair: R. Lillis, B. Sanchez-Cano and M. Crismani

09:30 Ionospheres of the Terrestrial Planets (keynote)
Cravens T
University of Kansas, (USA)

10:00 Hybrid plasma modelling of the planetary atmospheres and ionospheres (invited)
Modolo R
LATMOS/IPSL, UVSQ Université Paris-Saclay, UPMC Sorbonne Université, CNRS, France

10:20 Radio Sounding of the Mars Ionosphere over a full Solar Cycle by the Mars Express RadioScience Experiment (MaRS)
Pätzold M
Rheinisches Institut für Umweltforschung, Cologne, Germany

10:40 Spatial, seasonal and solar cycle variations of the total electron content (TEC): Is the TEC a good tracer for atmospheric cycles?
Sanchez-Cano B
University of Leicester, Leicester, UK [2]ESA/ESTEC, The Netherlands

11:00 Coffee break

11:30 Variability of the Martian upper ionosphere and factors controlling this variability.
Dubinin E
Max Planck Institute for Solar System Research, Germany

11:50 Variability of the Venusian and Martian nightside ionosphere after solar storms
Gray C
Apache Point Observatory, USA

12:10 Characterization of Mars' Persistent Meteoric Ion Layer
Crismani M
LASP, University of Colorado, USA

12:30 Comparison of Terrestrial and Martian TEC at Dawn and Dusk during Solstices
Burrell A
University Of Texas at Dallas, USA

12:50 Lunch

14:00 Observations and Modeling of Low-Altitude Ionospheric Responses to 2017 Sept Solar Flare at Mars
Xu S
University of California, Berkeley, USA

14:20 MAVEN observations of solar wind driven magnetosonic waves heating the Martian dayside Ionosphere
Fowler C
LASP, University of Colorado, USA

14:40 Control of the Nightside Structure of the Venusian Ionosphere
Brecht S
Bay Area Research Corp., USA

15:00 Small scale excess electron densities in the lower ionosphere of Mars: Interpretation of Mars Express radio science observations in combination with MAVEN measurements
Peter K

Rheinisches Institut für Umweltforschung, Cologne,Germany

15:20 Coffee break

Aeronomy and Plasma Environment of Exoplanets
Chair: D. Titov

15:50 Are "Habitable" Exoplanets Really Habitable? -- A perspective from atmospheric loss (invited)
Dong C
Princeton University, USA

16:10 Using Hybrid Simulations to Understand How Ion Loss Varies with Planetary Radius
Egan H
University of Colorado, USA

16:30 Poster Session 1

19:00 End of day 2

Wednesday 16 May 2018

Magnetospheres and Space Weather
Chair: S. Fatemi, S. Shuvalov, J. Halekas, and O. Witasse

09:30 Comparison of induced magnetospheres (invited)
Ma Y
EPSS, UCLA, USA

09:50 Earth's magnetosphere and its interaction with the solar wind (invited)
Milan S
University of Leicester, UK

10:10 The Complex Martian Magnetosphere: Recent Insights Based on MAVEN Magnetometer Observations
Espley J
Nasa Goddard Space Flight Center, USA

10:30 Momentum Transfer and Boundary Layer Structure at Mars
Halekas J
University of Iowa, USA

10:50 Coffee break

11:20 Magnetic topology during quiet and extreme conditions at Mars
Curry S
UC Berkeley, SSL, USA

11:40 Impact ionization of neutrals by foreshock electrons at Mars
Mazelle C
RAP / CNRS - University of Toulouse - UPS - CNES, France

12:00 The Structure and Properties of Martian Magnetosphere at ~ 70° Solar-Zenith Angle in MSE Coordinates as Observed on MAVEN Spacecraft
Vaisberg O
Space Research Institute, Russia

12:20 Study of ICME effects at Mars: energy deposition and feedback from enhanced thermosphere
Regoli L
University of Michigan, USA

12:40 Lunch

14:00 Magnetospheres of the Giant Planets (invited)
Masters A
Imperial College London, United Kingdom

14:20 The Strange Menagerie at the Magnetopause: High-Resolution Magnetospheric Multiscale Data Reveals Diverse Phenomena near the Boundary with the Magnetosheath
Russell C
Earth Planetary and Space Sciences, University of California, USA

14:40 Comparative planetary foreshocks: Results from recent studies
Meziane K
University of New Brunswick, Canada

15:00 Mass loading influence on the structure of Martian bow shock
Shuvalov S
Space Research Institute of the Russian Academy Of Sciences (IKI), Russia

15:20 Coffee break

15:50 A Generalized Magnetospheric Disturbance Index: Initial Application at Unmagnetized Bodies
Gruesbeck J
University of Maryland, USA

Solar wind interaction with atmosphereless bodies
Chair: O. Witasse

16:10 The solar wind interaction with the Moon (invited)
Fatemi S
Swedish Institute of Space Physics, Sweden

16:30 The Solar Wind Interaction with Ceres (invited)
Villarreal M
University of California, USA

16:50 The Solar Wind Interaction with Vesta and Ceres: Implications for their Magnetic Moments
Russell C
Earth, Planetary and Space Sciences, University of California, USA

17:10 To What Extent Does Solar Wind Forcing Affect the Occurrences of Energetic Electron Events in the Hermean Magnetosphere?
Lentz C
University of Colorado, USA

18:00 Dinner

Thursday 17 May 2018

Atmospheric Escape
Chair: M. Holmström, F. Leblanc, Ph. Escoubet, and M. Chaffin

09:30 Ion and neutral gas escape from the terrestrial planets (invited)
Barabash S
Swedish Institute of Space Physics, Sweden

09:50 Atmospheric Escape from Mars (invited)
Brain D
University of Colorado, USA

10:10 Signatures of sputtering at Mars: a first evidence?
Leblanc F
LATMOS/IPSL, UPMC Univ. Paris 06 Sorbonne Universités, UVSQ, CNRS, France

10:30 Cold Ion Escape from Mars - Observations by Mars Express and MAVEN
Fraenz M
MPI for Solar System Research, Germany

10:50 The Origin and Evolution of Nitrogen in Outer Planet Atmospheres through Comparative Planetology
Mandt K
Johns Hopkins University Applied Physics Laboratory, USA

11:10 Coffee break

11:40 Cold Ion Outflow and Magnetic Topology in Mars' Magnetotail
Mitchell D
University of California, Berkeley, USA

12:00 Estimating the Escape of Hydrogen and Deuterium from the Atmosphere of Mars
Clarke J
Boston University, USA

12:20 Seasonal Variability of Mars H Escape in the MAVEN IUVS dataset
Chaffin M
LASP, University of Colorado, USA

12:40 Solar cycle dependence on the H+/O+ flux ratio in Venus' magnetotail
Persson M
Swedish Institute of Space Physics, Sweden

13:00 Lunch

14:00 Escape and precipitation rates at Venus
Kollmann P
JHU / Applied Physics Laboratory, USA

14:20 Atmospheric Escape on Earth (invited)
Strangeway R

14:40 Ion Outflow from the Terrestrial Atmosphere: Sources, Mechanisms, Transport and Consequences (invited)
S. Haaland
Max-Planck-Institute, Germany

15:00 Simultaneous detection of terrestrial ionospheric molecular ions in the Earth's inner magnetosphere and at the Moon
<ins>*Dandouras I*</ins>
IRAP, Université de Toulouse, CNRS, UPS, CNES, France

15:20 Coffee break

15:50 Atmospheric loss from Earth's plasma mantle and its dependence on solar wind conditions
<ins>*Schillings A*</ins>
Swedish Institute of Space Physics (IRF), Sweden

Evolution and Climates
Chair: M. Chaffin

16:10 Mars Atmospheric Loss at the Present and Integrated Loss Through Time as Observed by MaVEN (invited)
<ins>*Jakosky B*</ins>
University of Colorado, USA

16:30 The Role of Magnetic Fields in Terrestrial Planets Evolution (invited)
<ins>*Lillis R*</ins>
Space Sciences Laboratory, University of California Berkeley, USA

16:50 Constraining the early evolution of terrestrial planets via noble gas isotope and K/U ratios (invited)
<ins>*Scherf M*</ins>
Austrian Academy of Sciences, Austria

17:10 Evolution of the Martian Climate (invited)
<ins>*Forget F*</ins>
CNRS, France

17:30 Poster Session II

20:00 End of day 4

Friday 18 May 2018

Missions and Data Archives
Chair: E. Sefton-Nash

09:30 Cluster observations of Earth atmospheric escape (invited)
Escoubet C
Esa/Estec, Netherlands

09:50 Geospace research contributions from ESA's Swarm constellation (invited)
Floberghagen R
European Space Agency, Italy

10:10 Status of the MAVEN Mission at Mars
Jakosky B
University of Colorado, United States

10:30 Mars Express science highlights and future plans
Titov D
ESA-ESTEC, Netherlands

10:50 Getting ready for BepiColombo: a modeling approach to infer the solar wind plasma parameters upstream of Mercury from magnetic field observations
Fatemi S
Swedish Institute of Space Physics, Sweden

11:10 Coffee break

11:40 Discussion. Where do we go from here?

13:00 End of 52^{nd} ESLAB Symposium

Posters

Upper Atmospheres

1 Comparison between IUVS-MAVEN limb dayglow observations and modeling
Gkouvelis L
University Of Liege, Belgium

2 Combining Observations and Modeling to Promote upper Atmospheres Research and Exploitation
Rosenblatt P
ACRI-ST, France

3 Capabilities of the Exomars Trace Gas Orbiter to study the Mars' upper atmosphere
Lopez-valverde M
Instituto de Astrofísica de Andalucía / CSIC, Spain

4 The LMD-Mars Global Climate Model and the Mars Climate Database: applications for the study of the upper atmosphere
Gonzalez-Galindo F
Instituto de Astrofísica de Andalucía-CSIC, Spain

5 Synthetic Retrievals of H2O and CO2 in the Mars Upper Atmosphere Using Solar Occultation Spectra for the NOMAD and ACS Instruments of the ExoMars TGO Mission
Hill B
Instituto De Astrofisica De Andalucia, Spain

6 Comparison of the thermal structure derived using SOIR on board Venus Express with a 1-D non-LTE radiative transfer model
Mahieux A
The University Of Texas At Austin, USA

7 Comparisons Between MAVEN/NGIMS Thermospheric Neutral Wind Observations and M-GITM Model Simulations
Roeten K
Climate and Space Sciences and Engineering Department, University Of Michigan, USA

8 Proton Aurora on Mars
Ritter B
Université de Liège, Liège, Belgium,

Ionospheres

9 The Ionospheric composition of Mars and its dependence on magnetic configuration
Fraenz M
Max Planck Institute For Solar System Research, Germany

10 Wave Structures in the Ionosphere and Upper Atmosphere of Mars as seen by the Mars Express Radio Science Experiment (MaRS)
Tellmann S
Rheinisches Institut für Umweltforschung (RIU), Germany

11 Conductivity Structures in The Martian Ionosphere
AlShehhi A
Mohammed Bin Rashid Space Center, United Arab Emirates

12 Energization of electrons trapped in the crustal magnetic field of Mars
Akbari H
Laboratory For Atmospheric And Space Physics, University Of Colorado At Boulder, USA

13 Horizontal Magnetic Fields and Currents in the Ionosphere of Mars and Their Dependence on the Interplanetary Magnetic Field
Fillingim M
Space Sciences Laboratory, University Of California, Berkeley, USA

14 Empirical Model of Electron Impact Ionization on Mars' Nightside
Lillis R
Space Sciences Laboratory, University Of California Berkeley, USA

15 Seasonal Changes in the Polar Ionosphere and Thermosphere on Mars
Pilinski M
Laboratory for Atmospheric and Space Physics, USA

Magnetospheres and Space Weather

16 Magnetic structure and propagation of a solar flux rope from the Sun to Saturn
Palmerio E
University Of Helsinki, Finland

17 A statistical study of thermal, dynamic, and magnetic pressures on the dayside of the induced magnetosphere of Mars as observed by MAVEN
Holmberg M
IRAP, University of Toulouse, CNRS, UPS, CNES, France

18 Modeling of energetic ions observations by MAVEN in the crustal field regions
Kotova A
IRAP, Université de Toulouse, CNRS, UPS, CNES, France

19 Effects of the Crustal Magnetic Fields and Changes in the IMF Orientation on the Magnetosphere of Mars
Romanelli N
Laboratoire Atmosphères, Milieux et Observations Spatiales (LATMOS), IPSL, CNRS, UVSQ, UPMC, France

20 Extracting hidden knowledge from data archives using machine learning and open data approaches for space weather effects autonomous investigation
Boumghar R
Esoc, Darmstadt, Germany

21 The Dependences of the Structure and Properties of Martian Dayside Magnetosphere on Solar Zenith Angle and IMF Clock Angle as observed on MAVEN
Ermakov V
Space Research Institute of the Russian Academy of Sciences, Russia

22 A multiscale structure of the cross-tail CSs and its relation to the ion composition according to MAVEN observations in the Martian magnetotail
Grigorenko E
Space Research Institute, Russia

23 The solar wind interaction with Mars: current systems and electromagnetic fields in the Martian ionosphere
Ledvina S
University Of California, USA

24 Effect of solar wind source variation events on planetary plasma environments
Opitz A
Wigner RCP, Budapest, Hungary,

25 Investigating space weather events at Mars with Mars Express housekeeping data
<u>*Witasse O*</u>
European Space Agency, The Netherlands

Solar Wind Interaction with Atmosphereless Bodies

26 MESSENGER X-ray observations of electron precipitation events on the dayside surface of Mercury
<u>*Lindsay S*</u>
University Of Leicester, UK

27 Sodium pick-up ion observations in the solar wind upstream of Mercury
<u>*Jasinski J*</u>
University of Michigan, USA

28 Solar wind-magnetosphere interaction at Mercury during passage of coronal mass ejections
<u>*Jarvinen R*</u>
Aalto University, School of Electrical Engineering, Department of Electronics and Nanoengineering, Finland

Atmospheric Escape, Evolution, and Climates

29 Atmospheric escape at early Mars and constraints on the evolution of the Martian atmosphere
<u>*Scherf M*</u>
Space Research Institute, Austrian Academy Of Sciences, Austria

30 Dependence of O+ escape rates from Venus on the solar wind and the solar activity
<u>*Persson M*</u>
Swedish Institute of Space Physics, Sweden

31 2-Dimensional Model of the Martian Exosphere Applied to HST Observations
<u>*Bhattacharyya D*</u>
CSP, Boston University, USA

32 Modeling deuterium from surface to space to understand Mars atmospheric evolution
<u>*Cangi E*</u>
Laboratory For Atmospheric And Space Physics, USA

33 Modeling of Ion and Photochemical Losses to Space over the Martian History
<u>*Dong C*</u>
Princeton University, USA

34 A parametric study of Enceladus plumes based on DSMC calculations for retrieving the outgassing parameters as measured by Cassini instruments
<u>*Mahieux A*</u>
The University Of Texas At Austin, USA

35 The terrestrial paleo-magnetosphere during the late Hadean and Archean: Implications on the evolution of the terrestrial atmosphere
<u>*Scherf M*</u>
Space research Institute, Austrian Academy Of Sciences, Austria

36 O+ escape at Earth during the magnetic storm on September 4th - 10th, 2017
<u>*Schillings A*</u>
Swedish Institute of Space Physics (IRF), Sweden

Missions and Data Archives

37 A concept for permanent stations on Phobos and Deimos: Study of the Mars space environment
Sefton-Nash E
European Space Agency (ESTEC), Netherlands

38 The Mars Express/ASPERA-3 and Venus Express/ASPERA-4 Solar Wind Databases
Holmstrom M
Swedish Institute of Space Physics, Sweden

39 ESCAPE (European SpaceCraft for the study of Atmospheric Particle Escape): a planetary mission to Earth, proposed to ESA in response to the M5-call
Dandouras I
IRAP, France

40 Solar SENTINEL: a satellite constellation mission concept for early forecasting of Coronal Mass Ejections
Rodrigues J
University Of Cambridge, UK [2]University of Bristol, UK

Abstracts

Monday 14 May 2018

History of Planetary Aeronomy

Nagy A[1]
[1]*University of Michigan, Ann Arbor, United States*

This talk will give a brief and concise review of planetary aeronomy activities covering the period from the beginning of the space age to recent times (e.g. Mariners, Veneras, Pioneers. Voyagers, Galileo, MGS).

Thermospheres of Terrestrial Planets including Coupling with the Lower Atmosphere

Bougher S[1]

[1]*University of Michigan, Ann Arbor, United States*

1. Basic Thermospheric Features and Scope

The thermospheres of Venus (~100-200 km), Earth (~100-500 km) and Mars (~100-200 km) are intermediate atmospheric regions strongly impacted by coupling from below with the lower-middle atmosphere (e.g. ubiquitous gravity waves, planetary waves and tides, plus episodic Mars dust storms and Earth tropical convection) and coupling from above with the exosphere and ultimately the Sun (via solar radiation and solar wind particles, see Figure 1) [1, 2, 3]. The thermospheric layer extends from the top of the middle atmosphere (defined as the mesopause) to the beginning of space (exobase). Dayside thermospheric temperatures typically increase from the mesopause to the exobase, according to the magnitude and vertical placement of EUV heating (plus auroral and Joule heating for Earth). For all three planets, CO_2 15-µm cooling serves as the IR radiator at the base of the thermosphere, with NO 4.3-µm cooling also contributing strongly at Earth during magnetic storms. The role of CO_2 15-µm cooling varies widely from planet to planet in its control of dayside temperatures and their variations [1].

The thermosphere is also distinguished by a transition region called the homopause, below which atomic and molecular constituents are well mixed. Above in the heterosphere, individual species begin to separate according to their unique scale heights via molecular diffusion. Lower thermospheric neutral densities are dominated by CO_2 (Venus and Mars) plus O_2 and N_2 (Earth) that give way to atomic O at higher altitudes for all three planets. The general homopause altitudes of Venus (~130-136 km), Earth (~100-110 km) and Mars (~115-130 km) are each regulated by vertical mixing. It is postulated that the vertical mixing for Venus and Mars is stronger than for Earth, resulting in larger eddy coefficients and the higher homopause altitudes [4]. Alternatively, the vigorous thermospheric global circulation may also contribute to the vertical mixing, especially for Venus [1, 4, 5]. Mixing ratios can serve as important diagnostics. For instance, the O/N_2 ratio (at Earth) and the O/CO_2 ratio (at Venus and Mars) above the homopause are each very sensitive to the magnitude of eddy diffusion [4].

These terrestrial planet thermosphere-ionosphere systems can also change dramatically over time since they are strongly impacted by two highly variable components of the Sun's energy output: solar radiation (~0.1–200 nm) and the solar wind [1, 3]. For instance, the amount of soft X-ray (0.1–5 nm) and EUV (5–110 nm) solar radiation most responsible for heating the Venus and Mars thermospheres (and forming their ionospheres) varies significantly over time. These temporal variations result from the changing Mars heliocentric distance (~1.38–1.67 AU) and its obliquity (determining the local season), plus the changing solar radiation itself for both planets. Both solar rotation (~27 day periodic changes in the solar output) and solar cycle (~11 year periodic overall changes in solar output) variations of the solar X-ray and EUV fluxes are significant (up to factors of ~3 to 100, depending on the wavelength, producing dramatic variations in global thermospheric temperatures, composition, and winds for all three planets [1, 5].

For this talk, we will focus on the comparative and unique aspects of the thermospheres of the non-magnetic planets (Venus and Mars), and augment the discussion by comparing to the Earth's non-magnetic storm thermosphere when it is important to do so. This will particularly be the case for lower-upper atmosphere coupling, since all three planet thermospheres display a vigorous coupling with the lower atmosphere. Also, we will present modern spacecraft datasets to characterize important thermospheric features, and illustrate a few older spacecraft datasets to provide historical context.

2. Three Common Features and Processes to Contrast

A selection of key features common to all three planets will be examined with a view to uncover the relative importance of underlying processes in each unique planetary environment. For example, dayside thermal budgets will be examined for all three planets, based upon General Circulation Model (GCM) simulations whose densities and temperatures closely match observations. The relative roles of CO_2 15-µm cooling, molecular thermal conduction and global winds in controlling dayside temperatures will be addressed [1, 5, 6]. We will also examine the process of wind induced diffusion and how it regulates the measured helium distributions observed in the thermospheres of Venus, Earth, and Mars [7]. Finally, NO UV nightglow distributions (and their temporal and spatial variations) will be examined specifically for

Venus and Mars. These nightglow emissions are being simulated by large GCMs which seek to explain the airglow as a tracer of the time variable upper atmosphere circulation [8, 9]. Nevertheless, these same GCMs struggle to capture the large (and wild) variability observed on short timescales.

3. Lower to Upper Atmosphere Coupling with Examples from Spacecraft Datasets

Waves of various temporal and spatial scales are ubiquitous in the thermospheres of the terrestrial planets. They have been observed to have a profound impact upon the combined density, temperature and wind structure of these upper atmospheres. We will discuss the tides of Earth and Mars, planetary waves at Venus, and gravity waves at Venus and Mars [4]. For instance, the similar rotation rates of the Earth and Mars imply that the mathematical characteristics of the tidal modes of the Earth and Mars are similar. However, the excitation of these tides differs greatly between both planets and results from the unique characteristics of each planet's atmosphere and surface [4]. In general, due to the large Martian topographic variations, the manifestation of these tides in the Mars upper atmosphere is greater than on Earth. The impact of these tides will be discussed.

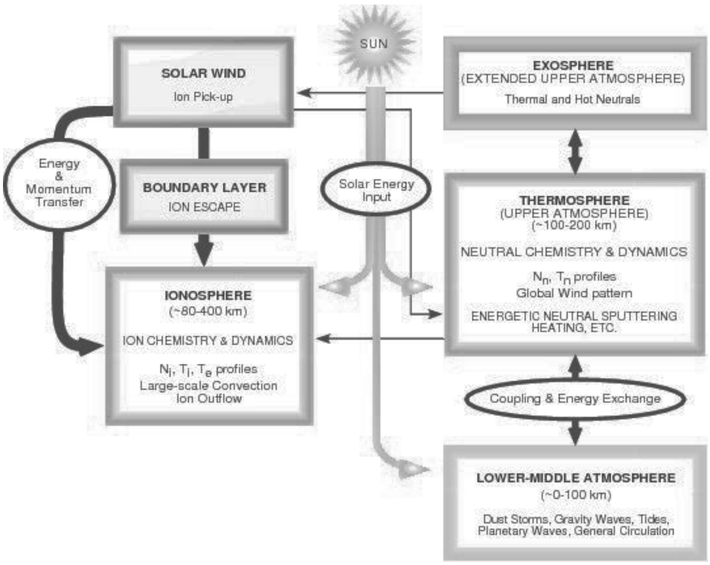

Figure 1: Cartoon of the basic Venus and Mars (non-magnetic planet) atmospheric regions and processes. Illustrates the coupling of atmospheric regions. From Bougher et al. (2015; 2017).

4. References

[1] Bougher, S. W., R. G. Roble, and T. J. Fuller-Rowell, "Simulations of the Upper Atmospheres of the Terrestrial Planets", in *AGU Monograph : Comparative Aeronomy* in *the Solar System*, Eds. M. Mendillo, A. F. Nagy, and J. H. Waite, (2002).
[2] Bougher, S. W. et al., Mars Global Ionosphere Thermosphere Model (M-GITM): I. Solar Cycle, Seasonal, and Diurnal Variations of the Upper Atmosphere, **JGR,** 120, 311-342, (2015).
[3] Bougher, S. W., D. A. Brain, J. L. Fox, F. Gonzalez-Galindo, C. Simon-Wedlund, P. G. Withers. Chapter 14: Upper Atmosphere and Ionosphere, in *The Atmosphere and Climate of Mars*, ed. B. Haberle, M. Smith, T. Clancy, F. Forget, R. Zurek, Cambridge University Press, (2017).
[4] Siskind, D. and S. W. Bougher, Aeronomy of the terrestrial planets, in *Heliophysics: Active Stars, their Astrospheres, and Impacts on Planetary Environments*, Cambridge University Press, Eds . C. J. Schrijver, F. Bagenal, and J. J. Sojka, (2016).
[5] Bougher, S. W., et al., Comparative Terrestrial Planet Thermospheres : 2. Solar Cycle Variation of Global Structure and Winds at Equinox, **JGR**, 104, 16591-16611, (1999).
[6] Bougher, S. W., et al., Solar Cycle Variability of Mars Dayside Exospheric Temperatures: Model Evaluation of Underlying Thermal Balances, **GRL,** 36, L05201, (2009).
[7] Elrod, M. K., et al., He bulge revealed: He and CO2 diurnal and seasonal variations in the upper atmosphere of Mars as detected by MAVEN NGIMS, **JGR**, 122, 2564-2573, (2017).
[8] Brecht, A., et al., Understanding the Variability of Nightside Temperatures, NO UV and O2 IR Nightglow Emissions in the Venus Upper Atmosphere, **JGR**, 116, E08004, (2011).
[9] Stiepen, A., et al., Nitric oxide nightglow and Martian mesospheric circulation from MAVEN/IUVS observations and LMD-MGCM predictions, **JGR,**122, 5782-5797, (2017).

Magnetospheres of Planets in the Inner Solar System. Sixty Years of the Space Age - Lessons Learned

Zelenyi L[1]
[1]*Space Research Institute Russian Academy of Science, Moscow, Russian Federation*

1. Introduction

Discovered of the Earth's magnetosphere started just after the launches of the first Soviet Sputnik and US Explorer-1 spacecraft. Originally it resembled the famous epoch of a great geographic discoveries - but very quickly new “in situ” measurements opened the door to a new physics - namely the physics of the hot collisionless plasma – which independently just started after WWII for nuclear fusion.

A number of fundamental physical processes – collisionless shocks, magnetic reconnection, wave particle interactions and nonadiabatic / chaotic particle dynamics have been thoroughly investigated by means of initially single- and later multi-point spacecraft measurements. Results of these intensive international efforts provided background for a very practical and well demanded now space weather predictions.

2. Magnetospheres of planets in the inner Solar System

Somewhat later- starting from 60-ies – Mars and Venus plasma envelopes also got a lot of interest due to their drastic difference with the one of the Earth’s. Absence (or partial absence) of intrinsic planetary magnetic field allowed to investigate completely new type of magnetospheres-induced ones produced by interaction of interplanetary magnetic field (mass loaded by ionospheric ions) with planetary ionosphere. Later VEGA and GIOTTO analysis of solar wind interactions with comet Halley provided another even more extreme evidence of such type of induced magnetospheric systems.

Mars have been the subject of intense debates about the intensity of Martian internal field. The puzzle have been solved by M. Acuna, who revealed the remnants of intrinsic magnetization in the southern hemisphere. One of the major challenges for Mars now, which might strongly influence the possibility of its human exploration, is the erosion of “gone with the solar wind” Martian atmosphere. Recent Maven results and their comparison with ESA MEX and historic Soviet Phobos-2 (1989) observations might shed a new light on the dependence of such escape processes on the particular conditions of a Solar cycle.

Somewhat counterintuitive - but basic plasma effects are working quite similarly in terrestrial and Martian magnetospheres despite the drastic difference of their topologies. Thin current sheets, which form in the Earth magnetotail at the periods of enhanced non-steady convection, are quite common in the Martian magnetic wake as well.

Mercury provides another example of a variety of solar wind interactions with celestial bodies. Planet has relatively strong (even surprisingly strong for its scale) internal magnetic field - and, instead of atmosphere, - only very rarified exosphere. Solar wind particles directly interact with planetary surface and complicated physical processes emerging from such interactions will be discussed in a separate presentations.

Author acknowledges the support of Russian Science Foundation (RSF grant Nr. 16-42-01103)

Living with the Sun

J.G. Luhmann[1*]; *L.K.Jian[2], Yan Li[1], C.O. Lee[1], M.L. Mays[2], Y. Futaana[3], T.L. Zhang[4], M. Holmstrom[3], J.S. Halekas[5], C.T. Russell[6].*
[1] Space Sciences Laboratory, University of California, USA,
[2] NASA Goddard Space Flight Center, USA,
[3] IRF, Kiruna, Sweden,
[4] IWF, Graz, Austria,
[5] University of Iowa, Iowa USA,
[6] IGPP UCLA, Los Angeles, USA.

1. Introduction

In addition to the effects of sunlight, the Sun influences the terrestrial planets through the particles and fields of the extended solar atmosphere - which can be highly influential in determining their aeronomical, near-space, and even surface conditions. In anticipation of the discussions of the individual planet aeronomy and solar wind interaction details by other speakers, this presentation takes a brief look at what we have learned from heliophysics observations about the the external conditions and events that the terrestrial planets experience. This essential 'space weather' information affects interpretations of processes causing features and phenomena from auroras to radiation belt enhancements to atmosphere escape, among others. The different consequences for each of the terrestrial planets, magnetized and unmagnetized, are integral to the definition of their solar wind obstacles, the nature of variability in their coupled atmospheres/magnetosphere systems, and even long term evolution. This topic also raises an important consideration regarding our current knowledge- of the other planets in particular- due to limited temporal sampling of solar conditions. We describe the existing coverage and our current capabilities for keeping an eye on the Sun and its consequences as new observations are obtained.

Mars Dayglow, Nightglow & Aurora observed by MAVEN's Imaging UltraViolet Spectrograph

N.M. Schneider[1] *and the MAVEN Imaging UltraViolet Spectrograph Team*
[1]*LASP, U. Colorado, Boulder, USA*

1. MAVEN's Imaging UltraViolet Spectrograph (IUVS)

The Mars Atmosphere and Volatile EvolutioN mission (MAVEN) is a Mars orbiter equipped with instruments to study the current state of the Mars atmosphere, atmospheric loss processes, and their fundamental drivers. Most instruments make *in situ* measurements of particles and fields in the Mars environment and upper atmosphere. IUVS is the only remote sensing instrument for the study of Mars' atmosphere and its interaction with the plasma environment [8]. The instrument has two main channels for the study of the upper atmosphere at far-UV and Mid-UV wavelengths, plus an echelle channel capable of spectrally resolving hydrogen and deuterium Lyman alpha lines to measure the D/H ratio [1]. The instrument uses a scan mirror to obtain limb scans or disk maps, and is mounted on an Articulated Payload Platform (APP) which maintains Mars pointing while the spacecraft bus and solar arrays maintain sun-pointing. The spacecraft travels on an elliptical orbit allowing limb scans to be obtained at periapse and full-disk imaging at apoapse, and scans of Mars corona in between [3]. Thanks to the scan mirror, APP, and routine planning, the instrument observes with >50% duty cycles in a variety of repeating modes. On a bimonthly basis, the instrument performs two-day stellar occultation campaigns [5] to probe atmospheric structure.

2. Key science results related to aeronomy and the plasma environment

By virtue of broad instrument capabilities and extensive observations, IUVS has observed the vast majority of phenomena discovered by prior UV instruments, and revealed a significant number of new phenomena as well. Observations of different phenomena can be individually optimized for spectral and two-dimensional resolution (through binning), as well as for sensitivity on daytime vs. night-time phenomena.

2.1. Dayglow

MAVEN/IUVS dayglow observations build on a rich history of prior UV studies by the Mariner missions and the SPICAM instrument on Mars Express. The dominant MUV emissions derive from solar excitation, ionization and dissociation of CO_2, and subsequent ionization and dissociation products. The brightest FUV emissions are atomic emissions from the constituent atoms of CO_2 and H_2O, plus additional molecular bands originating with CO_2 and its breakdown products. In addition to all spectral features observed by prior missions, IUVS has unambiguously observed and mapped the N_2 Vegard Kaplan bands [4, 11], and observed and mapped Mg+ from meteor ablation [2]. The instrument also recorded the aftermath of the most intense meteor shower observed with scientific instrumentation, after the close passage of Comet Siding Spring past Mars in October 2014 [9]. Limb scan dayglow observations have been powerful studies of spatial, seasonal and short-term variations in the thermosphere [6]. Longitudinal non-migrating tides have been observed in the peak emission altitudes [7].

2.2. Nightglow

The primary form of nightglow observed by IUVS is nitric oxide chemoluminescence. Nitrogen and oxygen atoms are liberated through molecular photodissociation on Mars' dayside. The atoms are then carried by thermospheric and mesospheric circulation patterns towards the winter pole, where they recombine and emit in the gamma and delta band of NO. IUVS limb scan observations [13] confirmed the basic geographic and seasonal emissions distribution predicted by modelling and observed by MEX/SPICAM. These observations also showed that the observed latitudinal emission distribution was not as sharply peaked at the winter poles as in models, an indication the circulation models may be missing important processes. Wave-3 tides were observed in equatorial regions at some seasons. Further apoapse imaging work with broader local time coverage is likely to distinguish between migrating, nonmigrating and stationary waves, offering further insights on their origin.

2.3. Aurora

Aurora at a planet lacking a global magnetic field would be expected to differ significantly from Earth's and other planets with a dominant dipole magnetic field. MEX/SPICAM detected occasional discrete auroral patches associated with the remanent crustal magnetic fields. The emissions were interpreted as originating from local particle acceleration during magnetic reconfiguration between the rotating planet and the solar wind. IUVS discovered a distinctly different form of aurora which can engulf the planet globally. Solar energetic particles accelerated at the Sun encounter little or no magnetic obstacle when encountering Mars, and therefore can penetrate as deep as 70km altitude in the Mars atmosphere over much or all of the planet [10]. In September 2017, an extreme space weather event impacted Mars and created global aurora observed with IUVS's apoase imaging mode.

2.4. Data Access

All data, including higher-level products are archived for public use at NASA's Planetary Data System (PDS). All team publications indicate the data types used, and reference the time period(s) utilized in the analysis. An instrument description and data format document ("Software Interface Specification) is also provided at the PDS.

3. References

[1] Clarke, J.T. et al., "Variability of D and H in the Martian Upper Atmosphere Observed with the MAVEN IUVS Echelle Channel", *J. Geophys. Res. Space Physics*, 122, 2017.
[2] Crismani, M. M. J. et al., "A persistent meteoric metal layer in the Martian atmosphere", *Nature Geoscience*, 10, 401–404, 2017.
[3] Deighan, J., et al., MAVEN IUVS observation of the hot oxygen corona at Mars, *Geophys. Res. Lett., 42*, 2015.
[4] Evans, et al., Retrieval of CO2 and N2 in the Martian thermosphere using dayglow observations by IUVS on MAVEN, *Geophys. Res. Lett., 42*, 2015.
[5] Gröller, H., et al., "Probing the Martian atmosphere with MAVEN/IUVS stellar occultations", *Geophys. Res. Lett., 42*, 2015.
[6] Jain, S. K., et al., "The structure and variability of Mars upper atmosphere as seen in MAVEN/IUVS dayglow observations", *Geophys. Res. Lett., 42*, 2015.
[7] Lo, D.Y., et al., "Non-migrating tides in the Martian atmosphere as observed by MAVEN IUVS", *Geophys. Res. Lett., 42*, 2015.
[8] McClintock, W.E., et al., "The Imaging Ultraviolet Spectrograph (IUVS) for the MAVEN Mission", Space Science Reviews, 2015.
[9] Schneider, N. M., et al., "MAVEN IUVS observations of the aftermath of the Comet Siding Spring meteor shower on Mars", *Geophys. Res. Lett*., 42, 4755–4761, 2015.
[10] Schneider, N.M., et al., "Discovery of diffuse aurora on Mars", *Science* 350, 2015.
[11] Stevens, M.H, et al., "New observations of molecular nitrogen in the Martian upper atmosphere by IUVS on MAVEN", *Geophys. Res. Lett., 42*, 2015.
[12] Stevens, M.H. et al., "Martian Mesospheric Cloud Observations by IUVS on MAVEN", *Geophys. Res. Lett.,* 44, 2017
[13] Stiepen, A., et al., "Nitric Oxide Nightglow and Martian Mesospheric Circulation from MAVEN/ IUVS Observations and LMD-MGCM Predictions", *J. Geophys. Res. Space Physics*, 122, 2017.

Variability of UV dayglow in the Martian thermosphere from measurements by SPICAM/Mars Express and global simulations

F. González-Galindo[1*]; *J.-Y. Chaufray[2], F. Forget[3], M. García-Comas[1], F. Montmessin[2], M.A. López-Valverde[1], S. Jain[4], and A. Stiepen[5]*
[1]Instituto de Astrofísica de Andalucía-CSIC, Spain
[2]LATMOS, France.
[3]Laboratoire de Météorologie Dynamique, France
[4]Laboratory for Atmospheric and Space Physics, USA
[5]Space sciences, technologies and astrophysics research institute, Université de Liège, Belgium

1. Introduction

Remote sensing of UV atmospheric emissions has been used since the first Martian missions to derive information about the temperature and composition of the upper atmosphere of Mars (e.g. [1, 2, 3, 4]). Dayglow arising from Mars is dominated by the CO Cameron bands and the CO_2^+ UV doublet, ultimately produced by the effects of UV solar radiation and photoelectrons on CO_2, the main constituent of the Martian atmosphere. Analysis of the scale height of these emissions has allowed derivation of thermospheric temperatures [2,3], assuming that the contribution from CO was minor in the case of the Cameron bands. Nightglow is dominated by the emission in the NO bands [5]

The UV channel of the SPICAM instrument on board Mars Express observed the Martian dayglow during 4 Martian Years. While the full dataset has been used to derive temperatures [3], the peak magnitudes (intensity at the emission peak and altitude of the peak) have only been analysed for the first Mars year of observations [2, 6]. Different theoretical models have been developed in order to simulate the Martian UV dayglow spectra [6, 7, 8, 9, 10]. All these are 1D models, that is, they only consider variations with altitude. This has the advantage of allowing for a detailed treatment of the different processes producing atmospheric emission, but decouples these models from the atmospheric variability produced by a variety of photochemical and transport processes.

We have included in the LMD Mars Global Climate Model (LMD-MGCM) a physical model of the Martian dayglow, providing a natural coupling between the UV airglow and the atmospheric variability. Here we will compare the predictions of the model with the SPICAM full dataset of dayglow observations, and present the dayglow global maps produced by the model.

2. Model description and selected results

The dayglow model has been incorporated into the most recent version of the ground-to-exosphere LMD-MGCM [11]. The creation and the energy degradation of photoelectrons, an important source of emission, have been simulated using the Analytical Yield Spectra technique [12].

Comparison of the modelled dayglow with SPICAM observations supports previous results which suggested suggesting a reduction in the electron impact cross sections on CO_2 and CO to reconcile model and observations [6, 10]. The predicted peak altitude for both emissions fits well with SPICAM observations, indicating that the model is correctly predicting the atmospheric density in the upper atmosphere. An exception is an underestimation of the peak altitude during the global dust storm of MY28.

We have produced, to our knowledge, the first global maps of these emissions for Mars (Fig. 1). The seasonal variability of the peak emission is dominated by the variability of the Sun-Mars distance produced by the eccentricity of the Martian orbit. We have found a strong contribution of electron impact excitation on CO to the Cameron band, indicating that previous determinations of temperature from this emission may be flawed. This is under current investigation. We have also identified longitudinal variations in the emission, linked to the effects of tides in the density structure. This offers the possibility to use these emissions together with lower atmospheric sounding to better characterize this important component of the Martian atmospheric dynamics.

While developed for Mars, in principle the model could be easily adapted to Venus, and implementation in the LMD-Venus GCM [13] should be straightforward. This would allow also comparison with the Venus Express SPICAV measurements of the dayglow, and to use a broader planetary perspective for the importance of CO on the Cameron bands on Mars and Venus.

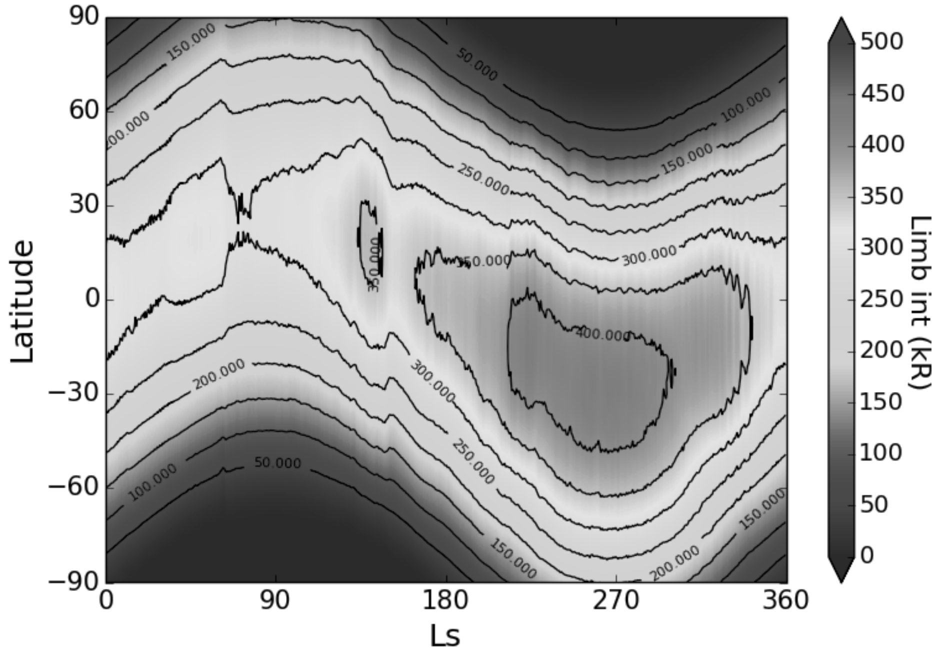

Figure 1 Seasonal and latitudinal variability of the peak limb intensity of the Cameron bands at noon

References:

[1] Stewart, A.I. et al., Icarus, 17, 469–474, 1972

[2] Leblanc, F., et al, JGR, 111(E9), E09S11, 2006.

[3] Stiepen, A. et al., Icarus, 245, 295-305, 2015.

[4] Jain, S.K. et al., GRL, 42, 9023–9030.

[5] Bertaux, J.-L., et al., Science, 307, 566-569, 2005

[6] Simon, C., et al., PSS, 57(8-9), 1008–1021, 2009

[7] Cox, C., et al., JGR 115(E4), E04010, 2010.

[8] Fox, J. L., and A. Dalgarno, JGR, 84, 7315–7333, 1979.

[9] Shematovich, V. I. et al., JGR, 113, E02011, 2008.

[10] Jain, S.K., and A. Bhardwaj, PSS, 6364, 110–122, 2010.

[11] González-Galindo, F. et al., JGR, 120, 2020–2035, 2015

[12] Bhardwaj, A., and S.K. Jain, JGR, 114, A11309, 2009

Acknowledgements: This work has been partially funded by the European Union Horizon 2020 Programme (H2020 Compet -08-2014) under grant agreement UPWARDS-633127 and by the Spanish National Research Council under "intramural" project CSIC 201450E022

Metastable oxygen O(^{1}S) Martian airglow: observations and model

J.-C. Gérard[1], L. Gkouvelis[1], B. Ritter[1], B. Hubert[1]; S. Jain[2]; N. Schneider[2]
[1]LPAP, Université de Liège, Belgium
[2]LASP, University of Colorado, USA

1. Introduction

Airglow observations are an efficient tool to probe composition and dynamics of planetary atmospheres since their altitude and horizontal distribution is directly dependent on the properties of the background atmosphere. The Imaging Ultraviolet Spectrograph (IUVS) on board MAVEN [1] has been collecting limb profiles of UV emissions for over 3 years and temperatures in the thermosphere have been deduced from the airglow vertical intensity distribution [2]. A detailed Monte Carlo model has been developed to calculate the photoelectron contribution to the excitation of several of the UV and visible emissions observed so far in the Mars and Venus airglow [3,4]. In this presentation, we will discuss some of the observed features of the O ^{3}P-^{1}S forbidden oxygen emission at 297.2 nm, based on comparisons between observations and model simulations. We will then review some of the new features and what can be learnt from this and other oxygen emissions.

2. Sources and sinks of metastable O(^{1}S) atoms in the Martian thermosphere

Atomic oxygen is a major constituent of the Martian upper atmosphere where it dominates the dayside chemical composition above □200 km. Although some of the production of atomic oxygen emissions such as the 135.6 nm doublet directly depends on the O density, some other are independent of the oxygen density such as the photo-dissociative production of O(^{1}S) from CO_2.

The main sources of O(^{1}S) atoms in the Martian upper atmosphere are:

- Photo-dissociative excitation of CO_2 : CO_2 + photon □CO + O(^{1}S) (1)
- photoelectron impact on O : O(^{3}P) + e_f □ O(^{1}S) + e (2)
- photoelectron impact on CO_2 : CO_2 + e_f □CO + O(^{1}S) + e (3)
- dissociative recombination of O_2^+ : O_2^+ + e_{th} □O + O(^{1}S) (4)

where e_f are (fast) photoelectrons and e_{th} thermal ionospheric electrons. The relative importance of these different sources depends on altitude.

Two types of loss processes must be considered:

- radiative relaxation:

  O(^{1}S) □O (^{3}P) + photon (297.2 nm)

  O(^{1}S) □O (^{1}D) + photon (557.7 nm)

- and collisional deactivation:

  O(^{1}S) + CO_2 □ O(^{1}D, ^{3}P) + CO_2

  O(^{1}S) + O □ O(^{1}D, ^{3}P) + O

Most of the relevant cross sections, rate coefficients, photon yields and branching ratios have been experimentally determined, so that the individual sources may be evaluated quantitatively. We first use outputs from an airglow-aurora Monte Carlo model that has been applied to calculate electron energy spectra in different planetary atmospheres. These energy spectra are integrated over excitation cross sections to determine the excitation rates from processes (2) and (3). These collisional processes are then combined with direct solar-induced source (1) and photochemical production (4) to obtain the total volume production rate of metastable O(^{1}S) atoms (Fig. 1).

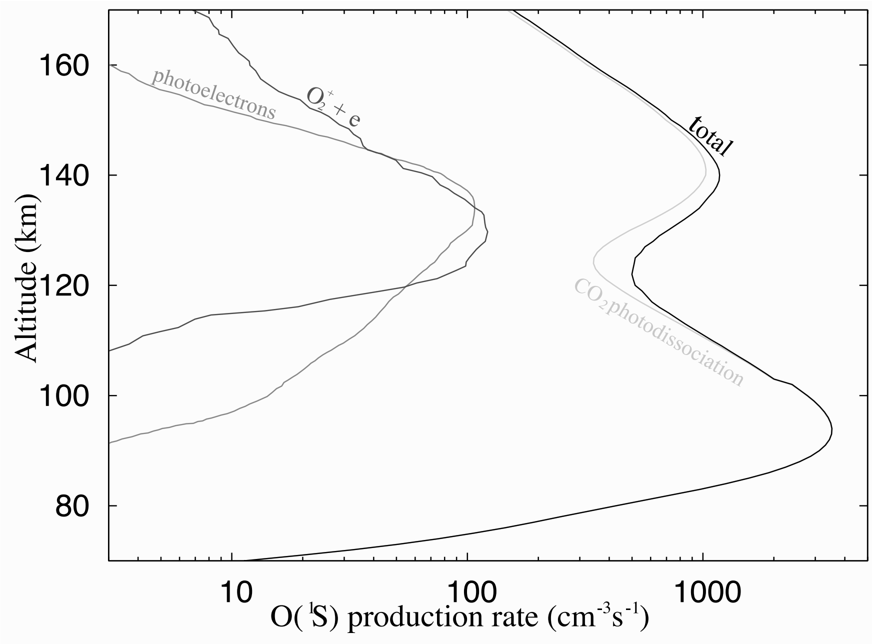

Figure 1: altitude distribution of the O(^{1}S) sources calculated for the conditions of the Viking 1 landing on the Mars surface. The neutral atmospheric and ionized densities are those measured with the mass spectrometer during the probe descent (Seiff and Kirk, 1977).

3. Comparison with observations

The simulated limb profiles based on sources (1) to (4) will be integrated to simulate limb observations and compared with IUVS-MAVEN observations of the 297.2 nm limb scans collected in conditions similar to those of the simulations. This comparison will be used to determine some of the uncertain model parameters and optimize them to best match the observations. Finally, the methodology to determine the density of O and CO_2 in altitude regions hardly accessible to *in situ* measurements will be demonstrated.

4. References

[1] McClintock, W.E. et al. Space Sci. Rev., 1-50,10-1007/s, 2014
[2] Jain, S.K., et al., GRL, 42, 2015.
[3] Shematovich, V.I. et al., JGR, 113, E02011, 2008.
[4] Gérard, J.C. et al., PSS, 56, 542-552, 2008.
[5] Seiff, A. and Kirk, D.B., JGR, 82, 364-4378, 1977.

Acknowledgements. This research was partly funded by the NOMAD PRODEX program managed by the European Space Agency with help of the Belgian Science Policy Office (BELSPO) and supported by BELSPO's SCOOP/BRAIN research contract.

Complex Molecules in Titan's Upper Atmosphere

P. Lavvas[1*]; R.V. Yelle[2]
[1]*Groupe de Spectrométrie Moléculaire et Atmosphérique, Université de Reims Champagne Ardenne, France,*
[2]*Lunar and Planetary Laboratory, University of Arizona, Tucson, USA*

1. Abstract

Results from the Cassini-Huygens mission reveal that Titan's upper atmosphere and ionosphere are far more complex than expected prior to the mission. Observations with the Ion Neutral Mass Spectrometer (INMS) detected 51 separate ion species (Fig. 1). Many of these ions are created by proton transfer reactions to ambient neutrals and thus imply the presence of similarly complex neutral molecules in the upper atmosphere [1]. Measurements by the Cassini Plasma Spectrometer (CAPS) show that positive ions with significant density extend to ~300 daltons [2]. This extraordinarily complex composition was unexpected and implies the existence of a vigorous ion chemistry at high altitudes in Titan's atmosphere. The compositions of the ions in the 100-300 dalton range, beyond the range of the INMS measurements, is unknown, but given the composition of the lower mass ions, it is certain that there is an abundance of large organic molecules.

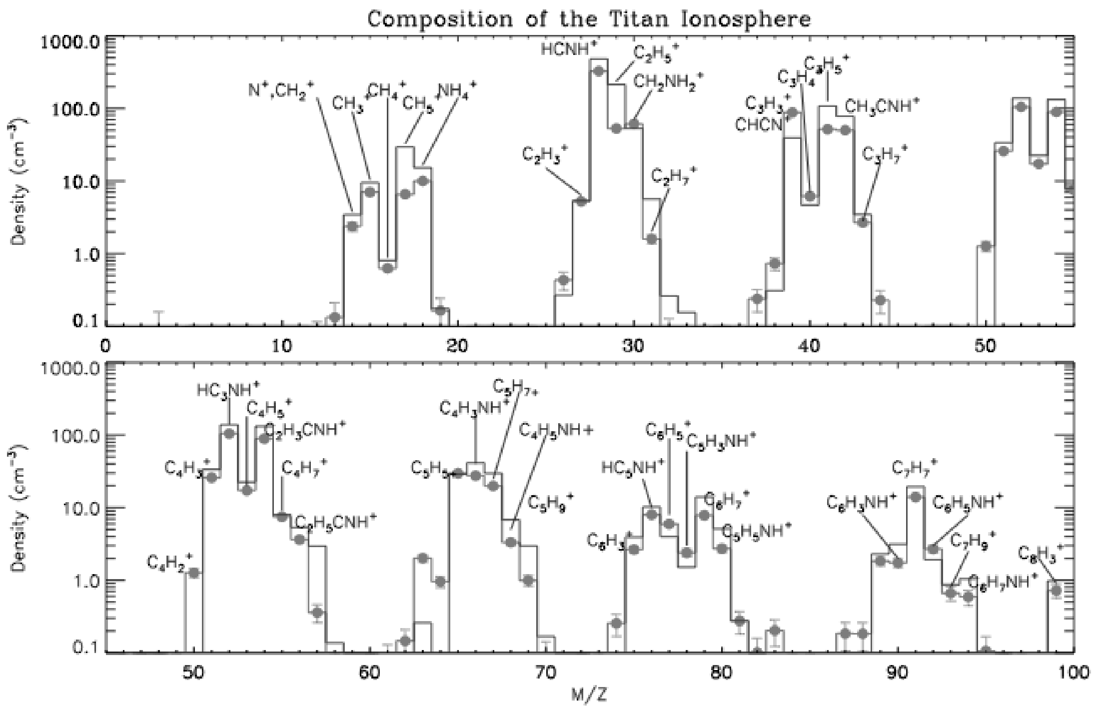

Figure 1:Positive ions in Titan's ionosphere (after Vuitton et al. 2007).

Measurements by the Electron Spectrometer channel of the CAPS instrument (CAPS/ELS) detected negative ions with masses from a few daltons to tens of thousands of daltons [3]. The heaviest negatively charged particles are better described as aerosols rather than molecules, thus the measurements bridge the transition from large molecules to aerosols. Nanometer-sized aerosols in the thermosphere are also observed through scattering of ultraviolet sunlight by the Ultraviolet Imaging Spectrometer (UVIS) [4]. Investigations into this molecular growth have emphasized the essential role of ion chemistry, both in the formation of seed molecules, such as benzene [5], and in the growth of aerosols in the thermosphere [6]. This talk will review these Cassini measurements and the status of photochemical models that seek to interpret the observations.

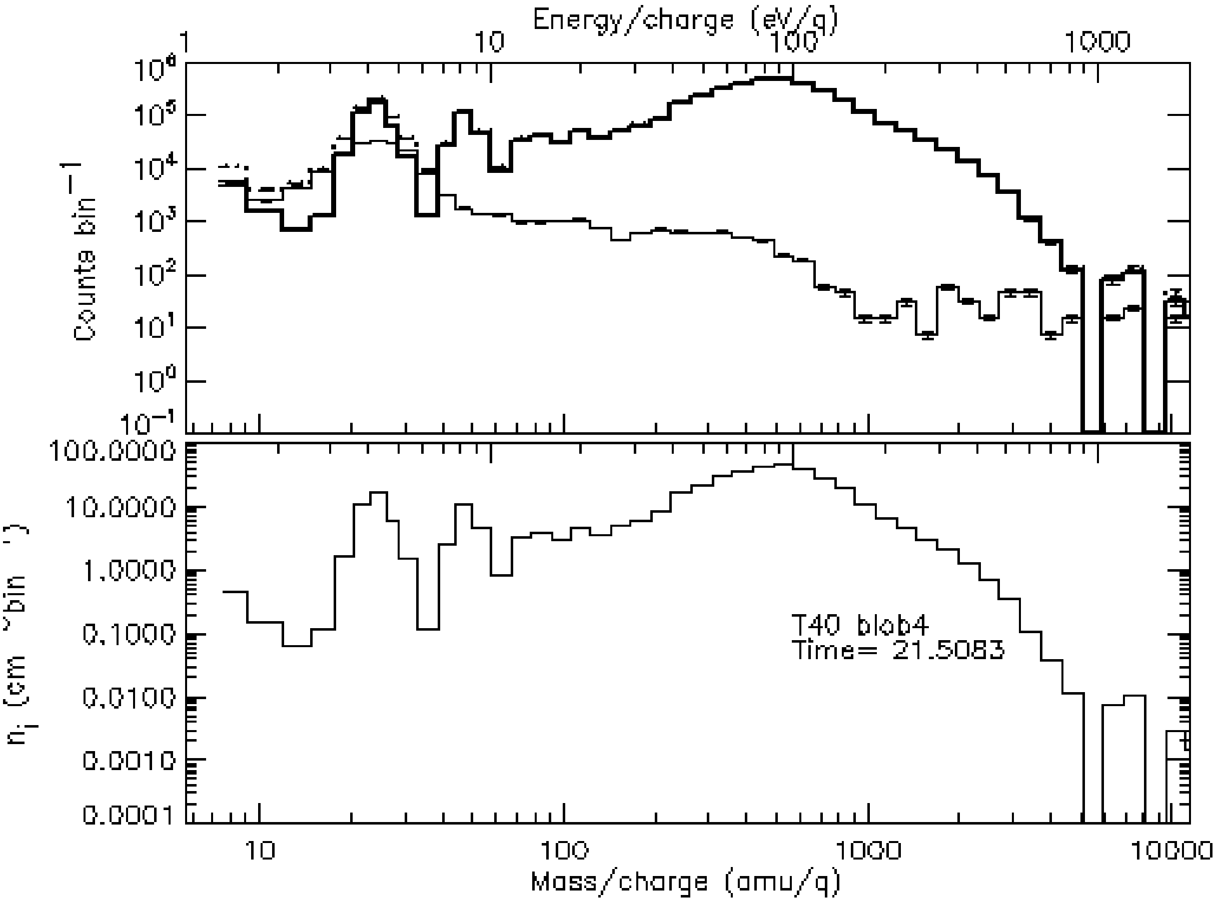

2. References

[1] Vuitton. V., R. V. Yelle, and M. McEwan (2007), Ion Chemistry and N-Containing Molecules in Titan's Upper Atmosphere, Icarus, 191, 722-742.
[2] Crary, F. J., B.A. Magee, K. Mandt, J.H. Waite Jr., J. Westlake, D.T. Young (2009). Heavy ions, temperatures and winds in Titan's ionosphere: Combined Cassini CAPS and INMS observations. Planet. and Space Sci. 57, 1847-1856.
[3] Coates, A. J., F. J. Crary,G. R. Lewis, D. T. Young, J. H. Waite Jr., and E. C. Sittler Jr. (2007). Discovery of heavy negative ions in Titan's ionosphere. Geophys. Res. Letts., 34, L22103, doi:10.1029/2007GL030978
[4] Koskinen, T. T., R. V. Yelle, D. Snowden, P. Lavvas, B. R. Sandel, F. J. Capalbo, Y. Benilan, and R. A. West (2011), The Mesosphere and Thermosphere of Titan Revealed by Cassini/UVIS Stellar Occultations, Icarus 216, 507–534.
[5] Vuitton, V., R. V. Yelle, and J. Cui (2008), Formation and distribution of benzene on Titan, J. Geophys. Res., 113, doi:10.1029/2007JE002997.
[6] Lavvas, P., R. V. Yelle, T. Koskinen, A. Bazin, V. Vuitton, E. Vigren, M. Galand, A. Wellbrock, A. J. Coates, J.-E. Wahlund, F. J. Crary, D. Snowden (2013), Aerosol growth in Titan's ionosphere, Proceedings of the National Academy of Sciences, 110 (8) 2729-2734.

Parameterizing Gravity Waves and Understanding their Impacts on Venus' Upper Atmosphere

A. S. Brecht[1]; S. W. Bougher[2], E. Yigit[3]*
[1] NASA Ames Research Center, USA
[2]CLaSP, 2418C Space Research Building, University of Michigan, USA.
[3]George Mason University, 4400 University Drive, MSN: 3F3, USA.

1. Introduction

The complexity of Venus' upper atmospheric circulation is still being investigated. Simulations of Venus' upper atmosphere largely depend on the utility of Rayleigh Friction (RF) as a driver and necessary process to reproduce observations (i.e. temperature, density, nightglow emission). Currently, there are additional observations which provide more constraints to help characterize the driver(s) of the circulation. This work will largely focus on the impact parameterized gravity waves have on Venus' upper atmosphere circulation within a three dimensional hydrodynamic model (Venus Thermospheric General Circulation Model).

2. Venus Thermospheric General Circulation Model (VTGCM)

The VTGCM's nominal set up utilizes two Rayleigh friction (RF) terms to help simulate mean thermosphere conditions observed by VEX (e.g. [2], [3]). One RF is symmetric about the sub-solar point with cos(latitude) variation which provide constant deceleration to the winds (RF-sym). The second RF is asymmetric about the sub-solar point with cos(latitude) variation in order to simulate the retrograde superrotation zonal wind (RSZ). The purpose of RF is to obtain first order approximation of the necessary wave momentum deposition to reproduce observations. Therefore, the RF provides guidelines for the implementation and adjustment of new wave momentum deposition parameterizations.

In the past, the VTGCM has been utilized to understand the impacts of gravity waves on the O_2 IR nightglow emission [10] and the zonal winds [9]. [10] had a shallower model but was able to show gravity wave deposition creating O_2 IR nightglow emission variations as observed. [9] demonstrated that gravity waves launched below 100km either broke below ~115 km or were reflected due to the internal reflection criteria of the deposition parameterization ([1]; [AD parameterization]). Overall, there was minimal impact on the circulation.

For this study, a different gravity wave momentum/energy deposition parameterization will be employed [8] within a more sophisticated VTGCM (compared to the version used in [10]) along with newly updated radiative processes (aerosol heating and 15 μm cooling parameterization). The radiative updates are important to properly simulate Venus' thermal structure which impacts the circulation and the behaviour of the gravity wave deposition parameterization.

2.1. Aerosol Heating

The VTGCM lower boundary is at ~70 km, which is near the cloud tops. Near this level, aerosols provide heat to the middle atmosphere. A parameterization guided by [7] has been incorporated and tested. The additional heating increases the scale heights in this altitude range (~75 – 90 km) and therefore augments density profiles (~100 – 130 km) and modifies wave propagation.

2.2. 15 μm Cooling Parameterization

We have adapted the updated simplified non-LTE formulation utilized within LMD-MGCM and LMD-VGCM ([6]; [5]). The non-LTE model uses five CO_2 levels and bands, instead of two molecular levels. It calculates the full exchange between atmospheric layers, instead of using the cool-to-space approximation which was the basis of the previous parameterization in the VTGCM ([4]; [2]). We expect to finid VTGCM temperatures warmer over ~80-110 km (day and night) and about the same (cool to space approximation is fine) in the Venus dayside and nightside thermosphere (above ~110-120 km).

2.3. Yiğit Gravity Wave Momentum Deposition Parameterization (GWMD-Y)

The GWMD-Y parameterization has been implemented into the VTGCM and testing has begun. It is a spectral non-linear parameterization [8]. It accounts for many wave dissipation processes that are important in the Venus upper atmosphere, including molecular diffusion and viscosity, plus radiative damping. The GWMD-Y parameterization is different from the AD parameterization because it allows waves to be saturated at multiple heights and the waves are not completely removed at a single breaking level. The computed momentum deposition ("drag") and heating/cooling rates are applied to the momentum and energy conservations equations, respectively. However, the GWMD-Y parameterization does not take into account total internal reflection as does the AD parameterization.

3. Discussion/Conclusion

The work to be presented will be the preliminary studies of the GWMD-Y parameterization incorporated into the VTGCM. The free parameters and their ranges for the parameterization will be discussed. Along with the impact the waves have on the thermal structure, wind structure, and O_2 IR nightglow emission.

4. References

[1] Alexander, M. J. and Dunkerton, T. J.: A Spectral Parameterization of Mean-Flow Forcing due to Breaking Gravity Waves, Journal of the Atmospheric Sciences, Vol. 56, pp. 4167-4182, 1999.
[2] Bougher, S. W., Dickinson, R. E., Ridley, E. C., and Roble, R. G.: Venus Mesosphere and Thermosphere: III. Three-Dimensional General Circulation with Coupled Dynamics and Composition, Icarus, Vol. 73, pp. 545-573, 1988.
[3] Brecht, A. S., Bougher, S. W., Gérard, J. –C., Parkinson, C. D., Rafkin, S., and Foster, B.: Understanding the variability of nightside temperatures, NO UV and O_2 IR nightglow emissions in the Venus upper atmosphere, JGR, Vol. 116, E08004, 2011.
[4] Dickinson, R. E. and Ridley, E. C.: Venus Mesosphere and Thermosphere Temperature Strcture: II. Day-Night Variations, Icarus, Vol. 30, pp.163-178, 1976.
[5] Gilli, G., Lebonnois, S, González-Galindo, F., López-Valverde, M. A., Stolzenbach, A., Lefèvre, F., Chaufray, J. Y., and Lott, F.: Thermal structure of the upper atmosphere of Venus simulated by a ground-to-thermosphere GCM, Icarus, Vol.281, pp. 55-72, 2017.
[6] González-Galindo, F., Chaufray, J. –Y., López-Valverde, M. A., Gilli, G., Forget, F., Leblanc, F., Modolo, R., Hess, S., and Yagi, M.: Three-dimensional Martian ionosphere model: I. The photochemical ionosphere below 180 km, JGR: Planets, Vol. 118, pp. 2105-2123, 2013.
[7] Haus, R., Kappel, D., and Arnold, G.: Radiative heating and cooling in the middle and lower atmosphere of Venus and responses to atmospheric and spectroscopic parameter variations, Planetary and Space Science, Vol. 17, pp. 262-294, 2015.
[8] Yiğit, E., Aylward, A. D., and Medvedev, A. S.: Parameterization of the effects of vertically propagating gravity waves for thermosphere general circulation models: Sensitivity study, JRG, Vol. 113, D19106, 2008.
[9] Zalucha, A. M., Brecht, A. S., Rafkin, S., Bougher, S. W., and Alexander, M. J.: Incorporation of a gravity wave momentum deposition parameterization into the Venus Thermosphere General Circulation Model (VTGCM), JRG: Planets, Vol. 118, pp. 1-14,. 2013.
[10] Zhang, S., Bougher, S. W., and Alexander, M. J.: The impact of gravity waves on the Venus thermosphere and O_2 IR nightglow, JGR, Vol. 101, pp. 23195-23205, 1996.

MAVEN/IUVS Observations of Martian Mesospheric Clouds in 2017: A Persistent Longitudinal Asymmetry at Southern Mid-Latitudes

M.H Stevens[1*]; S. Jain[2]; J.S. Evans[3]; J. Deighan[2]; N.M. Schneider[2]
[1] Space Science Division, Naval Research Laboratory, USA,
[2]Laboratory for Atmospheric and Space Physics, University of Colorado, Boulder, USA
[3]Computational Physics, Inc.,USA

1. Introduction

Observations of Martian mesospheric CO_2 ice clouds have been made sporadically for over 20 years [1] and are sometimes compared to their terrestrial counterpart, noctilucent clouds [7]. On Mars, mesospheric clouds are often used as diagnostics for dynamical variability [2] because the CO_2 frost point in the upper mesosphere (60-80 km) is very low at about 105 K [10]. Longitudinal asymmetries in mesospheric cloud observations have been identified, although these are primarily reported around the equator [6,7,9,10,11]. This spatial confinement of the cloud distribution has been linked to the interaction between migrating and non-migrating tides, allowing for important constraints to general circulation models [GCM; 2,5].

Here we report new observations of mesospheric clouds at southern mid-latitudes on Mars. Observations of Martian mesospheric clouds in the southern hemisphere are relatively rare [7] so the low temperatures required for such observations provide new constraints to Martian GCM. The southern hemisphere cloud population was observed in December 2017 between 80-160□ E longitude by the Imaging Ultraviolet Spectrograph (IUVS) on the Mars Atmosphere and Volatile Evolution (MAVEN) mission. We will compare these observations to concurrent IUVS observations of scale heights in the upper atmosphere to quantify the vertical coupling of the thermal tides controlling cloud formation in the mesosphere [5,10].

2. Observations

The MAVEN mission began orbiting Mars in September 2014 and has been operating continuously since then. MAVEN is in an elliptical orbit with an apoapsis altitude of 6200 km and a periapsis altitude of about 150 km [4]. IUVS on board MAVEN obtains 12 limb scans for each periapsis pass using a far-UV (FUV) and mid-UV (MUV) channel. The 0.06□ x 11□ field of view is divided into seven horizontal segments allowing for 84 separate profiles each orbit [3,8,10]. Many of these profiles extend down into the thermosphere, where Martian mesospheric clouds can be detected on the limb as excess solar scattered light above the background.

Martian mesospheric clouds typically appear between Ls=0-150□ [7] and IUVS was making daytime limb scans at southern mid-latitudes between Ls=95-108□ in December 2017. In contrast to many orbiting spacecraft at Mars, MAVEN observations are not locked in local time so that the entire diurnal cycle can be observed in about eight months. The observations presented herein are made between 8-10 local solar time, which is a time of day that has not been routinely sampled heretofore. We use the MUV spectral region between 185-205 nm to identify excess solar scattering from mesospheric clouds [10].

3. Results

Figure 1 shows 55 limb profiles identified with a mesospheric cloud along the line of sight. Also shown is the average clear air background for the same time period, which is relatively small so that the clouds are readily identified as bright layers above the background. We use the altitude region to search for excess radiance of solar scattered light between 60-80 km and conservatively flag as clouds those profiles with radiances +5□ above the clear air average [10]. Note that although the clouds are identified in the IUVS data between 60-80 km, many of the scans peak between 50-60 km altitude.

Figure 2 shows the horizontal distribution of the clouds as well as the clear air scans for the indicated time period. A longitudinal asymmetry in the cloud distribution is clearly identified at southern mid-latitudes between 80-160□ E.

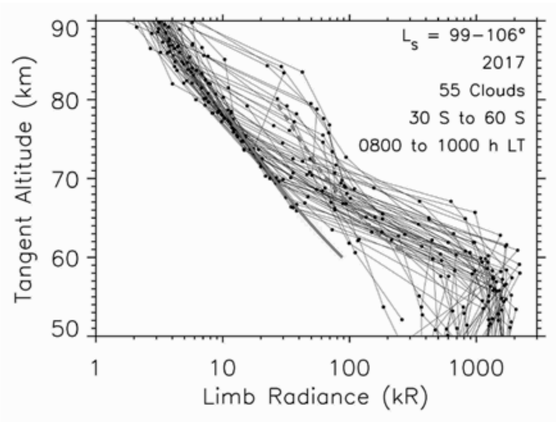

Figure 1: Limb radiances of solar scattered light from Martian mesospheric clouds observed between 11-25 December, 2017. Radiances are integrated between 185-205 nm. The average profile between 60-80 km for

clear air is shown as the solid red curve and the +5□ scatter is the dashed red curve. Detached mesospheric clouds are easily identified as the black profiles.

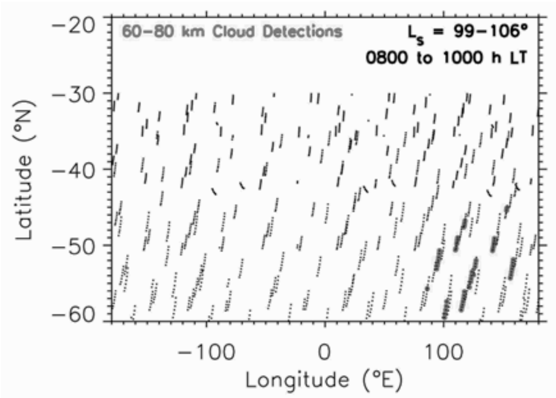

Figure 2: The spatial distribution of the mesospheric clouds identified in Figure 1 are shown as as the larger red symbols, which cluster between 80-160°E longitude. The smaller black symbols overplotted are all of the IUVS limb observations for the indicated conditions.

4. Summary

We report new observations of Martian mesospheric clouds between 40-60°S. These clouds show a persistent longitudinal asymmetry such that they are preferentially distributed between 80-160°E longitude. These MAVEN/IUVS observations are made between the heretofore sparsely sampled period of 8-10 local solar time and provide new constraints to GCM. We will quantify the vertical coupling of the non-migrating thermal tides that enable this spatial confinement using concurrent observations of lower thermospheric scale heights from IUVS observations.

References

[1] Clancy, R.T. and B.J. Sandor: CO_2 ice clouds in the upper atmosphere of Mars, Geophys. Res. Lett., Vol. 25, 489-492, 1998.
[2] González-Galindo, F. et al.: The martian mesosphere as revealed by CO_2 cloud observations and General Circulation Modeling, Icarus, 216, 10-22, 2011.
[3] Jain, S.K. et al.: The structure and variability of Mars upper atmosphere as seen in MAVEN/IUVS dayglow observations, Geophys. Res. Lett., 42, 9023-9030, doi:10.1002/2015GL065419, 2015.
[4] Jakosky, B.M. et al.: The Mars Atmosphere and Volatile Evolution (MAVEN) Mission, Space Sci. Rev., 195, 3-48, DOI 10.1007/s11214-015-0139-x, 2015.
[5] Kleinböhl, A. et al.: The semidiurnal tide in the middle atmosphere of Mars, Geophys. Res. Lett., Vol. 40, 1952-1959, doi:10.1002/grl.50497, 2013.
[6] Määttänen, A. et al.: Mapping the mesospheric CO_2 clouds on Mars: MEx/OMEGA and MEx/HRSC observations and challenges for atmospheric models, Icarus, Vol. 209, 452-469, 2010.
[7] Määttänen, A. et al.: Mesospheric Clouds on Mars and on Earth, in Comparative Climatology of Terrestrial Planets (S.J. Mackwell et al., eds.), 393-413. Univ. of Arizona, Tucson, DOI: 10.2458/azu_uapress_9780816530595-ch16, 2013.
[8] McClintock, W.E. et al.: The Imaging Ultraviolet Spectrograph (IUVS) for the MAVEN mission, Space Sci. Rev., 195, 75-124, doi:10.1007/s11214-014-0098-7, 2015.
[9] Montmessin, F. et al.: Hyperspectral imaging of convective CO2 ice clouds in the equatorial mesosphere of Mars, J. Geophys. Res., Vol. 112, E11S90, doi:10.1029/2007JE002944, 2007.
[10] Stevens, M.H. et al.: Martian mesospheric cloud observations by IUVS on MAVEN: Thermal Tides coupled to the upper atmosphere, Geophys. Res. Lett., Vol. 44, doi:10.1002/2017GL072717, 2017.
[11] Vincendon, M. et al.: New near-IR observations of mesospheric CO_2 and H_2O clouds on Mars, J. Geophys. Res., Vol. 116, E00J02, doi:10.1029/2011JE003827, 2011.

September 10-11, 2017 Solar Flare Event: Rapid Enhancement of the Martian Neutral Exosphere from the X-class flare as observed by MAVEN

M.K. Elrod[1, 2], *S.M. Curry[3], E.M.B. Thiemann[4], S. K. Jain[4]*
[1]NASA Goddard Spaceflight Center, [2] CRESST, University of Maryland, [3]SSL, [4]LASP, University of Colorado

Introduction

On September 10-11, 2017, there was a particularly strong x-class flare followed by an interplanetary coronal mass ejection (ICME) was observed at Mars. The flare began on September 10, 2017 at UTC 15:43:40, peaked at 16:07:50, as observed by GOES, with the hard x-rays arriving at Mars 10.7 minutes later. This was a unique solar event at Mars in that multiple assets like MAVEN, TGO, MRO, and Mars Express were able to observe the event with multiple instruments. This paper will focus on the observations made by the Mars Atmosphere and Volatiles EvolutioN (MAVEN) Neutral Ion Gas Spectrometer (NGIMS) analysis of the upper neutral atmosphere from 150-300km before and after the flare occurred. The closest MAVEN periapsis pass occurred on orbit 5718 and went from UTC 17:30 – 17:54. NGIMS measured a significant enhancement in the Martian neutral exosphere above 195km for the flare orbit (5718) and in the upper ionosphere (Thiemann et al. 2018). The enhancement from this flare, both before and after the flare event, stands out significantly for orbit 5718, among all major species measured by NGIMS (Ar, CO^2, CO, O and N_2). The O, CO and N2 are enhanced more than the CO2 and Ar likely due to ionization. This significant enhancement was brief, lasting only one orbit, suggesting the response of the neutral atmosphere to the flare was less than the 4.5h period MAVEN orbits Mars. The correlation of the flare and the enhancement in density and temperature in the upper atmosphere indicates that solar flare ionization is the most likely the main driver and has important implications for the effects of space weather events on terrestrial atmospheres.

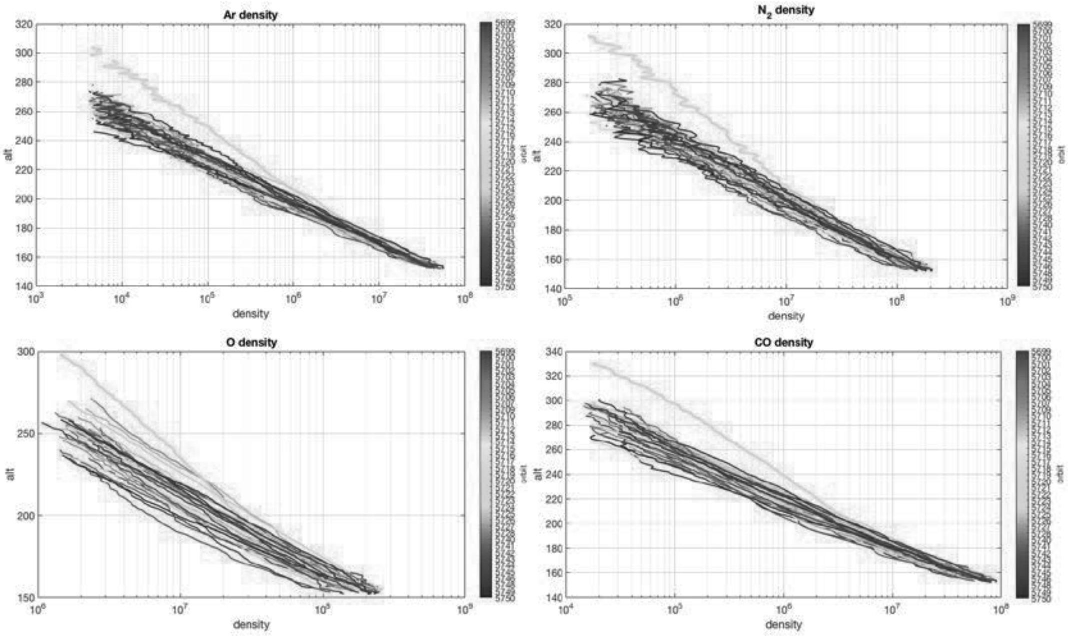

Fig 1- Ar, N2, O, CO density vs altitude for before, during and after the flare. The green highlighted orbit coincides with orbit 5718 when the flare peak reaches Mars. This significant enhancement in the neutral densities in all species coincident with the flare indicates heating from ionization due to the flare.

Protonated Ions and the Seasonal Variation of Hydrogen Observed by the MAVEN Neutral Gas and Ion Mass Spectrometer

S. W. Stone[1*]; *R. V. Yelle[1], M. Benna[2,3], M. K. Elrod[2,4], P. R. Mahaffy[5]*
[1]Lunar and Planetary Laboratory, University of Arizona, USA.
[2]Planetary Environments Laboratory, Code 699, NASA Goddard Space Flight Center, USA.
[3]CRESST, University of Maryland, Baltimore County, USA.
[4]CRESST, University of Maryland, USA.
[5]Solar System Exploration Division, Code 690, NASA Goddard Space Flight Center, USA

Introduction

H escape to space could account for the loss of up to 85% of the initial water inventory of Mars over the last 4 billion years. [1-3] Atomic and molecular hydrogen, products of the photolysis of H_2O high in the atmosphere, react with ions present in the atmosphere to form species such as H_2^+, HCO_2^+, and HCO^+. The Neutral Gas and Ion Mass Spectrometer (NGIMS) onboard the NASA Mars Atmosphere and Volatile EvolutioN (MAVEN) mission measures the abundance and variability of 22 atmospheric ions, including the relevant protonated species listed above, with unit mass per charge () resolution from an altitude of 500 km down to ~120 km, near the primary (F1) ionospheric peak. [4, 5] As the MAVEN orbit precesses, NGIMS densely samples the Martian upper atmosphere in local time and latitude.

Previous investigations have found an order of magnitude variation in upper atmospheric hydrogen and thus hydrogen escape rates on Mars. [6-8] We observe similar variation in numerous protonated ions, an example of which can be seen in **Figure 1**. Using NGIMS ion measurements, we investigate the composition and variation in time of the Martian ionosphere over the MAVEN mission so far. Combining these observations with photochemical models, we calculate H and H_2 densities to probe seasonal variations in these important atmospheric species over nearly 2 Martian years and explore implications for the escape of hydrogen from Mars.

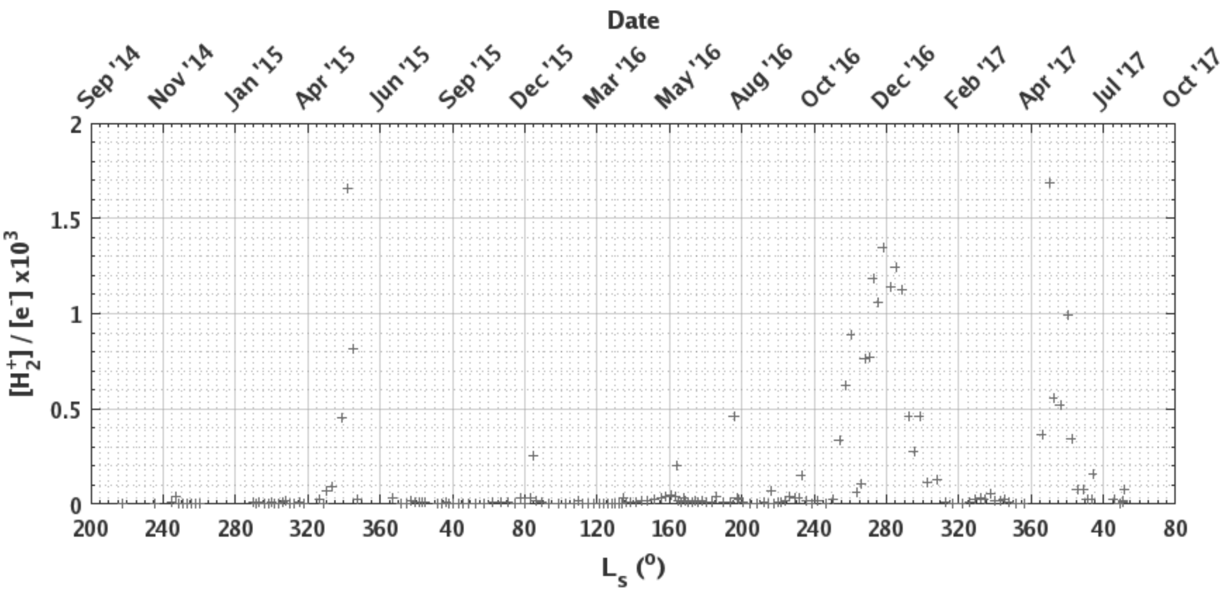

Figure 2. The mean $[H_2^+]$ / $[e^-]$ ratio over the MAVEN mission so far.

References

[1] Villanueva, G. L., et al. Strong water isotopic anomalies in the martian atmosphere: Probing current and ancient reservoirs, Science, Vol. 348(6231), pp. 218-221, 2015, doi:10.1126/science.aaa3630.
[2] Mahaffy, P. R., et al. The imprint of atmospheric evolution in the D/H of Hesperian clay minerals on Mars, Science, Vol. 347(6220), pp. 412-414, 2015, doi:10.1126/science.1260291.
[3] Krasnopolsky, V. A. Variations of the HDO/H_2O ratio in the martian atmosphere and loss of water from Mars, Icarus, Vol. 257, pp. 377-386, 2015, doi:10.1016/j.icarus.2015.05.021.
[4] Mahaffy, P. R., et al. The Neutral Gas and Ion Mass Spectrometer on the Mars Atmosphere and Volatile Evolution Mission, Space Science Reviews, Vol. 195(1-4), pp. 49-73, 2015, doi:10.1007/s11214-014-0091-1.

[5] Benna, M., et al. First measurements of composition and dynamics of the Martian ionosphere by MAVEN's Neutral Gas and Ion Mass Spectrometer, Geophysical Research Letters, Vol. 42(21), pp. 8958-8965, 2015, doi:10.1002/2015GL066146.
[6] Chaffin, M. S., et al. Unexpected variability of Martian hydrogen escape, Geophysical Research Letters, Vol. 41(2), pp.314-320, 2014, doi:10.1002/2013GL058578.
[7] Bhattacharyya, D., et al. A strong seasonal dependence in the Martian hydrogen exosphere, Geophysical Research Letters, Vol. 42(20), pp. 8678-8685, doi:10.1002/2015GL065804.
[8] Clarke, J. T., et al. Variability of D and H in the Martian upper atmosphere observed with the MAVEN IUVS echelle channel, Journal of Geophysical Research: Space Physics, Vol. 122(2), pp. 2336-2344, 2017, doi:10.1002/2016JA023479.

Tuesday 15 of May 2018

Ionospheres of the Terrestrial Planets

T. E. Cravens[1*]
[1]*University of Kansas, Lawrence, KS, USA,*

1. Introduction to Ionospheres

Ionospheres are formed when solar radiation or precipitating particles from the external environment (e.g., magnetosphere or solar wind) ionize the upper atmospheres of planets, satellites, or other neutral environments [2]. The Earth's ionosphere was the first to be studied, but over the past few decades remote and *in situ* measurements have been made of ionospheres throughout the solar system by many spacecraft. This makes comparative studies of ionospheres possible. This talk will start with an introduction to ionospheres in general. A brief review of the terrestrial ionosphere will follow and then a discussion of the ionospheres of Venus, Mars, and Titan.

The physical and chemical processes operating in all ionospheres are very similar. However, very different density structures, chemical compositions, temperatures, and dynamics result due to differences in the heliocentric distance, strength of the intrinsic magnetic field, size of the planet/object, and the underlying atmospheric composition. An important aspect of ionospheric behavior is magnetosphere-ionosphere coupling and/or the interaction with the solar wind.

2. Examples of Ionospheres

2.1. The Terrestrial Ionosphere

The neutral composition of the terrestrial thermosphere is dominantly N_2, O_2, O, N, and NO. The ionization rate is a maximum in the "E-region" near an altitude of 140 km. The O_2^+ and N_2^+ ions produced participate in chemical reactions including: O_2^+ + NO □NO^+ + O_2 and O^+ + N_2 – NO^+ + N. The resulting molecular ion species dissociatively recombine with electrons which removes ionization (e.g., O_2^+ + O □O + O). At higher altitudes (i.e., above 200 km) in the so-called F1 and F2 regions, O^+ becomes the dominant ion species. Plasma transport along the magnetic field, or perpendicular due to E X B drifts, associated with convective electric fields, becomes more important than chemistry at higher altitudes. In the auroral regions, ionization due to precipitation of energetic electrons and protons becomes important, and plays an important role in the coupling between the magnetosphere and the ionosphere.

2.2 Venus and Mars

The main sources of data for the upper atmosphere and ionosphere of Venus has been the Pioneer Venus (PVO) and Venus Express (VEX) missions. For Mars, the key missions have been Viking, Mars Global Surveyor (MGS), Mars Express (MEX), and the Mars Atmosphere and Volatile Evolution mission (MAVEN). CO_2 is the major neutral species and its dissociation products CO and O are also abundant in the thermosphere. Some N_2 and other species are also present. The most abundant ion species at both Venus and Mars is O_2^+ due to ion-neutral reactions (CO_2^+ + O □O_2^+ + CO and O^+ + CO_2□O_2^+ + CO). Note that the dissociative recombination of O_2^+ produces fast O atoms that populate the exospheres of these two planets (O_2^+ + e □O + O). A significant fraction of the O atoms produced by this reaction have speeds exceeding the escape speed at Mars, and can thus lead to significant atmospheric loss over geological time.

Venus and Mars do not have global-scale intrinsic magnetic fields, although Mars does have significant remnant crustal fields, especially in the southern hemisphere. A large magnetosphere exists around planets that possess large intrinsic fields (e.g., Earth, Jupiter, Saturn, and Neptune), but the solar wind interacts more directly with the ionospheres and atmospheres of "non-magnetic" bodies such as Venus, Mars, Titan, and comets. The solar wind- ionosphere interaction, and the associated induced magnetic fields, plays an important role in the dynamics and energetics of these ionospheres. Plasma flows in response to thermal pressure gradient forces and magnetic forces (that is, the J x B force). This plasma flow also leads to ionospheric (and atmospheric) loss from the planet.

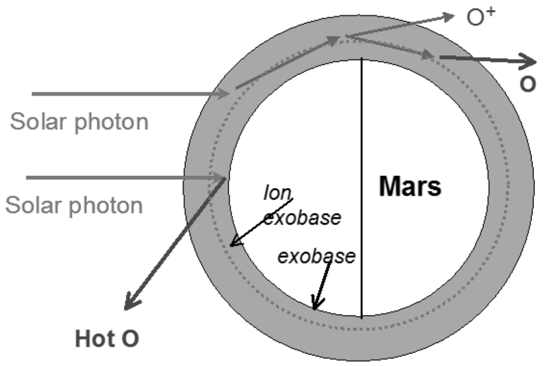

Figure 1: Schematic of oxygen loss from Mars due to ionospheric processes. Photoionization of neutrals at high altitudes leads to oxygen loss [1].

2.3 Other Ionospheres

Other "terrestrial" bodies are present in the solar system including larger satellites such as Titan, Triton, Europa, and Ganymede, all of which are known to have ionospheres. Perhaps Pluto can also be put into this category. The Cassini mission extensively studied Titan over more than a decade. The dense atmosphere contains N_2 and CH_4, as well as many complex organic species. A large number of ion species are present with measured mass spectra showing species up to hundreds of amu. Cassini also studied the interaction between Titan's ionosphere and the surrounding magnetosphere of Saturn.

3. References

[1] Cravens, T. E., Hamil, O., Houston, S., Bougher, S., Ma, Y., Brain, D., and Ledvina, S.: Estimates of Ionospheric Transport and Ion Loss at Mars, J. Geophys. Res., 122. https://doi.org/10.1002/2017JA024582, 2017.
[2] Schunk, R.W. and Nagy, A. F..: Ionospheres: Physics, Plasma Physics, and Chemistry, Cambridge Univ. Press, 2009.

Hybrid plasma modelling of the planetary atmospheres and ionospheres

R. Modolo[1]; F. Leblanc[2], J-Y Chaufray[2], L. Leclercq[3], N. Romanelli[2], B. Langlais[4], E Thebault[4].*

[1] LATMOS/IPSL, UVSQ Université Paris-Saclay, UPMC Sorbonne Université, CNRS, France

[2] LATMOS/IPSL, UPMC Sorbonne Université, UVSQ Université Paris-Saclay CNRS, France

[3] Materials Science and Engineering Department, University of Virginia,

USA

[4] Laboratoire de Planétologie et Géodynamique, Université de Nantes, CNRS, France

1. Introduction

Solar Wind interacts with solar system objects by exchanging momentum and energy. This transfer is particularly effective in the case of weakly magnetized bodies (Mars, Venus and comets) and small magnetosphere (Mercury, Ganymede). This interaction contributes to the erosion of the gaseous envelop and to the atmospheric dynamic and has therefore an important consequence on the atmospheric evolution of these objects. The electromagnetic coupling with these neutral environments takes place through ionization processes: ionization by solar photons, electron impact ionization (incident plasma electrons ionize the upper atmosphere), and charge exchange between ionized and neutral particles producing a cold ion and a fast neutral. As the solar wind or magnetospheric plasma flow approaches the ionospheric region, more and more of ions originating from the planet are incorporated. This mass loading becomes more important as we approach the object, contributes to the loss of momentum of the flow, and leads to a pile-up and a twist of magnetic field lines around the object, creating an induced magnetosphere. This deceleration is even stronger in presence of an ionosphere whose conductive layers represent the final obstacle.

In order to better represent plasma – planet interactions, modeling efforts have been conducted to develop the LatHyS simulation model, a generic 3D multi-species kinetic parallel simulation model for plasma planetary environments, where the spatial resolution approaches ionospheric scale heights [eg 1; 2].

2. Toward a more realistic description of neutral - plasma coupling for planetary environments

The characteristics and the description of the atmosphere/ionosphere are fundamental to understand the global interaction between the solar wind / magnetospheric plasma and the environment of a planet / moon. The different regions (surface – thermosphere – exosphere – ionosphere - magnetosphere) are coupled to each other by the means of energy exchange and transfer of momentum between the different layers. None of the simulation models can globally describe all physical processes required to characterize each of these region simultaneously.

Figure 1 presents a sketch of the Martian / Hermean neutral and ionized environment and the different simulation models appropriate for a given region. Although there are interconnections between the different regions, the dynamic is governed by physical processes having different spatial and temporal scales. A first order approach is to adapt models each other to provide a generic description of the entire interaction, meaning that outputs of one simulation model is used as input into a second model.

The strategy has been successfully tested in the framework of the ANR project HELIOSARES for Mars' environment. The coupling is achieved by using a general circulation model [3,4,5], a 3D exospheric model [6,7] and the hybrid model [1]. For instance, density distribution of several neutral species computed from the LMD-MGCM model [4,5] are used to fix the lower boundary condition for the exospheric model [6, 7]. The three-dimensional thermospheric and exospheric distribution is later used in the hybrid model to provide a realistic description of the Martian neutral reservoir. The hybrid model gives access to precipitated ion fluxes map on the topside atmosphere which can be used after to compute the sputtering contribution to the supra-thermal oxygen population [7].

The solar wind interaction with the hermean environment requires a good knowledge of the internal magnetic field. In the frame of the ANR project MARMITE, results of quasi-hemispheric model of the Hermean's magnetic field [8] as well as a 3D Hermean's exosphere [9] are used as input and boundary conditions in the hybrid simulation model.

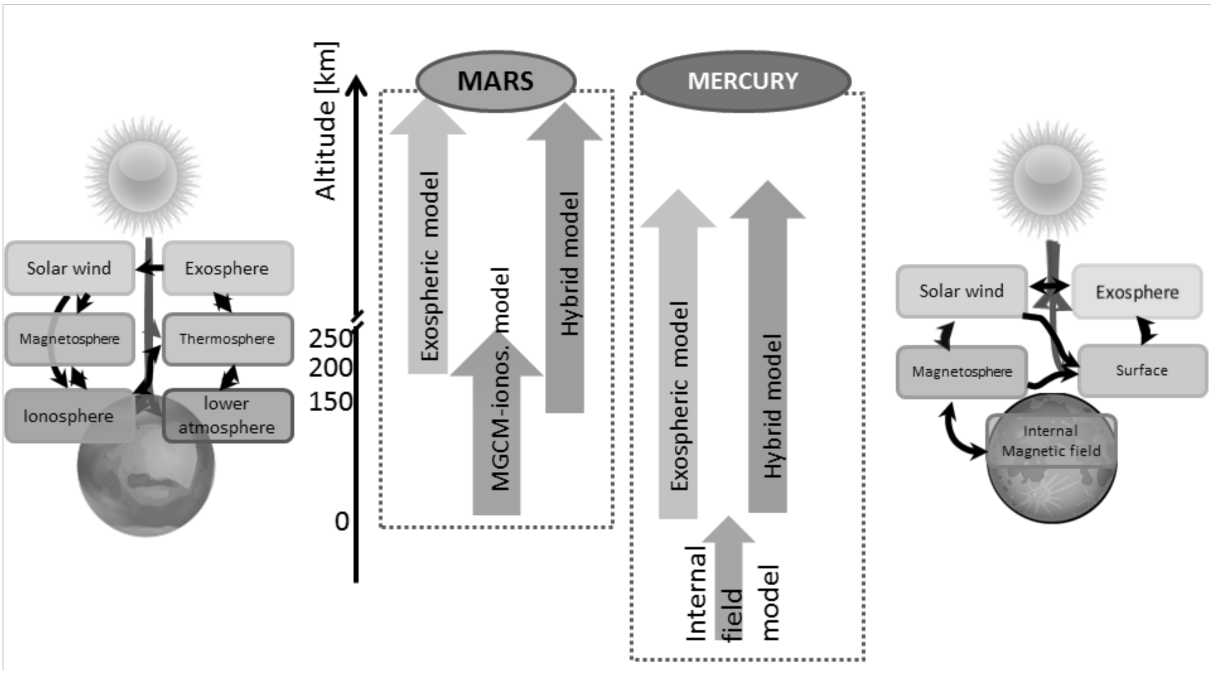

Figure 3 : Sketch representing the coupling between different simulation models describing the solar wind – planet (neutral land ionised) interaction. Left and right panels emphasize the exchange of energy and momentum with the different planetary regions for Mars and Mercury, while central panels illustrate the coupling between different simulation models.

Simulation results emphasizing the coupling between the neutral corona and the induced / intrinsic magnetosphere are presented.

3. References

[1] Modolo, R., et al. (2016), Mars-solar wind interaction: LatHyS, an improved parallel 3-D multispecies hybrid model, J. Geophys. Res. Space Physics, 121, 6378–6399, doi:10.1002/2015JA022324.
[2] Leclercq L., et al (2016), 3D magnetospheric parallel hybrid multi-grid method applied to planet-plasma interactions, Journal of Computational Physics, Elsevier, 309, pp.295-313. 10.1016/j.jcp.2016.01.005.
[3] Forget, F., et al (1999), Improved general circulation models of the Martian atmosphere from the surface to above 80 km. jgr, 104:2415524176.
[4] González-Galindo F., et al (2013), Three-dimensional Martian Ionosphere model: I. The photochemical ionosphere below 180 km, Journal of Geophysical Research. Planets, Wiley-Blackwell, 118 (10), pp.2105-2123.
[5] Chaufray J.-Y., et al (2014), Three-dimensional Martian ionosphere model: II. Effect of transport processes due to pressure gradients, Journal of Geophysical Research. Planets, Wiley-Blackwell, 119 (7), pp.1614-1636. 10.1002/2013JE004551.
[6] Yagi M. et al, (2012), Mars exospheric thermal and non-thermal components: Seasonal and local variations, Icarus, Elsevier, 221 (2), pp.682-693
[7] Leblanc et al (2017), On the Origins of Mars' Exospheric Non-Thermal Oxygen Component as observed by MAVEN and modeled by HELIOSARES, Journal of Geophysical Research. Planets, Wiley-Blackwell, in press. 10.1002/2017JE005336.
[8] Thebault E., et al (2018), A time-averaged regional model of the Hermean magnetic field, Physics of the Earth and Planetary Interiors, in press, 10.1016/j.pepi.2017.07.001
[9] Leblanc, F., et al, (2007), Mercury's exosphere origins and relations to its magnetosphere and surface. pss, 55:1069-1092.

4. Acknowledgments

Authors are indebted to the ANR projects HELIOSARES (ANR-09-BLAN-0223), MARMITE (ANR-13-BS05-0012), the Labex ESEP (ANR-2011-LABX-030) and the “Soleil-Heliosphere-Magnetospheres” and “Système Solaire” programs of the French Space Agency CNES for its support.

Radio Sounding of the Mars Ionosphere over a full Solar Cycle by the Mars Express Radio Science Experiment (MaRS)

M. Pätzold[*1]; *K. Peter[1], S. Tellmann[1], M.K. Bird[1], B. Häusler[2], D.P. Hinson[3,4], and G.L. Tyler[4]*
[1]Rheinisches Institut für Umweltforschung, Department of Planetary Research, Germany,
[2]Institut für Raumfahrttechnik und Weltraumnutzung, Universität der Bundeswehr Munich, Germany
[3]Carl Sagan Center, SETI Institute, USA
[4] Department of Electrical Engineering, Stanford University, USA

The Mars Express Radio Science Experiment MaRS sounds the ionosphere of Mars since 2004. It started during the declining phase of the past solar cycle in 2004, went through a pronounced deep and long solar minimum in 2008 and 2009 and covers most of the current solar cycle through its solar maximum. The great advantage of the MaRS experiment compared to other radio sounding experiments at Mars performed at only a single frequency is the dual-frequency radio sounding at X-band simultaneously at S-band. This helps to identify the true electron density distribution and to separate true ionospheric features, in particular in the topside, from contributions caused by the spacecraft.

The large-scale daytime ionosphere shows a two-layer structure of a main layer M2 and a lower layer M1 formed by mostly solar EUV and solar X-ray and secondary ionization, respectively. The base is typically identified at 90 km. Sometimes additional electron density may be found below the M1 layer which is suspected to be caused by short solar X-rays interacting with the neutral atmosphere (see presentation by K. Peter et al.).

The topside is defined by a transport region with varying plasma scale heights. The ionopause is rarely seen, mostly when the general electron density noise background is low which coincides with observations during planetary opposition.

The M1 and M2 peak densities are clearly under solar control and follow the solar zenith angle and the solar cycle. The altitudes of both layers change also with the solar zenith angle. Variations in altitude for a given solar zenith angle may be caused by atmospheric waves propagating through ionospheric altitudes (see presentation by Tellmann et al.).

The vertical electron content follows also the solar zenith angle and is dominated by the M2 layer which contains at least 50% of the total.

This presentation reviews the MaRS ionospheric soundings over 13 years and a full solar cycle.

Acknowledgments
The MaRS Experiment is funded by the German Space Agency (DLR) under grant 50QM1401 and 50QM1802.

Spatial, seasonal and solar cycle variations of the total electron content (TEC): Is the TEC a good tracer for atmospheric cycles?

Beatriz Sánchez–Cano[1*], *Mark Lester[1], Olivier Witasse[2], Pierre-Louis Blelly[3], Mikel Indurain[3], Francisco González-Galindo[4], Marco Cartacci[5], Álvaro Vicente-Retortillo[6]*
[1]Radio and Space Plasma Physics Group, Department of Physics and Astronomy, University of Leicester, United Kingdom.
[2] European Space Agency, ESTEC – Scientific Support Office, The Netherlands.
[3] Institut de Recherche en Astrophysique et Planétologie (IRAP), France.
[4] Instituto de Astrofísica de Andalucía, CSIC, Spain
[5] Istituto Nazionale di Astrofisica (INAF), Istituto di Astrofisica e Planetologia Spaziali (IAPS), Italy.
[6] Department of Climate and Space Sciences and Engineering, University of Michigan, USA

1. Introduction

The Martian atmosphere is a highly variable system in which the lower and upper parts are strongly coupled. The lower atmosphere is connected with the higher exosphere via the thermosphere. Additionally, the ionosphere is the ionized and very dynamic region of the thermosphere that is mainly created via EUV solar photoionization. Consequently, the ionosphere and the thermosphere are closely coupled, and influenced by several external and internal forcing mechanisms, such as space weather or gravity waves respectively among many others.

One of the most characteristic internal forcings mechanisms is the carbon dioxide (CO_2) cycle, in which the mass of the atmosphere varies during seasons. The CO_2 atmosphere condenses every winter at the Polar Regions forming the CO_2 polar ice caps, and then sublimates back into the atmosphere during the spring and summer seasons inducing a large semiannual variation in the daily averaged surface pressure all over the planet [e.g. 1]. This cycle occurs mainly at the surface and lower atmosphere level, and we evaluate in this work its possible effect on the upper atmosphere, which remains poorly understood.

2. Total Electron Content

The total electron content (TEC) of the ionosphere indicates the number of free electrons contained along the propagation path of a specific signal, such as from a radar. It can be used to characterize and monitor the ionosphere variability [2], and therefore, it is an excellent indicator of the variability of the ionosphere-thermosphere that can be used to assess the lower-upper atmospheric coupling.

In this work, we analyze the annual variation of 10 years of Mars Express TEC observations taken from the Mars Advanced Radar for Subsurface and Ionospheric Sounding (MARSIS) instrument. MARSIS TEC data come from its subsurface operational mode [3, 4] in which the TEC of the full atmosphere is retrieved (from the spacecraft to the surface of the planet).

Since the solar flux is the dominant factor for the atmospheric ionization, the TEC should follow the irradiance profile at the Mars' heliocentric distance, i.e. having a maximum at the orbit perihelion and a minimum at the aphelion. However, the annual averaged MARSIS TEC profile shows a secondary peak before aphelion which is not related to the solar irradiance variation. In this work we evaluate whether this TEC double peak structure is due to the seasonal variability of the thermosphere. In addition, we assess the latitudinal response of this atmospheric coupling (including the polar day and night ionosphere), its solar activity dependence, and the solar zenith angle effect.

3. Ionosphere-Thermosphere Simulation

A numerical simulation of the ionosphere of Mars during a Martian year has been performed in order to evaluate whether the neutral atmosphere is responsible for the TEC variation observed in the MARSIS dataset.

We have used the Mars version of the numerical/physical model IRAP plasmasphere-ionosphere model (IPIM) [5]. The IPIM model can be run from the Transplanet's Space Weather Prediction Center (http://transplanet.cdpp.eu). This model is coupled with the Mars Climate Dataset (MCD), which is a meteorological database built from the Global Circulation Model (GCM) of the Martian atmosphere Laboratoire de Meteorologie Dynamique (LMD).

The model was run for a fixed solar flux in order to avoid TEC variability due to space weather, and to assess the role that the neutral atmosphere has on the ionosphere as a function of season and latitude. Model outputs reproduce the double peaks in the annual TEC profile, and seem to confirm that they are consequence of this atmospheric coupling. The simulation also allows us to identify the neutral and ionized species that play a role in the thermosphere and ionosphere at each season.

Moreover, we evaluate and discuss whether the semiannual mass atmospheric change due to the CO_2 and water cycles play a role in the thermosphere-ionosphere coupling, and whether the double TEC peak observed by MARSIS is a result of the dynamic of the lower-upper atmospheric coupling.

4. Conclusions

In this work we show that the TEC observations routinely made by Mars Express-MARSIS can be used for useful monitoring of the Martian thermosphere.

5. References

[1] Forget, F., Spiga, A., Dolla, B., Vinatier, S., Melchiorri, R., Drossart, P., Gendrin, A., Bibring, J.-P., Langevin, Y., and Gondet, B.: Remote sensing of surface pressure on Mars with the Mars Express/OMEGA spectrometer: 1. Retrieval method, J. Geophys. Res., 112, E08S15, 2007. doi:10.1029/2006JE002871.

[2] Sanchez-Cano**,** B., Morgan, D.D., Witasse, O., Radicella, S.M., Herraiz, M., Orosei, R., Cartacci, M., Cicchetti, A., Noschese, R., Kofman, W., Grima, C., Mouginot, J., Gurnett, D.A., Lester, M., Blelly, P.-L., Opgenoorth, H., and Quinsac, G.: Total Electron Content in the Martian atmosphere: A critical assessment of the Mars Express MARSIS data sets, *J. Geophys. Res. Space Physics*, 120, 2166–2182, 2015. doi:10.1002/2014JA020630

[3] Cartacci, M., Amata, E., Cicchetti, A., Noschese, R., Giuppi, S., Langlais, B., Frigeri, A., Orosei, R., and Picardi, G.: Mars ionosphere total electron content analysis from MARSIS subsurface data, Icarus, 223, 423–437, 2013. http://dx.doi.org/10.1016/j.icarus.2012.12.011.

[4] Cartacci, M., Sánchez-Cano, B., Orosei, R., Noschese, R., Cicchetti, A., Witasse, O., Cantini, and F., Pio Rossi, A.: Improved estimation of Mars ionosphere total electron content, *Icarus*, 299, 396-410, 2018. https://doi.org/10.1016/j.icarus.2017

[5] Marchaudon, A., and Blelly, P.-L.: A new 16-moment interhemispheric model of the ionosphere: IPIM, J. Geophys. Res., 120, 2015, doi:10.1002/2015JA021193.

Variability of the Martian Upper Ionosphere and Factors Controlling this Variability. MEX and MAVEN Observations.

E. Dubinin[1*]; *M. Fraenz[1]; M. Pätzold[2]; J. McFadden[3]; J. Halekas[4]; J. Connerney[5]; F. Eparvier[6]; P. Mahaffy[5*]; D. Andrews[1*]; S. Barabash[8]*
[1]*Max Planck Institute for Solar System Research, Germany,*
[2]*Rheinisches Institut fuer Umweltforschung, Abteilung Planetforschung, Germany,*
[3]*University of California, USA,*
[4]*University of Iowa, USA,*
[5]*NASA Goddard Space Flight Center, USA,*
[6]*Laboratory for Atmospheric* and Space Physics, University of Colorado Boulder,
[7]*Swedish Institute of Space Physics, Sweden,*
[8]*Swedish Institute of Space Physics, Sweden,*

1. Introduction

At altitudes above ~200 km, the Martian ionosphere is no longer in photo-chemical equilibrium and strongly variable and complex. We will discuss how different external and internal factors control its variability. We present the observations in the upper ionosphere of Mars carried out by Mars Express and MAVEN spacecraft demonstrating a coupling of the ionosphere with the processes above and below it. Solar EUV flux remains to be important in the upper ionosphere. With increase of the solar irradiance the ionosphere expands above the nominal position of the induced magnetosphere and becomes denser [1,2]. Solar wind also affects its structure. For example, with increase of the solar wind strength the upper ionospheric layers are density depleted [3]. The upper ionosphere is sensitive to the IMF direction. In the hemisphere, in which the motional electric field is directed toward the planet, the ionosphere is denser and expands to higher altitudes as compared to the ionosphere in the opposite hemisphere [3]. Crustal magnetic field modifies the ionosphere structure producing a large bulge in the southern hemisphere [4,5]. All these features significantly affect ion losses at Mars [6].

2. References

1] Dubinin, E., Fraenz, M.; Pätzold, et al.: Effects of solar irradiance on the upper ionosphere and oxygen ion escape at Mars: MAVEN observations. J. Geophys. Res*.,* 122, doi:10.1002/2017JA024126, 2017.
[2] Dubinin, E., Fraenz, M.; Pätzold, et al.: Martian ionosphere observed by Mars Express: 2. Influence of solar irradiance on upper ionosphere and escape fluxes. Planet. Space Sci*.,* 144, 132, 2017.
[3] Dubinin, E., M. Fraenz, M.; Pätzold, et al.: Martian ionosphere observed by MAVEN. 3. Influence of solar wind and IMF on upper ionosphere, Planet. Space Sci. 2018, (in press).
[4] Dubinin, E. et al. Martian ionosphere observed by Mars Express. 1. Influence of the crustal magnetic fields, Planet. Space Sci. 124 (2016) 62–75, 2016, http://dx.doi.org/10.1016/j.pss.2016.02.004.
[5] Andrews, D.J., et al.: Determination of local plasma densities with the MARSIS radar: asymmetries in the high-altitude Martian ionosphere. J. Geophys. Res. 118, 6188–6196. http://dx.doi.org/10.1002/jgra.50593.
[6] Dubinin, E., M. Fraenz, M. Pätzold, et al.: The effect of solar wind variations on the escape of oxygen ions from Mars through different channels: MAVEN observations. J. Geophys. Res. Space Physics*, 122.* 2017*,* https://doi.org/10.1002/2017JA024741.

Variability of the Venusian and Martian nightside ionosphere after solar storms

C. Gray[1*]; Z. Girazian[2]; K. S. Peter [3], B. Häusler [4], M. Pätzold [3], S. Tellmann[3] ,
[1] New Mexico State University (Apache Point Observatory), 1320 Frenger Mall, United States
[2] NASA Goddard Space Flight Center, US
[3] Rheinisches Institut für Umweltforschung, Germany,
[4] Institut für Raumfahrttechnik und Weltraumnutzung, Germany

1. Introduction

Interactions between planetary atmospheres and the solar wind can be observed via atmospheric emission and ion/electron density profiles. The interaction of the solar wind with Venus and Mars is unique given that both planets lack an intrinsic magnetic field (or, in the case of Mars, only posesses a weak crustal field) and similar atmospheric composition (95% CO_2).

The Venusian and Martian nightside ionospheres have two distinct electron density peaks: the V1 and V2 peaks for Venus (located near 125 and 150 km), and the M1 and M2 peaks for Mars, (located near 100 and 150 km). These peaks are known to be be highly variable for both planets but the chemical pathways and processes, particularly for the V1 and M1 layers, are not well understood.

Both the V1 and M1 layers exhibit increases in density after intense solar storms, such as coronal mass ejections (CMEs) and solar flares [1, 2]. Figures 1, 2, and 3 illustrate the variability of both peaks during solar quiet time and after solar storms. These increases in density are observed almost immediately and are present on the deep nightside. While ions are transported from the dayside to the nightside of the planet, the time for this process to occur is much longer then the response seen in the electron density profiles. Thus, electron precipitation must play a key role in the variability of these ionospheres. Here, we study the variability of the Venusian and Martian nightside ionosphere and its connection to the solar wind, particularly after solar storms.

1. Observations

Using the Venus Radio Science Experiment (VeRa) instrument on Venus Express (VEX), Mars Radio Science Experiment (MaRS) on Mars Express (MEX), and Langmuir Probe and Waves (LPW) instrument on the Mars Atmosphere Volatile and EvolutioN (MAVEN) spacecraft, we compare electron density profiles of the Venusian and Martian nightside before and after solar storms. Additionally, we compare nightside ion density profiles observed by Neutral Gas and Ion Mass Spectrometer (NGIMS) onboard MAVEN.

2. Discussion

The MAVEN spacecraft is able to observe low ionsphere composition directly. [3] and [4] Giazian et al. 2017 shows that NO^+ is the dominate ion at the M1 level on the Martian nightside (Figure 4). NO^+ was predicted to be the source of the nightside V1 layer on Venus as well as a possible chemical pathway to the observed auroral emission of OI 5577.7 “oxygen green line” [5]. We propose that the the V1 and M1 layers are dominated by NO^+ and that production is sensitive to electron precipitation.

3. References

[1] Withers et al. (2012) JGR, 117, A12
[2] Gray et al. (2017) DPS poster presention.
[3] Girazian et al. (2016) GRL, 4712
[4] Girazian et al. (2017) GRL, 11, 248
[5] Gray et al. (2014) Icarus, 233, 342-347.

Figure 1: Venusian median nightside electron density profile calculated from 130 individual profiles using VeRA on VEX [5]. The V1 and V2 peaks are clearly observed with the V2 peak dominating. 1 sigma standard deviations are plotted as dashed lines.

Figure 2 – Venusian median nightside electron density profile calculated from 10 individual profiles after CME impacts [5]. The V1 and V2 peaks are clearly observed with the V2 peak dominating. 1 sigma standard deviations are plotted as dashed lines.

Figure 3: Martian nightside electron density profile observed during solar quiet time and after solar storms using MaRS on MEX [1]. The M2 peak is clearly observed in profiles 1-3 and 5 near 150 km. The M1 peak near 100 km is seen in profiles 2 and 3 which were observed after a solar storm.

Figure 4: Martian nightside ion profile observed using NGIMS onbaord MAVEN [4]. NO^+ is observed to peak low in the ionosphere.

Characterization of Mars’ Persistent Meteoric Ion Layer

M. Crismani[1], *N. Schneider[1,2], J. Plane[3], S. Jain[1], S. Evans[4], J. Deighan[1]*
[1]Laboratory for Atmospheric and Space Physics, United States
[2]University of Colorado, United States
[3]School of Chemistry, United Kingdom
[4]Computational Physics Inc., United States

1. Introduction

Interplanetary dust particles (IDPs) entering planetary atmospheres at orbital velocity melt and evaporate their constituent minerals as they undergo collisions with air molecules [6,2]. This process, called meteoric ablation, deposits a variety of atomic constituents at the µbar level. Meteoric ablation has been well studied for more than 40 years at the Earth, but only recently detected at another planet [4]. The Mars Atmosphere and Volatile EvolutioN (MAVEN) mission [7] was designed to study the response of Mars' upper atmosphere to solar influences [8], however it is coincidentally well equipped to detect the influence of IDPs. This capability was clearly demonstrated during the exceptionally close encounter of comet C/2013 A1 (Siding Spring) with Mars and the ensuing meteor shower [2,10,3] as well as in a persistent layer due to sporadic ablation [4]. Of the many elements that ablate from interplanetary dust particles, Mg^+ is the most readily detectable ion in ultraviolet (UV) remote sensing. Observations of meteoric ions have revealed unexpected dynamics [3], anomalous high altitude layers [5], surprising diurnal variation, and a response to regional dust storms. We investigate these phenomena and, where appropriate, compare them with our understanding of similar phenomena found at Earth.

2. Characterization of Variability

Metallic ions have been observed to have spatial distributions independent from other ambient ions, forming anomalous high altitude layers and scale heights inconsistent with the expected mass separation [3,5]. The unusual gradients seen after the comet Siding Spring encounter (Figure 1) and in high altitude transient metal layers [5] suggest there may be unique metal ion dynamics in the Martian ionosphere. Variability in metal emissions from scan to scan and from orbit to orbit has also been observed in the persistent layer, and this suggests that metallic species may not follow simple diffusive transport. However, this short-term variation may be due in part to competition between the faint Mg^+ emission and ambient emissions, and a systematic study will be necessary to determine which of these is the dominant driver of variability.

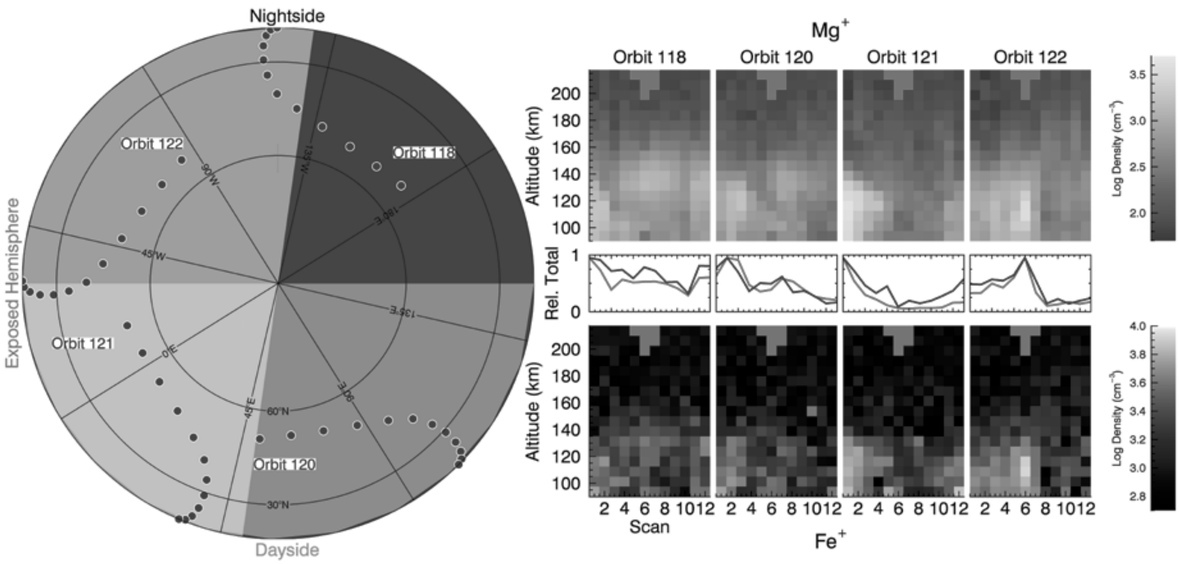

Figure 1: (Left) A geographical representation of observed regions of Mars at the predicted time of dust deposition by comet Siding Spring, where the tangent points of orbits 118, 120, 121, and 122 are shown with maroon circles, with scans beginning at high latitudes and ending near the equator. (Right) Orbit by orbit images of Mg^+ and Fe^+ (top and bottom) constructed by co-adding spectra by altitude (shown on the vertical axis), and adjacent scans are shown on the horizontal axis, which spans 1000 km. Line plots (Mg^+ = red, Fe^+ = green) in the center of the images indicate the total metallic content between 90 and 180 km normalized to each orbit.

The diurnal variation of Mg^+ seen by IUVS (Figure 2), is unexpected in context of current models. Mg^+ is created by charge exchange with O_2^+ and this diurnal variation may suggest inadequate modeling of the nightside ionosphere, day-night transport, or other ionospheric process. Investigation of Mg^+ is then a good proxy for understanding the ionosphere in the transition region between day and night.

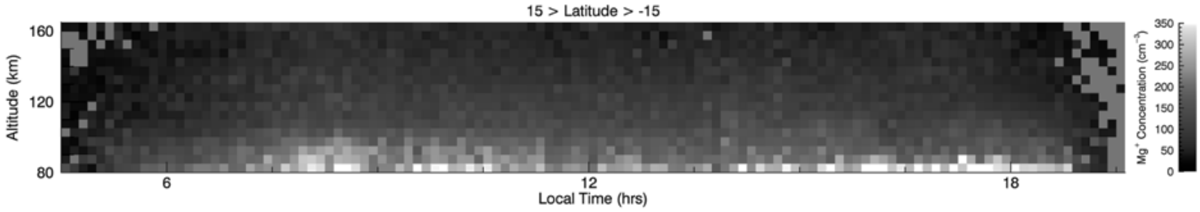

Figure 2: The mean Mg^+ density over the MAVEN mission, between 15 N and S with local time compared to altitude. This data is restricted to solar zenith angles less than 110 degrees. There exist local time variations that have not yet been explored, however the change in Mg^+ from 6 to 7 hours suggest Mg^+ is being created during this period, rather than only being illuminated.

Seasonal variability cannot be investigated without determining the source or sources of variability that exist on shorter timescales. In addition to the variability mentioned above, the ablation region at Mars has been observed to change in altitude, presumably in response to the changing atmosphere in which meteoric ablation takes place. Significant changes in ablation layer altitude suggest a close relationship with the ambient atmospheric profile. Orbits 4010 to 4035 followed a regional dust storm on Mars, and the presence of metal ions at high altitude suggests the entire atmospheric profile is responding to this event, as similarly seen in seasonal variations in Mars' homopause [9].

3. Summary

The persistent Martian meteoric ion layer displays unique characteristics, not found at Earth, whose drivers are not understood. The first attempt to address this problem consists of determining the frequency of anomalous horizontal and vertical profiles, and whether there are trends associated with such behaviour (either with season, geographic location, solar wind conditions, etc.). This catalogue will allow direct comparison of ionospheric features similar to Earth, and those features which may be more similar to other bodies, which are yet unidentified. Three-dimensional modeling that includes chemistry and self-consistent ionospheric transport is necessary to determine what may be causing these varied phenomena.

4. References

[1] Anderson, J., and Barth, C., "Rocket investigation of the Mg I and Mg II dayglow." *Journal of Geophysical Research* 76.16 (1971)
[2] Benna, M., et al. "Metallic ions in the upper atmosphere of Mars from the passage of comet C/2013 A1 (Siding Spring)." *Geophysical Research Letters* 42.12 (2015).
[3] Crismani, M., et al. "The Metals Delivered by Comet Siding Spring to Mars." *EGU General Assembly Conference Abstracts*. Vol. 19. 2017.
[4] Crismani, M., et al. "Detection of a persistent meteoric metal layer in the Martian atmosphere." *Nature Geoscience* 10.6 (2017)
[5] Grebowsky, J., et al. "Unique, non-Earthlike, meteoritic ion behavior in upper atmosphere of Mars." *Geophysical Research Letters* 44.7 (2017)
[6] Istomin, V. "Ions of extra-terrestrial origin in the earth's ionosphere." *Planetary and Space Science* 11.2 (1963)
[7] Jakosky, B., et al. "MAVEN observations of the response of Mars to an interplanetary coronal mass ejection." *Science* 350.6261 (2015).
[8] Jakosky, B., et al. "The Mars atmosphere and volatile evolution (MAVEN) mission." *Space Science Reviews* 195.1-4 (2015).
[9] Jakosky, B. *et al.* Mars' atmospheric history derived from upper-atmosphere measurements of 38Ar/36Ar *Science* (2017)
[10] Schneider, N., et al. "MAVEN IUVS observations of the aftermath of the Comet Siding Spring meteor shower on Mars." *Geophysical Research Letters* 42.12 (2015)

Comparison of Terrestrial and Martian TEC at Dawn and Dusk during Solstices

A.G. Burrell[1*]; B. Sanchez Cano[2], Mark Lester[2], Russell Stoneback[1], Olivier Witasse[3], Marco Cartacci[4]
[1]University of Texas at Dallas, Richardson, USA,
[2]Radio and Space Plasma Physics Group, Department of Physics and Astronomy, University of Leicester, United Kingdom.
[3]European Space Agency, ESTEC – Scientific Support Office, The Netherlands.
[4]Istituto Nazionale di Astrofisica (INAF), Istituto di Astrofisica e Planetologia Spaziali (IAPS), Italy.

1. Introduction

The Earth and Mars are often considered to be the most similar of the solar planets, with similar axial tilts and ionospheres that are formed primarily from EUV and X-ray radiation. These similarities invite comparisons, though care must be taken to account for the major differences, which include a strong, intrinsic magnetic field at Earth, a longer year at Mars, and the greater eccentricity of the Martian orbit. In this study, we compare the behaviour of the Terrestrial and Martian Total Electron Content (TEC) at dawn and dusk during summer and winter.

2. Data

Exploration of the characteristics of the Martian ionosphere have been made possible thanks to recent missions such as the Mars Global Surveyor, Mars Express, and MAVEN. This study takes advantage of a full solar cycle of near-continuous TEC measurements made by the Mars Advanced Radar for Subsurface and Ionosphere Sounding (MARSIS) [1] that is on board Mars Express, which began during the descending phase of the 23rd solar cycle. TEC from Mars Express is available for solar zenith angles (SZA) greater than 75˚ between the Martian surface and the spacecraft.

At Earth, the Global Positioning System (GPS) has been used since the mid- to late-1990's to provide regular, global TEC maps. The GPS satellites orbit at an altitude of 20,000 km above the surface of the earth, and so provide a measure of the column density that includes the entire ionosphere as well as the plasmasphere (when present). Due to the usefulness of this data source, there are many methods of calibrating TEC and repositories that make their data available. This study uses the MIT Haystack GPS TEC made available through the Madrigal Database [2]. This database includes GPS TEC from all open ground and space-based occultation sources, has been rigorously validated and updated when methods improve, and includes TEC with error estimates at a 1˚ latitude by 1˚longitude resolution over the globe at all SZAs.

3. Analysis

Due to the differences between the Terrestrial and Martian ionospheres, direct comparisons of TEC were not found to be practical. Instead, the slope of the TEC as a function of SZA was found using the Huber method (a robust linear fitting technique) and compared for different years, seasons, SZAs, and spatial regions. Data were divided by Martian years, but seasons were centred about the solstices, as is the convention at Earth. To ease the interpretation of the influence of Martian orbital and neutral atmospheric variations, only Northern hemisphere summer (25˚ < L_s < 155˚) and winter (205˚ < L_s < 335˚) are considered. Four SZA regions were examined: pre-dawn (135˚-90˚, after midnight), dawn (90˚-50˚, before noon), dusk (50˚-90˚, after noon), and night (90˚-135˚, before midnight), though the MARSIS TEC was allowed to extend beyond 135˚ in both the pre-dawn and night sectors when possible, since data availability was limited and the local time influence of a magnetic field was not important.

Spatial regions were chosen at each planet to reflect hemispheric and magnetic differences. At Mars, three regions were established: Northern, Southern without crustal fields, and Southern with crustal fields. At Earth, eight mid-latitude regions were established based on their hemisphere and the International Geomagnetic Reference Field (IGRF) [3] magnetic declination (see Figure 1). Breaking up the data into these regions enables the comparison of the Terrestrial and Martian ionospheres under different hemispheric and magnetic conditions, which is important at both planets since neither one exhibits perfect north-south symmetry.

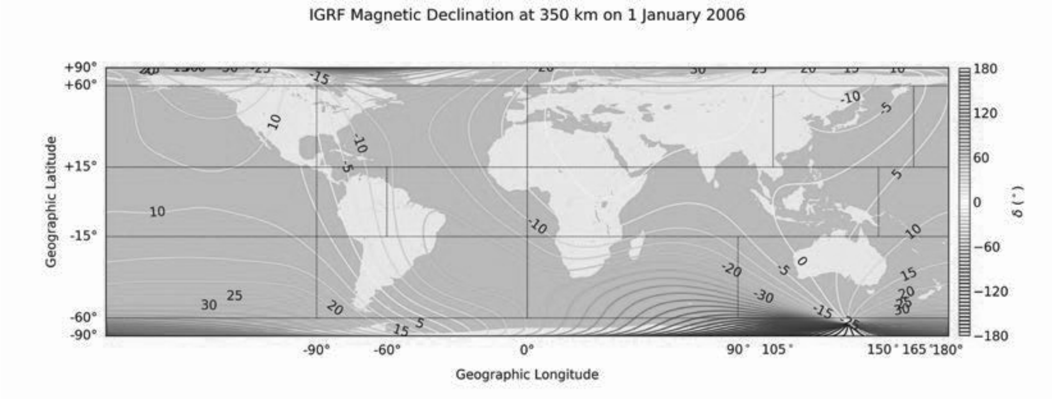

Figure 1: Spatial regions at Earth, plotted along with the IGRF magnetic declination.

4. Discussion

Initial results show that the Martian TEC exhibits consistent behaviour with region and season (the presence of a crustal field turns out to not significantly influence the ionospheric production and loss), showing only a slight dependence on the solar cycle. This solar cycle dependence is characterised by steeper TEC slopes as a function of SZA at dawn and dusk for years with higher solar activity. In contrast, the Terrestrial TEC is highly dominated by the magnetic declination. The most Mars-like region at Earth is found in the southern hemisphere at longitudes 270°-360°, where the magnetic declination varies between -23.2° and 26.4° (the smallest variation about zero). In this spatial region, the TEC shows the same type of SZA exhibited at Mars, and typically not expected in the Terrestrial F region. This suggests that the orientation and strength of the magnetic field is such that this region is dominated by production and loss processes at dawn and dusk. This study will expand on these initial results, expanding the Terrestrial analysis to cover all years currently available for Mars and further examine the role of magnetic field strength on the dawn and dusk behaviour of the TEC.

5. References

[1] Picardi, G., and Sorge, S: Adaptive compensation of ionosphere dispersion to improve subsurface detection capabilities in low-frequency radar systems. In: Proc. SPIE. Eighth International Conference on Ground Penetrating Radar, vol. 4084, pp. 624–629, 2000.

[2] Rideout, W., and A. J. Coster: Automated GPS processing for global total electron content data, GPS Solut, Vol. 10(3), pp 219–228, doi:10.1007/s10291-006-0029-5, 2006.

[3] Macmillan, S., and C. Finlay: The International Geomagnetic Reference Field, in Geomagnetic Observations and Models, pp. 265–276, Springer Netherlands, Dordrecht. 2010.

Observations and Modelling of Low-Altitude Ionospheric Responses to 2017 Sept Solar Flare at Mars

Shaosui Xu[1*]; *Ed Thiemann[2], David Mitchell[1], Frank Eparvier[2], David Pawlowski[3], Mehdi Benna[4], Laila Andersson[2], Michael Liemohn[5], Stephen Bougher[5], Tom Woods[2], Phil Chamberlin[2], Sonal Jain[2], Christian Mazelle[6].*

[1]Space Sciences Laboratory, University of California, USA,
[2]Laboratory for Atmospheric and Space Physics, University of Colorado, Boulder, USA
[3]Physics Department, Eastern Michigan University, Ypsilanti, USA
[4]NASA Goddard Space Flight Center, Greenbelt, USA
[5]Climate and Space Sciences and Engineering, University of Michigan, Ann Arbor, USA
[6]IRAP, CNRS - University of Toulouse - UPS - CNES, France

1. Introduction

Solar extreme ultraviolet (EUV, 10-100 nm) and X-ray (< 9 nm) photons are the main source of the Martian ionosphere, via photoionization of the neutral atmosphere, creating the M2 and M1 peaks at Mars, respectively. During a solar flare, these short wavelength photons can be enhanced by a factor of a few to orders of magnitudes. On September 10, 2017, the Mars Atmosphere and Volatile EvolutioN (MAVEN) mission [3] encountered the largest solar flare (~X9) to date. It is reported that the EUV flux and X-ray fluxes are increased by ~100% and ~1000%, respectively, for this flare event. In this study, we investigate the low-altitude ionospheric response to this solar flare event by simulating photoelectron spectra and ion production rates and densities for periods before the flare, during the flare peak, and during the first MAVEN in-situ observations after the flare peak with the SuperThermal Electron Transport (STET) model [4][8][9].

2. Methodology

Inputs for the STET model for pre-peak and post-peak flare periods include: solar spectra from EUVM L3 data [7], neutral and plasma density and temperature profiles from a combination of Neutral Gas and Ion Mass Spectrometer (NGIMS) data [5], simulation results from the Mars-Global Ionosphere and Thermosphere Model (M-GITM) [2], and also Langmuir Probe and Waves (LPW) data [1]. As the flare peaks during MAVEN's apoapsis passage, when the spacecraft is far above the ionosphere, we take pre-peak flare density and temperature profiles with the solar spectrum for peak flare to simulate the ionospheric response to the flare peak. We compare the modelled photoelectron energy spectra with measurements from Solar Wind Electron Analyzer (SWEA) [6] to constrain the solar spectra inputs and examine the photoelectron signature of the flare. Ion production rates from both photoionization and electron impact ionization by photoelectrons are obtained from STET simulations. Sequentially, ion densities (CO_2^+ and O_2^+) are calculated by assuming photochemical equilibrium, which is a good approximation below 180 km altitude.

3. Results

We find a good agreement between modelled (STET) and measured (SWEA) photoelectron spectra. Photoelectron fluxes at energies from 200 to 500 eV are enhanced by a factor up to 30 during this flare. In addition, the high photoelectron fluxes provide the statistics that allow us to clearly identify Carbon Auger electrons for the first time in the Martian ionosphere. The modelled ion densities are increased by 15%-40% above 150 km, which agrees with LPW data. Below 120 km (M1 layer), the ion density enhancement is up to ~160% and ~190% for post flare, ~300% and ~1500% for peak flare, for O2+ and CO2+ respectively, due to a combination of increased solar irradiance and an expanded thermosphere.

4. References

[1] Andersson, L., R. E. Ergun, G. T. Delory, Anders Eriksson, J. Westfall, H. Reed, J. McCauly, D. Summers, and D. Meyers. "The Langmuir probe and waves (LPW) instrument for MAVEN." Space Science Reviews 195, no. 1-4 (2015): 173-198.

[2] Bougher, S. W., D. Pawlowski, J. M. Bell, S. Nelli, T. McDunn, J. R. Murphy, M. Chizek, and A. Ridley (2015), Mars Global Ionosphere-Thermosphere Model (MGITM): Solar cycle, seasonal, and diurnal variations of the Mars upper atmosphere, J. Geo- phys. Res. Planets, 120, 311–342, doi:10.1002/2014JE004715.

[3] Jakosky, B. M., R. Lin, J. Grebowsky, J. Luhmann, D. Mitchell, G. Beutelschies, T. Priser, M. Acuna, L. Andersson, D. Baird, et al. (2015b), The mars atmosphere and volatile evolution (maven) mission, Space Science Reviews, 195(1-4), 3–48.

[4] Liemohn, M. W., D. L. Mitchell, A. F. Nagy, J. L. Fox, T. W. Reimer, and Y. Ma (2003), Comparisons of electron fluxes measured in the crustal fields at mars by the mgs mag- netometer/electron reflectometer instrument with a b field–dependent transport code, Journal of Geophysical Research, 108(E12), 5134.
[5] Mahaffy, Paul R., Mehdi Benna, Todd King, Daniel N. Harpold, Robert Arvey, Michael Barciniak, Mirl Bendt et al. "The neutral gas and ion mass spectrometer on the Mars atmosphere and volatile evolution mission." Space Science Reviews 195, no. 1-4 (2015): 49-73.
[6] Mitchell, D. L., C. Mazelle, J-A. Sauvaud, J-J. Thocaven, J. Rouzaud, A. Fedorov, P. Rouger et al. "The MAVEN solar wind electron analyzer." Space Science Reviews 200, no. 1-4 (2016): 495-528.
[7] Thiemann, E. M. B., P. C. Chamberlin, F. G. Eparvier, B. Templeman, T. N. Woods, S. W. Bougher, B. M. Jakosky (2017), The MAVEN EUVM model of solar spectral irradiance variability at Mars: Algorithms and results, J. Geophys. Res. Space Physics, 122, 2748–2767, doi:10.1002/2016JA023512.
[8] Xu, S., and M. W. Liemohn (2015), Superthermal electron transport model for mars, Earth and Space Science, 2(3), 47–64, doi:10.1002/2014EA000043, 2014EA000043.
[9] Xu, S., M. W. Liemohn, W. Peterson, J. Fontenla, and P. Chamberlin (2015), Comparison of different solar irradiance models for the superthermal electron transport model for mars, Planetary and Space Science, 119, 62–68.

MAVEN observations of solar wind driven magnetosonic waves heating the Martian dayside ionosphere

C.M. Fowler[1*]; *L. Andersson[1]; R.E. Ergun[1]; Y. Harada[2]; T. Hara[3]; G. Collinson[4]; W.K. Peterson[1]; J. Espley[4]; J. Halekas[2]; J. McFadden[3]; D.L. Mitchell[3]; C. Mazelle[5]; M. Benna[4]; B.M. Jakosky[1].*
[1]Laboratory for Atmospheric and Space Physics, University of Colorado, USA
[2]Department of Physics and Astronomy, University of Iowa, USA.
[3] Space Sciences Laboratory, University of California, USA.
[4]NASA Goddard Space Flight Center, USA.
[5]IRAP, University of Toulouse, CNRS, UPS, CNES, France.

The nature of the solar wind interaction with unmagnetized bodies can be very different to that at magnetized planets such as Earth. At unmagnetized bodies, the lack of a significant, global dipole magnetic field typically leads to an induced magnetosphere forming at the body. The solar wind stand-off distance is subsequently usually located much closer to the unmagnetized body than at magnetized equivalents. At Mars (an unmagnetized body), this solar wind stand-off distance typically lies at around 1.6 Mars radii upstream of the planet. This distance is comparable to the typical proton gyro radius in the solar wind and subsequently it is expected that particles and waves generated by the solar wind-Mars interaction may interact directly with the upper ionosphere of the planet. We present observations from NASA's Mars Atmosphere and Volatile EvolutioN (MAVEN) mission demonstrating the effects on the ionosphere of such interactions. Magnetosonic waves are observed propagating into the upper ionosphere close to the sub-solar point, driving large amplitude (~20-100%) variations in various plasma species densities and temperatures. These waves also drive significant ion heating down to altitudes just above the exobase region; the observed ions can be energized to energies greater than escape energy and this energy deposition appears to drive substantial ion outflow. This supports the idea that such waves may play an important role in driving ionospheric escape to space at Mars, and possibly at other unmagnetized bodies exposed to the solar wind as well.

Control of the Nightside Structure of the Venusian Ionosphere

S. H. Brecht[1] *and S. A. Ledvina*[2]
[1]*Bay Area Research Corp., USA*
[2]*Space Sciences Lab. UC Berkeley, 7 USA*

Introduction

The Pioneer Venus Orbiter, PVO, was the first mission to detect large-scale structure in the nightside region of Venus. This structure is often referred to as "tail rays" [1] Since this discovery, there has been continuous discussion as to the cause of the structure. There have been theoretical attempts to explain the structure but no definitive determination of the mechanism. Typically, the wavelengths of the structure were not always consistent with the theory. Three-dimensional hybrid simulations are reported that produce structure on the nightside of Venus. The structure seems consistent with the data.

Results

The results of the simulations as well as a variety of numerical tests offer some insight into the mechanism driving the development of the structure. The tests reveal that the ambipolar electric field, as produced by the gradient of the electron pressure, seems to be the root cause of the structure**.**
The hybrid simulations are three dimensional with neutral winds included in the simulations. The resolution of the simulation is 50 km/cell and lower. The spherical grid used in the simulations to handle chemistry and collisions has a resolution of 5 km radially and under 50 km in the angular directions. It is these high resolution simulations that produce the structure to be discussed in this paper, see figure 1 below.

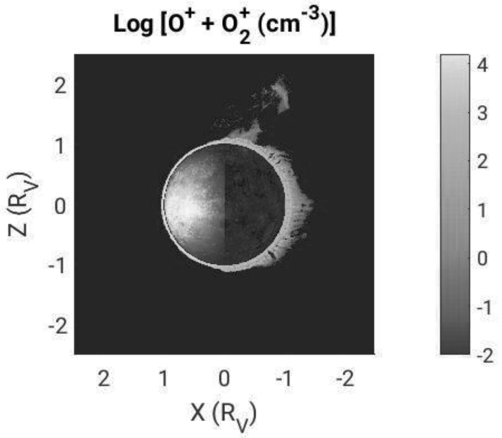

Figure 4: Simulation of Venus from HALFSHEL hybrid code.

In addition, the presentation will briefly discuss the effect of differing neutral atmospheric models on the location of the shock and will offer an explanation as to why the structure is not seen in the Martian tail.

[1] Brace, L.H. et al., "The Ionotail of Venus: Its Configuration and Evidence for Ion Escape", *J. Geophys. Res.*, **92**, 15-26, 1987.

Small scale excess electron densities in the lower ionosphere of Mars: Interpretation of Mars Express radio science observations in combination with MAVEN measurements

K. Peter[1]; M. Pätzold[1], F. González-Galindo[2], L. Andersson[3], M. K. Bird[1,4], M. Crismani[3], C. M. Fowler[3], B. Häusler[5], D. Larson[6], R. Lillis[6], G. Molina-Cuberos[7], N. Schneider[3], S. Tellmann[1] and O. Witasse[8]*
[1]Rheinisches Institut für Umweltforschung, Germany
[2]Instituto de Astrofísica de Andalucía, CSIC, Spain
[3]Laboratory for Atmospheric and Space Physics, University of Colorado at Boulder, USA
[4]Argelander Institut für Astronomie, Germany
[5]Universität der Bundeswehr München, Germany
[6]Space Science Laboratory, University of California, USA
[7]Universidad de Murcia, Spain
[8]Research and Scientific Support Department of ESA, ESTEC, The Netherlands

1. Introduction

The Mars Express radio science experiment MaRS observes the ionosphere and neutral atmosphere for more than 14 years. This resulted in more than 850 observations of the vertical structure of the ionospheric electron density, the neutral atmospheric pressure, density and temperature from the top of the ionosphere down to the surface. In 2005, Pätzold et al. identified an additional sporadic layer in the Martian dayside ionosphere below the well established structure of the ionospheric main and secondary peak [6]. Due to the fact, that radio science experiments can only sense the electrons but not the ion composition, the origin of these layers remained unknown.

In this work, the large MaRS database is used to explore potential origins of these sporadic layers. The identified excess electron densities are divided into two groups, excess electron density detached from (Md, Figure 1a) and excess electron densities merged with (Mm, Figure 1b) the ionospheric body. The focus of this work is on the origin and composition of the merged excess electron densities. A correlation of the identified Mm with derived environmental parameters provides information about their potential origin. A 1-D time-marching model of the Mars ionosphere with an included diurnal cycle is used to investigate the composition of the neutral atmosphere and ionosphere between 70 and 110 km altitude in dependence of the temporal variability of the short solar X-ray. In addition, the arrival of the MAVEN spacecraft at Mars in September 2014 provides new opportunities for further investigations of the origins of the identified excess electron densities.

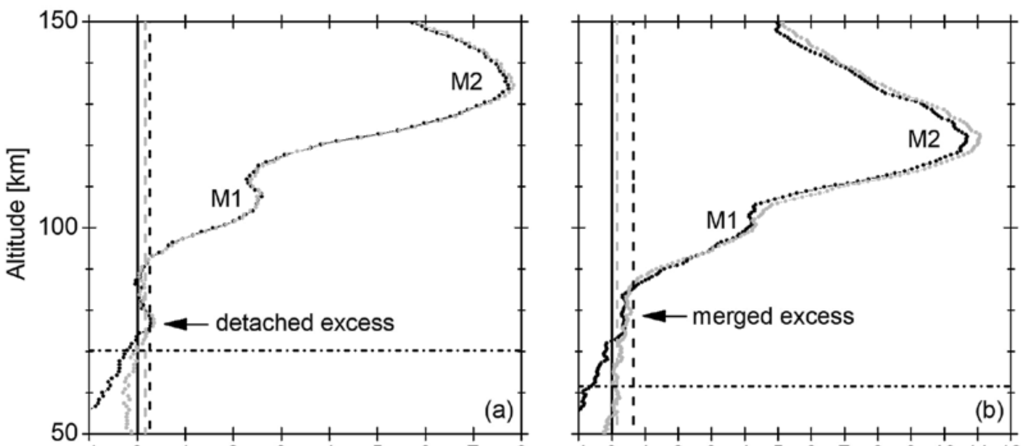

Figure 1: MaRS observation of (a) DoY 350 (2005) for a solar zenith angle □ of 74.1° and (b) DoY 111 (2006) for □ = 58.8°. The gray dots indicate the electron density derived from differential Doppler, while the black dots indicate the electron density derived from X-band. The straight black line is the zero line, while the dashed gray and black lines indicate three times the observational noise level for the respective observations.

2. Correlation between the derived Mm characteristics and environmental parameters

The characteristics of the MaRS merged excess electron densities from 2004 – 2014 are correlated with the SIP V2.38 [8] model solar flux and the Mars Global Surveyor Magnetometer crustal magnetic field magnitude in 400 km altitude [1]. The results indicate, that the ionization of the locally available neutral atmospheric components by short solar X-ray radiation seems to play a key role in the formation of the Mm excess densities:

- strong correlation of the Mm occurrence rate with the Sun's activity level
- high availability of the Mm excess densities for low underlying crustal magnetic fields
- Mm occurrences for all solar zenith angles in the investigated range from 50° - 90°
- slightly lower altitude of the ionospheric base for the MaRS observations containing Mm excess electron density profiles compared with the undisturbed observations.

3. The ionization of the local neutral atmosphere as potential source for merged excess electron densities

The 1-D time-marching photochemical and transport model IonA-2 simulates the ionization of the local neutral atmosphere by short solar X-ray as a potential origin for the merged excess electron densities. It is found, that the modelled Mm agree well with the characteristics of the MaRS observations in vertical total electron content (TEC), altitude range and peak electron density. The ionization of the local atmosphere by short solar X-ray provides satisfying agreement with the V-shaped merged excess electron densities (Figure 1b). Other potential sources might provide additional ion density and substructures, as there are meteoric Mg^+, solar energetic particles and internal gravity waves.

4. **Comparison of Mm characteristics with MAVEN observations**

The comparison of the Mm characteristics with the MAVEN IUVS Mg^+ observations ([5],[7],[2]), correlations of the Mm occurrences with the current X-ray measurements of the MAVEN Extreme Ultraviolet (EUV) monitor [3] at Mars and potential monitored solar energetic particle events during MaRS radio science observations by the MAVEN Solar Energetic Particle (SEP) instrument [4] will provide further insight into the formation processes of the merged excess electron densities.

4. References

[1] Connerney, J. E. P. et al.: The global magnetic field of Mars and implications for crustal evolution, *Geophysical Research Letters*, Vol. 28 (21), pp. 4015-4018, 2001.
[2] Crismani, M. M. J. et al.: Detection of a persistent meteoric metal layer in the Martian atmosphere, *Nature Geoscience,* Vol. 10, pp. 401–404, 2017.
[3] Eparvier, F. et al.: The Solar Extreme Ultraviolet Monitor for MAVEN, *Space Science Reviews,* Vol. 195 (1), pp. 293–301, 2015.
[4] Larson, D. E. et al.: The MAVEN Solar Energetic Particle Investigation, *Space Science Reviews, Vol.* 195 (1), pp. 153–172, 2015.
[5] McClintock, W. E. et al.: The Imaging Ultraviolet Spectrograph (IUVS) for the MAVEN Mission, *Space Science Reviews,* Vol. 195 (1), pp. 75–124, 2015.
[6] Pätzold, M. et al.: A Sporadic Third Layer in the Ionosphere of Mars, Science, Vol. 310, pp. 837-839, 2005.
[7] Schneider, N. M. et al.: MAVEN IUVS observations of the aftermath of the Comet Siding Spring meteor shower on Mars, *Geophysical Research Letters, Vol.* 42 (12), pp. 4755–4761, 2015.
[8] Tobiska, W. K. et al.: The Solar2000 empirical solar irradiance model and forecast tool, *Journal of Atmospheric and Solar-Terrestrial Physics*, Vol. 62 (14), pp. 1233-1250, 2000.

Are "Habitable" Exoplanets Really Habitable? -- A perspective from atmospheric loss

C. F. Dong[1*]
[1]*Department of Astrophysical Sciences, Princeton University, USA*

1. Introduction

In the last two decades, the field of exoplanets has witnessed a tremendous creative surge. Research in exoplanets now encompasses a wide range of fields ranging from astrophysics to heliophysics and atmospheric science. One of the primary objectives of studying exoplanets is to determine the criteria for habitability, and whether certain exoplanets meet these requirements. The classical definition of the Habitable Zone (HZ) is the region around a star where liquid water can exist on the planetary surface given sufficient atmospheric pressure, but this definition largely ignores the impact of the stellar wind and stellar magnetic activity on the erosion of an exoplanet's atmosphere. Amongst the many factors that determine habitability, understanding the atmospheric loss is of paramount importance [1-5]. Most of the recent attention has been centred around the study of exoplanets orbiting M-dwarfs since the latter are highly numerous in our Galaxy (and in the Universe). The study of these exoplanets has also received a major boost from the discovery of Proxima Centauri b (PCb) [6] and seven Earth-sized planets in the TRAPPIST-1 system [7].

2. Method

In our Solar system, the most sophisticated codes tend to use magnetohydrodynamic (MHD) models for modelling the interactions of the solar wind with magnetized (such as Earth) and unmagnetized (such as Mars and Venus) planets, and the interactions of planetary magnetospheric flow with its moons (such as Titan). We use the BATS-R-US MHD model [4,8,9] that has been well validated and applied to different solar system objects. For the stellar wind parameters (such as the stellar wind velocity, density and interplanetary magnetic field), we adopt the Alfvén Wave Solar Model (AWSoM) [10] to simulate those parameters based on the observed magnetograms of M-dwarf stars. The BATS-R-US MHD model is then adapted to exoplanet research by modifying the stellar wind inputs and exoplanetary atmospheric profiles, compositions, and photochemistry.

3. Results

Figure 1 presents the contour plots of the O^+ ion density, the magnetic field strength B and the magnetic field lines for unmagnetized and magnetized PCb [3]. The total ion escape rate varies from $\sim 10^{26}$ s^{-1} (magnetized) to $\sim 10^{27}$ s^{-1} (unmagnetized) over one PCb's orbital period, about 1-2 orders of magnitude higher than those of terrestrial planets in our Solar system. As the escape losses for PCb in the unmagnetized case are about two orders of magnitude higher than our Earth ($\sim 10^{25}$ s^{-1}), all of the atmosphere could be depleted much faster -- possibly in a span of $\square(10^8)$ years. In turn, this has very important ramifications for surface-based life as we know it, given the importance of elements like oxygen.

If gases such as oxygen are depleted on these short timescales, sufficient time may not exist for complex life to evolve. Our simulations indicate that the escape rates for PCb in the magnetized case are higher than that of the Earth, implying that some of the above conclusions for the unmagnetized case are also valid here. However, it is equally important to recognize that the magnetized case is quite sensitive to the values of the stellar wind parameters [3]. The atmosphere depletion could occur over $\square(10^8)$ and $\square(10^9)$ years for the magnetized case with minimum and maximum stellar wind dynamic pressure P_{dyn} over one PCb, respectively.

Figure 2 shows the total ion escape rate as a function of the semi-major axis for cases with both maximum (solid curve) and minimal (dashed curve) total pressure over each TRAPPIST-1 planet's orbit [5]. An inspection of Figure 2 reveals that the overall escape rate declines monotonically as one moves outwards, from TRAPPIST-1b to TRAPPIST-1h. Hence, taken collectively, this may suggest that TRAPPIST-1h ought to be most "habitable" planet amongst seven planets, when viewed purely from the perspective of atmospheric ion loss. However, it must be recalled that the presence of liquid water on the surface is a prerequisite for habitability, and TRAPPIST-1h is not expected to be conventionally habitable [7]. Hence, it seems likely that TRAPPIST-1g will, instead, represent the best chance for a habitable planet in this planetary system to support a stable atmosphere over long periods.

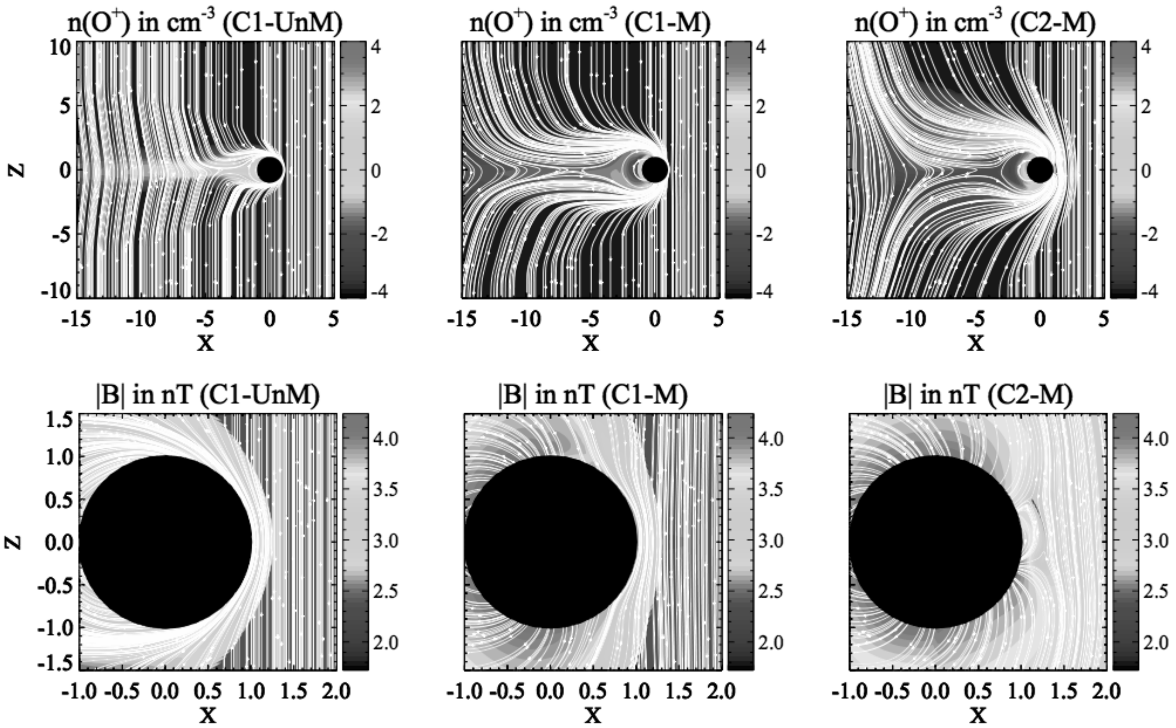

Figure 5: The logarithmic scale contour plots of the O^+ ion density (first row) and magnetic field strength (second row) with magnetic field lines (in white) in the meridional plane for the unmagnetized case 1 (C1-UnM), magnetized case 1 (C1-M) and magnetized case 2 (C2-M).

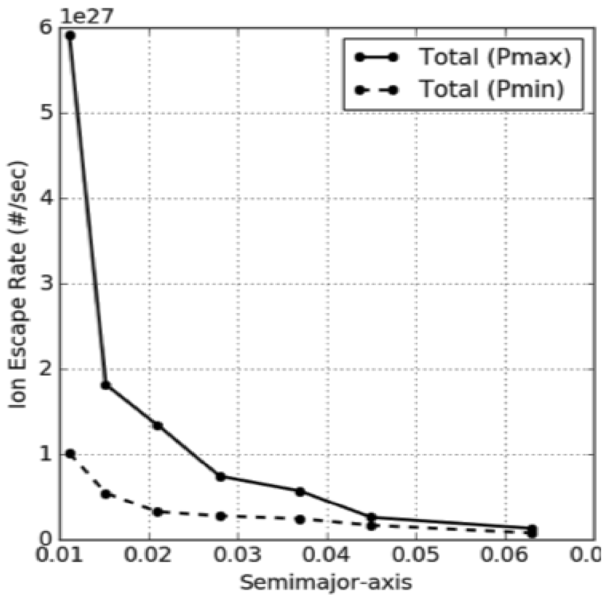

Figure 6: Total atmospheric ion escape rate as a function of the semi-major axis for cases with both maximum (solid curve) and minimal (dashed curve) total pressure over each planet's orbit. The seven distinct points on each curve represent the seven planets of the TRAPPIST-1 system.

4. References

[1] Lammer H. et al. (2009) Astron. Astrophys. Rev. **17**, 181.
[2] Ehlmann B. L. et al. (2016) JGR, **121**, 1927.
[3] Dong C et al. (2017a) ApJL **837**, L26.
[4] Dong C et al. (2017b) ApJL **847**, L4.
[5] Dong C et al. (2018) PNAS, **115**, 260.
[6] Anglada-Escude G., et al. (2016) Nature **536**, 437.
[7] Gillon M. et al. (2017) Nature **542**, 456.
[8] Tóth G. et al. (2012) JCP **231**, 870.
[9] Ma Y. et al. (2013) JGR **118** 321.
[10] van der Holst B. et al. (2014) ApJ **782**, 81.

Using Hybrid Simulations to Understand How Ion Loss Varies with Planetary Radius

H. Egan[1*]; D. Brain[1], R. Jarvinen[2]
[1]University of Colorado, USA,
[2]Finnish Meteorological Institute, Finland

1. Introduction

All planets undergo atmospheric evolution over the course of their lifetime; in particular non-thermal loss processes including those that act on ions are thought to be important to the evolution of secondary atmospheres. Observations show ion loss is currently taking place at Earth [11], Mars [8], Venus [10], and Titan [4]. Further understanding of ion loss in the terrestrial solar system planets has been developed using 3D global plasma models [eg. 9], but the results are rarely compared across planets, limiting the potential for better understanding the physics of ion escape.

Recent developments in exoplanet observation techniques have allowed the discovery of thousands of extrasolar planets, including dozens of small, rocky planets that are potentially habitable. Many current studies of exoplanet habitability use estimates of thermal loss [7] or turbulent entrained mass models [12] to estimate scaling of atmospheric evolution, although ion loss from terrestrial exoplanets has been studied for Proxima-b analogs [1,3] and the Trappist-1 planets [2]. In general ion loss models for exoplanets have taken the approach of starting with a planetary plasma model of a specific exoplanet and varying external drivers to match those of observed exoplanetary systems. While this is necessary work, with the abundance of planetary systems being discovered and the importance of characterizing planetary populations for follow-up observations, it is important to consider the diversity of planetary parameters and how ion escape processes work in general.

Here we present a systematic study of how ion loss processes vary with planetary properties, with a specific focus on planetary radius, under conditions appropriate for planets orbiting in the habitable zone of a typical M-dwarf or a young sun. By considering the solar system planets together with exoplanets, we build a generalized framework of understanding ion loss from terrestrial planets, that can be validated using current solar system observations.

2. Simulation Methods

For this project I will be using the hybrid plasma code RHybrid. Hybrid simulation codes treat ions as macroparticles representative of a population of ions that evolve kinetically according the Lorentz force, while electrons are treated as a charge-neutralizing fluid. This code has been adapted from the the HYB model [6], but is now fully parallelized. By using a hybrid model both Hall and finite larmor radius (FLR) effects are automatically included and the ion phase space distribution is fully three-dimensional. This makes it an ideal choice to use for global magnetospheric models where ion kinetic effects are likely to be important, ie., when ion gyroradii become comparable to the scale size of the planet, although it is also applicable for smaller gyroradius regimes.

3. Scaling

For rocky planets the overall density will be roughly constant and mass will scale as, and the corresponding escape energy energy scales as. However, the increase in escape velocity is not guaranteed to cause a proportional decrease in escape rate due to a variety of factors related to non-thermal escape mechanisms.

First, the additional energy sources available to ions will lead to non-thermal velocity distributions above the exobase, and bulk motion leading directly to escape. These additional sources may limit the effect of increasing escape energy as the ions may be accelerated to substantially above the escape energy. Second, an increase in mass causes a decrease in scale height (), which will in turn change how other processes, such as ion pickup, will interact with ions around the exobase. Finally, for small unmagnetized planets, ion gyroradii can be comparable to the size of the planet. This means that a given ion that appears to be escaping may instead gyrate back into the planet, leading to absorption or sputtering. These factors will all work together to complicate the picture of scaling with planetary mass/radius, necessitating global models.

4. Simulations

The simulations we have run vary the planetary radius from $R_P = R_M$ to $R_P = 5\ R_\oplus$ (where R_M is the radius of Mars, and $R_\oplus$ is the radius of the

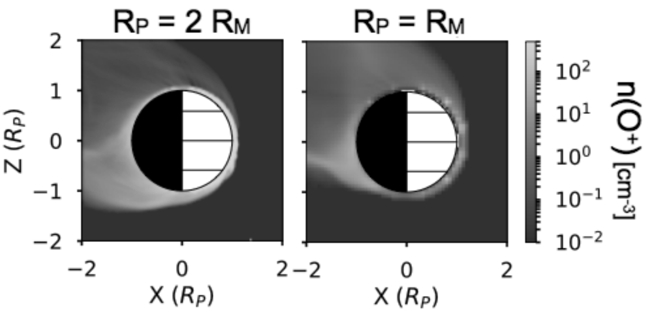

Earth). Fig. 1 shows slices of the O^+ number density for two models, with radii 1 R_M and 2 R_M. As evident in the shape of the escaping plume of ions in the +z hemisphere, the O^+ ion gyroradius changes relative to the size of the planet. **I**n this model set we have started by using an atmosphere that is Venus-like in composition with ion production rates scaled to values appropriate for the increased EUV emission from typical M-stars. This formulation places the planet in the energy-limited range of ion escape, as discussed in [5]; thus, slightly varying these rates is unlikely to have a substantial effect on the overall scaling we find for radius.

Figure 1: Slices of O^+ number density for a planet with R_P = $2R_M$ (*left*) and R_P = R_M (*right*).

5. Anticipated Analysis

I am currently in the preliminary stages of analyzing these simulations, but by May I will have taken two complementary approaches in understanding the outputs of the models:

1.) Deriving scaling laws for ion escape with radius and intrinsic magnetic field

2.) Using the model results to probe what dominates the change in ion escape rates as planetary parameters are varied.

As different escape processes and acceleration mechanisms scale differently with mass/radius, simply comparing global ion outflow rates across all models will not not lead to a deeper fundamental understanding of escape, nor to a well-constrained relationship. As such, I will systematically examine the spatial variation of ion energy distribution and corresponding energy inputs of a few representative models.

I will then compute scaling laws for ion escape rates over planetary radius (), fitting for the power law exponent *k*, for both overall escape rate and each escape channel. In addition to computing escape rates, I will examine total energy imparted by the variety of relevant electric fields, as well as the rate of ions reimpacting the planet through the lower boundary.

References

[1] C. Dong, et. al . The Dehydration of Water Worlds via Atmospheric Losses. ApJ, 847:L4, September 2017.

[2] C. Dong, M. Lingam, Y. Ma, and O. Cohen. Is Proxima Centauri b Habitable? ApJ, 837:L26, March 2017.

[3] K. Garcia-Sage, et. al On the Magnetic Protection of the Atmosphere of Proxima Centauri b. ApJ, 844:L13, 2017.

[4] D. A. Gurnett, F. L. Scarf, and W. S. Kurth. The structure of Titan's wake from plasma wave observations. J. Geophys. Res., 87:1395–1403, March 1982.

[5] R. Jarvinen, et. al Oxygen ion escape from Venus in a global hybrid simulation: role of the ionospheric O+ ions. Annales Geophysicae, 27:4333–4348, November 2009. doi: 10.5194/angeo-27-4333-2009.

[6] E. Kallio and P. Janhunen. Modelling the solar wind interaction with Mercury by a quasi-neutral hybrid model. Annales Geophysicae, 21:2133–2145, November 2003. doi: 10.5194/angeo-21-2133-2003.

[7] H. Lammer, et. al . Atmospheric Loss of Exoplanets Resulting from Stellar X-Ray and Extreme-Ultraviolet Heating. ApJ, 598:L121–L124, December 2003. doi: 10.1086/380815.

[8] R. Lundin, et. al. First measurements of the ionospheric plasma escape from Mars. Nature, 341:609–612, 1989.

[9] Y. Ma, A. et. al . Three-dimensional multispecies MHD studies of the solar wind interaction with Mars in the presence of crustal fields. Journal of Geophysical Research (Space Physics), 107: 1282, October 2002.

[10] T. Nordstrom, et. al, Venus ion outflow estimates at solar minimum: Influence of reference frames and disturbed solar wind conditions. Journal of Geophysical Research (Space Physics), 118:3592–3601, June 2013.

[11] R. J. Strangeway, R. E. Ergun, Y.-J. Su, C. W. Carlson, and R. C. Elphic. Factors con- trolling ionospheric outflows as observed at intermediate altitudes. Journal of Geophys- ical Research (Space Physics), 110:A03221, March 2005. doi: 10.1029/2004JA010829.

[12] J. Zendejas, A. Segura, and A. C. Raga. Atmospheric mass loss by stellar wind from planets around main sequence M stars. Icarus, 210:539–544, December 2010. doi: 10.1016/j.icarus.2010.07.013.

Comparison of induced magnetospheres

Y. J. Ma[1*]; C. T. Russel[1], A. F. Nagy[2], J. G. Luhmann[3], B. Jakosky[4].
[1] Earth, Planetary and Space Sciences, UCLA, USA
[2] Department of Climate and Space Sciences and Engineering, University of Michigan, USA
[3] Space Sciences Laboratory, UC Berkeley, USA
[4] Laboratory for Atmospheric and Space Physics, University of Colorado, USA

1. Introduction

Induced magnetospheres form around unmagnetized bodies that are electrically conducting. The characteristics of this region depend mainly on the conductivity of the obstacle and the pressure of the incoming solar wind (or corotating-magnetospheric) plasma flow. Similar to planetary magnetospheres, the induced magnetospheres become part of the obstacles to the incoming plasma flow, but the orientation of the field inside is largely controlled by the upstream magnetic field.

2. Comparison of Induced Magnetospheres

Venus, Mars and Titan are three well-known bodies in the solar system with substantial ionospheres. Despite the differences in their size, atmospheric thickness, existence of localized crustal field, EUV strength and upstream flow conditions, the induced magnetospheres show remarkable similarities due to the common physical processes that dominate. We will discuss the common features as well as major differences of the induced magnetospheres of the three bodies in line with recent observations and advances of numerical modelling.

2.1. Venus

Venus often serves as the prototype of the solar wind interaction with unmagnetized planets. Typical plasma interaction pattern at Venus is show in Figure 1a. Due to its closest distance to the Sun, solar wind dynamic pressure is the highest at Venus, and as a result, Venus has the strongest induced magnetosphere. It is also found that the induced magnetosphere is not a permanent structure and it could disappear on rare occasions when the IMF is nearly aligned with the solar wind flow [*1*].

2.2. Mars

Solar wind interaction with Mars is more complicated due to the non-uniformed distributed crustal magnetic field (Figure 1b). It is found that strong crustal fields near the subsolar point could raise the altitude of the MPB over the entire dayside [*2*]. As the crustal remnant field on Mars rotates with the planet, the magnetic field configuration interacting with the solar wind is constantly varying.

(a) (b)

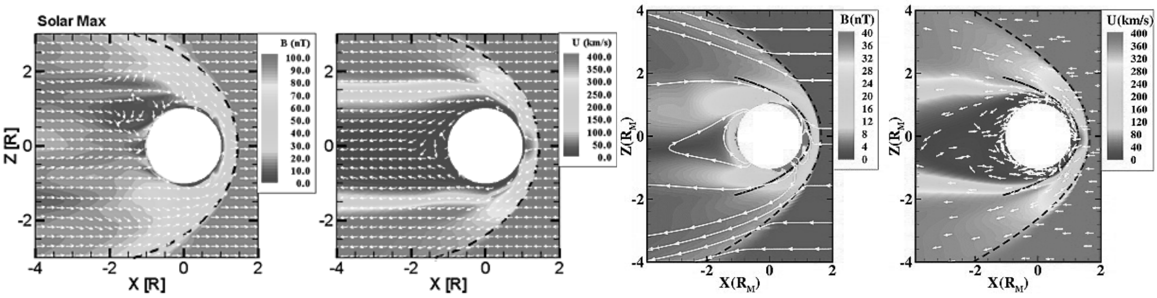

Figure 1: Solar wind interaction with Venus (a) and Mars (b), from *Ma et al.* [2013] and *Ma et al.* [2004].

2.3. Titan

Titan is located inside Saturn's magnetosphere for nominal solar wind conditions. As the plasma flow is sub-magnetosonic, there is no standing bow shock in front of Titan (see Figure 2 (a)). When the solar wind dynamic pressure is high, Titan could be in the sheath region [*3*] or directly exposed in the solar wind [*4*]. Under such circumstances, Titan's plasma interaction is similar to Venus and Mars, as shown in Figure 2(b).

(a) (b)

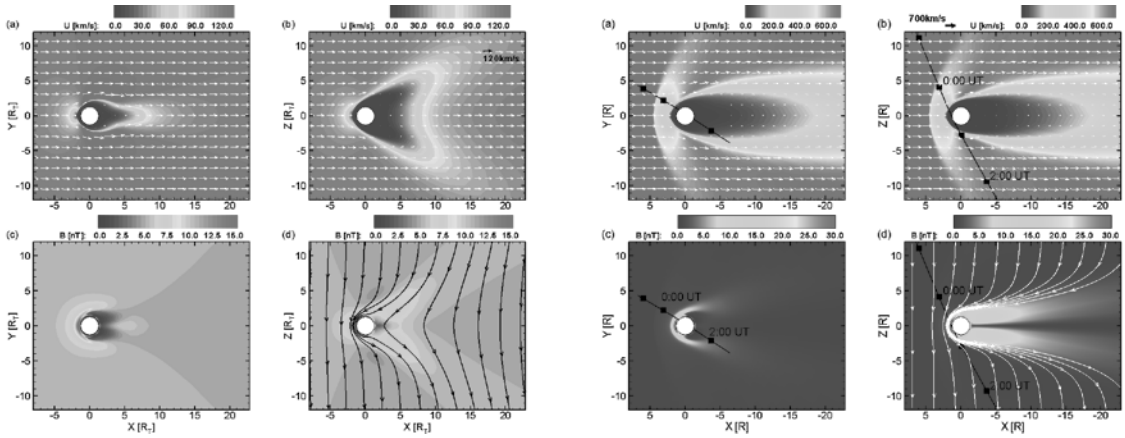

Figure 2: (a): Titan in the magnetosphere and (b): Titan in the solar wind.

3. Response time of the induced magnetospheres

We will also discuss the response time of the induced magnetospheres to typical variations in the upstream plasma flow, such as IMF direction change [*5*], Solar Wind dynamic pressure variations [*6*] and real ICME events [*7,8*], based on observations and numerical model results.

4. References

[1] Zhang, T. L., J. Du, Y. J. Ma, H. Lammer, W. Baumjohann, C. Wang, and C. T. Russel: Disappearing induced magnetosphere at Venus: Implications for close-in exoplanets, Geophys. Res. Lett., 36, L20203, 2009.

[2] Brain, D. A., J. S. Halekas, R. Lillis, D. L. Mitchell, R. P. Lin, and D. H. Crider: Variability of the altitude of the Martian sheath, *Geophys. Res. Lett.*, **32**, L18203, 2005.

[3] Bertucci, C., et al.: The magnetic memory of Titan's ionized atmosphere, Science, 321(5895), 1475-1478, 2008.

[4] Bertucci, C., D. C. Hamilton, W. S. Kurth, G. Hospodarsky, D. Mitchell, N. Sergis, N. J. T. Edberg, and M. K. Dougherty: Titan's interaction with the supersonic solar wind, Geophys. Res. Lett., 42, 193–200, 2015.

[5] Modolo, R., G. M. Chanteur, and E. Dubinin: Dynamic Martian magnetosphere: Transient twist induced by a rotation of the IMF, *Geophys. Res. Lett.*, **39**, L01106, 2012.

[6] Ma, Y. J., X. Fang, A. F. Nagy, C. T. Russell, and G. Toth: Martian ionospheric responses to dynamic pressure enhancements in the solar wind, *J. Geophys. Res. Space Physics*, **119**, 1272–1286, 2014.

[7] Jakosky, B. M., et al: MAVEN observations of the response of Mars to an interplanetary coronal mass ejection, *Science*, 350, aad0210-1-aad0210-7, 2015.

[8] Ma, Y. J., et al.: Variations of the Martian plasma environment during the ICME passage on 8 March 2015: A time-dependent MHD study, J. Geophys. Res. Space Physics, 122, 1714–1730, 2017.

Earth's magnetosphere and its interaction with the solar wind

S. E. Milan[1*]
[1]University of Leicester, UK

Abstract

In this talk I will outline our current understanding of the interaction of the solar wind with the terrestrial magnetosphere through magnetic reconnection, the excitation of magnetospheric convection and its link to ionospheric motions, the formation of electrical current systems and their relationship to auroral morphology, and the magnetotail response to dayside driving. The theoretical framework which underpins this understanding is the expanding/contracting polar cap (ECPC) model, a time-dependent version of the Dungey cycle. The ECPC will be used to explore the modes of behaviour of the system to solar wind driving, including substorms, steady magnetospheric convection (SMC) events, sawtooth events, and geomagnetic storms. Areas for future study will be identified.

The Complex Martian Magnetosphere: Recent Insights Based on MAVEN Magnetometer Observations

J. Espley[1*], G. DiBraccio[1], J. Gruesbeck[1, 3], Y. Soobiah[1, 3], A. Shane[4], G. Collinson[1], C. Fowler[5], J. Connerney[1,2]
[1]NASA Goddard Space Flight Center, USA,
[2]Space Research Inc., USA
[3] Department of Astronomy, University of Maryland, USA
[4] University of Michigan, USA
[5] Laboratory for Atmospheric and Space Physics, University of Colorado, USA

1. Introduction

The near-Mars space environment has been studied for decades with a variety on instruments on a variety of spacecraft. Recent observations from MAVEN have revealed that the induced martian magnetosphere has complexity beyond even what was previously known. This highly dynamic plasma laboratory offers us great opportunities to explore magnetospheres in general and to understand how escape to space shaped the martian climate over the aeons. We present highlights from several recent studies of this environment and discuss areas for future research.

2. The twisted martian magnetotail: a hybrid magnetosphere?

Recent work [1] has shown observationally that the martian magnetotail lobes exhibit a ~45° twist, either clockwise or counterclockwise from the ecliptic plane which is different than what would be expected for a purely draped (i.e. Venus-like) field configuration. Model field line tracings indicate that a majority of the twisted tail lobes are composed of open field lines, surrounded by draped IMF. We infer that dayside magnetic reconnection between the crustal fields and draped IMF creates these open fields and may be responsible for the twisted tail configuration. Figure 1 shows a schematic of this idea.

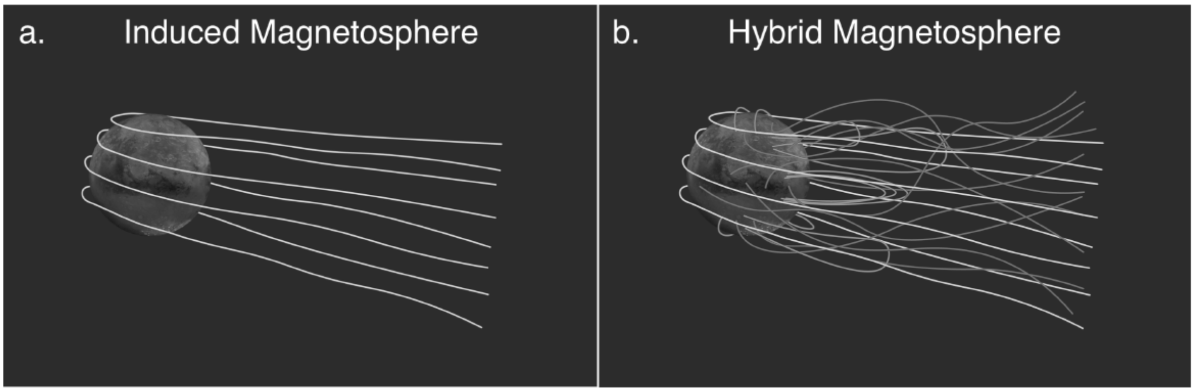

Figure 7 Schematics of a) an induced Martian magnetosphere similar to a Venus- or comet-like interaction with draped IMF magnetic fields (yellow) and b) a hybrid Martian magnetosphere including open (magenta), closed (cyan), and draped (yellow) field topologies.

3. Quantifying the Impact of Space Weather on the Martian Magnetosphere

For over a century, quantitative disturbance metrics have been employed at Earth, primarily relying on magnetometer observations. These metrics allow statistical studies of the effects of solar transient events such as stream interaction regions (SIRs) and interplanetary coronal mass ejections (ICMEs). Recent work [2] has used over 60 transient events observed by MAVEN at Mars to create a magnetospheric disturbance index. We discuss how this index can be used to explore the impacts of such events at Mars and at other bodies in the Solar System.

4. The Role of Solar Wind Waves in Heating the Ionosphere

Several recent studies [3, 4, 5] highlight the importance of waves originating in the solar wind in the heating of the ionosphere. These waves propagate downward and are absorbed by the ions. As the waves heat the ions, these ions are likely to be better able to escape permanently from the planet. Initial quantification of the impact of this heating on the escape rates has begun. We will discuss how further detailed analysis of the waves is necessary and also how we will require a better understanding of the frequency of occurrence (i.e. how often are IMF conditions such that such wave ionospheric heating occurs) in order to fully quantify the impact on atmospheric escape.

5. Plasma dynamics in the low altitude crustal regions

Recent work [6] reports on unusual ion flux intensifications in the Martian ionosphere in regions where magnetic cusps are likely formed by crustal magnetic fields. The energy dispersions of the plasma (ions and electrons) indicate that physical processes are occurring that take populations that were originally non-magnetized and, as they move into regions of stronger magnetic fields, entrap them and cause them to precipitate downward. The charge separation between the opposite tone electrons and ions indicate that field aligned current and electric fields are being produced in the process. The downward precipitating ions will have implications for sputtering and localized atmospheric heating.

6. References

[1] Dibraccio, G., et al., The Twisted Configuration of the Martian Magnetotail: MAVEN Observations, submitted to *Geophys. Res. Letters,* 2018.
[2] Gruesbeck, J. and J. Espley, A Magnetospheric Disturbance Index for Mars, in prep for submission to *J. Geophys. Res.*, 2018.
[3] Collinson, G. et al., Shaking the Martian sky: Ionospheric compression, energization, and escape resulting from the impact of ultra-low frequency magnetosonic waves generated upstream of Mars, submitted to *J. Geophys. Res.,* 2018.
[4] Fowler, C. et al., MAVEN observations of solar wind driven magnetosonic waves heating the Martian dayside ionosphere, submitted to *J. Geophys. Res.*, 2018.
[5] Shane, A. et al., A statistical analysis of magnetic waves in the Martian dayside magnetosphere and ionosphere as observed by MAVEN, submitted to *J. Geophys. Res.,* 2018.
[6] Soobiah, Y. et al., MAVEN case studies of plasma dynamics in low altitude crustal magnetic field at Mars: Dayside ion intensifications associated with radial crustal magnetic fields, in prep for submission to *J. Geophys. Res.*, 2018.

Momentum Transfer and Boundary Layer Structure at Mars

J.S. Halekas[1*]; D.A. Brain[2], Y. Ma[3], J.G. Luhmann[4], G.A. DiBraccio[5], S. Ruhunusiri[1], J.P. McFadden[4], D.L. Mitchell[4]
[1]Department of Physics and Astronomy, University of Iowa, USA,
[2]Laboratory for Atmospheric and Space Physics, University of Colorado, USA
[3]University of California, USA
[4]Space Sciences Laboratory, University of California, USA
[5]NASA Goddard Space Flight Center, USA

1. Introduction

The upper atmosphere and ionosphere of Mars interact directly with the solar wind. As a result, momentum transfer between the solar wind and planetary ions can occur, leading to acceleration and escape of planetary material. A variety of plasma processes mediate this momentum transfer, including motional electric field forces, magnetic pressure and tension forces, and particle pressure gradients, each of which plays an important role in individual regions of the Martian magnetosphere. In addition, fluid instabilities at the boundary between solar wind and planetary plasma can result in momentum transfer to coherent plasma parcels and thereby to so-called bulk escape. In order to determine the relative importance of these processes, we investigate the average structure of the fields, flows, and forces in the magnetosphere and characterize the variability and dynamics of this structure, with a particular focus on the boundary layer.

2. Flows, fields, forces, and momentum transfer

We utilize charged particle and magnetic field data from the Mars Atmosphere and Volatile EvolutioN (MAVEN) mission, organized by the upstream magnetic field, to investigate the morphology and variability of flows, fields, and forces in the Mars-solar wind interaction [1]. We find that the observed fields and flows in the magnetosheath, bow shock, and upstream regions have observable asymmetries controlled by the interplanetary magnetic field, with particularly large asymmetries found in the ion parallel temperature and anisotropy. The magnetosheath ion distribution is anisotropic, with the greatest ion temperature anisotropies occurring in quasi-perpendicular regions of the magnetosheath and under low Mach number conditions. These results have implications for the growth and evolution of wave-particle instabilities and their role in energy transport and dissipation. We utilize the measured parameters to estimate the average ion pressure gradient, $J \times B$, and $-v \times B$ macroscopic force terms. The pressure gradient force maintains nearly cylindrical symmetry, while the $J \times B$ force has larger asymmetries and varies in magnitude in comparison to the pressure gradient force. The $-v \times B$ force felt by newly produced planetary ions exceeds the other forces in magnitude in the magnetosheath and upstream regions for all solar wind conditions.

3. Boundary layer structure and dynamics

We utilize MAVEN observations to investigate the structure and variability of the boundary layer between magnetosheath plasma of solar wind origin and planetary plasma. While at some times this transition layer from solar wind to planetary plasma appears narrow and smooth, at other times it appears broader and displays considerable sub-structure, likely representing boundary layer irregularities and/or boundary motion. It remains unclear whether these different morphologies represent primarily spatial differences (i.e. different structure for different portions of the boundary layer) or whether they are influenced by external factors (solar wind Mach number, interplanetary magnetic field orientation, etc.) or the lower boundary conditions (e.g. the magnetization state of the ionosphere and the orientation of the crustal magnetic field – which may control magnetic reconnection that drives changes in magnetic topology). We analyse MAVEN observations throughout the mission to investigate which internal and/or external factors control the structure of this unique compositional boundary.

4. References

[1] Halekas, J.S., et al., Flows, fields, and forces in the Mars-solar wind interaction, J. Geophys. Res., 122. https://doi. org/10.1002/2017JA024772, 2017.

Magnetic topology during quiet and extreme conditions at Mars

S. M. Curry[1*]; S. Xu[1], J. G. Luhmann[1], C.F. Dong[2], D. M. Mitchell[1], G. DiBraccio[3], M. Elrod[3], J. Espley[3], J. McFadden[1]
[1]Space Sciences Laboratory, Univ. of California at Berkeley
[2]Department of Astrophysical Sciences, Princeton University, USA
[3]NASA Goddard Space Flight Center

1. Introduction

In the absence of a dipole magnetic field, terrestrial atmospheres are especially susceptible to scavenging, such as those of Mars and Venus. At both planets, the solar wind directly interacts with the upper atmosphere, creating a scenario where planetary ions are either picked up and swept away to space or precipitate back into the atmosphere causing neutral constituents to splash, or sputter, out [Luhmann et al. 1991, Leblanc et al. 2001]. At Mars, the trajectories of heavy planetary ions are influenced by the existence of remanent crustal magnetic fields, which are thought to create a shielding effect for escaping planetary ions. Mars' crustal magnetic fields also change the magnetic topology in its plasma environment because magnetic reconnection occurs between draped IMF and closed crustal magnetic fields, resulting in open field lines wind with one footprint attached to the planet [Brain et al. 2006]. Our results relating the magnetic field topology at Mars and planetary ion escape are an important aspect of magnetospheric physics and planetary evolution, as heavy ion loss and sputtering are thought to have been major drivers of atmospheric escape during earlier chapters of the Sun's history when it was thought to be more active.

2. Results

How the Martian magnetic topology responds to interplanetary coronal mass ejections (ICMEs) is a particularly important focus of understanding how the plasma environment responds to extreme conditions [Curry et al. 2018]. In particular, we focus on how the magnetic topology changes due to ICMEs. Two particular events are investigated: 2017 September ICME with Mars Atmosphere Volatile EvolutioN (MAVEN) data and the 2003 Halloween event with Mars Global Surveyor (MGS) data. We will compare the open, closed, and draped field patterns before/during/after ICME and correlate topology changes with upstream drivers.

With the use of magnetohydrodynamic (MHD) and test particle simulations, we will also explore the global topology and ion escape maps during both of these events. We will compare the MHD results with the ion and topology data from MAVEN and MGS, respectively. We will also compare escape rates for planetary ions and with open / closed magnetic field line maps.

3. Figures

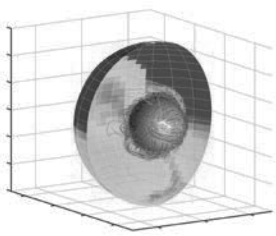

Figure 1: An example of open (green), closed (red) and draped (blue) field lines at Mars and a shell at 4 R_M depicting the heavy ion escape

4. References

[1] Luhmann et al., Evolutionary impact of sputtering of the Martian atmosphere by O(+) pickup ions, Geophysical Research Letters, Vol. 11, issue 21, 1992.
[2] Leblanc et al.: Sputtering of the Martian atmosphere by solar wind pick-up ions, Planetary Space Science, Volume 49, 2001.
[3] Brain et al.: The magnetic field draping direction at Mars from April 1999 through August 2004, Icarus, Volume 182, 2006
[4] Curry et al: MAVEN Observations of Atmospheric Escape During Space Weather Events in Solar Cycle 24, Journal of Geophysical Research, (under review), 2018

Impact ionization of neutrals by foreshock electrons at Mars

Mazelle C[1], Meziane K[2], Mitchell D[3], Espley J[4], Halekas J[5], Jakosky B[6]
[1]*IRAP / CNRS - University of Toulouse - UPS - CNES, France,*
[2]*Physics department, University of New Brunswick, Canada,*
[3]*Space Sciences Laboratory, University of California, , U.S.A.,*
[4]*NASA Goddard Space Flight Center, U.S.A.,*
[5]*Department of Physics and Astronomy, University of Iowa, U.S.A.,*
[6]*Laboratory for Atmospheric and Space Physics, University of Colorado Boulder, U.S.A.*

1. Observations

Foreshock backstreaming electrons emanating from the bow shock of Mars reported from the MAVEN / SWEA [1] observations show a flux fall off with the distance from the shock [2]. This feature is not observed at the terrestrial foreshock. The flux decay is observed only for electron energy E >~29 eV. A recent study indicates that Mars foreshock electrons are produced at the shock in a mirror reflection of a portion of the solar wind electrons [3]. In this context and given that the electrons are sufficiently energetic to not be affected by the IMF fluctuations, the observed flux decrease appears problematic.

2. Model

We have investigated the possibility that the flux fall off with distance results from the impact of backstreaming electrons with Mars exospheric neutral hydrogen. We have demonstrated that the flux attenuation is consistent with the electron-atomic hydrogen impact cross-section for a large range of energy [3]. A better agreement is obtained for energy where the impact cross section is the highest. One important consequence is that foreshock electrons can play an important role in the production of pickup ions at Mars far exosphere.

3. References

[1] Mitchell, D. L., C. Mazelle, J-A. Sauvaud, J-J. Thocaven, J. Rouzaud, A. Fedorov, P. Rouger et al. "The MAVEN solar wind electron analyzer." Space Science Reviews 200, no. 1-4 (2016): 495-528.
[2] Meziane, K., C. X. Mazelle, N. Romanelli, D. L. Mitchell, J. R. Espley, J. E. P. Connerney, A. M. Hamza, J. Halekas, J. P. McFadden, and B. M. Jakosky (2017), Martian electron foreshock from MAVEN observations, J. Geophys. Res. Space Physics, 122, doi:10.1002/2016JA023282.
[3] Meziane, K., Mazelle, C.X., Mitchell, D.L., Espley, J.R., Hamza, A., Halekas, J.S., and Jakosky, B.M., A Fast-Fermi Acceleration at the Mars Bow Shock, SM33B-2648, AGU Fall Meeting, 10-15 December 2017, New Orleans, U.S.A., 2017.
[4] Mazelle, C.X., Meziane, K., Mitchell, D.L., Garnier, P., Espley, J.R., Hamza, A., Halekas, J.S., and Jakosky, B.M., Evidence for Neutrals - Foreshock Electrons Impact Ionization at Mars, SM43E / SM33B-2647, AGU Fall Meeting, 10-15 December 2017, New Orleans, U.S.A., 2017.

The Structure and Properties of Martian Magnetosphere at ~ 70° Solar-Zenith Angle in MSE Coordinates as Observed on MAVEN Spacecraft

O. L. Vaisberg[1], V. N. Ermakov[1], S. D. Shuvalov[1], L. M. Zelenyi[1], J. Halekas[2], G. A. DiBraccio[3], J. McFadden[4], and E. M. Dubinin[5]

[1] Space Research Institute of the Russian Academy of Sciences, Russia

[2] Department of Physics and Astronomy, University of Iowa, USA.

[3] NASA Goddard Space Flight Center, USA.

[4] Space Sciences Laboratory, U.C., Berkeley, USA.

[5] Max-Planck-Institute for Solar System Research, Germany

1. Introduction

The obstacle to the solar wind flow at Mars has been observed for more than 45 years by several spacecraft. First crossings of the dayside magnetosphere with observations of increasing magnetic field up to ~30 nT [1] and ions of lower energy than magnetosheath ions were made by Mars-2 and Mars-3 [2]. The ion and magnetic tail at ~7 R_M with planetary ions outflow was found on Mars-5 [3, 4]. The magnetic field increase, solar wind proton depression and the presence of planetary ions measurements on Phobos-2 were interpreted in terms of the boundary layer existence on the dayside [5].

The ion composition within the magnetic barrier at dayside of Mars was measured on Mars-Express [6,7]. The cases of strong mass loading and the magnetic field pileup with discontinuity (the magnetic pileup boundary) were found as well as the crossings of the Martian magnetosphere on the dayside without a signature of a magnetic field pileup. The altitude of the magnetic barrier near subsolar point was 450-550 km independent on strong solar wind ram pressure variations. Rather sharp ionospheric boundary (PEB) with abruptly increasing photoelectron number density on this boundary up to ~10^3 cm^{-3} was found.

Halekas et al. [8] stated that "the magnetosphere of Mars forms as a result of the direct and indirect interaction of the solar wind with the Martian ionosphere, through a combination of induction effects and mass loading". The Martian magnetosphere is dominated by plasma of atmospheric origin, which forms the primary global obstacle to the solar wind through induction and mass loading, with additional contributions from localized crustal magnetic fields [9].

Matsunaga et al. [10] analyzed 10 months of MAVEN observations to determine the average locations of Ion Composition Boundary (ICB), Induced Magnetosphere Boundary (IMB) and Pressure Balance Boundary (PBB), They found that IMB almost coincide with ICB on the dayside.

The structure and properties of the dayside Martian magnetosphere is much less studied than the night side of it due to its small scale and insufficient temporal resolution of previous Martian satellites. Mars Atmosphere and Volatile EvolutioN mission (MAVEN) with comprehensive high-time resolution instruments suite provided an excellent possibility to study Martian environment. We analyze the structure and the properties of the dayside Martian magnetosphere near terminator in MSE coordinate system that shows the role of IMF direction in plasma and the magnetic properties of the dayside Martian magnetosphere.

2. Structure of magnetosphere at SZA~ 70^0 in MSE coordinates

In order to study influence of the solar wind electric field and pick-up on the structure of the magnetosphere we selected 44 inbound crossings of the solar wind-Mars interaction region and arranged them by the angle between electric field vector and the projection of spacecraft position radius vector in the YZ plane (Θ_E). All passes were divided into 3 angular sectors near 0°, 90° and 180° Θ_E angles in order to estimate the role of IMF direction in plasma and magnetic properties of dayside Martian magnetosheath and magnetosphere. The observations were performed from January 17 through February 4, 2016 when MAVEN was crossing the dayside magnetosphere at SZA ~ 70°. Magnetosphere as the region with prevailing accelerated planetary ions was always found between the magnetosheath and the ionosphere. Magnetic barrier forms in magnetosheath in front of the magnetosphere with strong magnetic field and extends within magnetosphere. Magnetopause was defined by the steep increase of $(n(O^+) + n(O_2^+))/n(p)$ ratio from 0.1 to 1. The number densities of O^+ and O_2^+ ions increase from magnetopause to the interface with ionosphere by the factor of 10^2 -10^3.

Within each angular sector of magnetic coordinates there are typical profiles of the magnetosheath, the magnetic barrier and the magnetosphere, and relative magnetic field magnitudes in these two domains vary. Plume ions frequently dominate the ion flow in magnetosheath and magnetosphere in the northern MSE sector (Θ_E ~ 0°-30°) where motion electric field is directed from the planet. The high flux of plume protons disturbs the structure of magnetosphere and magnetic barrier. In the equatorial sector (Θ_E ~ 60°-120°) magnetic barrier, magnetopause and magnetosphere are very irregular, triple crossings of magnetopause are observed, and magnetic barrier has small thickness. Velocity-dispersed ion beams are observed in the magnetosphere. The southern sector (Θ_E ~ 160°-180°)

is characterized by small scale and small magnitude magnetic barrier. Magnetosheath proton flux weakens but usually keeps the same energy distribution at the magnetopause. Magnetic field magnitude has a minimum at magnetopause. The gradient of planetary ions is steeper at magnetopause than in other sectors. The average height of the boundary with ionosphere is ~ 530 km and the average height of the magnetopause is ~ 730 km. The heights of magnetopause and the interface of magnetosphere with ionosphere in the southern sector are about by 150 km higher than ones in other sectors. Solar wind electric field direction controls magnetospheric parameters.

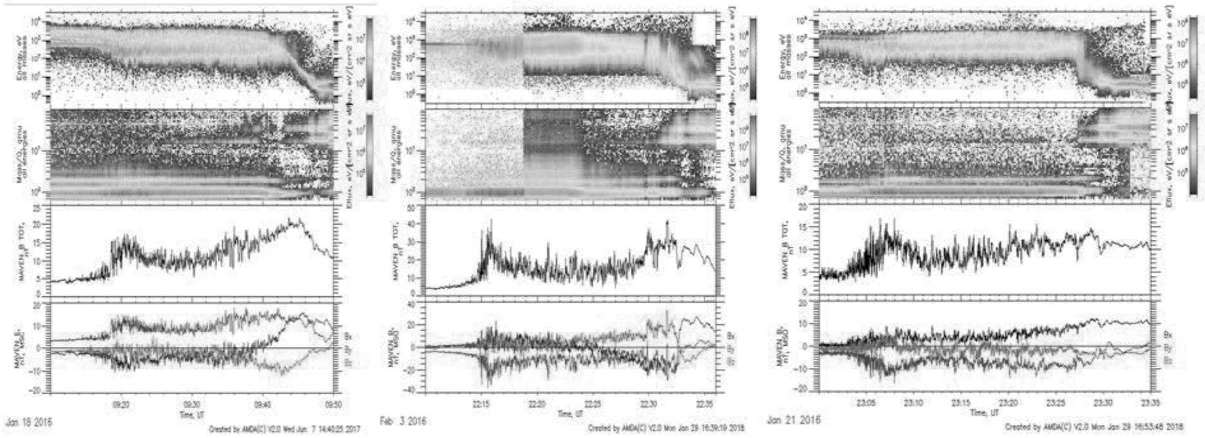

Figure 1. Examples of solar wind-Mars interaction regions for three sectors in MSE coordinates: left: Θ_E ~ 0°-30°, middle: Θ_E ~ 60°-120°, and right: Θ_E ~ 160°-180°.

3. References

1. Dolginov, Sh. Sh., et al., Magnetic field in the very close neighborhood of Mars according to data from the Mars-2 and Mars-3 spacecraft , Dokl. Akad. Nauk SSSR, 207(6), 1296, 1972.
2. Bogdanov, A. V. and Vaisberg, 0.L., Structure and variations of solar wind-Mars interaction region, J. Geophys. Res., 80, 487- 494,1975.
3. Vaisberg, O.L.et al., Mars-plasma environment. In:Williams,D.J.(Ed.), Physics of Solar Planetary Environment .AGU, Boulder ,pp. 854–871,1976.
4. Dolginov, Sh.Sh., On the magnetic field of Mars: Mars 2 and Mars 3 evidence, Geophys. Res. Lett, 5, 89-92, 1978.
5. Szego, et al., On the dayside region between the shocked solar wind and the ionosphere of Mars, J. Geophys. Res. 103 (A5), 9101–9111, 1998.
6. Dubinin, E., et al., Structure and dynamics of the solar wind/ionosphere interface on Mars: MEX-ASPERA-3 and MEX-MARSIS observations, Geophys. Res. Lett. 35, L11103, 2008.
7. Dubinin, et al., Plasma environment of Mars as observed by simultaneous MEX-ASPERA-3 and MEX-MARSIS observations (b), J. Geophys. Res., VOL. 113, A10217, 2008.
8. Halekas, J. S., et al. (2017a), Structure, dynamics, and seasonal variability of the Mars-solar wind interaction: MAVEN Solar Wind Ion Analyzer in-flight performance and science results, J. Geophys. Res. Space Physics, 122, 547–578,
9. Halekas, J. S., et al., Flows, fields, and forces in the Mars-solar wind interaction. Journal of Geophysical Research: Space Physics, 122, 2017.
10. Matsunaga, K., et al., Statistical study of relations between the induced magnetosphere, ion composition, and pressure balance boundaries around Mars based on MAVEN observations. J. Geophys. Res., 122, 9723–9737, 2017.

4. Acknowledgement

O.V., L.Z., V.E. and S.S. acknowledge support by Russian Science Foundation by grant 16-42-01103.

Study of ICME effects at Mars: energy deposition and feedback from enhanced thermosphere

L. H. Regoli[1*], X. Fang[2], Y. Lee[3], C. Dong[4], V. Tenishev[1], S. W. Bougher[1] and W. B. Manchester[1]
[1]Department of Climate and Space Sciences and Engineering, University of Michigan, USA,
[2]Laboratory for Atmospheric and Space Physics, University of Colorado Boulder, USA,
[3]NASA Goddard Space Flight Center, USA,
[4]Department of Astrophysical Sciences and Princeton Plasma Physics Laboratory, Princeton University, USA

1. Introduction

Due to the relatively small size of the induced magnetosphere of Mars, the upstream solar wind conditions have an important effect on the dynamics of the system as a whole. In March 2015, a series of interplanetary coronal mass ejections (ICMEs) impacted Mars, while the MAVEN spacecraft was gathering data both inside and outside the induced magnetosphere. This provided a rich dataset including measurements of the changing solar wind conditions and interplanetary magnetic field (IMF) as well as ion, electron and magnetic field data in the vicinity of the planet.

While the March 2015 event has drawn particular attention of researchers [3,6], the extent to which the heated thermosphere due to enhanced pickup ion precipitation in turn affects total ion escape rates has yet not been assessed. As demonstrated by [5], during extreme solar wind conditions, the precipitation of hot oxygen ions into the atmosphere can provide an extra heating term that can increase the thermospheric temperatures by up to a factor of 2.

In this study we focus on the feedback that the extra heating has on the total ion escape from Mars. We analyse the results from a number of iterations of four one-way coupled models in order to estimate how the total ion escape flow changes during the passage of the ICME and compare this to previously published results that studied the same event without taking into account the effects of the enhanced thermosphere.

2. The models

In order to provide a self-consistent picture of the Mars' system, we used four different numerical models, each of them focusing on a separate component and all of them coupled through flat files according to the schematic presented in .

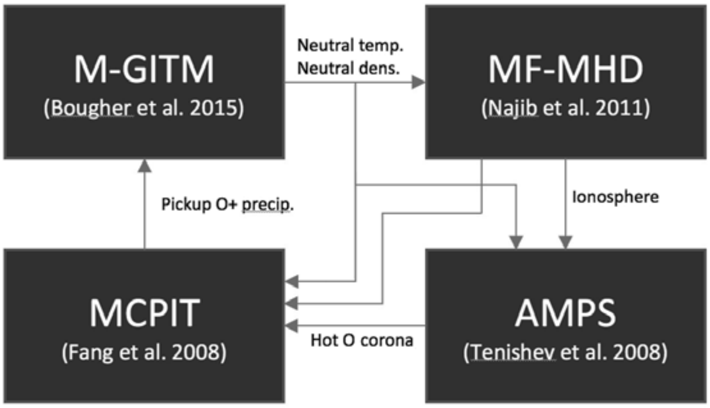

Figure 8. Block diagram of models used in this study.

2.1. Mars Global Ionosphere-Thermosphere Model (M-GITM)

M-GITM was originally developed as a thermosphere-ionosphere code for Earth and further adapted for the specific atmospheric conditions present at Mars [1]. It is a 3D ground-to-exosphere, solar-driven model that uses the monthly-averaged F10.7 proxy to calculate the atmospheric heating and dynamics. A $1/R^2$ scaling of the corresponding solar EUV-UV fluxes is applied for the seasonal/heliocentric distance variations of Mars. The code calculates the neutral and ion densities, as well as neutral temperatures and winds. It currently incorporates the main atmospheric constituents, namely CO2, CO, O, N2, O2, Ar, He and N(4S), and the main ionospheric species, namely O+, O2+, CO2+, N2+ and NO+.

2.2. Multi-fluid MHD (MF-MHD)

BATS-R-US is an MHD code originally developed at the University of Michigan [9]. The version of the code that will be used for this study is a multi-fluid code [8,2] that solves for separate continuity, momentum and energy equations for four ion species, namely O2+, O+, CO2+ and H+.

2.3. Adaptive Mesh Particle Simulator (AMPS)

AMPS is a Monte Carlo kinetic particle code that solves the Boltzmann equation for multi-species and multiphase environments with or without accounting for the collision integral [10]. The code has been already successfully applied for modeling of the exospheres of the Moon, Mars, Enceladus, Europa, simulating transport of the SEP and GCRs in Earth' magnetosphere, and for modeling of cometary comae. AMPS has been extensively used as a modeling support of the MAVEN mission by providing a model of Mars' extended hot oxygen and carbon coronas [7].

2.4. Monte Carlo Pickup Ion Transport (MCPIT)

MCPIT is a test-particle code specifically developed to study the interaction of Mars with the solar wind [4]. The code is used to generate and trace pickup O^+ ions in the induced magnetosphere. The ions are created by photoionization, charge exchange and electron impact ionization. Once the ions are generated, they are propagated upon the background electromagnetic fields generated by the MHD code, solving the Lorentz force equation using a staggered leapfrog numerical scheme.

3. References

[1] Bougher, S. W., Pawlowski, D., Bell, J. M., Nelli, S., McDunn, T., Murphy, J. R., Chizek, M. and Ridley, A.: Mars Global Ionosphere-Thermosphere Model: Solar cycle, seasonal, and diurnal variations of the Mars upper, Journal of Geophys. Res., Vol. 120(2), pp. 311-342, 2015.

[2] Dong, C., Bougher, S. W., Ma, Y., Toth, G., Nagy, A. F. and Najib, D.: Solar wind interaction with Mars upper atmosphere: Results from the one-way coupling between the multifluid MHD model and the MTGCM model, Geophys. Res. Letters, Vol. 41(8), pp. 2708-2715, 2014.

[3] Dong, C. et al.: Multifluid MHD study of the solar wind interaction with Mars' upper atmosphere during the 2015 March 8th ICME event, Geophys. Res. Letters, Vol. 42(21), pp. 9103-9112.

[4] Fang, X., Liemohn, M. W., Nagy, A. F., Ma, Y., De Zeeuw, D. L., Kozyra, J. U. and Zurbuchen, T. H.: Pickup oxygen ion velocity space and spatial distribution around Mars, Vol. 113(A2), 2008.

[5] Fang, X., Bougher, S. W., Johnson, R. E., Luhmann, J. G., Ma, Y., Wang, Y.-C. and Liemohn, M. W.: The importance of pickup oxygen ion precipitation to the Mars upper atmosphere under extreme solar wind conditions, Geophys. Res. Letters, Vol. 40(10), pp. 1922-1927.

[6] Jakosky, B. M. et al.: MAVEN observations of the response of Mars to an interplanetary coronal mass ejection, Science, Vol. 350(6261), 2015.

[7] Lee, Y., Combi, M. R., Tenishev, V. and Bougher, S. W.: Hot carbon corona in Mars' upper thermosphere and exosphere: 1. Mechanisms and structure of the hot corona for low solar activity at equinox, Journal of Geophys. Res., Vol. 119(5), pp. 905-924, 2014.

[8] Najib, D., Nagy, A. F., Tóth, G, and Ma, Y.: Three-dimensional, multifluid, high spatial resolution MHD model studies of the solar wind interaction with Mars, Journal of Geophys. Res., Vol. 116(A5), 2011.

[9] Powell, K. G., Roe, P. L., Linde, T. J., Gombosi, T. I. and De Zeeuw, D. L.: A solution-adaptive upwind scheme for ideal magnetohydrodynamics, Journal of Comp. Phys., Vol. 154(2), pp. 284-309, 1999.

[10] Tenishev, V., Combi, M. and Davidsson, B..: A Global Kinetic Model for Cometary Comae: The Evolution of the Coma of the Rosetta Target Comet Churyumov-Gerasimenko throughout the Mission, The Astrophys. Journal, Vol. 685(1), pp. 659-677, 2008.

Magnetospheres of the Giant Planets

M. K. Dougherty; *A. Masters.*
Imperial College London, United Kingdom

All of the giant planets have appreciable intrinsic magnetic fields, generated by interior dynamos, and the interaction with the solar wind confines each field to a giant planetary magnetosphere. However, there are differences between both the properties of the planetary fields and our understanding of how each giant planet magnetosphere works. Many of the characteristics of these systems are unexplained, representing major unsolved problems in planetary science. Here we review what we currently know about each giant planet magnetosphere and highlight key open questions. We discuss how past and present space missions have revolutionised our understanding of the giant planets (e.g., Juno, Cassini-Huygens), as well as the critical importance of future missions (e.g., the Jupiter Icy Moons Explorer).

The Strange Menagerie at the Magnetopause: High-Resolution Magnetospheric Multiscale Data Reveals Diverse Phenomena near the Boundary with the Magnetosheath

C.T. Russell[1*]; *C. Zhao[1], U. Schneck[1], Y. Qi[1], H.R. Lai[1], W. Paterson[2], B.L. Giles[2], J.L. Burch[3].*
[1]Earth Planetary and Space Sciences, University of California, USA
[2]National Aeronautics and Space Administration, USA.
[3]Southwest Research Institute, USA.

The magnetopause marks the boundary between the shocked solar wind plasma and the Earth's magnetic obstacle rooted in the planet. In situations when the magnetosphere is "closed," terrestrial magnetic lines have two lines rooted in the Earth, and solar wind plasma has magnetic fields lines that do not intersect the Earth's magnetosphere or zero magnetic connection with the Earth. The process of reconnection allows the solar wind plasma to be connected to the magnetosphere producing phenomena such as steady convection of the magnetospheric plasma, and time-varying magnetospheric substorms. The Magnetospheric Multiscale mission has high cadence measurements with fine-scale gradient measurements and can accurately measure pressure, forces and currents never before possible. These capabilities enable us to distinguish phenomena not recognizable previously. The magnetopause can be recognized as a region in pressure balance between the terrestrial plasma and magnetic field with the magnetosheath plasma and magnetic field. Since the magnetopause is flat, the total pressure (magnetic plus plasma) is constant during a magnetopause crossing. This is true for both northward and southward IMF conditions and for parallel and antiparallel magnetic fields on either side of the magnetopause. Magnetic flux transfer events are magnetic ropes of twisted magnetic field that are self-balanced structures in which the magnetic pressure in the center is confined by the twist of the outer field lines. The magnetic gradient force is in balance with the magnetic curvature force and no plasma need be involved in the force balance, quite unlike the magnetopause. During an FTE, the total pressure increases and decreases, and the field direction smoothly rotates. A feature that at first glance looks like a FTE having a central magnetic pressure enhancement has been termed a MFE or magnetosheath field enhancement. Quite as extraordinarily, the magnetic field rises in the enter without twisting or self-balancing. Instead of a rope configuration, the MFE has a thin current sheet near the field maximum. The plasma conditions change abruptly across the interface. The structure is not one of pressure balanced equilibrium. This suggests that there is material in the MFE that is not detected by the MMS instruments. It appears with a range of sizes.

In this presentation, we discuss the difference between the magnetopause, FTE flux ropes, and the new MFE events, as well as their similarities.

Comparative planetary foreshocks: Results from recent studies

Meziane K[1,2], *Mazelle C[2], Mitchell D[3], Romanelli N[4], Hamza A[1], Espley J[5], Halekas J[6], Jakosky B[7]*
[1]University of New Brunswick, Canada,
[2]IRAP-UPS-CNRS-CNES, France,
[3]Space Sciences Laboratory, University of California, USA,
[4]LATMOS-IPSL-CNRS, France,
[5]NASA Goddard Space Center, USA,
[6]University of Iowa, USA,
[7]University of Colorado, USA

The conventional approach to the study of the interaction of the solar wind with various planetary magnetospheres has always considered the terrestrial foreshock an archetype to be reproduced. More recently, however, satellite missions to a number of solar system planets have enabled the collection of in situ data from the planetary environments visited.

We propose to present an instructive comparison between the foreshocks of Earth, Venus, Mars, and to a lesser extent Saturn. We will primarily focus on the results of analysis of data collected by Cluster, Cassini, Venus Express and MAVEN, respectively.
Given the difference in nature of the various planetary obstacles to the flow of the solar wind, one would expect the observations to confirm the differences. However, some similar observational signatures have been revealed, and will be presented.

The comparative study will highlight some essential aspects of solar wind-planetary interactions.

Mass loading influence on the structure of Martian bow shock

S. Shuvalov [1*]; *O. Vaisberg[1],V. Ermakov[1], L. Zelenyi[1]*
[1]Space Research Institute of Russian Academy of Sciences, Russia,

1. Abstract

The structure of Martian bow shock is largely affected by mass loading processes which consist both of pickup occurring upstream of the shock, and plume which originates in magnetosphere. The first one is dependent on the intensity of extreme ultraviolet radiation from the Sun and on the density of oxygen corona which varies with season ([2], [3]). The latter is driven by the direction of motion electric field [1].

Depending on the conditions above, the bow shock can show different properties. Thus, the crossing presented in Fig.1 shows features common for a cometary-like shock with the width of the front approximately equal to the proton gyro radius.

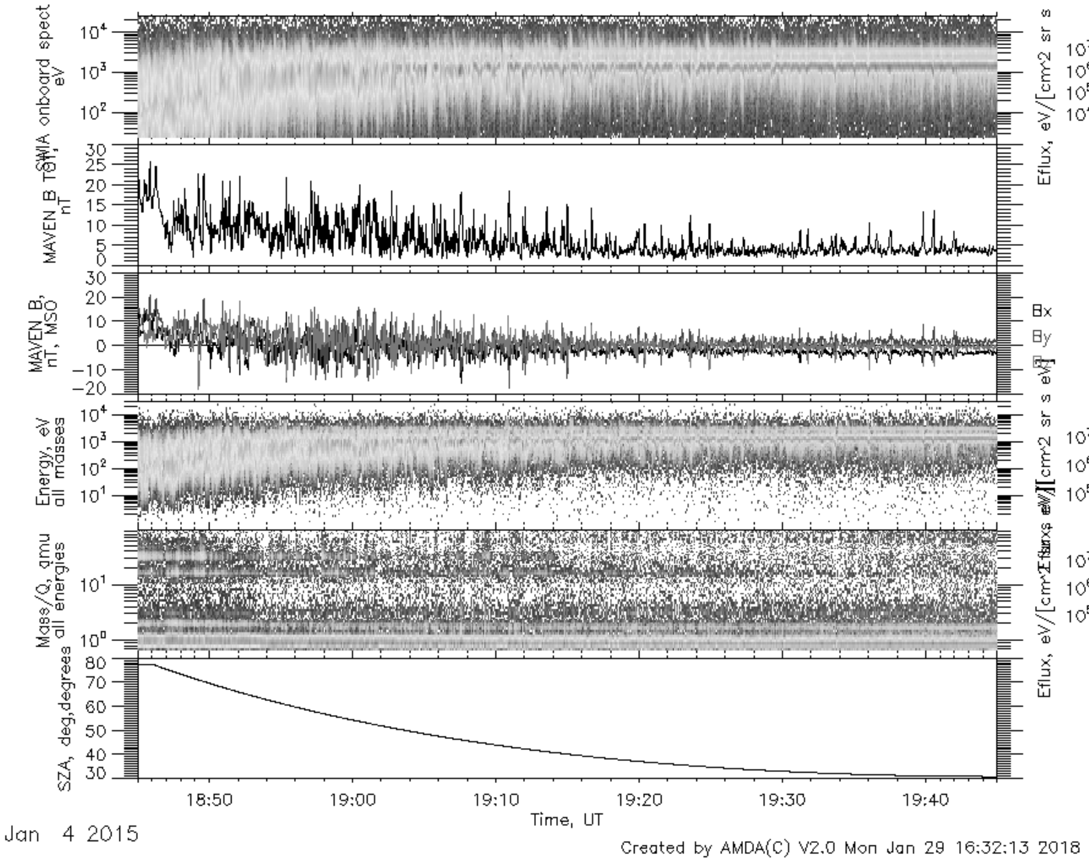

Figure 1: An example of cometary-like shock at Mars. From up to bottom: SWIA ion energy spectra, magnetic field magnitude, magnetic field components, STATIC ion energy spectra, STATIC ion mass spectra, solar-zenith angle.

Unlike the crossing presented in Fig. 1, the crossing in Fig. 2 is characterized by small mass loading with a well identified shock front.

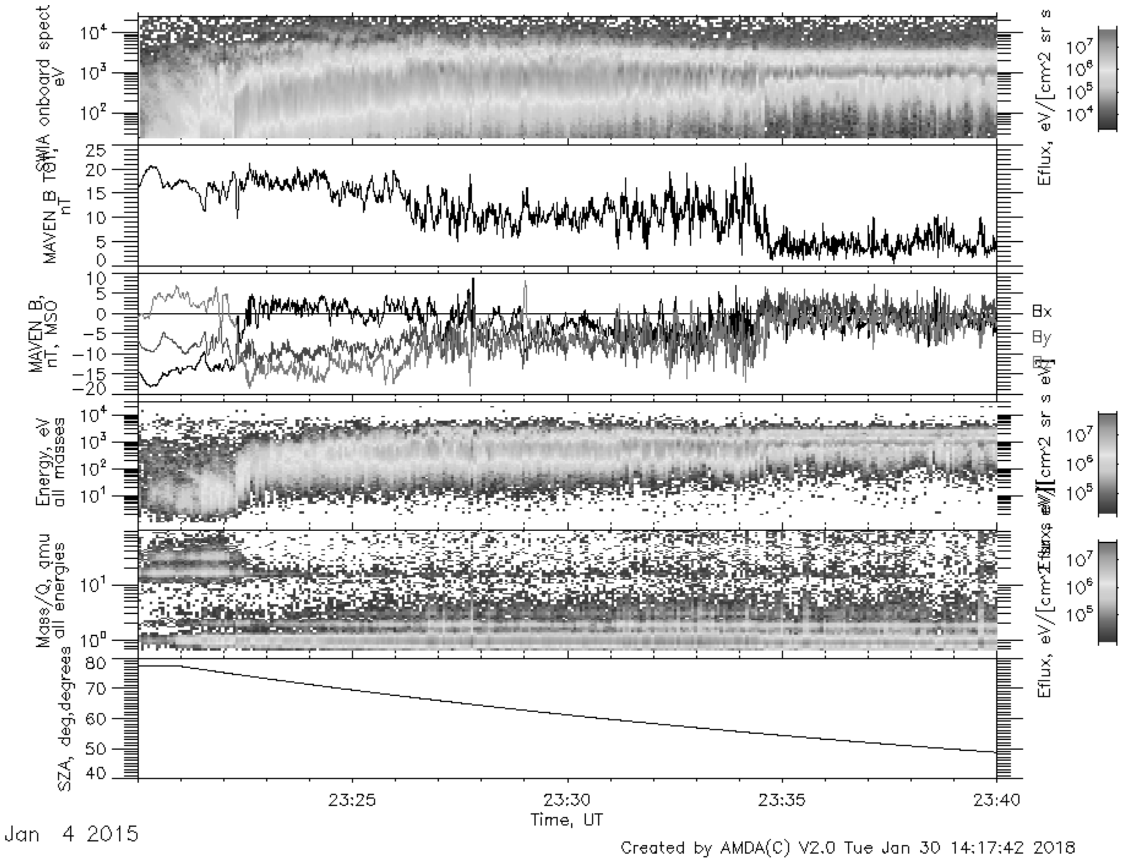

Figure 2: An example of Earth-like shock at Mars. From up to bottom: SWIA ion energy spectra, magnetic field magnitude, magnetic field components, STATIC ion energy spectra, STATIC ion mass spectra, solar-zenith angle.

In this work we study a number of Martian bow shock crossings by the MAVEN spacecraft within solar-zenith angle of ±30°, analyzing properties of the shock with respect to the degree of mass loading processes. We study the structure of the shocks depending on magnetic and sound Mach numbers, magnetic and plasma pressure balances.

2. References

[1] Dong, Y., X. Fang, D. A. Brain, J. P. McFadden, J. S. Halekas, J. E. Connerney, S. M. Curry, Y. Harada, J. G. Luhmann, and B. M. Jakosky (2015), Strong plume fluxes at Mars observed by MAVEN: An important planetary ion escape channel, Geophys. Res. Lett., 42, doi:10.1002/2015GL065346.
[2] Halekas, J. S. (2017), Seasonal variability of the hydrogen exosphere of Mars, J. Geophys. Res. Planets, 122, doi:10.1002/2017JE005306.
[3] Ramstad, R., S. Barabash, Y. Futaana, H. Nilsson, X.-D. Wang, and M. Holmstrцm (2015), The Martian atmospheric ion escape rate dependence on solar wind and solar EUV conditions: 1. Seven years of Mars Express observations, J. Geophys. Res. Planets, 120, doi:10.1002/2015JE004816.

A Generalized Magnetospheric Disturbance Index: Initial Application at Unmagnetized Bodies

J.R. Gruesbeck[1,2*]; J.R. Espley[1]
[1]Solar System Exploration Division, NASA Goddard Space Flight Center, USA
[2]Department of Astronomy, University of Maryland,

Introduction

Since MAVEN's arrival at Mars in 2014, in situ observations of the magnetic field have been made continually. During this time, the Martian magnetosphere has been disturbed by various solar transient events such as stream interaction regions (SIRs) and interplanetary coronal mass ejections (ICMEs). To understand the efficacy of solar transient events' abilities to disturb the Martian magnetosphere, statistical studies of large sets of events can be informative. Lacking an intrinsic global magnetic field, Mars' magnetosphere is a product of piled-up interplanetary magnetic field making the pre-disturbed background state of the system different event-to-event. For over a century, quantitative disturbance metrics have been employed at Earth, primarily relying on magnetometer observations [1, and references therein], which enable statistical studies of solar transient events on the various physical processes driven by solar wind-planetary interactions, such as aurorae and atmospheric loss. However, many of these indices require assumptions about the magnetic field background, which can be highly variable at bodies with an induced magnetosphere. We present early results on a generalized Magnetospheric Disturbance Index (MDI), which will be applicable to unmagnetized bodies. The MDI has been developed using MAVEN observations of over 60 solar transient events. Additionally, we demonstrate the MDI's use on Venus with Venus Express data.

A General Magnetospheric Disturbance Index

Over MAVEN's first few years in orbit about Mars, we have observed the transit of a number of moderate ICMEs and SIRs. While the exact nature of the disturbance of the system is different for every case, we do observe a few notable similarities for every event. The magnitude of the magnetic field inside the induced magnetosphere increases along with the variability of the magnetic field. Finally, we sometimes observe a changing of direction of the draped magnetic field. The left column of figure 1 illustrates these signatures in the magnetometer observations of the March 8, 2015 ICME event observed by MAVEN [3]. From top to bottom, we show the component magnetic field, the magnitude of the magnetic field, and the root mean square variability of the magnitude of the magnetic field.

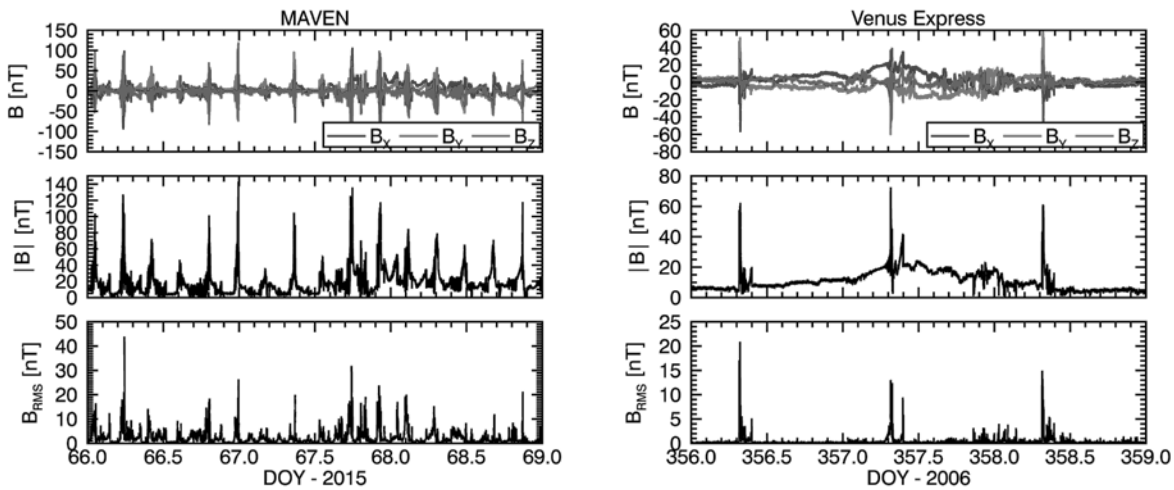

The right column of figure 1 shows magnetometer results obtained by the Venus Express mission from an ICME observed on December 23, 2006 [2] presented in the same order as the MAVEN observations. At Venus, we observe similar signatures, increasing magnitude and variability and a change in the orientation of the magnetic field direction. We use these common magnestospheric responses to create a generalized magnetospheric disturbance index. This index is the arithmetic combination of the normalized magnetic field magnitude deviation and the variability of the field. The mean of the induced magnetic field environment is used to normalize the deviation factors, accounting for the changing background in every event.

Comparison of MDI over MAVEN events

We have determined the MDI for the set of MAVEN events we have. Similar to the magnitude of the magnetic field, the MDI has a similar shape for all of the ICME and SIR events. We fit a simple Gaussian function to the MDI and superposed them, shown in figure 2, in order to directly compare the events. Figure 2 has both the March 8, 2015 ICME and the more recent September 12, 2017 ICME highlighted in blue and red respectively. Direct comparison of all events show that, at Mars the disturbance of ICMEs as well SIRs follow a similar profile lasting from 30 to 40 hours. The recent September ICME has the largest MDI to date, while the March 8 event has one of the smallest. The SIRs and ICMEs that MAVEN has been able to observe have all had similar values of MDI, however it should be noted that MAVEN has been in orbit at Mars during a particularly quiet solar cycle. We will present further results from the comparison of the MDI of the events at Mars, as well as comparison between Venus and Mars.

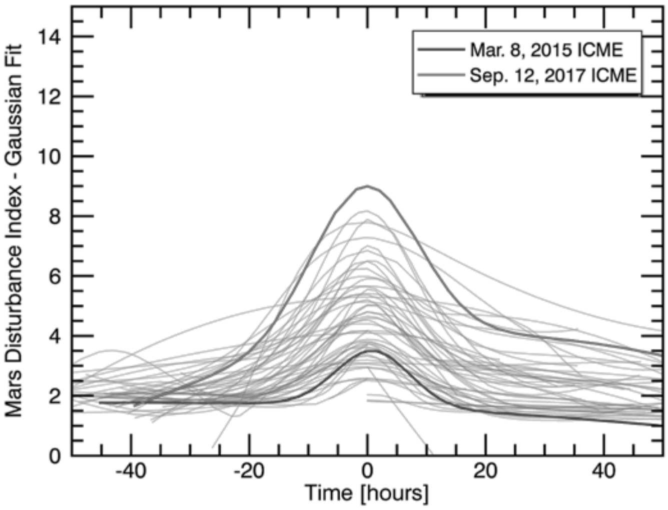

Figure 10. Gaussian fits of the Magnetospheric Disturbance Index for over 50 events superposed. The March 8, 2015 and September 12, 2017 ICME are highlighted in blue and red respectively.

References

[1] Borovsky, J. E. and Shrprits, Y. Y., Is the Dst index sufficient to define all geospace storms? Journal of Geophysical Research: Space Physics, Vol. 122, pp. 11543-11547, 2017.
[2] Collinson, G. A., et al., The impact of a slow interplanetary coronal mass ejection on Venus. Journal of Geophysical Research: Space Physics, Vol. 120, pp. 3489–3502, 2015.
[3] Jakosky, B. M., et al., MAVEN observations of the response of Mars to an interplanetary coronal mass ejection, Science, Vol. 350, pp. 1-7, 2015.

The solar wind interaction with the Moon

S. Fatemi[1*]; M. Holmström[1], A. R. Poppe[2], G. T. Delory[2], J. S. Halekas[3], S. Barabash[1]
[1]Swedish Institute of Space Physics, Sweden,
[2]Space Science Laboratory, Univ. of California, USA
[3]University of Iowa, USA

1. Introduction

A renewed interest in lunar exploration in the last two decades and an increasing probability of returning to the Moon with manned missions demand deep understanding on the plasma environment around this object. Despite previous thoughts, the physics of the solar wind interaction with the Moon is very dynamic and complex [1]. The interaction is not only about the plasma, but also provides detailed understanding about several processes occurring in the surrounding lunar environment, lunar surface, and even deep in the lunar interior.

2. Lunar plasma wake

Due to the lack of a global intrinsic magnetic field and dense atmosphere most of the solar wind ions impacting the lunar surface are absorbed by the Moon. This forms a wake structure downstream and leaves a plasma cavity behind the Moon. Observations and simulations have shown that the structure of the wake is very dynamic and controlled by the direction and intensity of the interplanetary magnetic field (IMF), plasma thermal pressure, and solar wind plasma beta [1, 2, 3, 4, 5]. Comparative data-model studies can reveal a wealth of new information about fundamental plasma interactions with a solid body.

3. Interaction with magnetic anomalies

Although the Moon does not have a global magnetic field, it does host small-scale incoherent magnetic anomalies with surface field strengths ranging from a few nano-Tesla to perhaps a few thousand nano-Tesla. The solar wind plasma interacts with these fields, gets deflected and/or reflected, and generates a broad range of plasma waves and instabilities upstream [6, 7]. Although no global bow shock forms upstream of the Moon, the reflected particles and their associated upstream waves share similarities with the terrestrial foreshock [8]. In addition, the interaction may also form small-scale localized bow shocks upstream of the magnetic anomalies, potentially the smallest collision-less shocks ever observed in planetary science [9].

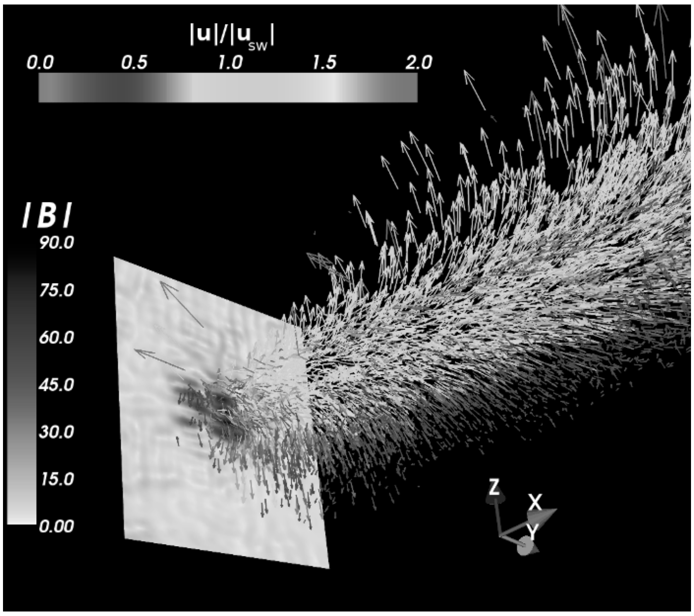

Fig 1. A snapshot of the solar wind plasma reflected from the Gerasimovich magnetic anomaly, taken from [7].

4. Lunar swirls

One of the seemingly unique aspects of the lunar surface in the solar system is the surface albedo anomalies, known as “swirls” [10]. The correlation between the spatial location and albedo markings of the swirls and crustal magnetic anomalies has suggested that the swirls are a manifestation of charged-particle space weathering effects. Recently, simulations have suggested that this correlation, together with understanding the solar wind plasma interaction with magnetic anomalies, provides key information about lunar surface weathering as well as the structure of the magnetic anomalies on the lunar surface [11, 12]. By using magnetic anomalies as “natural laboratories”, we can potentially distinguish the differing roles of charged particle irradiation and micrometeoroid bombardment in weathering planetary surfaces.

5. Plasma interaction with the surface

More than 80% of the incident solar wind plasma into the unmagnetized surface of the Moon is absorbed by the surface. However, nearly 1% reflect as charged particles and ~10-20% may reflect as energetic neutral atoms (ENAs) [13, 14, 15]. Intriguingly, observations have shown that the ENA reflection from areas surrounding lunar magnetic anomalies can increase considerably, leaving a “void” region of ENA reflection from the surface underneath the anomalies. Thus, ENA imaging is a powerful remote sensing tool to observe crustal fields and the rate at which solar wind ions are able to access the lunar surface underneath these crustal fields [16, 17].

6. Lunar interior structure

One of the most fundamental yet unanswered questions in lunar science is the structure and conductivity of the lunar interior. One method to determine the interior structure is to investigate the electromagnetic interior response to incident electromagnetic fluctuations, known as natural source electromagnetic sounding. The solar wind and its interaction with the Moon is the main source of incident electromagnetic fluctuations. The induced fields within the lunar interior couple with the Moon's ambient plasma environment, changing their final structure and topology and forming a non-linear complex system. Separating the inducing from induced magnetic fields is a critical obstacle towards understanding the interior; however, we have recently developed a self-consistent model that couples the electromagnetic interior response of the Moon to its ambient plasma environment. Using this model, we show that the induced fields are confined on the day side, but in contrast to previous work, they are not confined within the lunar wake, and may penetrate outside the wake. We have also shown the possibility that in certain locations on the lunar nightside the induced magnetic fields of the Moon have minimum perturbations from the surrounding plasma environment [18].

7. References

[1] Halekas J. et al. (2015), *Moon's plasma wake, 149-167.*
[2] Holmström M. et al. (2012) *EPS, 64(2)*.
[3] Fatemi S. et al. (2012) *JGR, 117(A10)*.
[4] Zhang H. et al. (2014) *JGR*, 119(7).
[5] Poppe A. et al. (2014) *GRL*, 41(11).
[6] Fatemi S. et al. (2014) *JGR, 119(8)*.
[7] Fatemi S. et al (2015a) *JGR, 120(6)*.
[8] Harada Y. and Halekas J., (2016) Upstream waves and particles at the Moon 216(307).
[9] Halekas J. et al., (2014) *GRL*, 41(21).
[10] Blewett D. et al., (2011) *JGR*, 116(E2).
[11] Poppe A. et al. (2016) *Icarus, 266*.
[12] Deca J. and A. Divin. (2016) *Astrophys. J.*, 829(2).
[13] Saito Y. et al., (2008) GRL, 35(L24205).
[14] Lue C. et al., (2014) *JGR*, 119(5).
[15] Vorburger A. et al., (2013) *JGR*, 118(7).
[16] Wieser M. et al., (2010) GRL, 37(5).
[17] Futaana Y. et al., (2013) GRL, 40(2).
[18] Fatemi S. et al. (2015b) *GRL, 42(17)*.

The Solar Wind Interaction with Ceres

M. N. Villarreal[1*], C. T. Russell[1], Y. D. Jia[1], T. H. Prettyman[2], N. Yamashita[2], C. A. Raymond[3], J. C. Castillo-Rogez[3], J. G. Luhmann[4], M. L. Mays[5], and C. O. Lee[4].
[1]Earth, Planetary, and Space Sciences, UCLA, United States,
[2]Planetary Science Institute, United States.
[3]Jet Propulsion Laboratory, United States.
[4]Space Sciences Lab, United States.
[5]Goddard Space Flight Center, United States.

1. Introduction

Ceres is an ice-rich dwarf planet located in the asteroid belt. The body does not possess a magnetosphere to shield itself from the incoming solar wind and thus its surface is directly exposed to incoming solar wind particles. However, Ceres has been observed to have a transient exosphere [1,2,3]. This intermittent exosphere is capable of mass-loading the solar wind and give rise to a temporary bow shock. Dawn's Gamma Ray and Neutron Detector (GRaND) has seen evidence for such a shock.

2. Energetic Electron Bursts and Evidence for a Bow Shock

In June 2015, Dawn's Gamma Ray and Neutron Detector [4] experienced short-lived enhancements in its exterior scintillators over the period of a week (Figure 1). These bursts were determined to be the result of bremsstrahlung created by energetic electrons impacting the spacecraft with energies greater than 20 keV [5]. The energetic electrons were detected on three consecutive orbits and were consistently located in the same locations in Ceres-Solar Orbital coordinates. Given the geometry and energy of these electron bursts, Russell et al. (2016) interpreted these bursts to be the result of the spacecraft passing through an electron foreshock created by a temporary bow shock. Jia et al. (2017) conducted single-fluid MHD simulations for a cerean bow shock and estimates this event was produced by a global water exosphere of ~9 kg/s, similar to telescopic measurements.

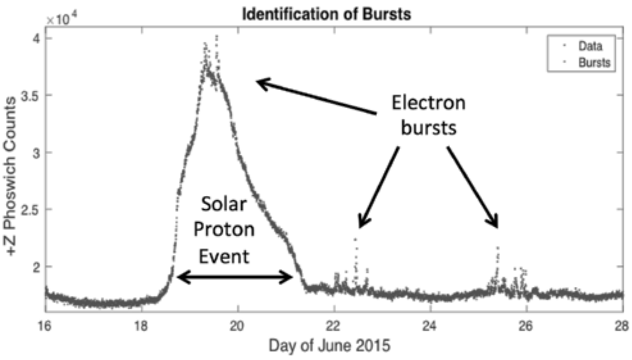

Figure 1: Energetic electron bursts (red) were observed to occur after the passage of a solar energetic particle event and repeat on three consecutive orbits before disappearing.

3. Production of a Cerean Exosphere by Solar Energetic Particle Events

The June 2015 event appeared to be triggered by a solar energetic particle (SEP) event. This is significant because exospheres on icy moons are known to be created via a sputtering process from the bombardment of energetic particles on their surfaces. The bow shock observation raised the question as to whether the solar energetic protons could explain the appearance of a transient cerean atmosphere on this, as well as other occasions. Villarreal et al. (2017) found a correlation between the water vapor production rates reported by telescopic campaigns and the energetic proton flux observed at 1 AU. They proposed a transient exosphere is created when the dwarf planet experiences a SEP event.

In order to test this hypothesis, how SEP events arrive at Ceres and their impact on the surface need to be better understood. Interplanetary shocks associated with solar coronal mass ejections are the sources of strong SEP events in interplanetary space. Solar energetic particles stream away from the shock surface along the Sun's interplanetary magnetic field (IMF) lines, allowing them to reach a wide range of heliolongitudes. A planet will experience a SEP event if the IMF lines at its location are connected to the shock surface. We analyzed the magnitude of SEP events at the Ceres' distance as observed by Dawn and compare with 1 AU measurements (Figure 2) and potential real-time SEP prediction models. This work will lay the foundation for a reactive telescopic campaign to observe the cerean exosphere with earth based telescopes immediately following a large SEP event.

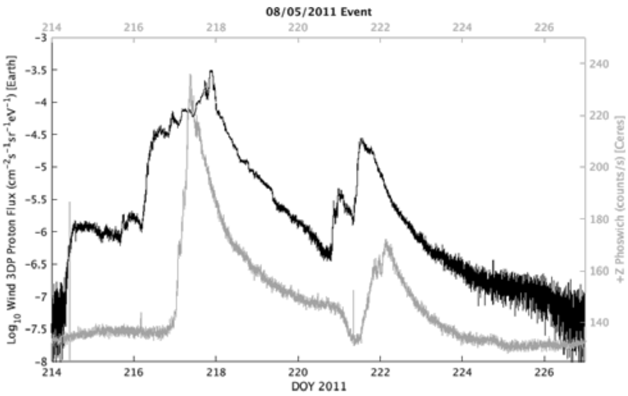

Figure 2. Comparisons of a solar energetic particle event observed by Wind at 1 au (black line; 4 MeV protons) and by Dawn's Gamma Ray and Neutron Detector at Vesta, located near the region of Ceres at ~2.4 AU (cyan line).

4. References

[1] A'Hearn, M. F. and P.D. Feldman (1992), Water Vaporization on Ceres, Icarus 98, 54-60.

[2] Rousselot, P. et al. (2011), A Search for Water Vaporization on Ceres, The Astronomical Journal, Vol 142, 125.

[3] Küppers, M. et al. (2014), Localized sources of water vapour on the dwarf planet (1) Ceres, Nature, 505, 525-527.

[4] Prettyman, T.H. et al. (2011), Dawn's gamma ray and neutron detector, *Space Sci. Rev.* **163**, 371-459, doi: 10.1007/s11214-011-9862-0

[5] Russell, C. T. et al. (2016), Dawn arrives at Ceres: Exploration of a small, volatile-rich world, Science, Vol 353, 1008-1010.

[6] Jia, Y.D. et al. (2017), Possible Ceres Bow Shock Surfaces Based on Fluid Models, J. Geophys. Res. Space Physics, 122, 4976-4987.

[7] Villarreal, M. N. et al. (2017), The Dependence of the Cerean Exosphere on Solar Energetic Particle Events, The Astrophysical Journal Letters, **838**, L8.

The Solar Wind Interaction with Vesta and Ceres: Implications for their Magnetic Moments

C.T. Russell[1*]; M.N. Villarreal[1], T.H. Prettyman[2], N. Yamashita[2], Y.D. Jia[1].
[1]Earth, Planetary and Space Sciences, University of California, USA
[2]Planetary Space Institute, USA.

Vesta and Ceres are the two most massive asteroids but are quite different in density and internal structure. Vesta has an iron core with a radius of about 100 km and an average density of 3456 km^{-3} [1], while Ceres has no resolvable core (thus far), and a density of 2162 g m^{-3} [2]. The iron core of Vesta may have once contained a magnetic dynamo, and had the dynamo solidified from the outside, could have been self-magnetized [3], leaving a magnetic moment that was present today. The Dawn spacecraft was designed to carry a magnetometer, but this instrument was removed from the payload during mission development. Thus we must resort to indirect techniques to infer if Vesta has any residual magnetic field today.

One way to do this is to examine the gain of the photomultiplier tube in the GRaND gamma ray and neutral detector. The GRaND detector is oriented to point its detectors at Vest as its orbits. If there were a sizeable magnetic field around Vesta, the gain of the photomultiplier would change as “multiplied” electrons were deflected by that magnetic field. This effect has been examined at Vesta, and no significant change in gain with position in orbit at Vesta is seen. This limits the magnetic moment to be less than 6 x 10^8 Tm^3.

A more indirect method is more sensitive. When a body deflects the solar wind by a magnetic field or an ionosphere (such as at Venus), or an atmosphere (such as at a comet), the solar wind is deflected and a bow shock is formed. This bow shock in turn can accelerate electrons forward and backward into the solar wind to energies greater than 20 keV. This process is called fast Fermi [4] acceleration and occurs as the reflection point of the electrons move rapidly. These electrons are sufficiently energetic to be detected by GRaND and were found at Ceres and interpreted in terms of the existence of a transient atmosphere at Ceres [2]. The transient atmosphere in turn was produced by Solar Energetic Protons [5].

This fast Fermi process is well studied at the Earth (e.g. [5]) and the signature in the GRaND detectors is understood and recognizable. Thus, its presence or absence at Vesta can be used to determine whether the Vesta magnetic moment is sufficiently large to deflect the solar wind above the surface of Vesta. To check if this occurred at Vesta, a survey of the types of electron burst detections or similarly appearing bursts was carried out independently by M.N. Villarreal and N. Yamashita.

Three types of events were seen at Vesta. Type 1 that consists of a negative peak followed by a positive peak was caused by a counter rollover These were not caused by bursty electron fluxes. Type 2 was found to occur in conjunction with gamma ray bursts from distant astrophysical objects and was detected with the appropriate delay at other points in the solar system. Type 3 was found to be associated with active regions on the Sun and their X-ray bursts. Thus we conclude that the magnetic moment of Vesta is too weak to deflect the solar wind and form a standing bow shock. Since the solar wind pressure drops a factor of 5.8 between the Earth and Vesta and Vesta’s radius is (250) times smaller than that of the Earth’s magnetopause, the maximum magnetic moment that Vesta might have and not produce fast Fermi electrons is 40 Tm^3.

Electron bursts at Ceres were apparently produced by fast Fermi electrons [2]. These electrons were seen for about a week after the solar proton event. Since the source of water production presumably ceased when the solar protons ceased, the water exosphere stayed around Ceres as long as predicted for a transient water exosphere [6]. After a week, the length we expect the exosphere to take to be reduced to zero, there were no more electron events. Hence the intrinsic magnetic moment of Ceres must be less than about 3 x 10^9 Tm^3.

In short, neither Vesta nor Ceres have sizably magnetized iron cores that affect their interaction with the solar wind. Generally the solar wind interacts with the crust of both planets and is absorbed. On occasion, in the presence of a strong flux of energetic solar protons, water is liberated from the crust and a temporary water atmosphere is present on Ceres. We have no evidence of such a process occurring at Vesta.

1. References

[1] Russell, C.T., Raymond, C.A., Coradini, A., McSween, H.Y., Zuber, M.T., Nathues A. et al: Dawn at

Vesta: Testing the protoplanetary paradigm, Science, Vol. 336, 684, 2012.
[2] Russell, C.T. et al.: Dawn arrives at Ceres: Exploration of a small, volatile-rich world, Science, Vol. 353, 6303, pp. 1008-1010, 2016.
[3] Fu, R.R., Weiss, B.P., Shuster, D.L., Gattacceca. J., Grove, T.L., Suavet, C., Lima, E.A., Li, L.Y., and Kuan, A.T.: An ancient core dynamo in asteroid Vesta, Science, Vol. 338, pp. 238-241, 2012.
[4] Leroy, M.M., and Mangeney, A.: A theory of energization of solar wind electrons by the Earth'w bow shock, Annales Geophys., Vol. 2, pp. 449-456, 1984.
[5] Villarreal, M.N., Russell, C.T., Luhmann, J.G., Thompson, W.T., Prettyman, T.H., A'Hearn, M.F., Kuppers, M., O'Rourke, L., Raymond, C.A.: The dependence of the Cerean exosphere on solar energetic particle events, Astrophys. J., Vol. 838, 1, 2017.
[6] Formisano, M., DeSanctis, M.C., Magni, G., Federico, C., Capria, M.T.: Ceres water regime: Surface temperature, water sublimation and transient exo(atmo)sphere. Mon. Not. R.A.S., Vol. 455, pp. 1892-1904, 2016.

To What Extent Does Solar Wind Forcing Affect the Occurrences of Energetic Electron Events in the Hermean Magnetosphere?

C.L. Lentz[1*]; D.N. Baker[1], A.N. Jaynes[2], T.W. Leonard[1], R.M. Dewey[3], D.J. Lawrence[4], W.J. Sun[3]
[1]University of Colorado, USA,
[2]University of Iowa, USA.
[3]University of Michigan, USA.
4 Johns Hopkins University, USA.

Abstract

The magnetic field of Mercury is strong enough to form a permanent magnetosphere under typical solar wind conditions. Earth's magnetosphere is often times used as a basis for qualitative comparison. However, due to the miniature size and lack of a substantial atmosphere and ionosphere, quantitative differences have led to queries regarding the dynamic aspect of the Hermean magnetosphere. A particular area of interest is the occurrence of energetic electron bursts, which are a result of substorm processes. These distributed events are detected at Earth in stable, long-lived radiation belts but at Mercury seem to occur only as transient phenomena in space and time. Mercury is not known to have a trapped population of energetic particles yet these energetic electron bursts appear to occur in specific regions of the magnetosphere. The curious nature of these energetic electron events begs the question as to what role they play in the active and dynamic Hermean magnetosphere. This study aims to provide some insight into the relationship between the occurrences of these energetic electron events and the environment outside the Hermean magnetosphere. Specifically, we focus on the relationship between solar transient events and the corresponding time-dependent shapes, or morphologies and the occurrence rate of energetic electron events.

Ion and neutral gas escape from the terrestrial planets

S. Barabash*; R. Ramstad
Swedish Institute of Space Physics, Sweden

1. Atmospheric escape: current paradigm

If the energy of gas particles (neutral or ionized) exceeds the escape energy, the particles escape to space and are lost from the atmosphere. This process is called atmospheric erosion. The thermal energy in atmospheres / ionospheres is a few 0.01 – 0.1 eV. The atomic oxygen escape energy is around 10 eV for Venus and Earth, and 2 eV for Mars, thus an energy source is required to erode the atmospheres of all terrestrial planets.

The neutral particles can gain energy from the redistribution of the inner or chemical energy in the atmosphere or from photochemical reactions, i.e, dissociative recombination, driven by solar radiation. Typical energy gain in these processes is a few eV. Therefore, the neutral gas escape of heavy species (helium and oxygen) is more efficient at low gravity Mars than at Venus and Earth. However, ions in the upper atmospheres / exospheres of planets can be accelerated by electric fields resulting from the planet – solar wind interaction. The electric fields acting on ions include the convective field of the solar wind (pick-up process), fields resulting from pressure gradients ("polar" wind), induced electric field (JxB-force), and fields of electromagnetic waves (wave-plasma interaction). The energy gain in this case can be from a few eV to 100s eV and is ultimately sourced from the kinetic energy of the solar wind.

While the neutral gas escape rate (number of particles lost to space per sec) is determined by the internal properties of the atmospheres (composition, density, temperature), the ion escape rate depends on the solar wind conditions, properties of the ionosphere (driven by solar EUV), and intrinsic magnetic field.

The present paradigm postulates that a magnetosphere created by an intrinsic magnetic fields "protects" the planetary atmosphere/ionosphere from the erosion resulted from the solar wind interaction as in the Earth case. The magnetospheric fields separate the moving interplanetary magnetic field "frozen-in" in the solar wind and the upper ionized part of the atmosphere, ionosphere. The ionospheric ions are not subjected to the induced and convective electric fields and cannot be accelerated to energies above the escape energy and leave the planet. Contrary to magnetized planets, atmospheres of non-magnetized Mars and Venus are subject to solar wind erosion because the interplanetary magnetic field can reach their ionospheres.

2. Comparative escape

Contrary to the conclusion from the present paradigm, the current rate of the planetary ions escape resulted from the interaction with the solar wind from Venus, Earth, and Mars is about the same and in the range 10^{24} – 10^{25} particles/s [1,2,3]. To understand this counterintuitive observations we put forward the idea that the ion escape rate is determined by the total energy transferred from the solar wind to the ionosphere and is thus limited by the transfer efficiency and the size of the interaction region. The intrinsic magnetic field creates a large size interaction region (magnetosphere) which can intercept and channel down to the ionosphere a significant energy increasing the ion escape rate in comparison to small-size interaction regions of un-magnetized Venus and Mars.

2.1. Escape from Mars

To develop this idea further we analysed 13 years of ion measurements at Mars on Mars Express to establish the dependence of the escape rate on the solar and solar wind conditions. It turned out the escape rate decreases with solar wind density for the fixed velocity [4], in line with the idea of reducing the total energy transferred to the planetary ions due to reducing the size of the interaction region. Figure 1a shows how the interaction region shrinks with increasing solar wind density [5]. Another argument in favor of the concept of escape rate driven by the energy transfer from the solar wind is the influence of the Martian magnetic anomalies on the escape rate. The long-term Mars Express measurements made possible to establish dependence of the escape rate on the magnetic anomaly solar zenith angle for fixed solar wind and solar UV conditions. It turned out that the escape rate is strongest when the Martian magnetic anomalies are at intermediate solar zenith angles of 60°-70°, it is indeed at these angles the mini-magnetospheres are the largest and "intercept" more energy [6].

The transfer efficiency from the solar wind to the planetary ions, or coupling function, can be determined as the ratio of the total energy of the escaping ions per sec to the total power available in the solar wind (the solar wind energy flux times the interaction area).

Figure 1b shows the transfer efficiency as a function of the solar wind dynamical pressure. Only 0.1% to 1% of all available energy is transferred to planetary ions. The coupling becomes weaker with increasing the dynamical pressure for fixed UV, and similarly decreases with solar UV flux for fixed dynamical pressure (Figure 1c) [5]. The decreasing ion escape rate from Venus with increased UV analogously indicates an increasingly energy-limited escape process [5,7].

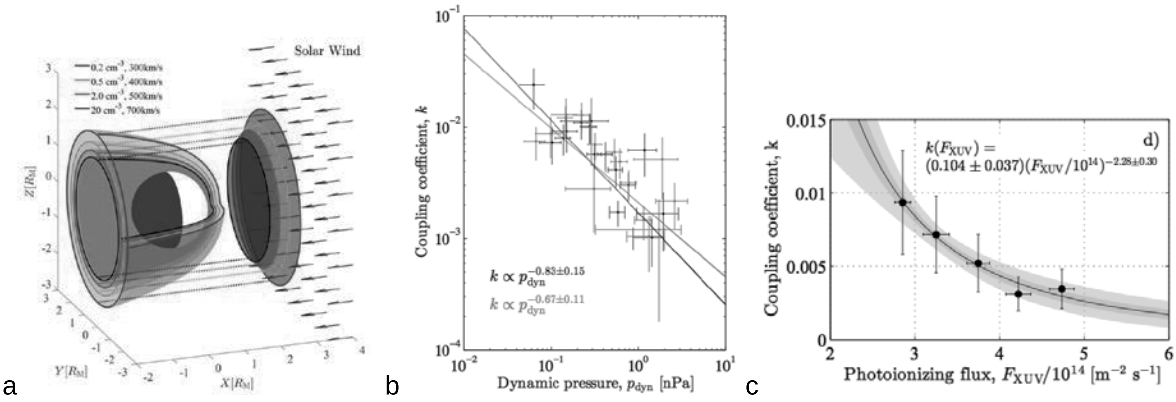

Figure 1: (a) Changing of the interaction cross-section area for varying upstream solar wind conditions [5].Dependence of the solar wind energy transfer efficiency (coupling function) to planetary ions on the solar wind dynamical pressure (b) and solar UV flux (c).

2.2. Impact of the ion escape on planetary evolution

The established dependence of the ion escape rate on the solar and solar wind conditions and known from the other stars variability of the Sun make possible to calculate the total amount of atmospheric gases lost due to the interaction with the solar wind. For Mars only about equivalent 10 mbar of the atmosphere would have been lost for the last 3.9 billion years as ions [8], an insignificant influence on Martian atmospheric evolution. The escape of neutral particles as results of atmospheric sputtering or/and photochemical reactions may contribute more to the atmospheric erosion, however, these mechanisms can be efficient only for low gravity Mars, not for Venus.

3. Paradigm shift

Following the above ideas, the concept of intrinsic magnetic fields “protecting” planetary atmospheres from solar wind erosion requires revision to conform to measurements. The intrinsic magnetic fields would rather facilitate planetary ion escape. Contrary, induced magnetospheres of non-magnetized atmospheric bodies are too small to “collect” significant amount of energy to power the atmospheric erosion.

4. References

[1] Fedorov, A., et al.: Measurements of the Ion Escape Rates From Venus for Solar Minimum, Journal of Geophysical Research: Space Physics, Vol. 116, A7, 2011.
[2] Nilsson, H., et al.: Hot and cold ion outflow: Spatial distribution of ion heating, Journal of Geophysical Research: Space Physics, Vol. 117, A11201, 2011.
[3] Brain, D., et al.: The spatial distribution of planetary ion fluxes near Mars observed by MAVEN, Geophys. Res. Lett*., 42, 9142*–9148, doi:10.1002/2015GL065293, 2015.
[4] Ramstad, R., et al.: The Martian atmospheric ion escape rate dependence on solar wind and solar EUV conditions: 1. Seven years of Mars Express observations, Journal of Geophysical Research: Planets, Vol. 120, 7, pp. 1298–1309, 2015.
[5] Ramstad, R., et al.: Global Mars-solar wind coupling and ion escape, Journal of Geophysical Research: Space Physics, Vol. 122, 8, pp. 8051-8062, 2017.
[6] Ramstad, R., et al.: Effects of the crustal magnetic fields on the Martian atmospheric ion escape rate, Geophysical Research Letters, Vol. 43, 20, pp. 10,574-10,579, 2016.
[7] Kollmann, P., et al.: Properties of planetward ion flows in Venus’ magnetotail, Icarus, Vol. 274, pp. 73-82, 2016.
[8] Ramstad, R., Ion Escape from Mars: Measurements in the Present to Understand the Past, PhD thesis, 2017.

Atmospheric Escape from Mars

D. Brain[1*]
[1]LASP / University of Colorado, USA

1. Introduction

It is inevitable that all planets lose atmospheric particles to space, as some particles are provided with enough energy to escape the planet's gravitational pull. Compared to Earth, Mars may be especially susceptible to atmospheric loss since it is smaller than Earth (leading to a lower escape velocity for atmospheric particles) and unmagnetized (so that the solar wind has more direct access to the upper atmosphere). Multiple lines of evidence suggest that liquid water was stable at the Martian surface long ago, which requires an atmosphere that was substantially thicker than the ~7 mbar present today. Atmospheric isotope ratios show an enrichment in heavy isotopes consistent with the loss to space of a large fraction of the atmosphere over time. Thus, the atmospheric escape processes active at every planetary body may, in the case of Mars, have combined to change the climate of a planet.

Atmospheric escape from Mars has been measured directly by several spacecraft (Phobos, Mars Express, MAVEN), and measurements relevant to escape stretch back more than 50 years. Theoretical calculations and computer simulations have also addressed atmospheric escape via different processes. Together, data and models provide the most complete picture of atmospheric escape, both at present and over time, from any planetary body.

2. Escape Processes

A variety of escape processes act at Mars, for both neutral and charged particles [1]. Every process energizes atmospheric particles to speeds in excess of the escape velocity.

Three different processes can remove neutral particles from the Martian atmosphere. Thermal escape is relevant only for the lightest atmospheric species – hydrogen, deuterium, and helium. Of these, hydrogen is the most abundant. Heavier species, such as oxygen, are instead removed primarily by photochemical processes, whereby a molecular ion (O_2^+, for example) is dissociated by sunlight and the constituent oxygen atoms recombine with enough energy to escape the planet. Sputtering is a final process, occurring when an incident particle (typically a high altitude atmospheric ion) encounters the exobase and, through collisions, exchanges energy with target atmospheric particles that escape as a result of their gained energy.

Escape rates for neutral escape processes are not measured directly; instead they can be inferred from measurements of the reservoirs for neutral particle loss: the exosphere and thermosphere. Thermal escape is calculated more or less directly from measurements of density and temperature near the exobase. Photochemical escape is similarly calculated from measurements of thermospheric and ionospheric densities, incident EUV sunlight, and electron concentrations. Sputtering is inferred from measurements of incident ions and knowledge of target particle populations near the exobase.

Similar to escape of neutral particles, three "processes" contribute to ion escape. These processes can be roughly associated with the three largest terms in the generalized Ohm's law: ion pickup (v x B), magnetic tension (J x B), and ambipolar electric fields (). All three electric field terms can contribute to accelerating an atmospheric particle away from Mars, though different terms are dominant in different regions.

Escape rates for ions can be measured directly at Mars, using in situ measurements of ion fluxes. In general, three different escape "channels" are identified in spacecraft observations. A "plume" of pickup ions escapes directly from the ionosphere near the exobase region in the direction of the convection electric field carried by the solar wind. Colder ions, "born" primarily on the dayside of Mars, escape down the Martian induced magnetotail. And particles ionized in the extended neutral exosphere escape downstream in the solar wind.

3. Escape Rates and Variability

Both measurements and models allow evaluation of present day atmospheric escape rates, and variability in escape rates in response to drivers. Using results from the ongoing MAVEN mission, estimated have been made for the escape rate from each process identified in Section 2. Ion loss via all three acceleration mechanisms removes roughly 10^{25} particles per second of O^+, O_2^+, and CO_2^+ from the Martian atmosphere [2]. Sputtering makes only a small contribution to present day loss, with rates of roughly 10^{24} s^{-1} [5]. Photochemical escape removes ~$4x10^{25}$ s^{-1} of oxygen [6]. And thermal escape removes as much as 10^{26} s^{-1} of hydrogen [3]. Together, MAVEN data suggest that a few x 10^{26} atmospheric particles per second are removed from the Martian atmosphere.

Each of these processes responds to drivers from the Sun and solar wind, as well as the Martian atmosphere below. Drivers that have been identified to date include the flux of EUV sunlight at Mars, the density and velocity of the flowing solar wind, and the subsolar longitude of Mars (which situates the Martian crustal fields with respect to the incident solar wind flow [see 1, eg.]. Atmospheric phenomena such as dust storms also appear to play a role in atmospheric escape by transporting hydrogen upward from the lower atmosphere, where it can subsequently escape [3]. Of these many drivers, EUV flux appears to be dominant in controlling the variability in escape rates.

4. Implications for Climate

The present day escape rate, if it has persisted throughout Martian history, is not large enough to account for a sufficiently large change in the Martian atmosphere to explain a transition in the planet's climate. A loss rate of 10^{26} s^{-1} over 4 Gy could account for the loss of ~100 mbar of CO_2 or, alternately, a ~2.5 m global surface layer of water. However, observations of Sun-type stars suggest that the solar drivers of atmospheric loss were more intense earlier in solar system history, so that loss rates could have been substantially greater as well. Moreover, present-day observations show that escape rates are enhanced during solar storm events (CMEs, flares, SEPs), which are believed to have been both more common and more intense earlier in solar system history. Thus, when both processes and changing driving conditions are accounted for, estimates for the total atmospheric loss over time range from a couple of hundred mbar to nearly 750 mbar [4]. It seems likely, therefore, that atmospheric loss from Mars has played a major role in changing the planet's climate.

5. References

[1] Brain, D., S. Barabash, S. Bougher, F. Duru, B. Jakosky, and R. Modolo: Solar Wind Interaction and Atmospheric Escape, in "The Mars Atmosphere", edited by R. Haberle, T. Clancy, F. Forget, and R. Zurek, 2017.
[2] Brain, D., et al.: The spatial *distribution of planetary ion fluxes near Mars observed by MAVEN*, Geophys. Res. Lett*.,* 42, 10.1002/2015GL065293, 2015.
[3] Chaffin, M., et al.: Unexpected variability of Martian hydrogen escape, Geophys. Res. Lett., 41, 10.1002/2013GL058578, 2014.
[4] Jakosky, B. et al.: Loss of the Martian atmosphere to space: Present-day loss rates determined, Icarus, submitted, 2017.
[5] Leblanc, F., et al.: Mars heavy ion precipitating flux as measured by Mars Atmosphere and Volatile EvolutioN, Geophys. Res. Lett*.,* 42, 10.1002/2015GL066170, 2015.
[6] Lillis, R., et al.: Photochemical escape of oxygen from Mars: First results from MAVEN in situ data, J. Geophys. Res., 122, 10.1002/2016JA023525, 2017.

Signatures of sputtering at Mars: a first evidence?

F. Leblanc[1*]; J.Y. Chaufray[2], M. Benna[3], A. Martinez[1], M. K. Elrod[3], P. Mahaffy[3], R. Modolo[2], J.G. Luhmann[4], R.E. Johnson[5], and B. Jakosky[6]
[1]LATMOS/IPSL, UPMC Univ. Paris 06 Sorbonne Universités, UVSQ, CNRS, France,
[2]LATMOS/IPSL, UVSQ Université Paris-Saclay, UPMC Univ. Paris 06, CNRS, France
[3]NASA Goddard Space Flight Center, USA
[4]Space Science Laboratory, University of California, USA
[5]Department of Material Science, University of Virginia, USA
[6]Laboratory for Atmospheric and Space Physics, University of Colorado, USA

1. Introduction

One of the potential driver of Mars' past atmospheric evolution is its escape into space following Mars' interaction with the solar radiation flux and solar wind [1]. To understand how the solar mass and energy can lead to the erosion of the atmosphere is one of the main goals of the Mars Atmosphere and Volatile Evolution MissioN (MAVEN) [2]. Among the processes that may have been at the origins of this erosion is the sputtering of Mars' atmosphere by heavy planetary ion picked up by the solar wind and precipitating into Mars [3]. This flux of precipitating heavy ion has been clearly identified by MAVEN [4], [5]. However, so far, no signature of the expected effects of these precipitating ion has been identified in Mars' atmosphere or exosphere [6].

In this presentation, we will describe a possible approach to disentangle the effect of the sputtering from other known sources of Mars' exosphere.

2. NGIMS/MAVEN measurements and HELIOSARES models

2.1. NGIMS data

For this work, we essentially used NGIMS measurements performed during the first one and a half year of MAVEN scientific measurements (from January 2015 up to August 2016). More specifically, NGIMS v06 products are selected to reconstruct the measured density profile of Mars upper atmosphere (typically above 150 km up to 500 km in altitude). No background has been subtracted for the time being from these measurements and we used only the inbound profiles and the Ar density because this species is the less subjected to calibration issues, wall absorption and mass identification problem.

2.2. HELIOSARES set of models

HELIOSARES is a set of coupled models describing the fate of Mars' environment from its surface up to the solar wind. In particular, HELIOSARES has been successfully used to reconstruct the oxygen component of the exosphere as measured by MAVEN for different seasons and at different solar zenith angles [6]. More recently, we used the typical measured precipitating flux by MAVEN to calculate the expected increase of the exospheric density induced by the sputtering [7].

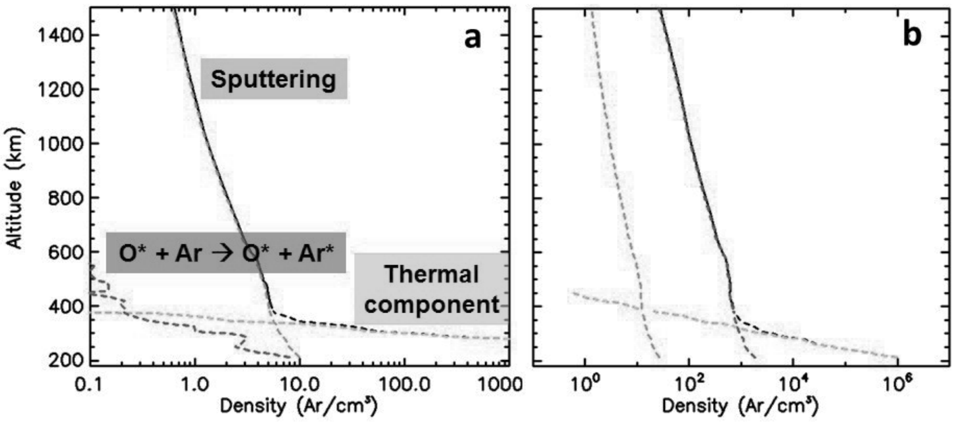

Figure 1: Density profile of the Ar as simulated by HELIOSARES set of models at Ls=180°, for solar minimum conditions and nominal solar wind conditions. The solid black line is the sum of all exospheric components modeled by HELIOSARES. The red, blue and green dashed lines are for the sputtering, thermal and photo-chemical processes respectively. Panel a: Solar Zenith Angle larger than 170°. Panel b: Solar Zenith Angle smaller than 10°.

In [7], we showed that, at present epoch, sputtering induced density in the exosphere remains much smaller than the density induced by thermal expansion of the atmosphere or by photo-chemical reactions. It is only for the heaviest atmospheric species, like CO_2 or Ar, and deep in the nightside, that the sputtering exospheric component dominates the other sources of exosphere as shown in Figure 1, panel a.

3. Comparison between NGIMS Ar measured profile and HELIOSARES simulated one

We therefore focused on NGIMS measurements of the Ar density when MAVEN periapsis was deep in the nightside. For each selected set of measurements, we calculated the simulated density along MAVEN path through HELIOSARES corresponding simulation (same Ls and solar activity).

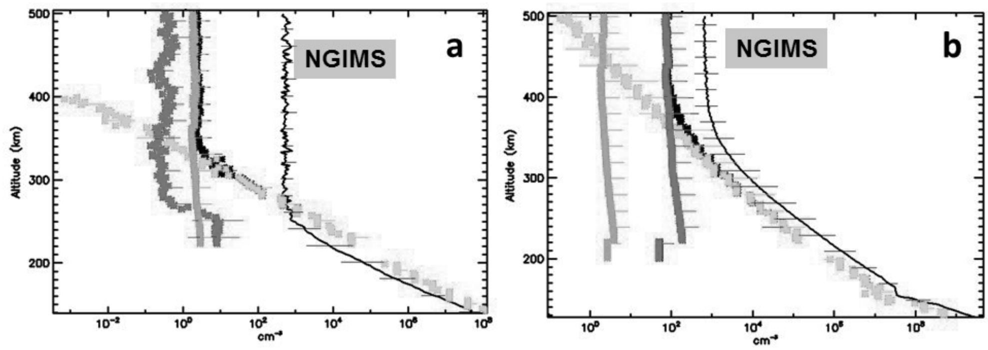

Figure 2: The symbols are for the simulated density (same colors as in Figure 1) whereas the solid black line is for NGIMS measured Ar density. Horizontal bars correspond to the one sigma dispersion of the measured and simulated densities. Panel a: measurements performed for SZA between 130 and 165°. Panel b: measurements performed for SZA between 4° and 55°.

As shown in Figure 2, NGIMS measured profile shows a clear change of slope above 350 km on the dayside and an almost constant density above in good agreement with the simulated profile. Part of the discrepancy between measured and simulated profiles is very probably due to the need to subtract a background to the measured density profile, a work which is in progress. But a very preliminary estimate of this background, based on apoapsis NGIMS dedicated measurements, suggests that at 500 km in altitude, part of the measured density is real which might imply that the measured profile on the nightside above 250 km is also partially real, a conclusion which is also suggested by the similar simulated and measured slopes above 350 km in panel a.

4. References

[1] Jakosky B.M., M. Slipski, M. Benna, P. Mahaffy, M. Elrod, R. Yelle, S. Stone, N. Alsaeed, (2017), Science 355, 1408–1410, doi: 10.1126/science.aai7721a.
[2] Jakosky, B. M., R. P. Lin, J. M. Grebowksy, J. G. Luhmann, and others (2015), Space Sci. Reviews, 195, 3–48, doi:doi:10.1007/s11214-015-0139-x
[3] Luhmann, J.G., Kozyra, J.U., (1991), J. Geophys. Res. 96, 5457-5467.
[4] Leblanc F., R. Modolo, S. Curry, J. Luhmann, R. Lillis, J. Y. Chaufray, T. Hara, J. McFadden, J. Halekas, F. Eparvier (2015), Geophys. Res. Lett., 42, doi:10.1002/2015GL066170
[5] Hara T., J. G. Luhmann, Leblanc F., Curry S.M., Seki K., Brain D.A., Halekas J.S., Harada Y., McFadden J.P., Livi R., DiBraccio G.A., Connerney J.E.P. and B. Jakosky, J. Geophys. Res. Space Physics, 122, 1083–1101, doi:10.1002/2016JA023348, 2017.
[6] Leblanc F., Modolo R., Chaufray J.Y. Leclercq L., Curry S., Luhmann J., Lillis R., Hara T., McFadden J., Halekas J., Schneider N., Deighan J. and B. Jakosky, J. Geophys. Res., doi: 10.1002/2017JE005336, 2017.
[7] Leblanc F., Modolo R., Chaufray J.Y., Curry S., Luhmann J., Lillis R., Hara T., McFadden J., Halekas J. and B. Jakosky, On Mars' Atmospheric Sputtering after MAVEN first Two Years of Measurements, Geophys. Res. Let., Submitted, 2018.

Cold Ion Escape from Mars – Observations by Mars Express and MAVEN

M. Fränz[1] , *E. Dubinin*[1], *L. Maes*[1], *J. McFadden*[2]
[1]*MPI for Solar System Research, Germany,*
[2]*Space Science Laboratory, Univ. of California, USA*

Measuring the escape of ions from Mars has been one of the main targets of the ASPERA-3 experiment on Mars Express since orbit insertion in 2004. But the Mars Express spacecraft is not optimized for this measurement since it lacks a magnetometer and a Langmuir probe to observe magnetic field and total plasma densities. Nevertheless, over the last 12 years several studies have been published attempting to determine the total escape flux and its variation with external parameters from ASPERA-3 observations [1,2,3]. Especially the contribution of the 'cold ions' with energies of less than 5eV to the escape flux has been debated because it is most difficult to measure.

Since October 2014 the MAVEN spacecraft is in orbit around Mars with a much larger instrumental suite optimized for measuring the ion outflow. In this paper we reassess observations made by the MEX ASPERA-3 and MARSIS experiments in the light of the MAVEN observations of tailside ion outflow observed between 2014 and 2017. We investigate the influence of the spacecraft potential on the derived flux values and compare ion density observations by the different MAVEN instruments.

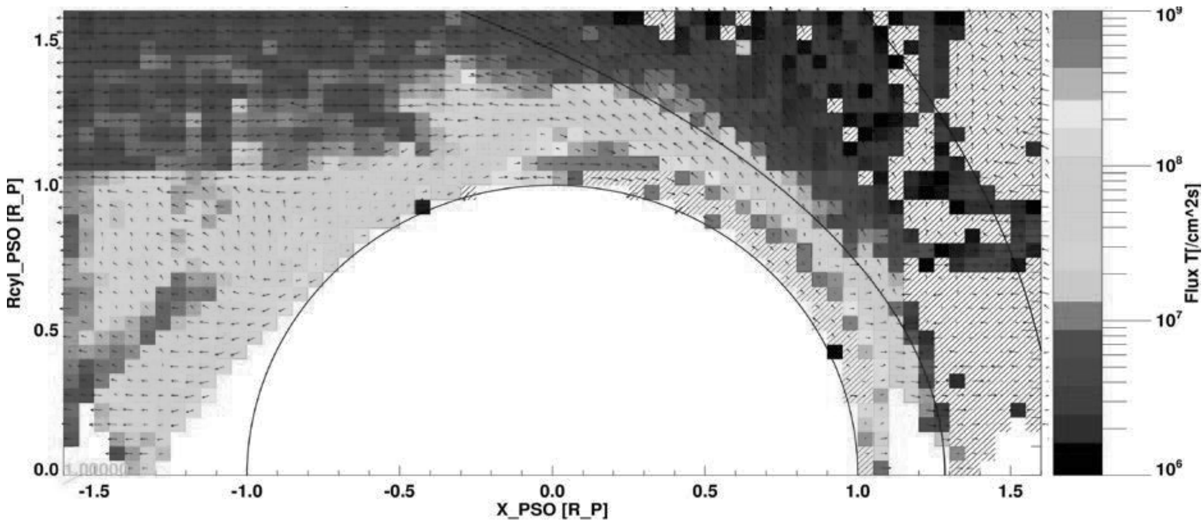

Figure 1: Total flux of heavy ions (O+ & O_2+) observed by MAVEN STATIC between 01 Dec 2014 and 15 Nov 2015, scaled in ions/cm^{2}s. The vertical component of vectors shows the deviation from the cylindrical symmetry axis.

References

[1] Fraenz, M. et al. Plan.Space Science, 119, 92, 2015
[2] Ramstad, R. etal. JGR, 10.1002/2017/JA024306, 2017
[3] Dubinin et al, JGR, 10.1002/2017JA024741, 2017

The Origin and Evolution of Nitrogen in Outer Planet Atmospheres through Comparative Planetology

K.E. Mandt[1*]; A. Luspay-Kuti[2], O. Mousis[3], P. Brandt[1].

[1]Johns Hopkins University Applied Physics Laboratory, USA
[2]Southwest Research Institute, USA,
[3]Aix Marseille Université, CNRS, LAM (Laboratoire d'Astrophysique de Marseille), France

1. Introduction

Stable isotope ratio measurements combined with modelling of isotope evolution help us to understand the origin of volatiles throughout the solar system [see 1 and references therein]. The evolution of the nitrogen isotope ratio, $^{14}N/^{15}N$, in the atmospheres of Titan, Pluto and Triton compared to measurements throughout the solar system (Fig. 1) can be used to determine the origin of nitrogen in each atmosphere. The goal is to determine if this nitrogen originated as N_2 or is derived from NH_3 in the protosolar nebula (PSN). The origin of Titan's nitrogen has been well constrained [2], but uncertainties due to lack of measurements and poor understanding of photochemistry and other processes leave Pluto [3,4] and Triton unconstrained. Therefore, our goal in this work is to provide guidance on measurements needed by a future Ice Giants mission to study Triton and any mission to follow New Horizons and Cassini in exploring Pluto and Titan.

2. The Origin and Evolution of Nitrogen

This work is part of an ongoing study to determine the origin of nitrogen in atmospheres throughout the solar system [2,3,4,5,6]. Measurements of $^{14}N/^{15}N$ throughout the solar system allow us to map out the origin and history of nitrogen in the solar system, as illustrated in Fig. 1 [adapted from 4, see references therein for individual measurements]. $^{14}N/^{15}N$ measured in the solar wind and the atmospheres of Jupiter and Saturn are presumed to be representative of N_2 in the PSN because the most abundant form of nitrogen in the PSN was N_2. Trace amounts of HCN and NH_3 were also present in the PSN, and $^{14}N/^{15}N$ for these constituents measured in comets are presumed to represent their primordial ratio.

On the other hand, $^{14}N/^{15}N$ measured in the atmospheres of the terrestrial planets, Titan and the lower limit for HCN in Pluto are known to have evolved from their primordial ratio over the history of the solar system. Modelling how the ratio changes over time helps us to understand the origin of nitrogen in these bodies. Our most recent work has evaluated Triton as a follow-up to our studies on Pluto [5,6] and Titan [2,3].

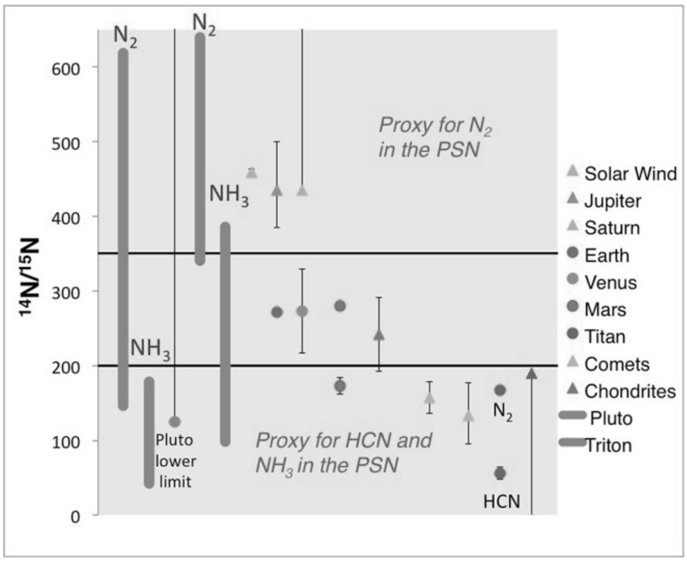

Figure 1: $^{14}N/^{15}N$ measured throughout the solar system [see 4 and refs. therein]. Triangles are primordial values while circles are ratios that have evolved. Estimated range of values for Pluto (left grey bars) and Triton (right grey bars) are also shown.

3. Lessons from Titan and Pluto

3.1. Escape

Escape preferentially removes the lighter isotope from the atmosphere, reducing the ratios illustrated in Fig. 1 over time. The higher ratio for Mars is thought to represent a primordial value that decreased through escape over time to the current ratio [see 6 and refs. therein]. However, escape from Titan's very dense atmosphere is not effective at changing $^{14}N/^{15}N$ [2,6]. We determined an upper limit for primordial $^{14}N/^{15}N$ similar to the $^{14}N/^{15}N$ in cometary NH_3 [2]. Hydrodynamic escape of nitrogen was predicted for Pluto's atmosphere prior to the *New Horizons* flyby. This would have a major impact on the isotope ratio over time [3]. However, observations by the *New Horizons* Alice UV spectrograph presented a much cooler atmosphere with nitrogen escaping rates that are orders of magnitude lower than predicted [7]. This significantly reduces the impact of escape on $^{14}N/^{15}N$ in Pluto's atmosphere [4].

3.2. Photochemistry

The difference in $^{14}N/^{15}N$ in N_2 and HCN in Titan's atmosphere (Fig. 1) is due to extreme fractionation by photochemistry in Titan's atmosphere [8]. Our preliminary study modelling the photochemistry of Pluto's atmosphere [4] does not find the same effect and is supported by the lower limit reported for $^{14}N/^{15}N$ in HCN [9]. It is unclear at this time why Pluto is so different from Titan, and more work needs to be done on this topic.

3.3. Other Processes

When evaluating photochemistry in Pluto's atmosphere, we also simulated the loss of HCN by condensation and sticking to aerosols [4] and found that this process appears to have a major impact on $^{14}N/^{15}N$ in HCN that does not agree with the lower limit [4,9]. This means that we have a poor understanding of the impact of these processes on $^{14}N/^{15}N$ and that more work is also needed.

4. Application to Triton

Updated estimates for Triton's atmospheric structure and the rate of nitrogen escape have been provided based on what has been learned about Pluto's atmosphere from *New Horizons* [10]. We apply these results and estimates for photochemical fractionation to determine the range of ratios that could be measured by a future Ice Giants mission to explore Triton (Fig. 1). Improved studies on photochemistry and other processes at Pluto will play an important role in reducing the uncertainty in these results.

5. Application to Triton

Measurements of $^{14}N/^{15}N$ in planetary atmospheres can be used to determine the origin of nitrogen for these bodies. We have determined that Titan's nitrogen originated as NH_3 in the PSN [2] and are working on constraints for current $^{14}N/^{15}N$ in the atmospheres of Pluto [3,4] and Triton in anticipation of future missions capable of making these measurements.

6. References

[1] Mandt K. E. et al.: Constraints from comets on the formation and volatile acquisition of the planets and satellites, Sp. Sci. Rev., Vol. 197, pp. 297–342, 2015a.
[2] Mandt, K. E. et al.: Protosolar NH_3 as the unique source of Titan's nitrogen, Astrophys. J., Vol. 788, pp. L24, 2014.
[3] Mandt, K. E., Mousis, O., Luspay-Kuti, A.: Isotopic constraints on the source of Pluto's nitrogen and the history of atmospheric escape, Planetary and Space Science, Vol. 130, pp. 104-109, 2016.
[4] Mandt, K. E. et al.: Photochemistry on Pluto: Part II HCN and nitrogen isotope fractionation, Monthly Notices of the Royal Astronomical Society, in press, 2017.
[5] Mandt, K. E. et al.: Isotopic evolution of the major constituents in Titan's atmosphere based on Cassini data, Planetary and Space Science, Vol 57, pp. 1917-1930, 2009.
[6] Mandt K. E., Mousis, O., Chassefière: Comparative planetology of the history of nitrogen isotopes in the atmospheres of Titan and Mars, Icarus, Vol. 254, pp. 259–261, 2015b.
[7] Gladstone, G. R. et al.: The atm. of Pluto as observed by New Horizons, Science, Vol. 350, pp. aad8866, 2016.
[8] Liang et al.: Source of nitrogen isotope anomaly in HCN in the atmosphere of Titan, Astrophysical Journal, Vol. 664, pp. L115, 2007.
[9] Lellouch et al.: Detection of CO and HCN in Pluto's atm. with ALMA, Icarus, Vol. 286, pp. 289-307, 2017.
[10] Strobel, D. F. & Zhu, X.: Comparative planetary nitrogen atmospheres: Density and thermal structures of Pluto and Triton, Icarus, Vol. 291, pp. 55-64, 2017.

Cold Ion Outflow and Magnetic Topology in Mars' Magnetotail

D. L. Mitchell[1*]; S. Xu[1]; J. P. McFadden[1]; T. Hara[1]; S. Curry[1]; J. G. Luhmann[1]; C. Mazelle[2,3,4]; L. Andersson[5]; C. Fowler[5]; G. A. DiBraccio[6]; and J. E. P. Connerney[6]
[1]Space Sciences Laboratory, University of California, U.S.A.,
[2] CNRS, Institut de Recherche en Astrophysique et Planétologie, France
[3] Université Paul Sabatier, France
[4] CNES, France
[5] Laboratory for Atmospheric and Space Physics, University of Colorado Boulder, U.S.A.
[6] NASA Goddard Space Flight Center, U.S.A.

1. Introduction

The enhancement of heavy isotopes in Mars' atmosphere indicates that loss of atmosphere to space has played an important role in transforming the planet's climate [7]. This loss can take place through a variety of mechanisms, and has been aided by a weak gravity and the cessation of a global magnetic field ~4 Ga ago. Jeans escape for hydrogen and photochemical escape for oxygen appear to be the dominant loss processes today [8]; however, ion outflow down the tail might contribute significantly. Ion outflow can take place through several processes, depending on the magnetic configuration and the acceleration mechanism (ambipolar, **V** x **B** and **J** x **B** electric fields, as well as wave heating). Magnetic topology plays an important role, since the configuration of Mars' magnetotail is complex and dynamic [3], and access to a dense source of planetary ions significantly affects the loss rate. Estimates of the total oxygen ion loss down the tail have increased tenfold over the past 10 years [1-2, 4, 6, 9-12], largely as a result of measuring and including lower energy ions in the calculation. Measuring the escape flux from ~10 eV down to the escape energy (~4 eV for O_2^+) is especially difficult, because corrections for spacecraft motion and spacecraft charging are large.

2. Observations

Since August 2016, the Mars Atmosphere and Volatile EvolutionN (MAVEN) spacecraft has been conducting a series of observing campaigns designed to measure cold ion outflow down to escape energy. As the orbit precesses and sweeps through the tail, the spacecraft reorients from 1200 to 5000 km altitude to optimize the fields of view for the Supra-Thermal and Thermal Ion Composition (STATIC) instrument and the Solar Wind Electron Analyzer (SWEA). Data from SWEA and the Magnetometer (MAG) are used to determine the magnetic field topology, and in particular whether field lines are open, closed, or draped, and if open or deeply draped whether they have access to the day-side or night-side ionosphere. STATIC, SWEA, and the Langmuir Probe and Waves (LPW) experiment determine the spacecraft potential throughout the Mars environment using multiple, cross-calibrated methods. Simultaneous observations by STATIC are used to measure the density, composition, and velocity of planetary ions on these same field lines, all corrected for spacecraft motion and spacecraft potential. Combining data from four sweeps of MAVEN's orbit through the tail (~600 orbits), we have built up a database from which we can map statistics and develop a picture of ion outflow in Mars' tail.

3. References

[1] Barabash, S., Fedorov, A., Lundin, R., and Sauvaud, J.-A.: Martian atmospheric erosion rates, Science, 315(5811), pp. 501–503, 2007.
[2] Brain D., *et al.*: MAVEN measurements of ion loss from Mars, abstract, Internat. Conf. Mars Aeronomy, Boulder, 2017.
[3] DiBraccio, G. A., Dann, J., Espley, J. R., Gruesbeck, J. R., Soobiah, Y., Connerney, J. E. P., Halekas, J. S., Harada, Y., Bowers, C. F., Brain, D. A., Ruhunusiri, S., Hara, Y., and Jakosky, B. M.: MAVEN observations of tail current sheet flapping at Mars, J. Geophys. Res., Space Physics, 122, pp. 4308-4324, 2017.
[4] Dong, Y., Fang, X., Brain, D. A., McFadden, J. P., Halekas, J. S., Connerney, J. E. P., Curry, S. M., Harada, Y., Luhmann, J. G., and Jakosky, B. M.: Strong plume fluxes at Mars observed by MAVEN: An important planetary ion escape channel, Geophys. Res. Lett., 42, 2015.
[5] Dubinin, E., Chanteur, G., Fraenz, M., and Woch, J.: Field-aligned currents and parallel electric field potential drops at Mars. Scaling from the Earth' aurora, Planetary and Space Science, 56(6), pp. 868-872, 2008.
[6] Fränz, M., Dubinin, E., Nielsen, E., Woch, J., Barabash, S., Lundin, R., and Fedorov, A.: Transterminator ion flow in the Martian ionosphere, Planet. Space Sci., 58(1), pp. 1442–1454, 2010.
[7] Jakosky, B. M., Slipski, M., Benna, M., Mahaffy, P., Elrod, M., Yelle, R., Stone, S., Alsaeed, N.: Mars' atmospheric history derived from upper-atmosphere measurements of $^{38}Ar/^{36}Ar$, Science 355(6332), pp. 1408-1410, 2017.
[8] Jakosky, B., and the MAVEN Science Team, Loss of the Early Mars Atmosphere to Space Determined

from MAVEN Observations of the Upper Atmosphere. Fourth International Conference on Early Mars, LPI Contribution No. 2014, 2017.
[9] Lundin, R., Barabash, S., Fedorov, A., Holmström, M., Nilsson, H., Sauvaud, J. A., and Yamauchi, M.: Solar forcing and planetary ion escape from Mars, Geophys. Res. Lett., 35(9), 09203, 2008.
[10] Lundin, R., Barabash, S., Holmström, M., Nilsson, H., Yamauchi, M., Dubinin, E. M., Fraenz, M.: Atmospheric origin of cold ion escape from Mars, Geophys. Res. Lett., 36(1), 17202, 2009.
[11] Nilsson, H., Carlsson, E., Brain, D. A., Yamauchi, M., Holmström, M., Barabash, S., Lundin, R., and Futaana, Y.: Ion escape from Mars as a function of solar wind conditions: A statistical study, Icarus, 206(1), pp. 40–49, 2010.
[12] Nilsson, H., Edberg, N., Stenberg, G., and Barabash, S.: Heavy ion escape from Mars, influence from solar wind conditions and crustal magnetic fields, Icarus, 215(2), pp. 475-484, 2011.

Estimating the Escape of Hydrogen and Deuterium from the Atmosphere of Mars

J.T. Clarke[1], *M. Mayyasi[1], D. Bhattacharyya[1], J.Y. Chaufray[2], J.L. Bertaux[2], M. Chaffin[3], N.M. Schneider[3], H. Gröller[4], J. Deighan[3], S. Jain[3], G. L. Villanueva[5], and B. Jakosky[3]*
[1]Center for Space Physics, Boston University, USA
[2]LATMOS, CNRS, France
[3]LASP, University of Colorado, USA
[4]Lunar and Planetary Lab., University of Arizona, USA
[5]GSFC, NASA, USA

1. Introduction:

A fundamental challenge in planetary atmospheres research is to understand the present-day processes by which hydrogen escapes into space from the atmosphere of Mars. Once the processes are well known, it will be possible to accurately extrapolate back in time to estimate the history of water on Mars. The measured ratio of D/H in the martian atmosphere is elevated compared with the Earth, consistent with the loss of a substantial amount of water into space over the life of the planet. However, recent measurements of HDO / H_2O in the lower atmosphere have shown a factor of 2 range in values [Villanueva *et al*. 2015], and observations of D and H from the MAVEN IUVS echelle channel have shown much larger variations in the D and H densities over a martian year. This presentation will give an update on the next steps needed to understand hydrogen escape, including quantifying the rate and controlling factors.

2. Observational Data:

Hubble Space Telescope (HST) images of the H Ly α exosphere of Mars have shown the altitude distribution and its large seasonal changes since 2007 [Clarke *et al*. 2014, Bhattacharyya *et al.* 2017]. MEX SPICAM [Chaffin *et al*. 2014] and MAVEN IUVS spectra [Mayyasi *et al.* 2017] have tracked changes in the H and D emissions with a higher duty cycle but within the extended exosphere. The HST and MAVEN observations are also presented at this conference by Bhattacharyya *et al*. and Chaffin *et al*. Both emissions are highly variable, with maxima during Mars southern summer and just after perihelion. Several factors may contribute to the seasonal variations, including the changing solar EUV flux [Chaufray *et al*. 2015] and an added water flux from the lower atmosphere that might be caused either by gradual seasonal changes or more sudden upwelling, perhaps tied to dust storm activity [Chaffin *et al.* 2016; Heavens *et al.* 2018]. The extended series of data now being obtained may reveal the controlling factors from the timing of the changes.

3. Interpretation and Modeling:

Deriving densities of H and D requires modeling the radiative transfer of resonantly scattered solar Ly α emission in the martian upper atmosphere. The D emission is optically thin, and the H is optically thick, thus the D/H ratio is nonlinear with the emission brightnesses. Accurate absolute calibrations of the instruments are needed to obtain accurate densities, and there is a degeneracy in the models between density and temperature. In addition, the global HST images do not reveal local time variations in temperature and density, both of which are needed to estimate the global escape flux. The problem is further complicated by the expected presence of superthermal hydrogen, which is difficult to distinguish from the thermal component due to the weak gravity and large extent of the exosphere. These uncertainties, and activities underway to estimate the various processes, will be presented. We have adopted approaches to handle each of these uncertainties, including 1) an updated absolute calibration for improved accuracy in number densities, 2) fixing the upper atmospheric temperature with values measured by the NGIMS instrument on MAVEN, 3) an assumed variation in exospheric density from noon to midnight based on theoretical modeling, and 4) added information about the superthermal component from new HST observations that extend to particularly high altitudes.

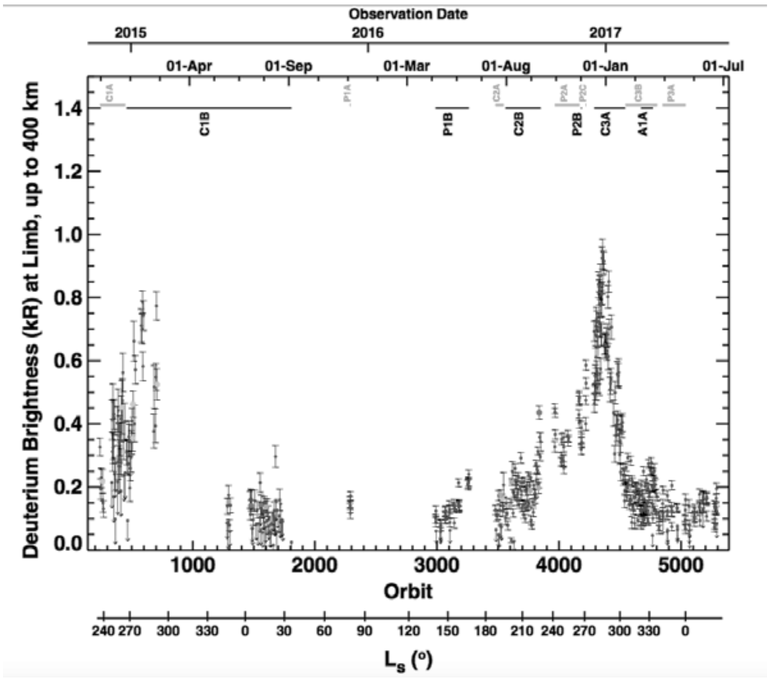

Figure 1: Measured brightness of the martian D Ly α emission measured with the MAVEN IUVS echelle channel, showing the large seasonal changes [Mayyasi *et al.* 2017].

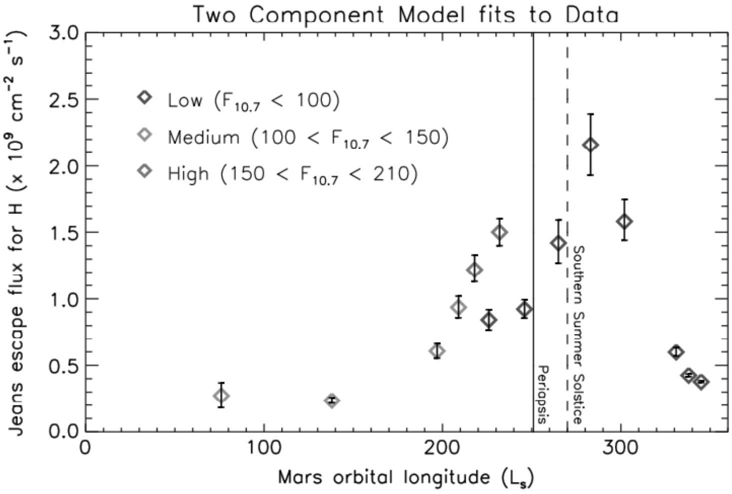

Figure 2: Derived hydrogen escape fluxes based on modeling HST images of the martian exosphere [Bhattacharyya *et al*., 2017].

4. References:

[1] Bhattacharyya, D. *et al*. (2017), *GRL, 4122*, 756-764.
[2] Chaffin, M. *et al.* (2014), *GRL, 41*, 314-320.
[3] Chaffin, M. *et al*. (2017), *Nature Geosci*., doi:10.1038/NGEO2887.
[4] Chaufray, J.L. *et al.* (2015), *Icarus, 245*, 282-294.
[5] Clarke, J.T. *et al.* (2014), *GRL, 41*, 8013-8020.
[6] Heavens, N. *et al.* (2018), *Nature Astr*., doi:10.1038/s41550-017-0353-4.
[7] Mayyasi, M. *et al.,* (2017), *J. Geophys. Res*., doi:10.1002/2017JA024666.
[8] Villanueva, G.L. *et al.* (2015), *Science, 348*, 218-221.

5. Acknowledgements:

This research was supported by NASA grants STScI GO-14752-01A to BU and MAVEN NNH1OCCO4C under a sub-contract to BU.

Seasonal Variability of Mars H Escape in the MAVEN IUVS dataset

M. Chaffin[1*], J.-Y. Chaufray[2], J. Deighan[1], N. M. Schneider[1], M. Mayyasi[3], J.T. Clarke[3], E. Thiemann[1], S.K. Jain[1], M. Crismani[1], A. Stiepen[4], F.G. Eparvier[1], W.E. McClintock[1], A.I.F. Stewart[1], G.M. Holsclaw[1], F. Montmessin[3], and B. M. Jakosky[1]
[1]LASP, Boulder, USA,
[2]LATMOS/IPSL, France,
[3]CSP, Boston University, Boston, USA,
[4]LPAP, University of Liege, Belgium

1. Mars Water Loss

Mars has lost a substantial fraction of its initial water, but an accurate determination of the integrated loss has proved elusive [1]. Multiple methods to estimate water loss exist, including extrapolation from D/H in near-surface water [2], and using inferred escape rates at present as a guide to loss throughout history [3,4,5]. Both methods suffer from incomplete information; D/H measured in water is not easily related to the global value, and contemporary escape rates cannot sample the range of conditions encountered by Mars in the past, including changes in obliquity and solar inputs. Here, we focus on interpreting MAVEN measurements of light scattered by thermospheric hydrogen to obtain present-day loss rates, filling in the timeline of Mars H loss as a function of season.

2. IUVS periapsis observations

MAVEN's elliptical orbit precesses in local time and latitude to sample a range of thermospheric conditions [6]. MAVEN's Imaging Ultraviolet Spectrograph observes at each periapsis [7], producing altitude profiles for 121.6 nm Lyman alpha scattered by thermospheric hydrogen (Figure 1).

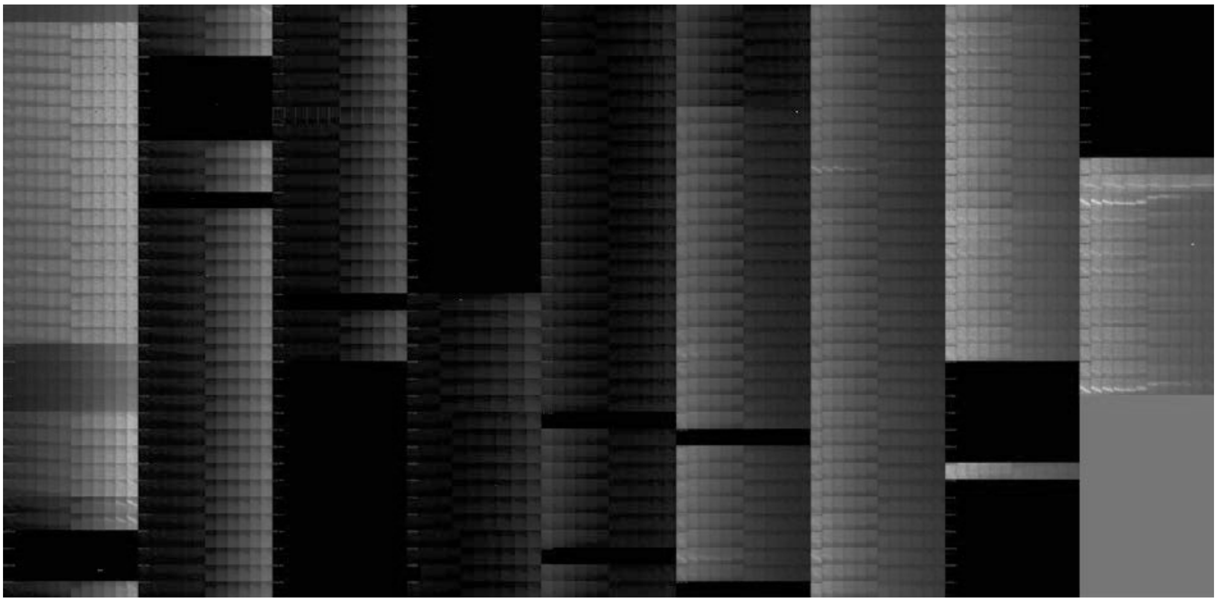

Figure 1: IUVS periapsis observed Lyman alpha for orbits 1-1000. Each orbit corresponds to a rectangle (orange box). Orbit number (time) for each periapsis pass increases down each column and subsequently across columns. Each pass contains 12 swaths, each swath contains 21 integrations and 7 bins along the slit. Altitude increases vertically in the first six swaths in each orbit, and reverses in the second six. Darkness at either end of a swath is produced by CO2 absorption at low altitudes, Proton aurora produces a distinct peak in some profiles, and some profiles are black due to instrument or data transmission issues.

Multiple scattering in the thermosphere and corona results in an optically thick emission, requiring a radiative transfer model to interpret brightness and produce H densities [8]. By comparing modelled and observed intensities, we can obtain estimates of escape rates from thermospheric emission (Figure 2). Simulated intensities do the best job of matching the data during Northern summer (Ls~90), but underpredict observed intensities in Southern summer, when the H corona has been observed to be most extended, and in observations made deep on the nightside, when in situ temperatures used in the modelling likely do not reflect local conditions. Of these two deficiencies, underprediction in southern summer is more problematic, and may indicated the presence of a seasonally-variable hot H population, as has been suggested in the past [5].

Building on these preliminary conclusions, we will present best-estimate H escape rates as a function of time based on MAVEN periapsis Lyman alpha measurements and compare with estimates based on in-situ data [9], producing a more complete record of Mars H escape rates. Further, we will compare processes and variability of Mars H escape with records of H escape at the Earth and Venus, which appear to exhibit far less dramatic seasonal variability than Mars.

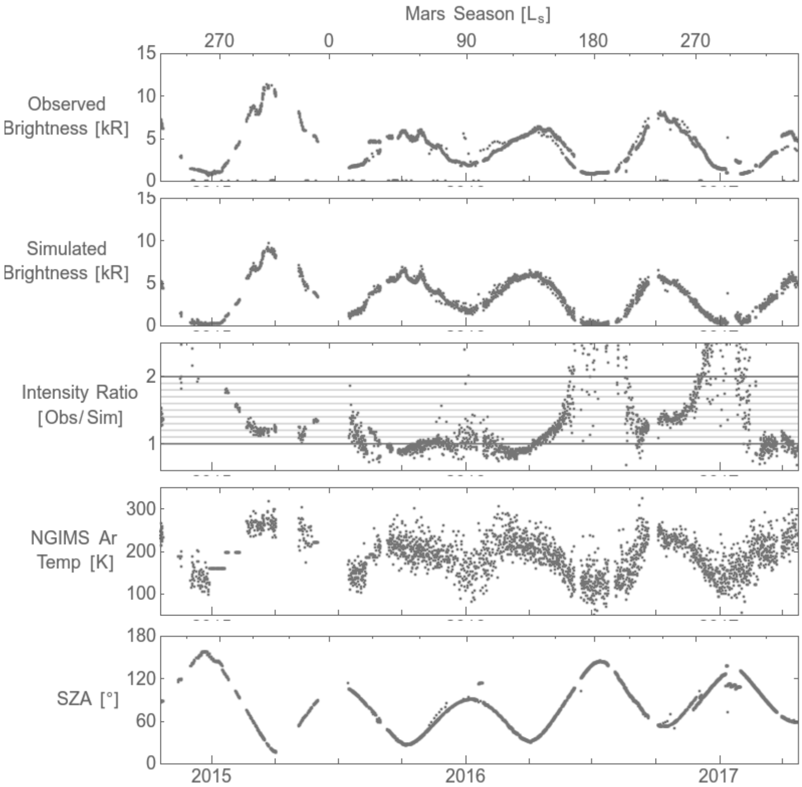

Figure 2: IUVS periapsis observations compared with model predictions. Panels show (from top to bottom) observed brightness from IUVS in the middle scan of each periapsis pass; best-fit simulated brightness for each observation; intensity ratio observed/simulated; in-situ Argon scale-height temperature from NGIMS, used to obtain best-fit simulated brightness; solar zenith angle of observation line-of-sight tangent point.

3. References

[1] Carr, M.H., and Head, J.W.: Martian surface/near-surface water inventory: Sources, sinks, and changes with time, Geophys. Res. Lett., Vol. 42, pp. 726–732, 2015.
[2] Villanueva, G.L. et al.: Strong water isotopic anomalies in the Martian atmosphere: Probing current and ancient reservoirs, Science, Vol. 348, pp. 218-221, 2015.
[3] Chaffin, M.S., et al.: Unexpected variability of Martian hydrogen escape, Geophys. Res. Lett., Vol. 41, pp. 314–320, 2014.
[4] Clarke, J.T. et al.: A rapid decrease of the hydrogen corona of Mars, Geophys. Res. Lett., Vol. 41, pp. 8013-8020, 2014.
[5] Bhattacharyya, D., et al.: A strong seasonal dependence in the Martian hydrogen exosphere, Geophys. Res. Lett., Vol. 42, pp. 8678–8685, 2015.
[6] Jakosky, B.M., et al.: The Mars Atmosphere and Volatile Evolution (MAVEN) Mission, Space Science Reviews, Volume 195, pp. 3-48, 2015.
[7] McClintock, W.E., et al.: The Imaging Ultraviolet Spectrograph (IUVS) for the MAVEN Mission, Space Science Reviews, Vol 195, pp. 75-124, 2015.
[8] Chaufray, J.-Y. et al.: Observation of the hydrogen corona with SPICAM on Mars Express, Icarus, Vol. 195, pp. 598–613, 2008

Solar cycle dependence on the H+/O+ flux ratio in Venus' magnetotail

M. Persson[1*]; *Y. Futaana*[1], *A. Fedorov*[2], *S. Barabash*[1]
[1]*Swedish Institute of Space Physics, Sweden,*
[2]*IRAP, CNRS, France*

1. Introduction

Billions of years ago, Venus was a humid planet. Today Venus' atmosphere is very arid. Water may have been lost through a number of different processes [1, 2]. Any water present in the upper atmosphere of Venus may be photo dissociated by the incoming solar EUV radiation and escape as H+ and O+ ions. The ratio of H+/O+ flux escaping from Venus have been investigated, using Venus Express (VEx) data, resulting in the ratio close to 2 [3-6], which is the stoichiometric ratio of a water molecule. All these studies were made during the solar minimum (2006-2009). In this study, we extend the analysis of the H+/O+ flux ratio in the magnetotail using all available data from Venus Express (VEx) during 2006-2014.

2. Data set

We use the data acquired from Ion Mass Analyser (IMA), a part of the ASPERA-4 (Analyser of space plasma and energetic atoms) instrument package, onboard the VEx mission [7]. VEx had a polar orbit around Venus during 2006-2014, with a nominal pericentre of 250 km and a 24-hour orbit, which gave more than 3000 orbits in total [8]. The IMA instrument uses electrostatic deflector plates to determine the direction of the ions, which with its cylindrical symmetry gives a 2□ sr field-of-view. An electrostatic analyser measures the ion energy per charge (0.01-15 keV) and an assembly of permanent magnets separate the mass per charge of the ions onto the detector plate [7].

3. Results

We use the density and velocity vector of the protons and heavy ions [4] to calculate the flux of each species. We then produced maps of ion fluxes in the Venus' magnetotail. We then calculate the escape rates through dividing the full data set (2006-2014) into several time periods, corresponding to different solar activities. Our results indicate that the H+/O+ ratio in the Venusian magnetotail is strongly dependent on the solar activity. Near solar maximum the H+/O+ flux ratio was found to be higher than during solar minimum. However, it is not straightforward to calculate the escaping flux, particularly for protons, since the separation of the solar wind and planetary protons is challenging [3]. In addition, a complicated velocity field in the magnetotail during solar maximum, with a strong azimuthal flow [9] that potentially represents a different proton dynamics than that during solar minimum, makes the calculations more complex. In this presentation, we will discuss the dynamics of H+ and O+ in the Venusian tail, and the escape ratio dependence on the solar cycle.

4. References

[1] Lammer *et al*.: Loss of hydrogen and oxygen from the upper atmosphere of Venus, Planetary and Space Science, Vol. 54, Nr. 13, pp. 1445-1456, 2006.

[2] Futaana *et al*.: Solar wind interaction and impact on the Venus atmosphere, Space Science Reviews, Vol. 212, Nr. 3, pp. 1453-1509, 2017.

[3] Barabash, S. *et al*.: The loss of ions from Venus through the plasma wakes, Nature, Vol. 450, pp. 650-653, 2007.

[4] Fedorov *et al*.: Measurements of the ion escape rates from Venus for solar minimum, Journal of Geophysical Research, Vol. 116, Nr. A07220, 2011.

[5] Nordström *et al*.: Venus ion outflow estimates at solar minimum: Influence of reference frames and disturbed solar wind conditions, Journal of Geophysical Research: Space Physics, Vol. 118, Nr. 6, pp. 3592-3601, 2013.

[6] Lundin *et al*.: Ion acceleration and outflow from Mars and Venus: An overview, Space Science Reviews, Vol. 162, Nr. 1, pp. 309-334, 2011.

[7] Barabash, S. *et al*.: The analyser of space plasmas and energetic atoms (ASPERA-4) for the Venus Express mission, Planetary and Space Science, Vol. 55, pp. 1772-1792, 2007.

[8] Svedhem *et al*.: Venus Express – the first European mission to Venus, Planetary and Space Science, Vol. 55, pp. 1636-1652, 2007.

[9] Kollman *et al*.: Properties of planetward ion flows in Venus' magnetotail, Icarus, Vol. 274, pp. 73-82, 2016.

Escape and precipitation rates at Venus

P. Kollmann[1*], P. C. Brandt[1], G. Collinson[2], Z. Jin Rong[3], Y. Futaana[4], T. L. Zhang[5]
[1]The Johns Hopkins University Applied Physics Laboratory (JHU/APL), USA
[2] NASA Goddard Spaceflight Center (GSFC), USA
[3] Swedish Institute of Space Physics (IRF), Sweden
[4] Chinese Academy of Sciences, China
[5] Space Research Institute (IWF), Austria

1. Introduction

Venus is continuously losing parts of its atmosphere into space. A large fraction of this escape occurs in the form of ions flowing down along Venus' magnetotail. Many studies followed these ions in order to constrain the atmospheric escape [1, 2]. Interestingly, there are also ions in the magnetotail that return to Venus (Fig. 1). These flows, their properties, and possibilities for the underlying physics have been barely studied in the past.

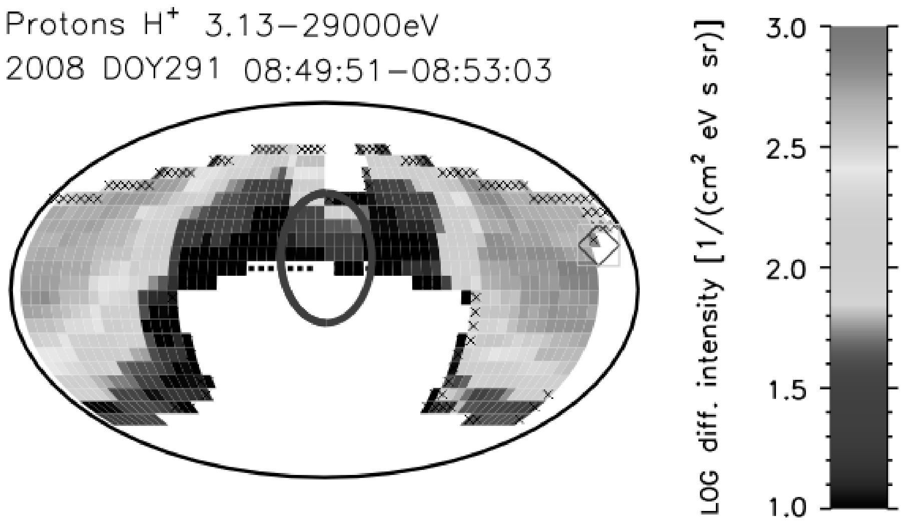

Figure 1: Illustration of protons in Venus' magnetotail that are flowing back the planet instead of escaping. The figure shows the directional distribution of proton intensities in a Mollweide projection. The violet circle in the centre is the limb of Venus. Red areas on the sides indicate high intensities coming from "behind" and flowing towards Venus. The centre of the bulk flow is marked with a green square.

2. Results

In our analysis [3], we find that the planetward flow rate decreases with EUV irradiance (Fig. 2). This irradiance changes over the 11-year solar cycle and over the age of our Sun. Since we also find that the planetward return rate is comparable to the escape rate, the relation between EUV and return flows also affects the net atmospheric escape. It turns out that the relation between net escape and EUV irradiance scales opposite to Mars [4], even though Mars is an unmagnetized planet as Venus (Fig. 2). This needs to be taken into consideration for theoretical studies on exoplanetary atmospheres.

Planetary flows, as we observe them at Venus, are often associated with magnetic reconnection. However, we find that the bulk of these flows do not correlate with proximity to the magnetotail current sheet, as it would be expected from magnetic reconnection. Instead, we find that the flows we observe are consistent with flows that naturally emerge from pickup ions moving in the magnetic environment of Venus.

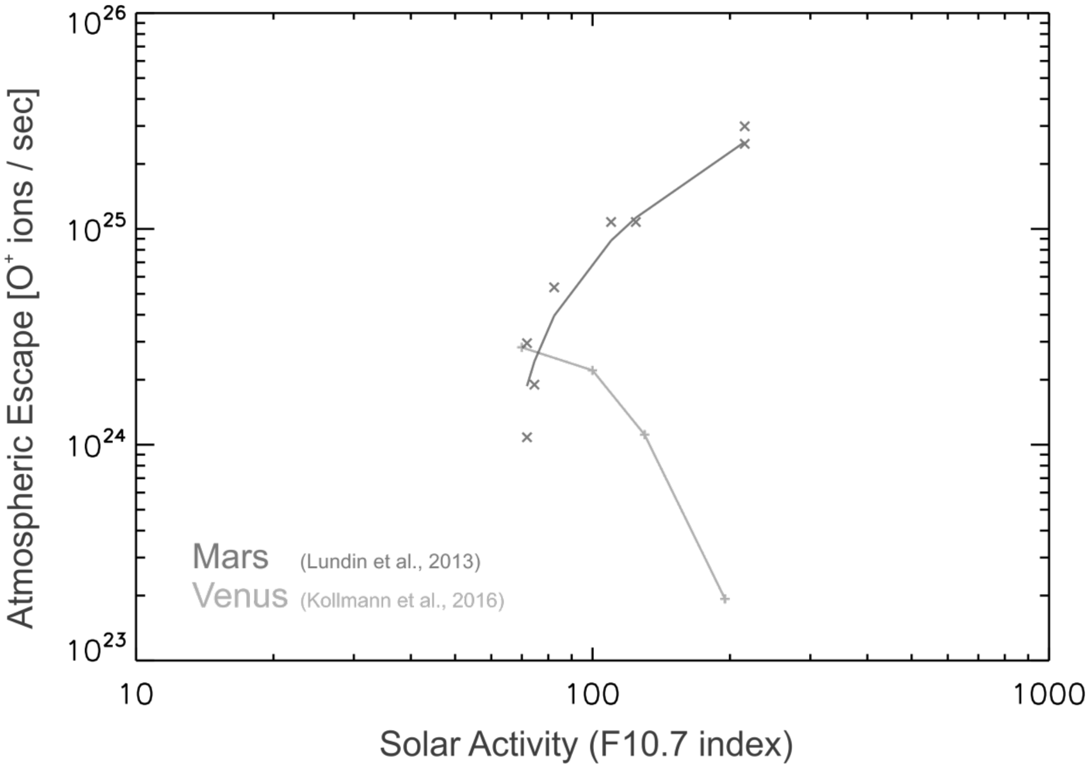

Figure 2: Net atmospheric ion escape rates of Venus (blue) and Mars (red) as a function of solar activity.

3. References

[1] Fedorov, A., et al.: Measurements of the ion escape rates from Venus for solar minimum, J. Geophys. Res., doi:10.1029/2011JA016427, 2011.
[2] Masunaga, K., et al.: Dependence of O^+ escape rate from the Venusian upper atmosphere on IMF directions. Geophys. Res. Lett,. doi:10.1002/grl.50392, 2013.
[3] Kollmann, P., et al.: Properties of planetward ion flows in Venus' magnetotail, Icarus, doi:10.1016/j.icarus.2016.02.053, 2016.
[4] Lundin, R., et al.: Solar cycle effects on the ion escape from Mars, Geophys. Res. Lett., doi:10.1002/ 2013GL058154, 2013.

Atmospheric Escape on Earth

R. J . Strangeway[1*]; C. T. Russell[1]; J. G. Luhmann[2]; T. E. Moore[3]; J. C. Foster[4]; S. V. Barabash[5]; H. Nilsson[5]; D. Brain[6]
[1]Dept. of Earth, Planetary and Space Science, UCLA, USA,
[2]Space Sciences Laboratory, USA
[3]NASA Goddard Space Flight Center, USA
[4]MIT Haystack Observatory, USA
[5]IRF Swedish Institute of Space Physics, Sweden
[6] Laboratory for Atmospheric and Space Physics, University of Colorado, USA

1. Introduction

The contemporary ion outflow rates for the terrestrial planets Earth, Mars, and Venus are all comparable, of the order 10^{25} ions/s. For Venus and Mars these rates depend on a variety of factors, but the primary of these are solar EUV and the dynamic pressure of the solar wind. The presence of crustal magnetic fields at Mars further complicates the picture, but in general at Venus and Mars ion outflows are through direct interaction with the solar wind. This is not the case at the Earth, which has a large magnetic field. Here the interaction is more indirect. The solar wind couples to the Earth's magnetosphere through magnetic field reconnection. This allows both electromagnetic and plasma energy fluxes to propagate into the polar ionosphere. These energy fluxes result in energization of ionospheric ions, which can escape into the magnetosphere. Here we review the underlying processes that drive ionospheric escape at the Earth, as well as the possible loss of these ions to the solar wind.

2. Connections between inflowing energy fluxes and outflowing ions

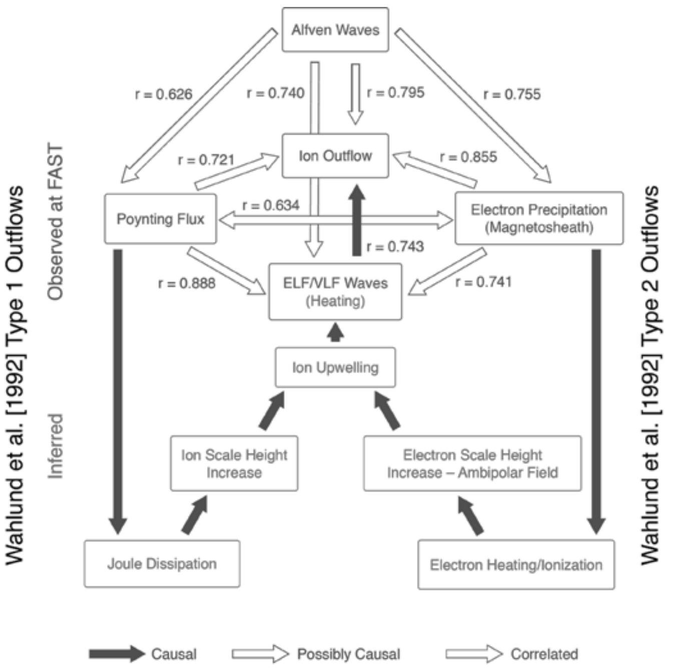

Figure 1: Connections between inflowing energy and outflowing ions.

Observations from the low altitude Fast Auroral Snapshot Small Explorer [FAST] have been used to relate Poynting flux and electron precipitation to ion outflows [1], and, more recently, to Alfvén waves [2]. The connections between the observables at FAST and the associated processes are shown in Figure 1 (adapted from [1] to include the results of [2]). The upper half of the flow chart shows the phenomena observed by FAST, with the numbers giving the correlation coefficients from log-log regression of the connected parameters. The lower half of the diagram refers to the physical processes that lead to the outflows observed at FAST. While labelled "inferred" because they were not directly observable by FAST, radar observations [3] show the connection between ion and electron heating and upwelling, with outflows associated with Joule dissipation labelled as Type 1 outflows, whereas outflows driven by electron heating are referred to as Type2.

The processes marked in red in Figure 1 are also incorporated in physics based models for the polar wind. One such model has recently been extended to include wave-induced transverse heating, which is not normally included in the models [4]. This heating is necessary to provide the energization to several tens of eV required for oxygen ions to escape the gravitational potential well. One characteristic of the modelling effort is that the ion fluxes have a maximum value. The results of the model are compared with FAST data in Figure 2.

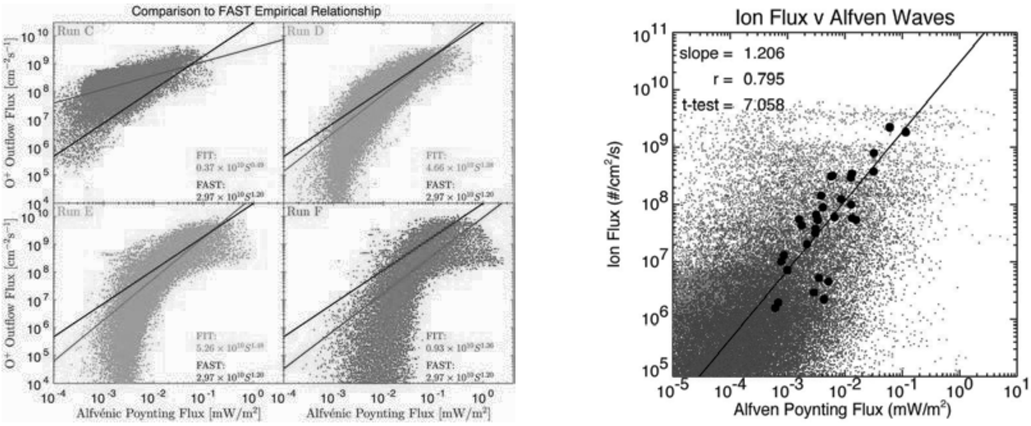

Figure 2: Flux limitation from a set of simulations [4] (left) compared to FAST observations (right).

The left hand set of plots in Figure 2 show the outflow fluxes for several runs of the simulation model described in [4]. The right hand plot shows the data used to generate the scaling law that is compared to the model. The black dots are the orbit averages used to derive the scaling law, while the red dots show 1 second averages for the dayside, and the blue dots 1 second averages for the nightside. Both the model and the data show an upper limit below 10^{10} $cm^{-2}s^{-1}$. If the fluxes are assumed to be coming from a 10˚ by 10˚ area at the ionosphere, the net escaping flux would be of order 10^{26} ions/s, comparable to the net storm time flux reported by [5].

3. Consequences for atmospheric loss

The peak net flux cited above is larger than typical outflows at Venus and Mars, but this flux is highly variable. In addition, it is not clear how much of this flux would eventually leave the Earth's magnetosphere and be lost. One pathway for escape is transport downtail on lobe field lines, but some of the lobe ions will also be transported onto closed field lines, to form part of the ring current and plasma sheet. These ions could in turn be lost through the dayside magnetopause. The models are becoming sufficiently sophisticated, however, that it will be possible in future studies to better quantify both the outflows and the net loss to the solar wind of the Earth's ionosphere as function of the solar wind drivers. This will in turn enable us to extrapolate to earlier times to compare global loss rates for the terrestrial planets for the young solar system, when Venus and Mars are thought to have lost most of their water.

4. References

[1] Strangeway, R. J., R. E. Ergun, Y.-J. Su, C. W. Carlson, and R.C. Elphic, Factors controlling ionospheric outflows as observed at intermediate altitudes, J. Geophys. Res., 110, A03221, doi:10.1029/2004JA010829, 2005.
[2] Brambles, O. J., W. Lotko, B. Zhang, M. Wiltberger, J. Lyon, and R. J. Strangeway, Magnetosphere sawtooth oscillations induced by ionospheric outflow, Science, 332(6034), 1183-1186, doi:10.1126/science.1202869, 2011.
[3] Wahlund, J.-E., H. J. Opgenoorth, H. I. Häggström, K. J. Winser, G. O. L. Jones, EISCAT observations of topside ionospheric ion outflows during auroral activity: revisited, J. Geophys. Res., 97, 3019-3037, 1992.
[4] Varney, R. H., M. Wiltberger, B. Zhang, W. Lotko, and J. Lyon, Influence of ion outflow in coupled geospace simulations: 1. Physics-based ion outflow model development and sensitivity study, J. Geophys. Res. Space Physics, 121, 9671–9687, doi:10.1002/2016JA022777, 2016.
[5] Yau, A. W., M. André, Sources of ion outflow in the high latitude ionosphere, Space Sci. Rev., 80, 1-25, 1997.

Ion Outflow from the Terrestrial Atmosphere: Sources, Mechanisms, Transport and Consequences.

S. Haaland[1,2]
[1]BCSS, University of Bergen, Norway
[2]Max-Planck-Institute, Germany

1. Introduction

The terrestrial ionosphere is a significant contributor of plasma to the magnetosphere. In this talk, we review some of the recent results from the Cluster mission with focus on cold ion escape from the polar cap regions. Characteristics of the outflow, including species involved, source regions, acceleration mechanisms, transport and fate of the escaping ions are discussed. We also briefly discuss possible consequences of cold ions magnetospheric properties and processes.

Simultaneous detection of terrestrial ionospheric molecular ions in the Earth's inner magnetosphere and at the Moon

I. Dandouras[1*]; A. R. Poppe[2,3], M. O. Fillingim[2], L. M. Kistler[4], C. G. Mouikis[4], and H. Rème[1]
[1]IRAP, Université de Toulouse, CNRS, UPS, CNES, France
[2]Space Sciences Laboratory, University of California, Berkeley, USA
[3]Solar System Exploration Research Virtual Institute, NASA Ames Research Center, USA
[4]Department of Physics and Space Science Center, University of New Hampshire, USA

1. Introduction

Heavy molecular ions escaping from a planetary atmosphere can contribute to the long-term evolution of its composition.

The ARTEMIS (Acceleration, Reconnection, Turbulence, and Electrodynamics of the Moon's Interaction with the Sun) spacecraft has recently observed outflowing molecular ions at lunar distances in the terrestrial magnetotail [1]. Backward particle tracing indicated that these ions should originate from the terrestrial inner magnetosphere.

Here we have examined Cluster spacecraft data acquired by the CIS-CODIF (Cluster Ion Spectrometry-Composition Distribution Function) ion mass spectrometer, obtained in the terrestrial magnetosphere. Events were selected for which the orbital conditions were favourable and the Cluster spacecraft were in the high-latitude inner magnetosphere a few hours before the ARTEMIS molecular ion detection, a time compatible with the transfer to lunar distances.

2. Results

Our analysis shows that during these events the CIS-CODIF instrument detected, in upwelling ion beams and in the ring current, a series of energetic ion species including not only O^+ but also a group of molecular ions around ~30 amu, which could include N_2^+, NO^+, or O_2^+. The events were during active periods, with CME (Coronal Mass Ejections) arrivals followed by a northward rotation of the IMF (Interplanetary Magnetic Field).

Although energetic heavy molecular ions have been detected in the storm time terrestrial magnetosphere in the past (e.g. [2], [3]), these events constitute the first coordinated observation in the Earth's inner magnetosphere and at the Moon. They show that molecular ion escape, during active periods, is an additional escape mechanism (with respect to the atomic ion escape). Quantifying these mechanisms is important in order to understand the long-term (billion years scale) evolution of the atmospheric composition, and in particular the evolution of the N/O ratio, which is essential for habitability. Terrestrial heavy ions, transported to the Moon, suggest also that the Earth's atmosphere of billions of years ago may be preserved on the present-day lunar regolith [4].

3. Perspectives

Future missions, as the proposed ESCAPE mission, should investigate in detail the mechanisms of atomic and molecular ion acceleration and escape, their link to the solar and magnetospheric activity, and their role in the magnetospheric dynamics and in the long-term evolution of the atmospheric composition.

4. References

[1] Poppe, A. R., Fillingim, M. O., Halekas, J. S., Raeder, J., and Angelopoulos, V.: ARTEMIS observations of terrestrial ionospheric molecular ion outflow at the Moon, Geophys. Res. Lett., doi: 10.1002/2016GL069715, 2016.
[2] Klecker, B., Möbius, E., Hovestadt, D., Scholer, M., Gloeckler, G., and Ipavich, F. M.: Discovery of energetic molecular ions (NO^+ and O_2^+) in the storm time ring current, Geophys. Res. Lett., 13(7), 632–635, 1986.
[3] Christon, S. P., et al.: Energetic atomic and molecular ions of ionospheric origin observed in distant magnetotail flow-reversal events, Geophys. Res. Lett., 21(25), 3023–3026, 1994.
[4] Terada, K., et al.: Biogenic oxygen from Earth transported to the Moon by a wind of magnetospheric ions, Nature Astro., doi: 10.1038/s41550-016-0026, 2017.

Atmospheric loss from Earth's plasma mantle and its dependence on solar wind conditions

A. Schillings[1,2*]; R. Slapak[3], H. Nilsson[1], M. Persson[1], R. Ramstad[1], Y. Futaana[1].
[1]Swedish Institute of Space Physics, Sweden,
[2] Division of Space Technology, Luleå University of Technology, Sweden
[3] EISCAT Scientific Association, Sweden

1. Introduction

The Earth's atmospheric loss is an important phenomenon affecting the evolution of the atmosphere on geological timescales. The Earth's ion escape response to the solar wind conditions provided by magnetic storms are of particular interest as these are thought to be similar to the magnetic conditions billion years ago in the ancient solar system [1]. This terrestrial phenomenon is driven by atmospheric ions, mainly oxygen ions (O^+) heated through different processes and with sufficient energy to escape the gravity, and becoming outflow. Outflowing O^+ can take different paths, flowing back in the plasma sheet (low velocity O^+), escaping through the far magnetotail or directly escaping into the solar wind for the highest velocity ions [2].

The outflowing ions are observed at low and high altitudes in the open magnetic field line regions called the polar cap, cusp and plasma mantle. The polar cap and plasma mantle configuration changes under strong solar wind conditions (high density and velocity), which allows higher solar wind flux to penetrate these regions. However, it is not well understood how strong solar wind affects the O^+ escape rate even though several studies have already investigated this topic [3], [4]. Thus, this study aims to answer how the O^+ escape rate depends on the solar wind parameters.

2. Data and method

To calculate the O^+ escape rate under different solar wind constraints, we used the O^+ data from the CODIF instrument onboard the European Cluster spacecraft 4 [5], the solar wind data propagated at Earth from the ACE satellite (NASA) and the EUV flux measured by the SEE instrument onboard TIMED [6]. The O^+ escape rate is calculated over a five years period (2001-2005). In this study, we limit the discussion on O^+, which have an atmospheric origin. We may further investigate the H^+ flux, but it is beyond the scope of this study.

Similar to previous studies of ion escape at Mars by [7], [8], we defined solar wind constraints by plotting the distribution between the solar wind velocity and density for time period with available O^+ observations in the plasma mantle (Fig. 1). In Fig. 1, we divided the upstream solar wind density/velocity parameter space in low, medium, and high (thus we have 9 solar wind constraints). Measurements of O^+ outflow in the plasma mantle under similar (binned) conditions are combined to yield maps of average O^+ outflow. Subsequently, integration over shells gives the total escape rates in the plasma mantle. Analogously, we also investigated the O^+ escape rate dependence on solar EUV flux (defined as the ratio of the EUV intensity over the photon energy) and the solar wind dynamic pressure.

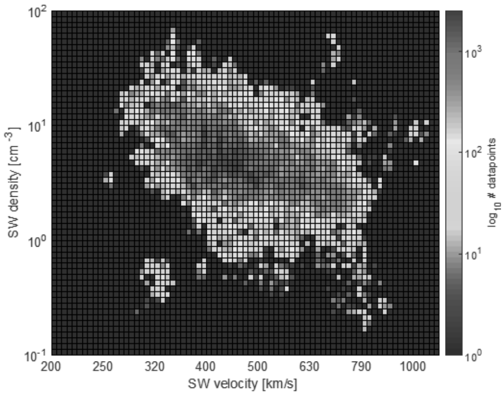

Figure 1: Distribution of upstream ACE solar wind parameters for Cluster measurements of O^+ in the plasma mantle between 2001 and 2005. The colourbar represents the number of observations in each bin. Note that all axes are scaled logarithmically.

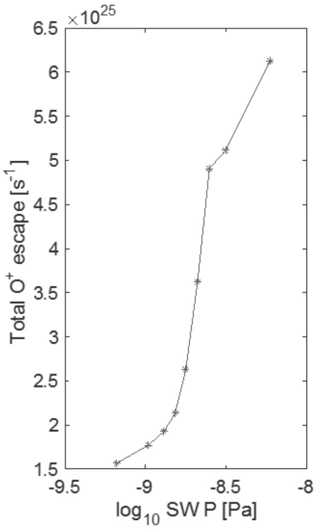

Figure 2: Total O^+ escape rate [s^{-1}] as a function of the solar wind dynamic pressure [Pa]. The O+ escape increases with the dynamic pressure.

3. Results

For the first solar wind constraints, the O^+ flux in the plasma mantle increases with increased solar wind velocity and density. Consequently, the O^+ escape rate follows this tendency and is higher as well. The O^+ escape rate also increases with solar wind dynamic pressure as shown in Fig. 2. However, the EUV flux does not have a significant influence on the O^+ escape rate.

4. Discussion

The terrestrial atmospheric loss, in particular for O^+, is affected by different solar wind conditions. Our results demonstrate that a higher O^+ escape rate is observed under higher solar wind density, velocity and consequently dynamic pressure (see Fig. 2). This result can be explained by considering that energetic (high solar wind velocity, density and dynamic pressure) solar wind penetrates into the dayside magnetosphere. The stronger convection in the cusp regions provides a greater energy transfer from the penetrating solar wind, heating and accelerating O^+. During those disturbed conditions, a significant amount of atmospheric O^+ are flowing upwards and gain sufficient energy to escape into the solar wind. However, the O^+ escape rate is independent of the EUV flux, which is unexpected because EUV flux has a strong influence on outflow from Martian atmosphere. Despite the denser source region, it seems that the outflow does not increase in a period of high EUV flux as compared to those with less EUV. This may indicate that the ion escape process is energy limited rather than source region density limited.

5. Conclusion

We estimated the O^+ escape rate in the plasma mantle region for different solar wind conditions. Our results imply that the higher solar wind flux penetrates into the magnetosphere, the higher O^+ rates. Therefore, atmospheric loss (including O^+) depends on solar wind conditions. Considering that solar wind from the young Sun was stronger [9], solar wind driven O^+ escape can be expected to have had a significant influence on the evolution of the Earth's atmosphere. Questions remain regarding how does the intrinsic magnetic field protect Earth from significant solar wind penetration and our atmosphere from atmospheric loss, and will the atmosphere continue to lose O^+ on a longer timescale and become a Martian-like atmosphere.

6. References

[4] Elliott H. A., R. H. Comfort, P. D. Craven, M. O. Chandler and T. E. Moore, "Solar wind influence on the oxygen content of ion outflow in the high-altitude polar cap during solar minimum conditions," *J.Geophys. Res.: Space Physics,* vol. 106, pp. 6067-6084, 2001.

[5] Escoubet C. P., M. Fehringer and M. Goldstein, "IntroductionThe Cluster mission," *Ann.Geophys.,* vol. 19, pp. 1197-1200, 10 2001.

[1] Krauss S., B. Fichtinger, H. Lammer, W. Hausleitner, Y. N. Kulikov, I. I. Ribas, V. I. Shematovich, D. Bisikalo, H. I. M. Lichtenegger, T. V. Zaqarashvili, M. L. Khodachenko and A. Hanslmeier, "Solar flares as proxy for the young Sun: satellite observed thermosphere response to an X17.2 flare of Earth's upper atmosphere," *Ann. Geophys.,* vol. 30, pp. 1129-1141, 8 2012.

[3] Lennartsson O. W., H. L. Collin and W. K. Peterson, "Solar wind control of Earth's H^+ and O^+ outflow rates in the 15-eV to 33-keV energy range," *J. Geophys. Res. (Space Physics),* vol. 109, p. A12212, 12 2004.

[7] Ramstad R., S. Barabash, Y. Futaana, H. Nilsson and M. Holmström, "Global Mars-solar wind coupling and ion escape," *J. Geophys. Res.: Space Physics,* vol. 122, pp. 8051-8062, 2017.

[8] Ramstad R., S. Barabash, Y. Futaana, H. Nilsson, X.-D. Wang and M. Holmstr{\~A}¶m, "The Martian atmospheric ion escape rate dependence on solar wind and solar EUV conditions: 1. Seven years of Mars Express observations," *J. Geophys. Res.: Planets,* vol. 120, pp. 1298-1309, 2015.

[2] R. Slapak, H. Nilsson, L. G. Westerberg and A. Eriksson, "Observations of oxygen ions in the dayside magnetosheath associated with southward IMF," *Journal of Geophysical Research (Space Physics),* vol. 117, p. A07218, 7 2012.

[9] Wood, B.E "The solar wind and the Sun in the past", Space Sci. Rev., 126, 3-14, doi:10.1007/s11214-006-9006-0

[6] Woods T. N., S. Bailey, F. Eparvier, G. Lawrence, J. Lean, B. McClintock, R. Roble, G. J. Rottman, S. C. Solomon, W. K. Tobiska and O. R. White, "TIMED Solar EUV experiment," *Physics and Chemistry of the Earth, Part C: Solar, Terrestrial & Planetary Science,* vol. 25, pp. 393-396, 2000.

Mars Atmospheric Loss at the Present and Integrated Loss Through Time As Observed by MAVEN

B. M. Jakosky[1] *and the MAVEN Science Team*
[1]*Laboratory for Atmospheric and Space Physics, University of Colorado at Boulder, USA*

1. Introduction There is compelling evidence that liquid water was abundant on early Mars, despite Mars being too cold today to sustain significant amounts of liquid water. The most likely explanation, especially in the face of the Sun having been dimmer early in its history, is that early Mars had a more-effective greenhouse atmosphere. Measurements from spacecraft and from the surface over the last several decades indicate that there are insufficient carbonate deposits to hold enough CO_2 from this early, thicker atmosphere to provide significant warming. In that context, the *Mars Atmosphere and Volatile Evolution* (*MAVEN*) mission was designed to explore in detail the loss of gas to space occurring at the present epoch; this would allow determination of the integrated loss to space through time and the ability of loss to space to explain the changes inferred for the Martian climate. We report here the loss rates derived through a full Mars year of *MAVEN* observations, and use these loss rates to extrapolate back in time to get the time-integrated loss to space. These will allow us to determine the role that loss to space played in the changes in climate inferred from the surface morphology and mineralogy.

MAVEN has been observing the Mars upper atmosphere, ionosphere, and magnetosphere, along with the solar and solar-wind energetic inputs into the system. The goals are to determine the composition, structure, and behavior of the system and how they are controlled by the energetic drivers, the current rates of loss to space and how they are controlled by the energetic drivers, and properties that allow us to determine the integrated loss to space through time. *MAVEN* has made science observations for about 1.75 Mars years as of the time of the conference.

2. Results: *MAVEN* observations have been used to derive the rates of loss of gas to space:

2.1. Hydrogen loss*.* Hydrogen is created in the upper atmosphere from the photodissociation of H_2O in the lower and middle atmosphere and the transport of the H upward. The H atom is light enough that those atoms in the high-energy tail on the Boltzmann distribution and residing above the nominal exobase will have enough energy to escape to space. This thermal (or Jeans) escape is likely to be the main mechanism by which H is lost to space. The combination of escaping atoms and atoms having sufficient energy to travel ballistically to high altitudes but not to escape creates an extended corona of H atoms surrounding Mars; this corona can extend out past 10 R_M or greater. For the range in observed column abundance and temperature of H in the corona, the loss rate is inferred to vary with season during the Mars year between ~ 1-11 x 10^{26} H s^{-1}. This is equivalent to a loss rate of ~ 160-1800 g H s^{-1}. At this rate, the entire column of atmospheric water at present (nominally, about 10^{-3} g/cm^2) would be removed in between ~ 3000 - 30,000 years. Over 4 b.y., loss at this rate would be able to remove a global layer of water between ~ 3-24 m thick.

2.2. Oxygen ion loss*.* Ion loss occurs via the acceleration of ions in an electric field. The electric field can be generated by the moving magnetic field of the impinging solar wind or by the motion of ions around the magnetic field in magnetic cusp regions associated with the crust. The integrated escape is obtained by summing up the loss across the planet, breaking the loss into separate O^+ and O_2^+ rates. The net global loss rate for O is 5 x 10^{24} s^{-1}, equivalent to a loss rate of ~130 g O s^{-1}. If loss occurred at this constant rate, the entire column of atmospheric O (present mainly as CO_2) would be removed in 3 b.y.

2.3. Photochemical loss*.* Photodissociation can ionize O_2 or N_2. When the electrons and ions recombine, the energy is released via one of multiple pathways. In some of the recombinations, the energy is sufficient both to break the O_2 bond and to give each of the resulting O atoms an amount of energy (as kinetic energy) greater than the escape energy from Mars; when recombination occurs above the exobase, such that the upward-moving atom will not hit anything, it will escape to space. *MAVEN* does not measure the escaping neutral O atoms. But it does measure the upper-atmospheric ion composition and electron properties, allowing the photodissociation and recombination rates and the resulting escape rate to be calculated. The loss rate can be calculated for each orbit. The average O loss rate inferred from these observations is 5 x 10^{25} O s^{-1}, equivalent to 1300 g O s^{-1}. At this rate, the O present as CO_2 in today's atmosphere would be lost in 300 m.y.

2.4. Sputtering loss*.* The electric field generated by the solar wind will accelerate ions in one hemisphere (relative to the magnetic field) away from the planet causing them to escape, and from the other hemisphere into the planet where they collide with molecules in the upper atmosphere. When these ions collide at high velocities (up to twice the solar-wind velocity, or nearly 1000 km/s), they can physically knock upper-atmospheric constituents out of the atmosphere. This sputtering process can be very effective in removing neutral atoms (and is the only significant mechanism for removing species such as argon, which is a noble gas). *MAVEN* does not measure escaping neutrals. However, we can measure the properties of the incoming ions (composition and speed) and the composition of the upper-atmospheric target onto which they impinge. From these, we can calculate the sputtering loss yield based on well-developed theories of sputtering. For the coverage obtained during the year of observations, the average loss rate is ~3 x 10^{24} O s^{-1}, equivalent to ~80 g O s^{-1}. At this loss rate, it would take more than 4 b.y. to remove the atmospheric column of O.

2.5. Integrated loss rates. We can sum up the loss as observed or inferred during this one Mars year. The loss of H, over 4 b.y., would result in loss of an equivalent of a global layer of H_2O between 3 – 24 m thick. The total loss rate of O at present is 6 x 10^{25} O s^{-1}. At this rate, the present column of atmospheric O would be lost in about 250 m.y.; equivalently this would remove a total of ~75 mbar of CO_2 over 4 billion years.

2.6. Extrapolation back in time*.* These rates are not expected to have been constant in time. The major factors that were different early in Mars history were the EUV flux from the Sun and the nature of the solar wind. These were recognized as being important drivers of the escape rate by each of the above processes by Luhmann et al. (1992), and the extrapolations to early times indicated that loss rates could have been orders of magnitude greater than they are today. These models have been updated as our understanding of the evolution of sun-like stars and of the escape processes themselves have improved. We use the most-recent integrated model, that of Chassefiere and Leblanc (2013), to extrapolate back in time.

When integrated through time, the integrated loss of O is equivalent to loss of greater than 0.5 bar of CO_2, 15 m global equivalent layer of water, or some combination of the two depending on the source of the O. Our extrapolation makes these numbers a conservative estimate, with the actual loss possibly being considerably larger.

Loss of H is more difficult to extrapolate into the past. We do not as yet fully understand what drives the seasonal behavior of the abundance of H in the corona and of the escape rate. While the suggestion of dust allowing H_2O to rise higher during southern summer and be photodissociated closer to the exobase is plausible, it has not been cleanly demonstrated. Even if it is correct, we do not as yet understand the seasonal variability in either the dust cycle or the lower-atmosphere water cycle well enough to determine whether the year observed by *MAVEN* is representative of the current epoch, or even whether the extreme high or low values of H escape rate might be representative. Even if we understood the present-day H loss rate, it would be difficult to extrapolate to ancient times. On the one hand, loss could have been greater in ancient times than it is today based on the increased solar EUV flux. The EUV would have provided additional heating of the upper atmosphere, increasing the H escape rate. On the other hand, loss of H could have been less in ancient times if, by having a more-Earth-like atmosphere, the Martian middle atmosphere had a more-efficient cold trap that kept the H_2O from getting as high in the atmosphere.

3. Conclusions: Combined with the previous results on loss derived from the Ar isotopes (Jakosky et al., 2017), these results provide a direct indication that the bulk of the early Martian atmosphere has been lost to space. The timing of this loss as determined from the history of the Sun is consistent with that inferred from the geology of the surface. Combined with the lack of evidence for a substantial CO_2 reservoir on the surface or in the subsurface, we conclude that loss to space was the major process by which the Mars atmosphere evolved from an early, warmer and wetter climate to the cold, dry climate that we see today.

The Role of Magnetic Fields in Terrestrial Planet Evolution

R. Lillis[1*]; D. Brain[2], R. Strangeway[3], J. Luhmann[1], Y. Ma[3], S. Sakai[4]
[1] Space Sciences Laboratory, UC Berkeley, USA
[2] Laboratory for Atmospheric and Space Physics, University of Colorado, USA
[3] Institute for Geophysics and Planetary Physics, University of California Los Angeles, USA
[4] Department of Earth and Planetary Science, University of Tokyo, Japan

1. Introduction

Magnetic fields have negligible effects on the bulk neutral atmosphere of terrestrial planets. However, in the partially-ionized upper atmospheres of such planets, magnetic fields play an important role in guiding the motion of electrons and ions into, within, and out of, these environments. Therefore, particularly over geologic time, the strength, geometry and topology of planetary magnetic fields (both intrinsic and induced) can profoundly impact the total pressure and composition of terrestrial planet atmospheres, and hence the evolution of their climates. Simple comparisons between the terrestrial planets are of limited use because the terrestrial planets Venus, Earth and Mars differ in many more respects than just their magnetic fields: gravity, outgassing rates, solar wind average speed and density, as well as atmospheric pressure, temperature and composition [1]. Nonetheless, we can broadly consider how the configuration and strength of planetary magnetic fields affects the sources and sinks of terrestrial planet atmospheres and hence climate evolution.

2. Magnetic fields of the three terrestrial planets.

Figure 1 shows schematic views of the three terrestrial planets' interaction with the solar wind. Venus does not possess any known intrinsic magnetic fields and so its interaction with the solar wind produces an induced magnetosphere, whereby the solar wind slows and is diverted around, and the interplanetary magnetic field (IMF) drapes around, the conducting obstacle of the dayside ionosphere [2]. Earth has a strong, internally generated, largely dipolar global magnetic field which stands off the solar wind out to ~15 R_E and which connects with the IMF only in the polar regions, wherein plasma can precipitate and escape along the field lines. Mars does not possess a global dipole field today, but did in its first few hundred million years [3], and so its interaction with the solar wind is somewhat Venus-like globally, though inhomogeneous and locally strong crustal magnetic fields concentrated in the southern hemisphere alter the plasma environment in complex ways and can stand off the solar wind up to 1000 km [4].

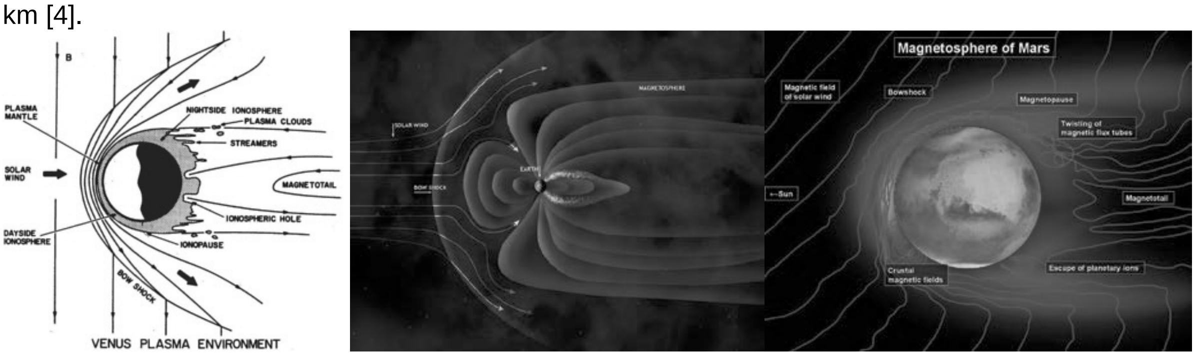

Figure 1: schematic diagrams of the solar wind interaction with the three terrestrial planets: Venus, Earth and Mars from left to right. Courtesy of J. Luhmann, S. Bartlett, and E. Dubinin respectively.

3. The impact of planetary magnetic fields on escape rates

Terrestrial planet atmospheric escape can be categorized by the charge state of the atoms/molecules when they receive sufficient energy to escape, and further by the physical process which imparted the energy. We discuss how these processes differ with respect to different magnetic field configurations.

3.1. Ion escape

Ions are accelerated to escape energies by a combination of processes operating near and above the planetary exobase:

3.1.1. Solar wind pickup

Newly-created planetary ions in the exosphere are swept away by the solar wind convection electric field in a process known as solar wind pickup. Pickup is less efficient in the presence of a global magnetic field for two reasons: first, only one of three ionization processes - photoionization - can operate inside the magnetosphere; the other two - solar wind charge exchange and electron impact ionization – are greatly diminished. Second, new ions born on (the mostly) closed magnetic field lines cannot escape the magnetosphere [1].

3.1.2. Ion outflow

Second, ions near the exobase can be heated/energized by collisions or wave-particle interactions and carried out to space where IMF-connected field lines thread the ionosphere. Without a global magnetic field, this is the case for a large fraction of the planet, particularly at higher dayside solar zenith angles (SZA) and on the nightside. In contrast, where a global magnetic field exists, only the polar cap regions allow ionospheric outflow. However, recent work has shown that total energization of ionospheric plasma in earth's magnetic cusp regions may exceed global energization at Venus and Mars [5], the question of whether ion outflow is helped or hindered by a global magnetic field is as yet unresolved.

3.1.3. Bulk escape

Bulk ion loss process, such as ionospheric stripping via the Kelvin Helmholtz instability, occur when magnetic or velocity shear exists between the surrounding plasma environment and the ionosphere. With a global magnetic field, the flowing plasma would be kept far above the ionosphere, causing shear and hence bulk escape to be inhibited.

3.2. Neutral escape

Neutral loss occurs by three main processes: sputtering, thermal escape and photochemical escape.

3.2.1. Sputtered escape

Exospheric ions can be accelerated by the solar wind convection electric field back into the atmosphere, transferring escape energy and momentum to thermal neutrals, in a process known as sputtering which, though negligible today, may have been the dominant escape process for early Mars [6]. A global magnetic field would prevent the vast majority of these ions from reaching the exobase and cause sputtering.

3.2.2. Thermal escape

Neutrals near the exobase receive little heating from precipitating solar wind plasma, so the presence or absence of a global magnetic field should not change thermal escape rates significantly.

3.2.3. Photochemical escape

Dissociative recombination of O_2^+ ions can provide the resulting hot O atoms with sufficient energy to escape from Mars (though not Earth or Venus). The rate of this reaction is controlled mostly by the temperature of ambient electrons, which can be heated by suprathermal electrons precipitating along magnetic field lines, so this escape rate may be slightly lower if Mars had a global magnetic field, though this is not expected to be a significant effect.

4. Summary and Future Needed Measurements

Overall, it is undoubtedly true that a global magnetic field will alter the magnitude of atmospheric escape and its dependence on heliospheric conditions. However, at this time we do not necessarily know whether escape rates would be higher or lower, given that the much larger cross-sectional area of a global magnetic field could absorb significantly more energy from the solar wind than a small induced magnetosphere and funnel it into the polar cap regions [5]. Indeed, a comprehensive understanding of the impact of magnetic fields on climate evolution is still a way in the future, because a) several different but overlapping physical processes operate to determine plasma inflows to and outflows from planetary upper atmospheres from today, b) sufficient data do not yet exist to constrain the relative importance of these processes, and c) the boundary conditions and atmospheric compositions within which these processes operated were different in the past.

5. References

[1] Brain, D., Leblanc, F., Luhmann, J.G., Moore, T.E., Tian, F., Planetary Magnetic fields and Climate Evolution, In Comparative Planetology of Terrestrial Planets (SJ Maxwell et al. eds.), pp 487-501. Univ. of Arizona, Tucson, 2013.
[2] Venus solar wind interaction reference
[3] Lillis, R. J., H. V. Frey, and M. Manga, Rapid decrease in Martian crustal magnetization in the Noachian era: Implications for the dynamo and climate of early Mars, Geophys. Res. Lett., 35, 2008.
[4] Brain, D, Bagenal, F., Acuña, M., Connerney, J. Martian magnetic morphology: Contributions from the solar wind and crust, J. Geophys. Res., 108(A12), 2003
[5] Strangeway, R. J., C. T. Russell, J. G. Luhmann, T. E. Moore, J. C. Foster, S. V. Barabash, H.

Nilsson, Does a Planetary-Scale Magnetic Field Enhance or Inhibit Ionospheric Plasma Outflows? Abstract SM33B-1893, Fall AGU Meeting, San Francisco, December 13-17, 2010.
[6] J.G. Luhmann, R.E. Johnson, M.H.G. Zhang, Evolutionary impact of sputtering of the Martian atmosphere by O(+) pickup ions. Geophys. Res. Lett. 19, 1991.

Constraining the early evolution of terrestrial planets via noble gas isotope and K/U ratios

H. Lammer[1], M. Scherf[1], M. Leitzinger[1], P. Odert[1], C. Burger[2], C. Johnstone[2], M. Güdel[2], N. Tosi[3,4], A. Nikolaou[3,4], D. Kubyshkina1, T. Maindl[2], E. Marcq[5], N. V. Erkaev[6,7], L. Noack[8], K. G. Kislyakova[2,1], L. Fossati[1], E. Pilat-Lohinger[2], R. Dvorak[2], E. A. 2Dorfi[2]
[1]Space Research Institute, Austrian Academy of Sciences, Austria
[2]Department of Astrophysics, University of Vienna, Austria
[3]German Aerospace Center, Institute for Planetary Research, Department of Planetary Physics, Germany
[4]Technical University of Berlin, Department of Astronomy and Astrophysics, Germany
[5]LATMOS, Université de Versailles Saint-Quentin-en-Yvelines, France
[6]Institute of Computational Modeling SB RAS, Russian Federation
[7]Siberian Federal University, Russian Federation
[8]Freie Universität Berlin, Department of Earth Sciences, Germany

1. Introduction

Compositional variations between the solar nebula, chondrites and the chemical abundances of the terrestrial planets provide evidence that some sort of elemental and isotopic fractionation should have taken place early in the history of the solar system. Some of those fractionations can be explained via atmospheric loss [1] and the collisional erosion of the early differentiated body [2], whereas others remained poorly understood.

During the disk-embedded phase, early in the evolutionary history of the solar system, protoplanetary cores are believed to accumulate hydrogen gas and to form thin planetary H_2-envelopes. According to the "Grant-Tack" scenario [3], those protoplanetary cores (proto-Earth and proto-Venus) should have accumulated a size of 0.5-0.75 Earth- and Venus-masses, respectively, until the solar nebular evaporated. Afterwards, EUV-driven hydrodynamic escape started to slowly erode the accumulated hydrogen-envelopes of the proto-planets. In addition, constant bombardment of impacting material, delivered further material to growing proto-Earth and -Venus. This presentation will show how noble gases and potassium can be dragged away via hydrodynamic escape, adding up to the observed elemental and isotopical fractionations as observed at the terrestrial planets.

2. Fractionation of the noble gases and potassium

Lighter elements, such as potassium (K) compared to uranium (U), as well as isotopes, as for example ^{36}Ar compared to ^{38}Ar, or ^{20}Ne compared to ^{22}Ne can escape easier from proto-Earth and proto-Venus due to H-drag from a nebula-captures hydrogen-envelope compared to a magma ocean related outgassed steam atmosphere, whereas heavier elements and isotopes cannot be dragged away that easily. Our simulations of the hydrodynamic escape of the accumulated hydrogen envelope around proto-Earth and proto-Venus show that this effect can explain initial compositional variations between the terrestrial planets and the solar nebula. It is also shown that in the case of the Earth delivery of chondritic material is necessary to reproduce the observed fractionations. These model results are also supporting the Grant-Tack scenario [3], and are in agreement with ^{182}Hf-^{182}W chronometric fast accretion scenarios of the Earth with a late Moon-forming giant impact [4] and ^{142}Nd-^{144}Nd ratios [5]. In addition, the observed noble gas isotope and K/U ratios at Venus and Earth can only be reproduced with a slow rotating early Sun.

3. References

[1] Odert P., Lammer H., Erkaev N.V., Nikolaou A., Lichtenegger H.I.M., Johnstone C.P., Kislyakova K.G., Leitzinger M., Tosi N.: Escape and fractionation of volatiles and noble gases from Mars-sized planetary embryos and growing protoplanets, Icarus, in press, 2018.
[2] O'Neill, H.S.C., Palme, H.: Collisional erosion and the non-chondritic composition of the terrestrial planets, Phil. Trans. R. Soc. A. 366, 4205-4238, 2008.
[3] O'Brien, D.P., Walsh K.J., Morbidelli A., Raymond S. N.: Water delivery and giant impacts I the 'Grand Tack' scenario, Icarus, 239, 74-84, 2014.
[4] Yu, G., Jacobsen, S.B.: Fast accretion of the Earth with a late Moon-forming giant impact, PNAS, 108, 17604-17609, 2011.

4. Acknowledgement

The authors acknowledge the support of the FWF NFN project Pathways to "Habitability: From Disks to Active Stars, Planets and Life", in particular its related sub-projects S11604-N16, S11606-N16 and S11607-N16.

Evolution of the Martian Climate

F. Forget.
Laboratoire de Météorologie Dynamique, IPSL, CNRS, Sorbonne Université, France

1. Introduction

The planet Mars that we study today have strongly varied in the past due to various processes that have completely changed its environment. This can be studied by analyzing the geological records and by using numerical climate models. Two major processes have induced climate change. First, throughout its history, Mars have undergone variations of its orbital and rotation parameters (in particular its obliquity) which have resulted in major changes in its environment and its atmosphere. Second, in the distant past, Mars must have been covered by a different atmosphere than today, possibly thicker and with a different composition, and which must have been able to allow liquid water to flow on its surface.

The study of these different planets Mars is of interest in a symposium on aeronomy and plasma environment for several reasons. Firstly atmospheric escape is thought to have played a major role in the evolution of the atmosphere and the habitability of Mars. Second, the changes in the environment throughout history (and notably the one due to obliquity variations) could have affected the behavior of the upper atmosphere and thus the atmospheric escape.

2. Climate variations induced by obliquity variations.

The present-day Mars climate is a complex system in which the atmospheric dynamic is coupled with the dust cycle, the CO_2 cycle and the water cycle. This system is influenced by the variations of Mars orbital and rotation parameters (in particular its obliquity) which control the distribution of insolation. Calculations have shown that Mars' obliquity can vary widely between 0° and more than 60° [1] with a ~10^5 year cycle (consequence of the differential spin axis and orbital plane precession rates) modulated on a more eratic ~10^6 year cycle (resulting from slow oscillations in the inclination of the Martian orbital plane). What kind of climate changes have been and will be induced by such variations?

Clues are provided by the geological record. While water ice is currently unstable at the surface of Mars outside the polar regions, Mars is partly covered by landforms resulting from the local accumulation of ice, such as debris-covered glaciers and ice mantles. It is likely that they were created when Mars was experiencing an obliquity different than today. The kilometers-thick polar ice caps themselves exhibit thousands of layers that are most likely related to periodic climate changes,

At obliquity lower than today, we can expect the seasonal variations to be small and the poles to become relatively colder all year long since the Sun is always lower in the sky. It is expected that the fraction of the atmosphere constantly held as CO_2 ice, and which is presently near the southern pole will increase. The atmospheric pressure may collapse and mostly contain Argon and Nitrogen. Must work remains to be done to understand what really happened on Mars during these periods

The environment of Mars at obliquities larger than today have been studied in more details using Global Climate Models. The surface pressure was probably higher than today due to the release of frozen CO_2 at the south pole and the desorption of high latitude subsurface CO_2 (to first order, we can expect a doubling of the atmosphere/seasonal cap inventory).

A key, early finding of GCMs is the fact that at obliquity larger than about 40°, ice can accumulate outside the polar regions [2-6], until the polar reservoir is depleted to form glaciers in the tropics and at mid-latitudes often in remarkable agreement with geological observations of glaciers-related landforms. However, more work is needed to better simulate the atmosphere (including the upper atmosphere) notably to better take into account the effect of the thick clouds that are thought to have played a key role in the climate system.

3. Different climates induced by a different atmosphere

There is compelling evidence and widespread agreement that water flowed on the surface on early Mars, at least episodically. However, we still do not know which climate processes operated. Each proposed solution has its difficulties. In any cases, for liquid water to flow on the surface, the atmospheric pressure must have been significantly higher than today. Yet the origin of this atmosphere (could an early atmosphere accumulate without escaping before 4.1 Ga?) and its fate (can atmospheric escape explain everything?) remains a topic of active research.

A pure CO_2-H_2O atmosphere under early Mars conditions cannot easily warm the planet to explain the geo-logical record. Yet, 3D simulations of early Mars with a CO_2 atmosphere thicker than today have simulated an interesting environment, different than today. The key difference is related to the fact that, if the surface pressure is high enough, the elevated regions are colder than the low lying plains [10], providing a cold trap where water tends to accumulate as snow and ice in high altitude [11], and a process to constant-ly replenish these reservoirs. Interestingly, the resulting distribution of glaciers is in somewhat good agreement with the observed valley networks [11-13].

If a thick Mars CO_2 atmosphere only yields a cold and icy planet, one has to take into account additional processes to warm it and melt significant amounts of water to explain the geological record. The climatic impact of impacts is, within that context, a key process to study and work is ongoing to evaluate if impacts could explain at least a fraction of the fluvial geology and mineralogy of the most ancient terrains. Volcanic activity could have supplemented such an early atmosphere with additional greenhouse gases such as SO_2, H_2S, CH_4, NH_3, and H_2 and boost the greenhouse effect for some time if their concentration could be raised to an adequate level and for a sufficient duration. None of these gases provide an easy solution to the early Mars enigma. In particular SO_2 was found to be incapable of creating a sustained greenhouse on early Mars because of its limited greenhouse effect and the formation of sulfate aerosols that can actually cool the surface [e.g. 15]. Recently Ramirez et al. [16] argued that H2 emitted from volcanoes into a thick CO_2-dominated atmosphere could have significantly warmed the planet assuming a very reducing mantle and a very high rate of volcanism. This scenario was thus not easy to prove right. However, Wordsworth et al. [17] recently showed that in this study the strength of the greenhouse effect induced by the CO_2–H_2 collision-induced absorption could have been significantly underestimated (by using the available spectroscopic properties, originally derived for an N_2 atmosphere instead of CO_2). Furthermore, they reported that methane could also have acted as a powerful greenhouse gas on early Mars due to CO_2–CH_4 Collision Induced Adsorption in the critical 250–500 cm^{-1} spectral window region. The required outgassing fluxes become more realistic, and the scenario is very interesting. At the conference, we will present new simulations performed with atmospheres including H_2 and CO_2 and discuss the possible behavior of the upper atmosphere

References

[1] Laskar et al. Icarus, 170:343{364
[2] Toon et al. Icarus, 44:552–607. (1980).
[3] Jakosky, B. M. Space Sci. Rev., 41:131–200. (1985).
[4] Mischna et al. JGR (Planets), pages 16–1. (2003).
[5] Levrard et al., Nature, 431:1072–1075. (2004)
[6] Forget et al. Science, 311:368–371. (2006).
[10] Forget, F., Wordsworth, R., Millour, E., et al. (2013) *Icarus*, 222, 81– 89 (2013)
[11] Wordsworth R, Forget F, Millour E, Head JW, Madeleine JB, Charnay B. 2013. Icarus 222:1–19
[12] Wordsworth et al. J. Geophys. Res. Planets 120:1201–19 (2015)
[13] Bouley et al., *Nature*, 531:344-347, 2016.
[14] Turbet et al. 2017. Fourth International Conference on Early Mars:
[15] Kerber L, Forget F, Wordsworth RD. 2015. Icarus 261:133–48.
[16] Ramirez et al. 2014.. Nat. Geosci. 7:59–63
[17] Wordsworth et al., Geophys. Res. Lett., 44, 665–671 (2017)

Cluster observations of Earth atmospheric escape

C. P. Escoubet[1*]; *H. Laakso[2], A. Masson[2], M. L. Goldstein[3]*
[1]ESA/ESTEC, The Netherlands
[2]ESA/ESAC, Spain,
[3]SSI/GSFC, USA

After more than 17 years in space, the Cluster mission is continuing to deliver ground-breaking results, thanks to its ability to move the four spacecraft with respect to each other, according to the science topic to be studied. The main goal of the Cluster mission, made of four identical spacecraft, carrying each 11 complementary instruments, is to study in three dimensions the key plasma processes at work in the main regions of the Earth's environment: solar wind and bow shock, magnetopause, polar cusps, magnetotail, and auroral zone. Atmospheric escape and ion outflows were not one of the prime objectives of the Cluster mission. However, with its orbit crossing the Earth's polar regions and the plasmasphere, Cluster could perform, for the first time, multi spacecraft measurement of plasma escaping Earth's atmosphere. We will present science highlights obtained such as the cold plasma distribution in the magnetosphere, the continuous leakage of plasma from the plasmasphere, the role of centrifugal acceleration on ion outflows, the solar wind illumination control of the polar wind, north-south asymmetries in cold plasma density, intermittent thermal plasma acceleration linked to sporadic motions of the magnetopause, statistics of outflows and plumes at the magnetopause as well as enhanced atmospheric oxygen outflow on Earth and Mars during a corotating interaction region. We will also present the Cluster Science Archive, which was implemented to provide, for the first time for a plasma physics mission, a permanent and public archive of all the high-resolution data from all instruments.

Geospace research contributions from ESA's Swarm constellation

R. Floberghagen[1]
[1]*Directorate for Earth Observation Programmes, European Space Agency, Italy*

1. Introduction

The Earth-orbiting three-satellite Swarm constellation continuously delivers high-quality data on the thermosphere- ionosphere region using in-situ measurements of the magnetic field vector, the ionospheric plasma environment and thermosphere neutral density. This presentation will highlight examples of current research utilising Swarm data, and provides an outlook for the future. Following in the footsteps of the CHAMP mission, Swarm extends the available magnetic field, ionosphere and thermosphere data into the next solar cycle, and for the first time provides multi-point measurements of this environment. This enables investigations of the response of the thermosphere to energy inputs and cooling processes over a wide range of external conditions. The high accuracy magnetic and electric field data of the Swarm satellites contribute to improved climatologies of the high-latitude current system and energy exchange. In addition, the high temporal resolution of these measurements enables the investigation of these currents at much smaller scales than has been possible before, uncovering details on the relationship between small and large scale currents. Based on a highly successful nominal mission Swarm has recently received an extension. The satellites are in excellent overall health and carry sufficient propellant for a prolonged on-orbit lifetime. The Swarm team is continuing to invest to improve its data products and science output, bringing together observations on the drivers and response of the thermosphere-ionosphere system, which can feed into improvement of models. In the near future, we can look forward to an excellent synergy with observations of the thermosphere-ionosphere from NASA's GOLD and ICON missions, promising to bring both a global overview for context of the in-situ measurements, as well as increased detail of the dynamics of the system at mid- and low latitudes. The Swarm experience should also be of importance for the definition of the next US flagship mission Geospace Dynamics Constellation.

Status of the MAVEN Mission at Mars

B. M. Jakosky[1]
[1]LASP, University of Colorado, USA

1. Introduction

The Mars Atmosphere and Volatile Evolution (MAVEN) mission has been orbiting Mars since September 2014. It has completed nearly two Mars years of observations of the upper atmosphere, ionosphere, magnetosphere, and solar and solar-wind interactions. The goal is to understand the structure and dynamics of the integrated system today, along with the processes controlling them; the rate at which atmospheric gases are being lost to space today, and the processes controlling them; and the extrapolation through time in order to determine the integrated loss to space throughout Mars' history.

2. Status and future

MAVEN continues to operate both as a science mission and in support of communications relay with rovers on the surface. Its projected lifetime based on fuel exhaustion date is out past 2030. Status and future will be reported in detail at the meeting. Topics to be discussed include:

2.1. Current status (along with status as of this writing)

- Operational status of spacecraft (performing nominally)
- Operational status of instruments (performing nominally)
- Pipeline processing of science data and release through the Planetary Data System (data being released on three-month centers)
- Science results to date and in process (to be presented)
- Current extended mission (EM-2, funded through 30 Sept. 2018)

2.2. Future plans

- Proposal for next extended mission (EM-3, beginning 1 Oct. 2018)
- Science objectives for EM-3
- Aerobraking into a lower-apoapsis orbit to improve relay operations
- Planning for combined science plus relay operations
- Relay operations for upcoming rovers and landers
- Ongoing and future science collaboration/coordination with other orbiters and landers

3. Summary

MAVEN continues to operate nominally and to obtain valuable, high-quality science data. We anticipate that we will be able to carry out both science and relay operations during EM-3 and beyond, and that MAVEN will continue to be a high-quality science orbiter. Based on anticipated fuel-exhaustion date, we expect to be able to obtain science data through at least 2030; this would give us measurements through about eight separate Mars years and through more than an entire eleven-year solar cycle.

Mars Express science highlights and future plans

D. Titov[1*]; J.-P. Bibring[2], A. Cardesin[3], T. Duxbury[4], F. Forget[5], M. Giuranna[6], F. González-Galindo[7], M. Holmström[8], R. Jaumann[9], A. Määttänen[10], P. Martin[3], F. Montmessin[10], R. Orosei[11], M. Pätzold[12], J. Plaut[13], MEX SGS Team[3]
[1]ESA-ESTEC, The Netherlands
[2]IAS-CNRS, France
[3]ESA-ESAC, Spain
[4]George Mason University, , USA
[5]LMD, France
[6]IAPS-INAF, , Italy
[7]IAA, Spain
[8]IRF, Sweden
[9]IPF-DLR, Germany
[10]LATMOS/ IPSL, CNRS, France
[11]IRA-INAF, Italy
[12]RIU-Uni Cologne, Germany
[13]JPL, USA

Mars Express remains one of ESA's most scientifically productive missions whose publication record now exceeds 1050 papers. Characterization of the geological processes on a local-to-regional scale by HRSC, OMEGA and partner experiments on NASA spacecraft has allowed constraining land-forming processes in space and time. Recent results suggest episodic geological activity as well as the presence of large bodies of liquid water in several provinces (e.g. Eridania Planum, Terra Chimeria) in the early and middle Amazonian epoch and formation of vast sedimentary plains north of the Hellas basin. New analysis of the subsurface dielectric properties by MARSIS radar sounder revealed that the deposits in Meridiani Planum, previously interpreted as ice-rich, may contain little or no ice at all. Mars Express observations and experimental teams provided essential contribution to the selection of the Mars-2020 landing sites.

More than a decade-long record of the atmospheric parameters such as temperature, dust loading, water vapor and ozone abundance, water ice and CO2 clouds distribution, collected by SPICAM, PFS and OMEGA spectrometers as well as subsequent modeling have provided key contributions to our understanding of the martian climate.

More than 10,000 crossings of the bow shock by Mars Express allowed ASPERA-3 to characterize complex behavior of the magnetic boundary topology as function of the solar EUV flux. ASPERA-3 observations of the ion escape during complete solar cycle revealed important dependencies of the atmospheric erosion rate on parameters of the solar wind and EUV flux and established global energy balance between the solar wind and escaping ion flow. This led to important conclusion that the ion escape at Mars is production rather than energy limited.

The structure of the ionosphere sounded by the MARSIS radar and the MaRS radio science experiment was found to be significantly affected by the solar activity, the crustal magnetic field, as well as by the influx of meteorite and cometary dust. MARSIS and ASPERA-3 observations suggest that the sunlit ionosphere over the regions with strong crustal fields is denser and extends to higher altitudes as compared to the regions with no crustal anomalies. Reconnection of solar magnetic field lines carried by the solar wind with field lines of crustal origin opens channels through which the ionospheric plasma escapes to space, producing strong and narrow cavities in the density. The situation is very different on the night side where the ionosphere has patchy structure. Such patchy ionizations are observed in the regions where field lines have a dominant vertical component. Through these patches the ionospheric plasma from the dayside penetrates and supplies the nightside ionosphere.

Mars Express has successfully passed the solar eclipse season in 2017 and completed the observation programme. The mission extension till the end of 2020 was approved. The extension plan includes both augmenting the coverage and extending long-time series, as well as new elements and potentially new opportunities for discoveries. It will be boosted by collaboration and synergies with NASA's MAVEN, ESA-Roscosmos Trace Gas Orbiter (TGO) and other missions. In 2018 the mission will pass through the bi-annual extension review and will elaborate the science case for new extension till the end of 2022. The talk will give the Mars Express status, review the recent science highlights, and outline future plans focusing on synergistic science with TGO.

Getting ready for BepiColombo: a modelling approach to infer the solar wind plasma parameters upstream of Mercury from magnetic field observations

S. Fatemi[1*]; *N. Poirier[2], M. Holmström[1], J. Lindkvist[3], M. Wieser[1], S. Barabash[1].*
[1]Swedish Institute of Space Physics, Sweden
[2]École Nationale Supérieure de Mécanique et d'Aérotechnique, France
[3]Department of Physics, Umeå University, Sweden

1. Introduction

The lack of an upstream solar wind plasma monitor when a spacecraft is inside the highly dynamic magnetosphere of Mercury limits interpretations of observed magnetospheric phenomena and their correlations with upstream solar wind variations. A detailed and accurate knowledge about the solar wind plasma and its variations as it interacts with Mercury is crucial to better understand the morphology of the interaction, structure of the magnetosphere of Mercury, and its associated phenomena and their correlations with solar wind variations.

2. Methodology

We use AMITIS, a three-dimensional GPU-based hybrid model of plasma (particle ions and fluid electrons) [1] to infer the solar wind plasma parameters upstream of Mercury by comparing our simulation results with Messenger magnetic field observations inside the magnetosphere of Mercury. We select a few orbits of Messenger, which have been already analysed and compared with simulations before. Then, we run nearly 40 simulation runs for each orbit with different solar wind plasma parameters to find the best agreement between our simulations and Messenger magnetic field observations inside Mercury's magnetosphere.

3. Results and Discussion

We show that there is a good agreement between our hybrid simulation results and Messenger observations for the estimated solar wind plasma parameters upstream of Mercury [2]. We also use our model to determine the location of the magnetospheric boundaries, i.e., bow shock, magnetopause, and magnetotail, and their correlations and variations with the solar wind plasma and compare them with those previously estimated from observations [2]. We show that our model can be used as an upstream solar wind plasma monitor for Mercury to provide estimates of the solar wind variations from magnetic field observations inside Mercury's magnetosphere. These results have important implications for observations by Messenger, and for the future ESA/JAXA mission to Mercury, BepiColombo [2].

4. References

[1] Fatemi et al., (2017) *J. of Phys.*, 837(1)
[2] Fatemi et al., (2018) *A&A*, (submitted)

Comparison between IUVS-MAVEN limb dayglow observations and modeling

L. Gkouvelis[1*], J.-C. Gérard[1], *B. Ritter*[1], *B. Hubert*[1], *V. I.* Shematovich[2], *D.V.* Bisikalo[2], *N. Schneider*[3]
[1]*LPAP, University of Liege, Belgium.*
[2]*Institute of Astronomy, Russian Academy of Sciences, Russia*
[3]*Laboratory for Atmospheric and Space Physics, University of Colorado, USA.*

Introduction

Limb observations of airglow emissions is a standard technique to study the altitude profiles of the chemical elements in the Martian atmosphere and its thermal structure. Several previous missions have performed observations in the past (Mariners, Mars Express). Recently the IUVS Ultraviolet spectrograph (McClintock et al. 2014) on board MAVEN has been collecting thousands of airglow (Jain et al. 2015) and auroral (Schneider et al., 2015) limb profiles in the range 120 to 340 nm. We have analyzed more than three years of airglow observations and compared them to model simulations. The objective is to study the CO_2, O, CO and other density profiles as well as thermospheric temperatures.

1. IUVS-MAVEN observations

The Imaging Ultraviolet Spectrometer is a remote sensing instrument on MAVEN, equipped with two ultraviolet channels. MUV (middle ultraviolet) and FUV (far ultraviolet) detectors that cover the 115-190 nm and 180-340 nm spectral ranges respectively. MAVEN has collected over three years of quasi-continuous airglow observations covering more than a full Martian year and various latitudes ranges per epoch. We have analyzed the data and produced mean altitudes profiles for many of the emission features, grouping them in epoch, solar zenith angle and latitude ranges of interest. An example of simultaneous limb scans of several emissions is shown in Figure 1. The limb brightness profile of each spectral feature was obtained by using a multiple linear regression method to fit each observed spectrum.

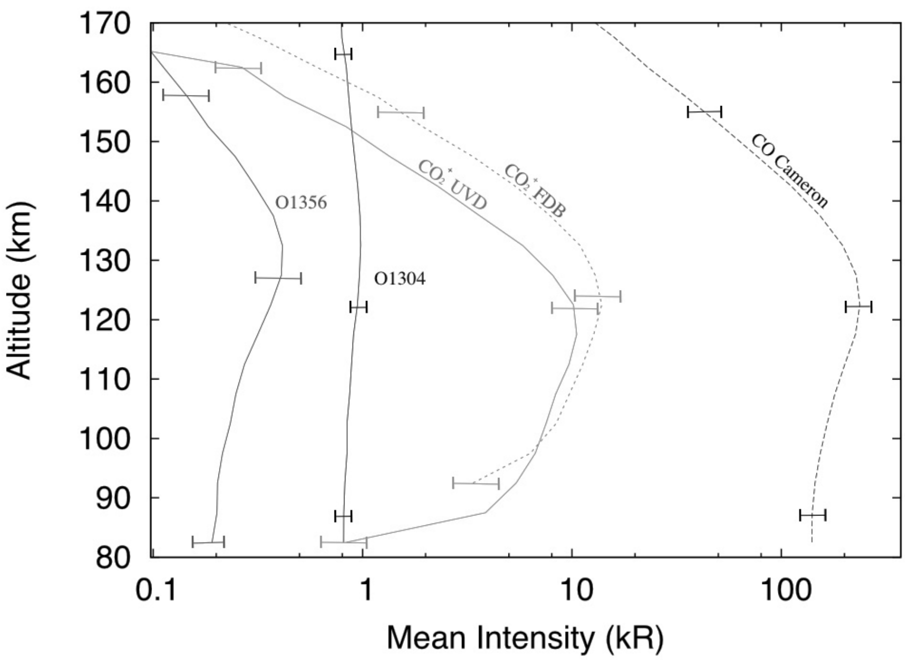

Figure 1: example of airglow emission features obtained by averaging IUVS limb scans for solar zenith angles between 50° and 60° degrees; orbits: 3000-3400, Ls: 100°-150°(data available from NASA/PDS archives).

2. Dayglow modeling

To model the dayglow emissions of the Martian atmosphere we adopt a three-step approach. First, we construct neutral atmosphere distribution of the main constituents for different seasons, latitudes and solar zenith angles based on the MGITM model (Bougher et al., 2015). Second, we use Monte Carlo simulations to calculate the photoelectron energy spectrum as a function of altitude for the latitude, solar longitude, local time and solar activity corresponding to the observations. The model uses the Direct Simulation Monte Carlo (DSMC) method that has been developed over the years (Shematovich et al. 2008; Gérard et al., 2008) to calculate the brightness profiles of a series of spectral features of the Earth, Jupiter, Saturn, Venus and Mars atmospheres. Once the energy spectrum of the photoelectrons is calculated at fixed grid points, it is folded with relevant electron impact excitation cross sections to derive the corresponding excitation rates. Finally, the production rates from these collisional processes are combined with other solar-induced or photochemical sources to obtain the total volume production rates. In the case of an optically thick emission a radiative transfer code is used to calculate the emerging nadir or limb intensity. Collisional deactivation is accounted for in the case of metastable excited states.

Comparison between observed and modeled limb profiles of several features will be presented and differences will be interpreted in terms of parameters in the model and/or corrections to the neutral model densities.

3. References

[1] Bougher et al., **JGR**, 10.1002/2014JE004715

[2] Jain, S.K., et al., ***GRL**, 42*, 2015.

[3] Gérard, J.C. et al., ***PSS**, 56,* 542-552, 2008.

[4] McClintock, W.E. Et al. **Space Sci. Rev.**, 1-50,10-1007/s, 2014

[1] Shematovich, V.I. et al., ***JGR**, 113*, E02011, 2008.

[5] Schneider, N. M. et al. **Science**, 350,6261, aad0313, 2015

Acknowledgements. This research was partly funded by the NOMAD PRODEX program managed by the European Space Agency with help of the Belgian Science Policy Office (BELSPO) and supported by BELSPO's SCOOP/BRAIN research contract.

Combining Observations and Modeling to Promote upper Atmospheres Research and Exploitation

P. Rosenblatt[1*]; *S. Bruinsma[2], F. Forget[3], A. Jaeggi[4], F. Montmessin[5], M.A. Lopez Valverdei[6], A.-C. Vandaele[7]*
[1]ACRI-ST, Sophia-Antipolis, France
[2]CNES, France
[3]LMD, France
[4]Universitaet Bern, Switzerland
[5]LATMOS, France
[6]IAA-CSIC, Spain
[7]IASB, Belgium

1. Introduction

The upper atmospheres of terrestrial planets are extremely active regions, which provide unique natural laboratories to study geophysical fluid dynamics, wave processes and atmospheric physical phenomenon. Until recently, sparse observations were available to study these regions and learn from them. Space missions, and notably the ESA's Mars Express (MEX), Venus Express (VEX), and trace Gas Orbiter (TGO) are now providing an unprecedented dataset. Our basic goal is to combine experience in diverse research lines in order to exploit this dataset to enhance the scientific return of those missions.

1. Data (re-)processing and modelling approach

Our team is planning to combine and process accelerometer and tracking data as well as stellar and solar occultation observations in a comprehensive manner to support the scientific investigations of these three ESA missions in combination with NASA's mission data. This combined dataset should provide a larger ever spatio-temporal sampling of the upper atmosphere of the two planets allowing for monitoring variations of the density field. These data could be further combined with novel analysis and retrieval tools, and the statement-of-the-art climate model for both planets. The TGO tracking data shall also allow improving the time-variable gravity of Mars related to seasonal mass exchange in the lower atmosphere.

Other ambitious expectations are to enhance our understanding of the processes governing the high-altitude atmospheric variability. Our plan shall also improve the European Mars Climate Database and thrust a similar database for Venus up to upper atmosphere to support aerobraking phases of future planetary missions. Further, this could even help to initiate a combination center for planetary geodesy in Europe.

Capabilities of the Exomars Trace Gas Orbiter to study the Mars' upper atmosphere

M. A. López-Valverde[1*]; J.-C. Gerard[2], F. González-Galindo[1], A.-C. Vandaele[3], O. Korablev[4], M. R. Patel[5], S. Jiménez-Monferrer [1], M. García-Comas[1], A. Cardesin[6], M.S. Chaffin[7], M. López-Puertas[1] , B. Hill[1], J.J. López-Moreno[1], Julio Rodríguez[1]
[1]Instituto de Astrofísica de Andalucía-CSIC, Spain
[2]Laboratoire de Physique Atmosphérique et Planétaire, Université de Liège, Belgium
[3]IASB, Belgium
[4]IKI, Russia
[5]Open University, UK
[6]ESAC, Spain
[7]LASP, USA

1. Introduction

The Martian mesosphere and thermosphere (altitudes above about 60 km), is not the primary target of the ExoMars 2016 mission but its Trace Gas Orbiter (TGO) will explore these altitudes and hopefully address many scientific open issues, either in-situ during the aerobreaking period or remotely during its regular mission. In addition to the nominal atmospheric observations (in solar occultation and nadir pointing) with its two spectrometers NOMAD and ACS, exploring the limb off-the-terminator (i.e. the night and dayside hemispheres) is also possible. These new possibilities would extend the capabilities of the TGO investigations and permit novel studies of the Martian aeronomy [1]. In this presentation we will review all these observational strategies and the science benefits associated to them.

2. Exomars TGO nominal operations

TGO carries two instruments designed for the detection of trace species, NOMAD and ACS, which will use the very sensitive solar occultation technique. With 6 signals/telescopes, they will cover from the UV to the infrared (see Figure 1 below). Further details on the instruments can be obtained from recent reviews [2,3]. These signals will supply regular sounding at the terminator (1 sunset and 1 sunrise every orbit, i.e., every 2 hours approximately) up to very high altitudes and in many molecular bands and atmospheric species (CO2, CO, O3, H2O, O2 and aerosols among them). We expect an extensive and precise dataset of densities and hopefully temperatures (from the rotational structure of spectra or from the scale height of the species densities), suitable to clarify hot topics like the high altitude H2O abundance and its impact on escape rates [4,5,6], couplings with the lower atmosphere [6,7], and the homopause/mesopause variability [8,9]. Even the nadir emissions in the dayside might be exploited to infer the temperature in the upper atmosphere, as it was done from Venus orbit using VIRTIS/Venus Express measurements of the fluorescent CO2 emissions at 4.3 mm in the illuminated hemisphere [10].

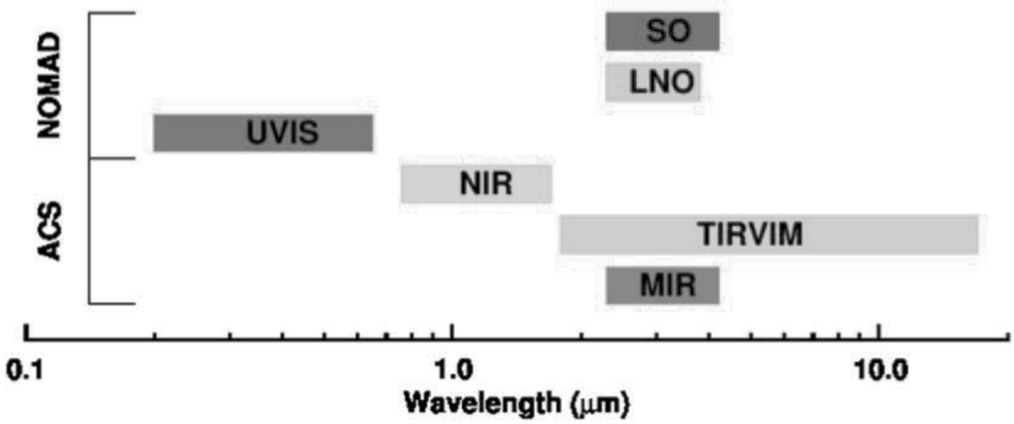

Figure 1: Spectral coverage obtained combining the six NOMAD and ACS channels.

3. Additional capabilities

3.1 Aerobraking phase

The aerobraking phase of TGO progressed as expected to date [11], peeking into thermospheric altitudes in a broad range of latitudes and during a long continuous period. Its analysis shall supply along-track densities and temperatures which could give information on lower thermosphere variability, about gravity wave propagation, and also permit a stringent validation of current global models [1].

3.2 Limb emissions off the terminator

In addition to the solar occultation with the NOMAD-SO and ACS-MIR channels, specifically designed for this geometry, it is also possible to perform limb observations with the NOMAD-LNO, the NOMAD-UVIS and the ACS-TIRVIM channels [2, 3]. There are four possible configurations, depending on the pointing that may be achieved [1], and they will be discussed in this presentation. Our simulations suggest that airglow emissions from the UV to the IR might be observed outside the terminator. If eventually confirmed from orbit, they would supply new information about atmospheric dynamics and variability. The first obvious benefit is the building of vertical profiles off the terminator, extending the mapping of the daily cycle of minor species. Also nightglow, Martian aurora and non-LTE fluorescent emissions could add information about the density and thermal structure. Other science windows could be open due to serendipity under new viewing conditions never performed on Mars before; let us recall the open debate about the high altitude clouds on Mars [12]. It is important to recall that the optimal exploitation of these alternative observational modes requires special spacecraft pointings, currently not considered in the regular operations, although feasible in our opinion.

4. Synergies with other missions

The synergy between the TGO instruments, specially the wide spectral range achieved by combining them, allows for coordinated operations with other ongoing Mars missions capable of supplying simultaneous measurements of the upper atmosphere, specifically, Mars Express, Maven and MRO. Further, possibilities for joint studies with the James Web Space Telescope as well as with ground based observations at hgh spectral resolution should also be exploited. These synergies and their science impact will also be discussed in this presentation.

5. References

[1] López-Valverde, M.A. et al., Space Sci Rev (2018) 214: 29. doi:10.1007/s11214-017-0463-4
[2] Vandaele, A.-C. et al, Space Sci Rev, in press
[3] Korablev, O. et al., Space Sci Rev (2018) 214: 7. doi:10.1007/s11214-017-0437-6
[4] Fedorova, A. et al., Icarus, 300, pp.440-457, 2018.
[5] Chaffin, M.S. et al., Nature Geoscience (2017), 10: 147. doi:10.1038/ngeo2887
[6] Heavens, N. et al., Nature Astronomy, 2, pp126–132, 2018.
[7] Imamura, T. et al., Icarus 267, 51–63 (2016). doi:10.1016/j.icarus.2015.12.005
[8] Jakosky, B.M. et al., Science 355(6332), 1408–1410 (2017). doi:10.1126/science.aai7721
[9] González-Galindo, F. et al., J. Geophys. Res., Planets 114(E13), 4001 (2009).
[10] Peralta, J. et al., A&A, 585 (2016) A53 doi:10.1051/0004-6361/201527191
[11] http://blogs.esa.int/rocketscience/2017/12/06/keeping-up-with-tgo/
[12] Sanchez-Lavega et al., Nature (2015) **518**, 525–528. doi:10.1038/nature14162

Acknowledgements: This work has been partially funded by the European Union Horizon 2020 Programme under grant agreement UPWARDS-633127, by the Spanish National Research Council under "intramural" project CSIC 201450E022 and by the Spanish Ministry of Economy and Innovation and by the FEDER funds under grant ESP2015-65064-C2-1-P (MINECO/FEDER).

The LMD-Mars Global Climate Model and the Mars Climate Database: applications for the study of the upper atmosphere

F. González-Galindo[1*], *E. Millour[2], F. Forget[2], J.-Y. Chaufray[3], M.A. López-Valverde[1], A.Spiga[2], J.-B. Madeleine[2], L. Montabone[2,4], M. Vals[2], V. Zakharov[2], F. Lefevre[3], and F. Montmessin[3]*
[1]Instituto de Astrofísica de Andalucía-CSIC, Spain
[2]Laboratoire de Météorologie Dynamique, France
[3]LATMOS, France
4 Space Research Institute, USA

Introduction

The development of whole-atmosphere Global Climate Models (GCM) has boosted our understanding of the processes affecting the upper atmosphere (UA) of Mars in the last decade [1]. The LMD-MGCM was the first of such whole-atmosphere models for Mars [2,3,4]. It can simulate the temperature, density, composition (including the ionosphere), wind structure, and some UV atmospheric emissions, among other fields of interest for the UA. The model has been validated against observational data, including aerobraking datasets, Mars Express/SPICAM stellar occultations and observations of atmospheric emissions and MGS, MAVEN and Mars Express ionospheric measurements, and also against other Mars GCM [5]. In an effort to make the model outputs available to the whole community, they have been compiled to build the Mars Climate Database (MCD), a freely available tool useful for the scientific and engineering communities.

The LMD-MGCM: study of Mars' upper atmosphere

Initially placed at 80 km, the model top of the LMD-MGCM was moved upwards in different steps as models for the physical processes important in upper layers were added: non-LTE processes [6], UV heating and photochemistry of the UA, molecular diffusion and thermal conduction [3]. The model is forced by a day-to-day variable UV solar flux [7]. The dust variability in the lower atmosphere, known to potentially affect the state of the UA, is also taken into account by including an instrument-derived dust climatology for the last 8 Martian Years [8]. The model has been applied to many different topics of importance for the UA of Mars: the variability of temperatures in the UA [4,7] (fig. 1), the mesospheric winds and the presence of mesospheric clouds [9], the ionosphere [6], different UV atmospheric emissions [10,11] or the balance between different heating/cooling mechanisms [12]. The LMD-MGCM has been coupled to an exospheric and a magnetospheric model, allowing for simulation of atmospheric escape [13] or the interaction with the solar wind [14].

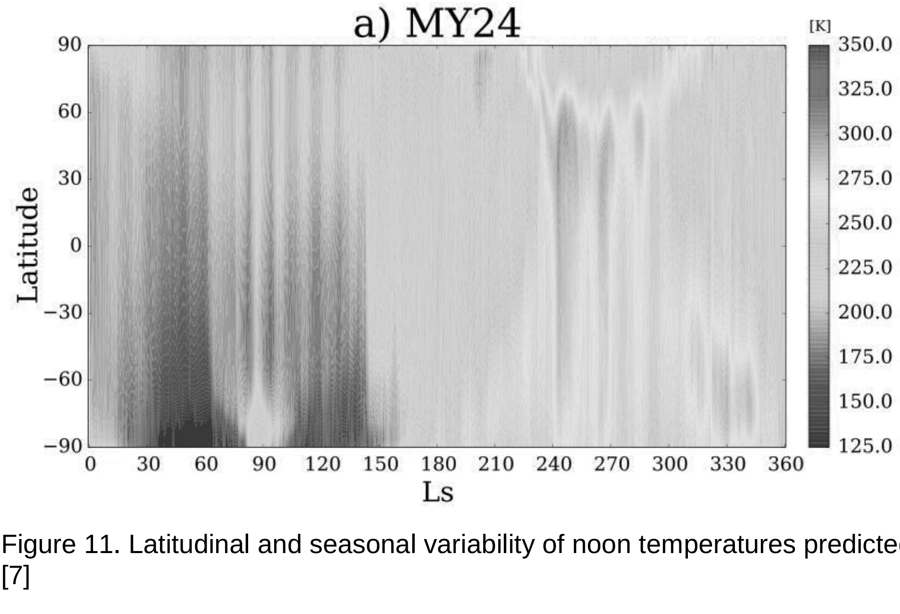

Figure 11. Latitudinal and seasonal variability of noon temperatures predicted by the LMD-MGCM. From [7]

The Mars Climate Database

The MCD is freely distributed and intended to be useful and used in the framework of engineering applications as well as in the context of scientific studies which require accurate knowledge of the state of the Martian atmosphere. Over the years, various versions of the MCD have been released and handed to more than 300 teams around the world. Current version (v5.3) can be obtained upon request (simply contact millour@lmd.jussieu.fr or forget@lmd.jussieu.fr), or through a simplified web interface for quick browsing at MCD outputs is available on http://www-mars.lmd.jussieu.fr. As the main driver of the Martian climate is the dust loading of the atmosphere, the MCD provides climatologies over a series of dust scenarios: standard year, cold (i.e: low dust), warm (i.e: dusty atmosphere) and dust storm. The influence of UV solar radiation is included with 3 UV scenarios (solar minimum, average and maximum inputs). In addition, we also provide additional “add-on” scenarios which focus on individual Martian Years (MY 24 to 32), using the observed day-to-day variability of the dust abundance and the UV solar radiation. The MCD provides mean values and statistics of different atmospheric variables, including many of interest for the UA: atmospheric temperature, density, pressure, winds, concentrations of species such as CO2, O, N2, CO, H2, H, He and electrons, and the Total Electron Content. It also offers the possibility to reconstruct realistic conditions by combining the provided climatology with additional large scale and small scale perturbations schemes. Examples of recent applications of the MCD to the study of the UA of Mars are the analysis of the atmospheric reconstruction from MSL EDL [15], the comparison with temperatures derived from MAVEN stellar occultations [16], or using the MCD as input for an ionospheric model [17] or for a gravity wave propagation scheme [18].

References

[1] Bougher, S.W. et al., Upper neutral atmosphere and ionosphere, on “The atmosphere and climate of Mars”, Cambridge University Press, 2017
[2] Angelats i Coll, M. et al., The first Mars thermospheric general circulation model: The Martian atmosphere from the ground to 240 km, Geophys. Res. Lett., Vol. 34, L04201, 2005
[3] González-Galindo, F. et al., Extension of a Martian general circulation model to thermospheric altitudes: UV heating and photochemical models, J. Geophys. Res., Vol., 110, E09008, 2005
[4] González-Galindo, F. et al., A ground-to-exosphere Martian general circulation model: 1. Seasonal, diurnal, and solar cycle variation of thermospheric temperatures, J. Geophys. Res.,114, E04001, 2009
[5] González-Galindo, F. et al., Thermal and wind structure of the Martian thermosphere as given by two General Circulation Models, Planet. Space Sci., Vol. 58, pp. 1832-1849, 2010
[6] González-Galindo, F. et al., Three-dimensional Martian ionosphere model: I. The photochemical ionosphere below 180 km, J. Geophys. Res., Vol. 118, pp. 2105-2123, 2013
[7] González-Galindo, F. et al., Variability of the Martian thermosphere during eight Martian years as simulated by a ground-to-exosphere global circulation model, J. Geophys. Res., Vol., 120, pp. 2020-2035, 2015
[8] Montabone, L. et al., Eight-year Climatology of Dust Optical Depth on Mars, Icarus, Vol. 251, pp. 65-95, 2015
[9] González-Galindo, F. et al., The martian mesosphere as revealed by CO 2 cloud observations and General Circulation Modeling, Icarus, Vol. 216, pp. 10-22, 2011
[10] Gagné, M.E., et al., Modeled O2 airglow distributions in the Martian atmosphere, J. Geophys. Res., Vol. 117, E06005, 2012
[11] Stiepen, A. et al., Nitric oxide nightglow and Martian mesospheric circulation from MAVEN/IUVS observations and LMD-MGCM predictions, J. Geophys. Res. Vol. 122, pp. 5782-5797, 2017
[12] Medvedev, A. et al., Cooling of the Martian thermosphere by CO2 radiation and gravity waves: An intercomparison study with two general circulation models, J. Geophys. Res., Vol. 120, pp. 913-927, 2015
[13] Chaufray, J.-Y. et al., Variability of the hydrogen in the martian upper atmosphere as simulated by a 3D atmosphere-exosphere coupling, Icarus, Vol. 245, pp. 282-294, 2015
[14] Modolo, R. et al., Mars-solar wind interaction: LatHyS, an improved parallel 3-D multispecies hybrid model, J. Geophys. Res., Vol. 121, pp. 6378-6399, 2016
[15] Holstein-Rathlou, C., Maue, A., and Withers, P., Atmospheric studies from the Mars Science Laboratory Entry, Descent and Landing atmospheric structure reconstruction, Planet. Space Sci., Vol. 120, pp. 15-23, 2016
[16] Gröller, H. et al., Probing the Martian atmosphere with MAVEN/IUVS stellar occultations, Geophys. Res. Lett., Vol. 42, pp. 9064-9070, 2015
[17] Peter, K. et al., The dayside ionospheres of Mars and Venus: Comparing a one-dimensional photochemical model with MaRS (Mars Express) and VeRa (Venus Express) observations, Icarus, Vol. 233, pp. 66-82, 2015
[18] Yigit, E. et al., High-altitude gravity waves in the Martian thermosphere observed by MAVEN/NGIMS and modeled by a gravity wave scheme, Gesophys. Res. Lett., Vol. 42, pp. 8993-9000, 2015

Synthetic Retrievals of H2O and CO2 in the Mars Upper Atmosphere Using Solar Occultation Spectra for the NOMAD and ACS Instruments of the ExoMars TGO Mission

B. N. Hill[1*]; *M. A. López-Valverde[1]; B. Funke[1], S. Jiménez-Monferrer[1]; F. Gonzalez-Galindo[1]; M. López-Puertas[1].*
[1]Instituto de Astrofísica de Andalucía (IAA/CSIC), Spain

Introduction

After finishing its aerobraking phase, the ExoMars Trace Gas Orbiter (TGO) will soon start taking science measurements of the Martian atmosphere. From that point TGO will be making systematic solar occultation observations for the first time of the Martian atmosphere. One of the key goals of this mission is to gain a better understanding of the namesake trace gases of the Martian atmosphere with the NOMAD and ACS spectrometers.

This mission presents us with a unique opportunity to explore the atmospheric vertical structure (composition and temperature) at high vertical resolution, and hopefully in a wide range of altitudes extending into the upper thermosphere. Making good use of this data requires specialized tools, specifically a line-by-line radiative transfer model and an appropriate inversion scheme.

As part of the NOMAD and ACS science teams, our group at the Instituto de Astrofísica de Andalucía (IAA/CSIC) has experience in simulating CO2 emissions in the upper atmospheres of the three terrestrial planets under conditions of non-local thermodynamic equilibrium (non-LTE) [1, 2, 3]. We also performed successful retrievals of CO densities in the Venus atmosphere [4] and our team has helped develop, in partnership with IMK / Karlsruhe Institute of Technology, a line-by-line radiative transfer model (KOPRA) [5] used to simulate emission and absorption spectra primarily of the Earth's atmosphere. We expect that with some additional adaptations this tool will become a valuable asset for us in taking advantage of the solar occultation data from ExoMars TGO instruments in other spectral regions in the near-IR.

CO2 is the primary component of the martian atmosphere but its abundances in the upper atmosphere have not been adquately measured, especially its variability with season, solar cycle and latitude. Water vapor is a key ingredient of Martian photochemistry. Its variability is a hot topic, and its presence has been detected at high altitudes in abundances much higher than previously expected [6]. Also, water vapor abundance has recently been found to be heavily influenced by lower and middle atmospheric processes [7].

In this talk, we would like to go over the adaptations that we have made to our radiative transfer model KOPRA in order to handle solar occultation measurements, the application of the modified tool to specific selections of NOMAD spectral intervals containing detectable H2O and CO2 lines, and the incorporation of the effects of the NOMAD and ACS instruments' responses on synthetic spectra. We present results from our synthetic retrievals of H2O and CO2, a comparison of results from both instruments (NOMAD and ACS), and our plans to apply it to other atmospheric species like methane and CO.

1. Acknowledgements

This work was supported by the Spanish Ministry of Economy and Innovation and by the FEDER funds under grant ESP2015-65064-C2-1-P (MINECO/FEDER).

2. References

[1] López-Puertas, M. and Taylor, F., Non-LTE radiative transfer in the atmosphere. Ed. World Scientific, 2001.
[2] Gilli, G., Lopez-Valverde, M.A., Funke, B.: Non-LTE CO limb emission at 4.7 μm in the upper atmosphere of Venus, Mars and Earth: Observations and modeling, Planetary and Space Science, Vol 59, pp1010-1018, 2011. doi: 10.1016/j.pss.2010.07.023.
[3] López-Valverde, M. A., Lopez-Puertas, M., Funke, B.: Modeling the atmospheric limb emission of CO 2 at 4.3 m m in the terrestrial planets, Planetary and Space Science, Vol 59, pp 988–998, 2011. doi: 10.1016/j.pss.2010.02.001
[4] Gilli, G., Lopez-Valverde, M.A., Peralta, J.: Carbon monoxide and temperature in the upper atmosphere of Venus from VIRTIS/Venus Express non-LTE limb measurements, Icarus, Vol 248, pp 478-498, 2015. doi: 10.1016/j.icarus.2014.10.047
[5] Stiller, G.P., Clarmann, T., Funke, B.: Sensitivity of trace gas abundances retrievals from infrared limb emission spectra to simplifying approximations in radiative transfer modelling, Journal of Quantitative Spectroscopy and Radiative Transfer, Vol 72(3), pp249–280, 2002. doi:10.1016/S0022-4073(01)00123-6
[6] Fedorova, A., Bertaux, JL., and Betsis, D.: Water vapor in the middle atmosphere of Mars during the 2007 global dust storm, Icarus, Vol 300, 15 January, pp 440-457, 2018.
[7] Heavens, N., Kleinböhl, A., and Chaffin, M.: Hydrogen escape from Mars enhanced by deep convection in dust storms, Nature Astronomy, Vol 2, February 2018, pp126–132, 2018.

Comparison of the thermal structure derived using SOIR on board Venus Express with a 1-D non-LTE radiative transfer model

A. Mahieux[1,2,3]; *R. V. Yelle[2], A. C. Vandaele[3], V. Wilquet[3]*
[1] The University of Texas at Austin, USA
[2] The University of Arizona, USA
[3] Belgian Institute for Space Aeronomy, Belgium

1. Introduction

The SOIR infrared spectrometer on board Venus Express probed the Venus terminator region from mid-2006 till end of 2014. The measurements were taken at both morning and evening terminators, covering all latitudes from pole to pole. The wavelength range of 2.2 to 4.3 µm allowed a detailed chemical inventory of the Venus atmosphere [1-6], including CO_2, CO, H_2O, HCl, HF, SO_2 and aerosols. CO_2 was detected from 70 km up to 165 km, CO from 70 km to 140 km, and the minor species typically below 110 km down to 70 km.
Number density profiles of these species are computed from the measured spectra. Temperature profiles are obtained while computing the spectral inversion of the CO_2 spectra combined with the hydrostatic law [3].
These temperature measurements show a striking permanent temperature minimum close to the homopause (~125 km, ~100 K) and a weaker temperature maximum (100-115 km, 200-250 K). The time variability of the CO_2 density profiles spans over two orders of magnitude, and a clear trend is seen with latitude. The temperature variations are also important, of the order of 35 K for a given pressure level, but the latitude variation are small. Results from the morning and evening terminators are quite similar. The mean SOIR vertical profiles are given in . The O profile is taken from [7] and the N_2 profile is taken as 3.5% of the total density.

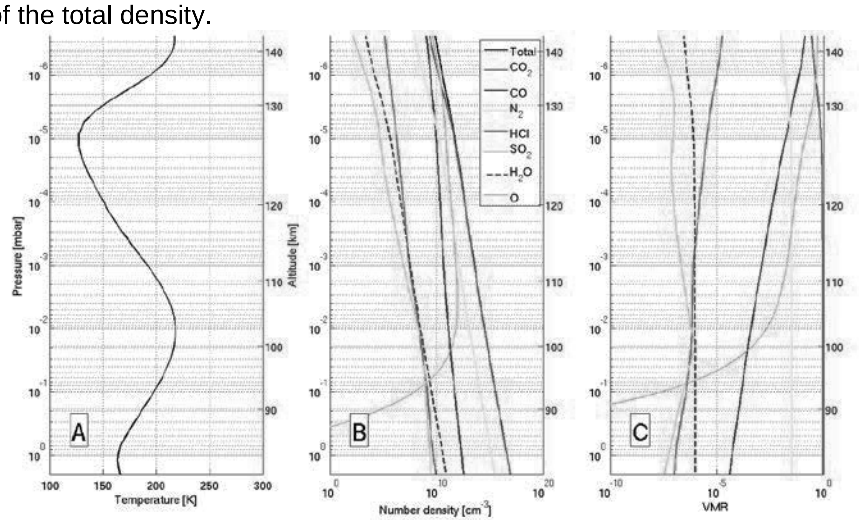

Figure 12: Mean profiles derived from the SOIR measurements, as a function of the pressure, covering the 2 mbar to 10^{-7} mbar (80 km to 143 km) region. The altitudes are indicated on the right side of each panel. Panel A: mean temperature profile; Panel B: mean number density profiles of the different species considered in this study; Panel C: mean VMR profiles.

2. Radiative model

A 1-D radiative transfer model has been developed to interpret the SOIR terminator profiles. This model solves the coupled, time-dependent energy balance, diffusion, and continuity equations in the vertical direction. It accounts for heating and cooling radiative terms originating from CO_2 non local thermodynamical equilibrium (LTE), by grouping the population levels between 4 and 15 µm into 8 groups, and solving the corresponding radiative transfer equations and energy levels populations, while considering collisional de-excitation by CO_2, CO, O and N_2.
UV heating by CO_2, CO and O are also taken into account, as well as radiative rotational cooling by minor species detected by SOIR (e.g. HCl, SO_2, and H_2O) which are found to be small in comparison to the CO_2 non LTE cooling. Aerosol cooling in the 60-110 km altitude range may be important to the thermal balance.

3. Discussion

There is a good agreement between the 1D model temperature profile and the mean SOIR temperature profile, when aerosols cooling is considered in the mesosphere. Modes 1 and 2 are considered in the current study, in agreement with mean vertical profiles derived from the SOIR spectra [6]. We note that H_2O cooling plays a large effect, together with CO_2 non-LTE heating below the mesopause in the lower atmosphere, while CO_2 non-LTE cooling and UV heating are dominant in the upper atmosphere. Further we can suggest parameters that can be adjusted to improve the agreement between the model and measurements. The remaining differences can be attributed to the atmosphere dynamics at the terminator.

4. Future prospects

This model will be adapted to Mars in order to study the temperature profiles derived instruments on-board the MAVEN mission and by the NOMAD instrument on-board ExoMars.

5. Acknowledgments

The research program was supported by the Belgian Federal Science Policy Office and the European Space Agency (ESA – PRODEX program). The research was performed as part of the “Interuniversity Attraction Poles” programme financed by the Belgian government (Planet TOPERS). The authors also recognize the support from the FP7 EuroVenus project (G.A. 606798) as well as that of the HiResMIR International Scientific Coordination Network (GDRI). A. Mahieux would like to thank the FNRS (Belgium) for his Chargé de Recherches position and for supporting two stays at the University of Arizona.

6. References

[1] Bertaux, J.L., et al., *A warm layer in Venus' cryosphere and high altitude measurements of HF, HCl, H_2O and HDO.* Nature, 2007. **450**(29 November): p. 646-649, doi:10.1038/nature05974.
[2] Vandaele, A.C., et al., *Carbon monoxide short term variability observed on Venus with SOIR/VEX.* Planet. Space Sci., 2015. **113-114**: p. 237-255.
[3] Mahieux, A., et al., *Update of the Venus density and temperature profiles at high altitude measured by SOIR on board Venus Express.* Planet. Space Sci., 2015. **113-114**: p. 309-320.
[4] Mahieux, A., et al., *Venus mesospheric sulfur dioxide measurement retrieved from SOIR on board Venus Express.* Planet. Space Sci., 2015. **113-114**: p. 193-204.
[5] Mahieux, A., et al., *Hydrogen Halides measurements in the Venus upper atmosphere retrieved from SOIR on board Venus Express.* Planet. Space Sci., 2015. **113-114**: p. 264-274.
[6] Wilquet, V., et al., *Optical extinction due to aerosols in the upper haze of Venus: Four years of SOIR/VEX observations from 2006 to 2010.* Icarus, 2012. **217**(2): p. 875-881.
[7] Bougher, S.W., et al., *Venus Mesosphere and Thermosphere. III. Three-Dimensional General Circulation with Coupled Dynamics and Composition.* Icarus, 1988. **73**: p. 545-573.

Comparisons Between MAVEN/NGIMS Thermospheric Neutral Wind Observations and M-GITM Model Simulations

K. Roeten[1*]; S. Bougher[1], M. Benna[2], P. Mahaffy[2], Y. Lee[2], D. Pawlowski[3], F. González-Galindo[4], M. López-Valverde[4]
[1]Climate and Space Sciences and Engineering Department, University of Michigan, USA
[2]NASA GSFC Planetary Environments Laboratory, USA
[3]Physics & Astronomy Department, Eastern Michigan University, USA
[4]Instituto de Astrofisica de Andalucia/CSIC, Spain

Introduction

The MAVEN (Mars Atmosphere and Volatile Evolution) mission is currently providing systematic observations of the Martian upper atmosphere [4]. Additionally, the NGIMS (Neutral Gas and Ion Mass Spectrometer) instrument on MAVEN is producing a new dataset of thermospheric neutral wind measurements [2]. These are the first in-situ observations of thermospheric winds at Mars, and as such, provide a unique opportunity to add to our understanding of the dynamics of the Martian upper atmosphere. Furthermore, when these wind observations are compared to model simulations, the processes driving the winds (and their variations) in the upper atmosphere can be examined and better understood. Here, the Mars Global Ionosphere-Thermosphere Model (M-GITM) is utilized for data-model comparison.

Neutral Wind Observations

With this new observational technique, NGIMS has the capability to measure horizontal winds in-situ along orbit passes from periapsis up to ~200 km. The technique involves nodding the Articulated Payload Platform (APP) to rapidly vary the instrument's pointing by ±6º from the ram direction as well as utilizing the spectrometer's retarding potential analyzer capability. With this method, wind velocities can be determined for both cross-track and along-track flow (relative to the spacecraft ram direction). Horizontal winds can be measured up to 350 m/s with an accuracy of 30 m/s for cross-track winds and 100 m/s for along-track winds [2]. Using spacecraft geometry, cross-track and along-track velocities are then converted to zonal and meridional velocities.

Wind observations are done in monthly campaigns in which, nominally, five orbits of neutral wind measurements and five orbits of ion wind measurements are taken consecutively [2]. The first wind campaign took place in September 2016, and campaigns have been carried out on a near monthly cadence since January 2017. These five consecutive neutral wind measurements in a campaign are averaged to find a representative wind velocity profile for each campaign. This serves to smooth out potential longitudinal variability, as MAVEN circles the planet once about every five orbits [4]. Significantly, looking at mean winds over time should also allow seasonal-length trends in thermospheric winds to be more readily observable. Currently, the neutral wind dataset spans over half a Martian year.

Data-Model Comparisons

These NGIMS neutral wind campaigns have been compared to simulations from the Mars Global Ionosphere-Thermosphere Model (M-GITM), a ground to exosphere 3-D global circulation model [1]. From the M-GITM simulations, winds are extracted along the same track flown during each MAVEN orbit using the spacecraft's trajectory information. These model "flythroughs" allow for a more direct comparison to the in-situ NGIMS wind observations.

A preliminary comparison with M-GITM simulations has shown that the NGIMS wind measurements in many cases do not match the simulated thermospheric winds in speed, direction, or both. Yet, in a few cases, both direction and magnitude of the simulated and observed winds are similar. The M-GITM model is currently primarily driven by solar EUV forcing at thermospheric altitudes. Thus, it is likely that for cases where simulated and observed winds are similar, EUV heating is the primary mechanism driving the thermospheric winds. However, large discrepancies between simulated and observed winds in other campaigns may indicate at those times the winds are strongly impacted by other physical processes which the model is presently lacking or handles poorly.

Notably, there have been recent upgrades in the M-GITM code to improve data-model comparisons. First, a modern CO_2 NLTE 15-µm cooling scheme [3] has been added to accurately capture the feedback of atomic O densities and large diurnal temperature variations on the cooling rates. Second, the solar EUV fluxes measured at Mars by the MAVEN EUVM (Extreme Ultraviolet Monitor) have been used to assemble the FISM-M (Flare Irradiance Spectral Model - Mars) empirical model, yielding daily averaged full solar spectra from ~0-190 nm in 10 nm bin intervals [6]. The wavelength bins used by M-GITM are populated using these daily averaged datasets to provide solar EUV fluxes corresponding to MAVEN-specific orbit observations.

Four NGIMS neutral wind campaigns were selected for more in-depth study and comparison with the upgraded M-GITM simulations. These campaigns were specifically chosen so that cases with a better match in direction but worse match in speed (September 2016, December 2017), a case with a better match in speed but poor match in direction (May 2017), and a case with extremely poor match in direction and speed (January 2017) would be analyzed. Additionally, campaigns with a range of conditions, i.e., different seasons (aphelion, perihelion, and equinox), local times (midnight, noon, and near the evening terminator), and latitudes, are represented in the analysis. This was done in order to try to capture some of the wind variability induced by these widely different conditions.

The M-GITM simulations (with the addition of the new 15-µm cooling code and FISM-M output) can thus be used to better understand the extent of the role of solar EUV heating in driving thermospheric winds through these data-model comparisons. These simulations and comparisons will also serve as a baseline for future studies as new physics is added to the model.

Specifically, gravity waves are believed to have large thermal and dynamical impacts in the thermosphere, and are expected to significantly modify the thermospheric structure and circulation [5]. Presently, a spectral nonlinear gravity wave parameterization scheme [7] is being incorporated into M-GITM to identify the relative importance of gravity wave effects during these MAVEN wind campaigns.

References

[1] Bougher, S. W., D. Pawlowski, J. M. Bell, S. Nelli, T. McDunn, J. R. Murphy, M. Chizek, and A. Ridley: Mars global ionosphere-thermosphere model: Solar cycle, seasonal, and diurnal variations of the Mars upper atmosphere, J. Geophys. Res. Planets, Vol 120, pp. 311–342, 2015.

[2] Bougher, S. W., K. Roeten, K. Olsen, P. Mahaffy, M. Benna, M. Elrod, J. Bell, and B. Jakosky: Variability of the thermospheric wind structure of Mars: MAVEN NGIMS measurements and corresponding global model simulations, Abstract # P13D-05, AGU, 12-16 December 2016, San Francisco, CA, USA, 2016.

[3] González-Galindo, F., J.-Y. Chaufray, M. A. López-Valverde, G. Gilli, F. Forget, F. Leblanc, R. Modolo, S. Hess, and M. Yagi: Three-dimensional Martian ionosphere model: I. The photochemical ionosphere below 180 km, J. Geophys. Res. Planets, Vol. 118, pp. 2105-2123, 2013.

[4] Jakosky, B. M., et al.: The Mars Atmosphere and Volatile Evolution (MAVEN) mission, Space Sci. Rev., Vol 195, pp. 3–48, 2015.

[5] Medvedev, A. S., and E. Yigit: Thermal effects of internal gravity waves in the Martian upper atmosphere, Geophys. Res. Lett., Vol. 39, pp. L05201, 2012.

[6] Thiemann, E. M. B., P. C. Chamberlin, F. G. Eparvier, B. Templeman, T. N. Woods, S. W. Bougher, and B. M. Jakosky: The MAVEN EUVM model of solar spectral irradiance variability at Mars: Algorithms and results, J. Geophys. Res. Space Physics, Vol. 122, pp. 2748–2767, 2017.

[7] Yigit, E., and A. S. Medvedev: Heating and cooling of the thermosphere by internal gravity waves, Geophys. Res. Lett., Vol. 36, pp. L14807, 2008.

Proton Aurora on Mars

B. Ritter,[1,2*]; J.-C. Gérard[1]; B. Hubert[1]; L. Rodriguez[2]; L. Gkouvelis[1]
[1]LPAP, Université de Liège, Belgium
[2]Royal Observatory of Belgium

Introduction

Three kinds of aurora have been detected on Mars by the ultraviolet spectrometers SPICAM (Spectroscopy for the Investigation of the Characteristics of the Atmosphere of Mars) on board Mars Express and IUVS on board MAVEN: the discrete aurora [1,2,3,4], the diffuse aurora [5] and the proton aurora [6,7]. We present a brief overview of the three kinds of aurorae and measurement results from SPICAM for the proton aurora.

Electron Aurorae

The discrete and the diffuse aurora are seen on the Martian nightside. Both result from energetic electron impact on the upper atmosphere. Their emission in the UV includes features from CO (Cameron bands, Fourth Positive bands), CO_2^+ and atomic oxygen.

The discrete aurora is spatially confined and linked to the topology of the crustal magnetic field of Mars. It is seen at altitudes of about 140 km. The diffuse aurora on the other hand is neither restricted in location nor linked to the Martian magnetic field, but is thought to be globally extended. The long lasting (days) features extend down to altitudes of 60 km and are observed following periods of enhanced solar activity.

SPICAM observations of the proton aurora

The proton aurora has been observed on the dayside of Mars. It originates from precipitating protons onto the Martian hydrogen corona that partially convert by charge transfer to fast neutral hydrogen atoms. It can be identified by an intensity enhancement over the ubiquitous Lyman-□ dayglow at 121.6 nm at altitudes between 120 and 150 km (). It is not related to the residual Martian magnetic field. Its occurrence is correlated with the arrival at Mars of coronal mass ejections or corotating interaction regions from the Sun. During an observational period of 7 years of Mars Express data, Lyman-□ emission signatures of the proton aurora have been positively identified in about 4% of the limb observations of the dayside of the planet.

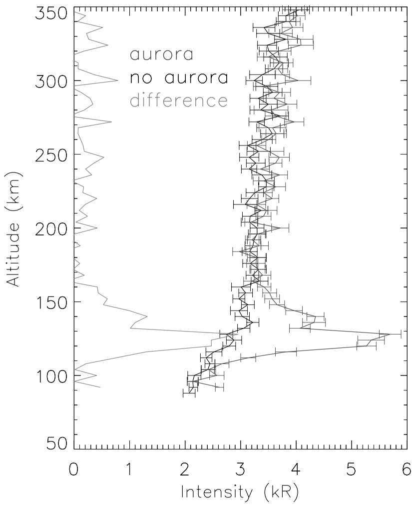

Figure 13: Lyman-α a limb profile of a proton aurora on Mars observed with SPICAM [7].

References

[1] Bertaux, J.-L., Leblanc, F., Witasse, O., Quemerais, E., Lilensten, J., Stern, S. A., Sandel, B., and Korablev, O.: Discovery of an aurora on Mars, Nature, 435(7043), 790–794, 2005.
[2] Leblanc, F., Chaufray, J.Y., Witasse, O., Lilensten, J., and Bertaux, J.-L.: The martian dayglow as seen by SPICAM UV spectrometer on Mars Express, Journal of Geophysical Research, 2006.
[3] Gérard, J.-C., Soret, L., Libert, L., Lundin, R., Stiepen, A., Radioti, A., and Bertaux, J.-L.: Concurrent observations of ultraviolet aurora and energetic electron precipitation with Mars Express, Journal of Geophysical Research: Space Physics, 120(8), 6749-6765,2015.
[4] Soret, L., Gérard, J.-C., Libert, L., Shematovich, V. I., Bisikalo, D. V., Stiepen, A., and Bertaux, J.-L.:

SPICAM observations and modeling of Mars aurorae, Icarus, 264, 398-406, 2016.
[5] Schneider, N. M., Deighan, J. I., Jain, S. K., Stiepen, A., Stewart, A. I. F., Larson, D. et al.: Discovery of diffuse aurora on Mars, Science, 350(6261), 0313, 2015.
[6] Deighan, J. et al.: Discovery of Proton Aurora at Mars, AGU, Fall General Assembly, #P13D-01, 2016.
[7] Ritter, B., Gérard, J.-C., Hubert, B., Rodriguez, L., and Montmessin, F.: Observations of the Proton Aurora on Mars with SPICAM on board Mars Express, Geophysical Research Letters, 45, 2018.

Acknowledgements. This research was partly funded by the NOMAD PRODEX programme managed by the European Space Agency with help of the Belgian Science Policy Office (BELSPO) and by BELSPO's SCOOP/BRAIN research contract.

The Ionospheric composition of Mars and its dependence on magnetic configuration

L. Maes[1*]; M. Fraenz[1], E. Dubinin[1], J. McFadden[2].
[1]Max Planck Institute for Solar System Research, Germany
[2]University of California, Space Science Laboratory, U.S.A

Introduction

The solar wind has a strong effect on the Martian ionosphere. It's pressure and magnetic field configuration control the magnetization and structuring of the ionosphere of Mars. Using data from the Suprathermal and Thermal Ion Composition (STATIC) onboard the MAVEN satellite, we will analyze the composition and layering of the ionosphere under different magnetic conditions, during specific passes through the ionosphere around Maven's pericenter. By combining data from the Magnetometer (MAG) and electron data from the Solar Wind Electron Analyzer (SWEA), we can analyze the magnetic structure with magnetic field, and its effect on the ionospheric composition. These results may help constraining ionospheric models of Mars and interpreting the ionospheric composition data from the ASPERA instrument on Mars Express.

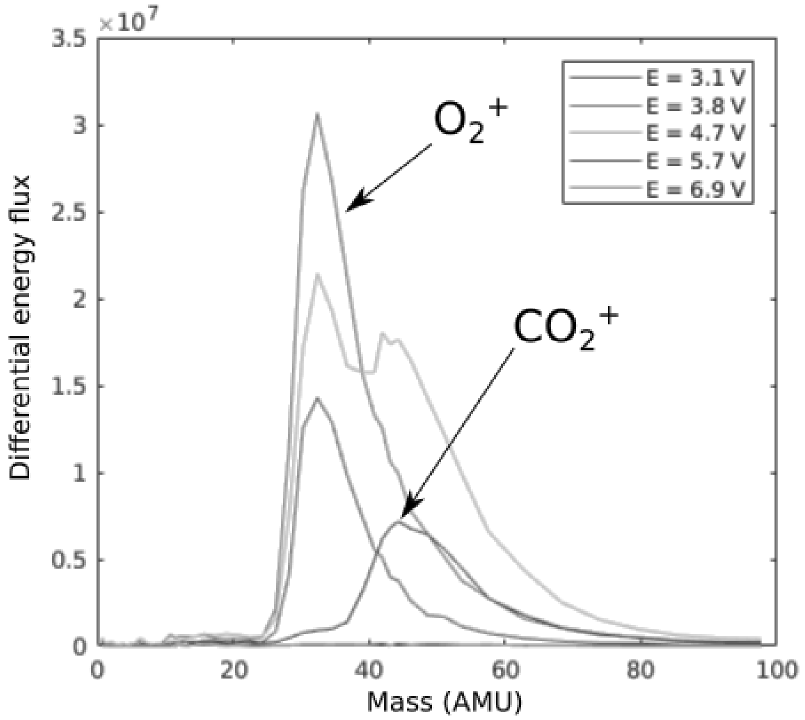

Figure 14: An example of a time-of-flight mass spectrogram by the STATIC instrument onboard MAVEN

Wave Structures in the Ionosphere and Upper Atmosphere of Mars as seen by the Mars Express Radio Science Experiment (MaRS)

S. Tellmann[1*]; K. Peter[1], M. Pätzold[1], B. Häusler[2], D.P. Hinson[3,4], and G.L. Tyler[4]
[1]Rheinisches Institut für Umweltforschung, Department of Planetary Research, Germany
[2]Institut für Raumfahrttechnik und Weltraumnutzung, Universität der Bundeswehr Munich, Germany
[3]Carl Sagan Center, SETI Institute, USA
[4] Department of Electrical Engineering, Stanford University, Stanford, USA

Introduction

Atmospheric waves play a crucial role in all stably stratified planetary atmospheres. They contribute significantly to the redistribution of momentum, energy and dust between the different atmospheric regions.

Several different kinds of waves are known to exist in the Martian atmosphere. Almost all kinds of waves have been detected in the lower and middle atmosphere of Mars (e.g. stationary and transient waves [1], baroclinic waves as well as migrating and non-migrating thermal tides [2], gravity waves, etc...). In the thermosphere, thermal tides have been observed e.g. by radio occultation or accelerometer measurements on MGS [3, 4]. Recently, the NGIMS instrument on MAVEN reported gravity waves in the thermosphere of Mars [5].

The Radio Science Experiment MaRS on Mars Express

The Mars Express Radio Science Experiment (MaRS) retrieves refractivity profiles from the lower atmosphere (a few hundred metres above the surface) to the topside of the ionosphere. These refractivity profiles are used to analyse temperature, pressure and neutral number density profiles in the lower atmosphere (up to ~ 40-50 km) and electron density profiles in the ionosphere of Mars [6,7, 8] with a high vertical resolution of only a few hundred metres.

In the lower atmosphere, MaRS could observe large scale stationary waves that dominate the northern winter atmosphere (lat: 64.8° - 65.1°, LT: 12.97—14.9; Ls = 6.7°-16.3°). Electron density profiles, retrieved during the same occultation experiments and additional electron density profiles are now used to study atmospheric waves in the upper atmosphere and ionosphere. Two coherent frequencies (X- & S-band) allow to discriminate between plasma density fluctuations in the ionosphere and Doppler related frequency shifts caused by spacecraft movement.

Waves in the Upper Atmosphere and Ionosphere

In the ionosphere, large scale waves propagating from the lower atmosphere upwards lead to altitude changes of the main ionospheric peaks as a function of planetary longitude. These waves can be identified as thermal tides influenced by the Martian topography. An ionospheric time stepping model (Ion-A2; [9]) is used to study the influence of neutral atmospheric density shifts on the Martian ionosphere.

Small scale wavelike structures have also been detected below the main ionospheric layers (M1 & M2) and in the topside of the ionosphere. A careful analysis of the observed electron density fluctuations in combination with simulations based on ray tracing methods and comparisons with Mars atmospheric model predictions is used to classify the observed features.

References

[1] Noguchi, K., Y. Morii, N. Oda, T. Kuroda, S. Tellmann, and M. Pätzold, Role of stationary and transient waves in CO2 supersaturation during northern winter in the Martian atmosphere revealed by MGS radio occultation measurements, *J. Geophys. Res. Planets*, *122*, 912–926, doi:10.1002/2016JE005142, 2017.
[2] Withers, P., Pratt, R., Bertaux, J.L., and Montmessin, F., Observations of thermal tides in the middle atmosphere of Mars by the SPICAM instrument, J. Geophys. Res., 116, E11005, doi:10.1029/2011JE003847, 2003.
[3] Bougher, S.W., Engel, S., Hinson, D.P., and Forbes, J.M., Mars Global Surveyor Radio Science electron density profiles: Neutral atmosphere implications, Geophys. Res. Lett., 28, 16, 3091 - 3094, 2001.
[4] Cahoy, K.L., Hinson, D.P., and Tyler, G.L., Characterization of a semidiurnal eastward-propagating tide at high northern latitudes with Mars Global Surveyor electron density profiles, Geophys. Res. Lett., 34, L15201, doi:10.1029/2007GL030449, 2007.
[5] Yigit, E., England, S.L., Liu, G., Medvedev, A.S., Mahaffy, P.R., Kuroda, T., and Jakosky, B.M., High-

altitude gravity waves in the Martian thermosphere observed by MAVEN/NGIMS and modeled by a gravity wave scheme, Geophys. Res. Lett., 42, 8993 - 9000, 2015.
[6] Pätzold, M., et al., Mars Express 10 years at Mars: Observations by the Mars Express Radio Science Experiment (MaRS), Plan. Space Sci., 127, 44 - 90, 2016.
[7] Pätzold, M., et al. MaRS: Mars Express Radio Science Experiment, SP-1291. Mars Express: The Scientific Investigations. European Space Agency, Special Publication, pp.217–245, 2009.
[8] Tellmann, S., Pätzold, M., Häusler, B., Hinson, D.P., Tyler, G.L., The structure of Mars lower atmosphere from Mars Express Radio Science (MaRS) occultation measurements. J. Geophys. Res. Planets118, 306–320. http://dx.doi.org/ 10.1002/jgre.20058, 2013.
[9] Peter, K., et al., The dayside ionospheres of Mars and Venus: Comparing a one-dimensional photochemical model with MaRS (Mars Express) and VeRa (Venus exppress) observations, Icarus, 233, 66—82, 2014.

Acknowledgments
The MaRS Experiment is funded by the German Space Agency (DLR) under grant 50QM1401.

Conductivity Structures in The Martian Ionosphere

AlShehhi [1]: *M. O. Fillingim* [2]
[1]*Mohammed Bin Rashid Space Center, UAE*
[2]*Space Sciences Laboratory, University of California, USA*

Ionospheric conductivity is an extremely important quantity in determining the electrodynamics of planetary upper atmospheres. During its elliptical, approximately 4.5 hours orbit, the MAVEN spacecraft repeatedly passes through the upper atmosphere of Mars providing in-situ measurements of the neutral atmospheric density and composition, the plasma density, composition, and temperature, as well the ambient magnetic field. From these measurements, we calculate the different types of conductivity (Parallel, Pedersen, and Hall conductivities) -using the Equations below [1]- and characterize their behavior with respect to season, time of day, solar zenith angle, magnetic field strength, and altitude.

Parallel Conductivity:
Pedersen Conductivity:
Hall Conductivity:

The behavior of the conductivities with these various parameters are presented. Results are shown in the figures below.

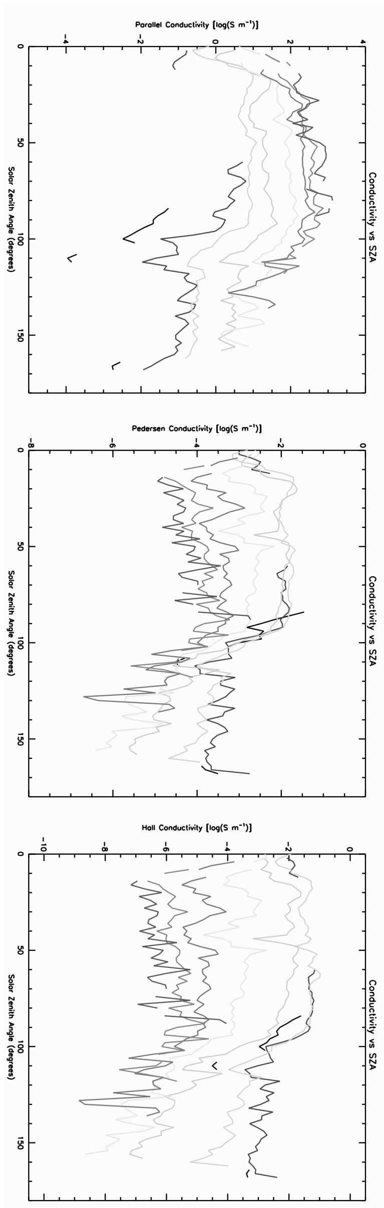

Figure 15: Types of conductivity vary due to change in solar zenith angle.

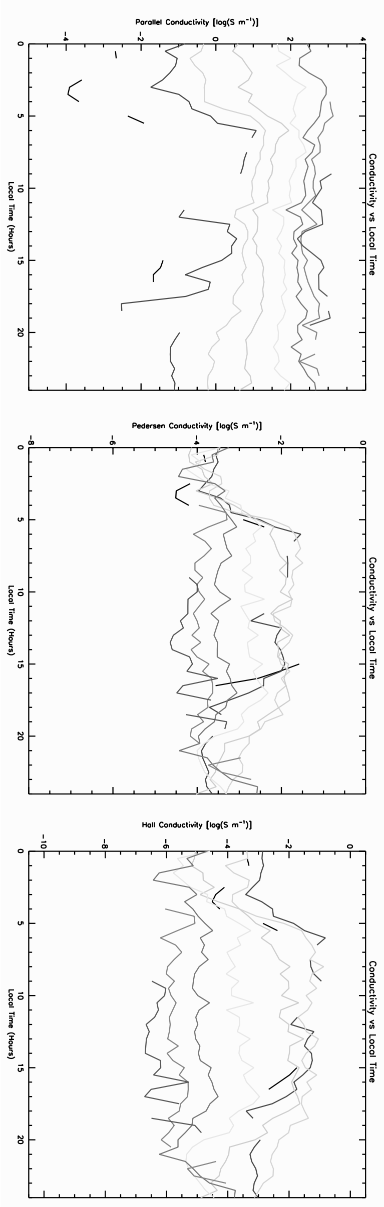

Figure 16: Types of conductivity vary due to change in local time.

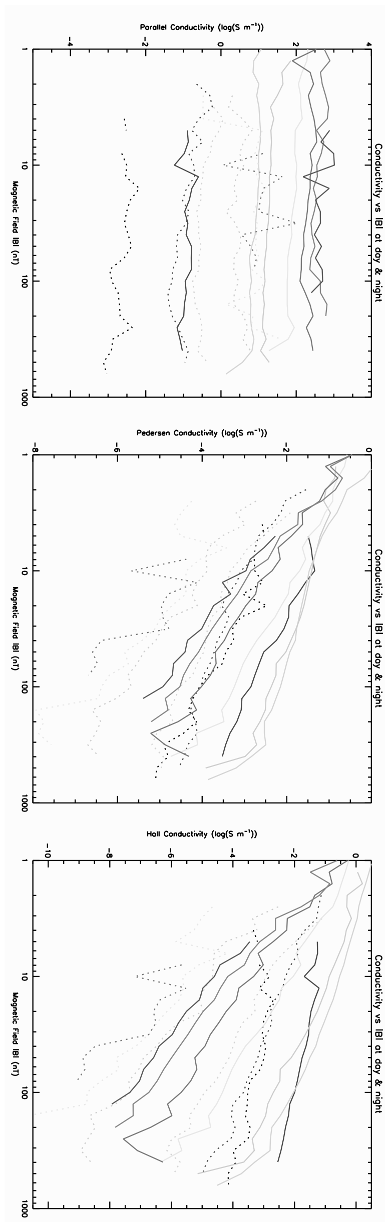

Figure 17: Types of conductivity vary due to change in magnetic field.

The change in colors resembles change in altitude. The colors index is illustrated below.

275 km - 300 km
250 km - 275 km
250 km - 250 km
200 km - 225 km
175 km - 200 km
150 km - 175 km
125 km - 150 km

To understand the behavior of conductivity even further, the behavior of dynamo region (the region where Hall conductivity is greater than Pedersen conductivity), ion density, and neutral density are studied with respect to the same parameters.

In general, the conductivities are lower in night time than in day time due to lower ion density. However, there is a dawn-dusk asymmetry in the behavior of the conductivities with a rapid increase in the conductivities at dawn and a relatively gradual decrease after dusk. Even though the parallel conductivity is independent of magnetic field strength, both Pedersen and Hall conductivities decrease as the magnetic field strength increases. This magnetic field effect is enhanced during night time in the absence of sunlight. Seasonal results are inconclusive as MAVEN has only collected data for approximately one Martian year. As MAVEN continues to collect more data, the seasonal behavior of the conductivity can be further investigated.

References:

[1] Boström, R. (1964), A model of the auroral electrojets, *J. Geophys. Res.*, *69*, 4983–4999.

Horizontal Magnetic Fields and Currents in the Ionosphere of Mars and Their Dependence on the Interplanetary Magnetic Field

M. O. Fillingim[1*]; A. L. Fogle[1], P. Dunn[1], J. E. P. Connerney[2], J. S. Halekas[3]
[1]Space Sciences Laboratory, University of California, USA
[2]Planetary Magnetospheres Laboratory, NASA Goddard Space Flight Center, USA
[3]Department of Physics and Astronomy, University of Iowa, USA

Introduction

How the solar wind interacts with a planetary object depends upon the object's properties, such as the presence of a magnetic field or an atmosphere. An un-magnetized object cannot deflect the flow of the solar wind unless it possess a substantial atmosphere which can be ionized by solar radiation creating a conductive ionosphere. Currents can then be induced in the ionosphere which act to cancel out the external interplanetary magnetic field (IMF) preventing it from reaching the surface. Here we present MAVEN observations of currents in the ionosphere of Mars and investigate their behavior with respect to the IMF direction.

Data and Methodology

During its elliptical, approximately 4.5-hour orbit, MAVEN repeatedly passes through the upper ionosphere providing in-situ measurements of the magnetic field from the magnetic field investigation (MAG) [1], [2] down to the periapsis altitude (~ 150 km). From these local measurements we calculate ionospheric currents from the curl of the magnetic field using Ampère's Law. However, in order to compute the curl of the magnetic field from single space-craft observations, we have to make assumptions about the uniformity of the magnetic field and the direction of magnetic field gradients. We assume that the principle gradient in the magnetic field is in the radial direction and that gradients in the horizontal directions are negligible. This assumption is most likely satisfied when the magnitude and variation of radial component of the magnetic field are small compared to the magnitude and variation of the horizontal components. In an attempt to satisfy this assumption, we restrict our analysis to a subset of the MAVEN MAG data where the ionospheric magnetic fields are approximately horizontal to the surface; i.e., the radial component of the magnetic field is small. Therefore, when computing ionospheric currents, we only use magnetic field data with a magnetic dip angle (the angle be-tween the magnetic field direction and the horizontal) less than 18o between 300 km altitude and the space-craft periapsis (~ 150 km). The calculated ionospheric currents are, therefore, likewise horizontal.

You will find an example of how to include your reference list at the end of this file. You may cite all references with [1], [2], [3], etc. The reference list should be in an alphabetical order. All references in the bibliography list should start with the reference number being put in square brackets.

Results

In the first two years of MAVEN data, we have identified nearly 200 orbits where these criteria are satisfied. In addition, we further subdivide these observations based on the average direction of the IMF measured during the preceding apoaspsis orbit segment (if MAVEN did in fact enter the solar wind during the preceding aposapsis orbit segment). We have identified 65 orbits where MAVEN encountered the solar wind and then subsequently measured horizontal magnetic fields in the ionosphere. During most of these orbits (49 orbits), the IMF direction was predominantly directed east-west (33 orbits with earthward IMF and 16 orbits with westward IMF), consistent with a Parker spiral orientation. Of the remaining 16 orbits, 9 had a north-ward IMF and 7 had a southward IMF.

At high altitudes (> ~ 200 km), the observed ionospheric magnetic fields are generally in the same direction as the IMF, consistent with a draped IMF. The magnetic field magnitude and direction are roughly constant and the derived current densities are small. Below ~ 200 km, in the ionospheric dynamo region, large rotations in the magnetic field direction and/or large changes in the magnitude of the magnetic field are often observed. These changes in the magnetic field are accompanied by significant ionospheric cur-rents with current densities on the order of a few 10-6 A m-2.

We consider two possibilities to explain the changing magnetic fields and currents at lower altitudes: either the conducting ionosphere is keeping a record of the highly variable IMF strength and direction or dynamics in the thermosphere/ionosphere are driving currents which modify the ionospheric magnetic field. Disentangling these effects is left for future work.

References

[1] Connerney, J. E. P.;,Espley, J., Lawton, P., Murphy, S., Odom, J., Oliversen, R., and Sheppard, D.: The MAVEN Magnetic Field Investigation, Space Sci. Rev., Vol. 195, pp. 257–291, 2015.

[2] Connerney, J. E. P., Espley, J. R., DiBraccio, G. A., Gruesbeck, J. R., Oliversen, R. J., Mitchell, D. L., Halekas, J., Mazelle, C., Brain, D., and Jakosky, B. M.: First results of the MAVEN magnetic field investigation, Geophys. Res. Lett., Vol. 42, pp. 8819-8827, 2015.

Seasonal Changes in the Polar Ionosphere and Thermosphere on Mars

M. Pilinski[1*]; L. Andersson[1], C. Fowler[1], E. Thiemann[1]
[1]Laboratory for Atmospheric and Space Physics, USA

The MAVEN satellite has now made two Martian-years of ionosphere-thermosphere (I-T) observations enabling the study of seasonal changes in the upper atmosphere. Based on previous MAVEN results, between 150-180 km altitudes, there is no statistical correlation between ionospheric properties and local magnetic field strength. This implies that the localized crustal magnetic fields at Mars (located primarily in the southern hemisphere) should not have a significant impact in this region. This is not unexpected due to the unmagnetized nature of ions at these low altitudes. The MAVEN dataset provides in-situ measurement coverage below 220 km altitudes in both the northern and southern polar regions. This enables a comparison between the I-T systems in each polar region, and an ability to distinguish any effects driven by the localized crustal magnetic fields. Given the aforementioned unmagnetized nature of ions below ~200 km altitudes at Mars, the large-scale dynamics of these polar regions should be driven primarily by seasonal and latitudinal differences, rather than localized crustal magnetic field structures.

The MAVEN mission has already enabled detailed studies of the equatorial ionosphere in recent years. These studies have revealed the morning electron temperature overshoot as well as a close dependence between electron temperatures and neutral densities. In this presentation, we will discuss how the summer and winter polar region ionospheres differ. Furthermore, we will discuss how changes in solar distance drive differences between the northern and southern summer ionospheres.

Magnetic structure and propagation of a solar flux rope from the Sun to Saturn

E. Palmerio[1*], E.K.J. Kilpua[1], M. Mierla[2,3], A.N. Zhukov[2,4], D. Barnes[5], O. Witasse[6], L. Rodriguez[2], A. Isavnin[7], C. Möstl[8], B. Sánchez-Cano[9], T. Nieves-Chinchilla[10,11], E. Roussos[12], A. Masters[13], N.P. Savani[14,11]
[1]Department of Physics, University of Helsinki, Finland
[2]Solar-Terrestrial Center of Excellence, SIDC, Royal Observatory of Belgium, Belgium
[3]Institute of Geodynamics of the Romanian Academy, Romania
[4]Skobeltsyn Institute of Nuclear Physics, Moscow State University, Russia
[5]STFC-RAL Space, Rutherford Appleton Laboratory, Harwell Campus, UK
[6]ESTEC, European Space Agency, Netherlands
[7]Center for Mathematical Plasma Astrophysics, Department of Mathematics, KU Leuven, Belgium
[8]Space Research Institute, Austrian Academy of Sciences, Austria
[9]Radio and Space Plasma Physics Group, Department of Physics and Astronomy, University of Leicester, UK
[10]Catholic University of America, United States
[11]NASA, Goddard Space Flight Center, United States
[12]Max Planck Institute for Solar System Research, Germany
[13]The Blackett Laboratory, Imperial College London, UK
[14]Goddard Planetary Heliophysics Institute, University of Maryland, United States

1. Introduction

The prediction of the magnetic structure, arrival time, and arrival speed of coronal mass ejections (CMEs) at different locations in the heliosphere is a subject of intense study and great importance for understanding how CMEs evolve after they erupt. CMEs form in the solar atmosphere as helical magnetic field structures known as flux ropes [1]. The magnetic structure of flux ropes at the time of their eruption can be inferred through indirect proxies based on the source region of the CME. These proxies allow us to reconstruct the “intrinsic flux rope type” at the time of the eruption. However, the knowledge of the magnetic structure of the flux rope at the Sun does not always imply a successful prediction of the magnetic structure at Earth, or in general in interplanetary space. This is because CMEs can change their orientation and shape due to deflections, rotations, and/or deformations [2].

2. The 11 May 2012 CME

In this work, we study in detail a filament eruption and related CME that took place on 11 May 2012, with the aim of estimating how the knowledge of the intrinsic flux rope type is useful in the case of CMEs that are associated with rotating filaments. We aim to compare the magnetic structure of the CME flux rope as seen at the Sun with observations at different planets. We use observations from multiple vantage points in order to analyse the evolution of the flux rope from the Sun throughout the heliosphere. Figure 1 shows the position of the planets and spacecraft involved in the study during 12 May 2012. We use remote-sensing observations of the solar disc, the corona, and the inner heliosphere, and *in situ* measurements taken at Venus, at Earth, at Mars, and at Saturn. The CME was directed towards Mars, and impacted Venus, Earth, and Mars during 13-17 May 2012, and Saturn on 16 June 2012.

2.1. Remote-sensing observations

We determine the intrinsic flux rope type by analysing several indirect proxies from remote-sensing multiwavelength observations [3]. We also reconstruct the 3D configuration of the filament by applying the tie-pointing technique [4], which is a triangulation method that can be used to evaluate the 3D rotation of erupting filaments. The orientation of the CME in the corona is estimated through the graduate cylindrical shell model [5] applied to coronagraph data.

2.2. Stereoscopic Self-Similar Expansion model

The evolution of the CME is then observed in Heliospheric Imagers data, where we triangulate the leading edge of the flux rope until it becomes too faint to be analysed. At this point, we apply the Stereoscopic Self-Similar Expansion model [6] to propagate the CME until the orbit of Saturn.

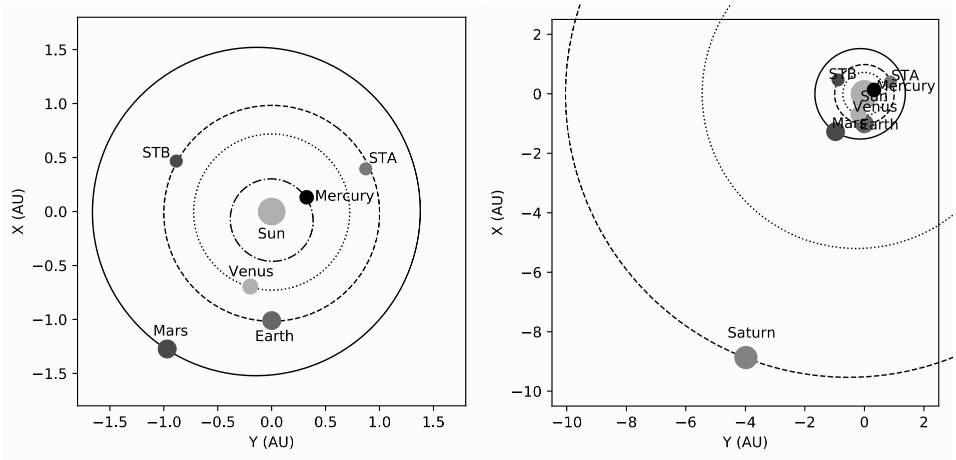

Figure 1: Positions of the planets and spacecraft, *left)* in the inner solar system (*i.e.*, until the orbit of Mars) and *right)* until the orbit of Saturn, during 12 May 2012.

2.3. *In situ* observations

We analyse the magnetic structure of the flux rope at Venus (in the solar wind), at Earth (in the solar wind), and at Saturn (in the magnetosheath). Mars had no spacecraft carrying a magnetometer outside of its magnetopause. Finally, we study galactic cosmic rays and energetic particles associated with the CME event (*i.e.*, Forbush decreases and solar energetic particles, SEPs) at different locations in the heliosphere.

3. Orientation of the flux rope axis

The flux rope axis was tilted ~65° Southeast at the eruption onset. Upon eruption, however, the filament apex rotated clearly clockwise (as expected for a right-handed flux rope), and left the SDO and STEREO field of view as a nearly-parallel to the ecliptic flux rope, with its axis pointing roughly to the East. During the filament eruption, the western leg was seen to rotate for about 2 hours after onset, while the eastern leg disappeared shortly and its evolution could not be followed. The magnetic structure of the CME at Venus and at Earth, however, suggests that the flux rope axis was pointing roughly to the Northwest, which means reversed by 180° in direction compared to what we would expect *in situ*.

Since coronagraph data do not show significant rotation of the CME, the causes of the mismatch between remote-sensing and *in situ* observations cannot be attributed to rotations of the whole CME body. Possible explanations are the filament's eastern leg having rotated a large amount, or the CME front being extremely distorted. Further investigation of the flux rope structure at Saturn may give new insights about the global structure and orientation of the CME.

4. References

[1] Antiochos, S.K., DeVore, C.R., and Klimchuck, J.A., A model for solar coronal mass ejections, Astrophys. J., 510, 485-493, 1999.
[2] Isavnin, A., Vourlidas, A., and Kilpua, E.K.J., Three-dimensional evolution of flux-rope CMEs and its relation to the local orientation of the heliospheric current sheet, Solar Phys., 289, 2141-2156, 2014.
[3] Palmerio, E., Kilpua, E.K.J., James, A.W., Green, L.M., Pomoell, J., Isavnin, A., and Valori, G., Determining the intrinsic CME flux rope type using remote-sensing solar disk observations, Solar Phys., 292, 39, 2017.
[4] Thompson, W.T., 3D triangulation of a Sun-grazing comet, Icarus, 200, 251-357, 2009.
[5] Thernisien, A., Vourlidas, A., and Howard, R.A., Forward modelling of coronal mass ejections using STEREO/SECCHI data, Solar Phys., 256, 111-130, 2009.
[6] Davies, J.A., Harrison, R.A., Perry, C.H., Möstl, C., Lugaz, N., Rollett, T., Davis, C.J., Crothers, S.R., Temmer, M., Eyles, C.J., and Savani, N.P., A self-similar expansion model for use in solar wind transient propagation studies, Astrophys. J., 750, 23, 2012.

A statistical study of thermal, dynamic, and magnetic pressures on the dayside of the induced magnetosphere of Mars as observed by MAVEN

M. K. G. Holmberg[1*]; N. André[1], P. Garnier[1], R. Modolo[2], L. Andersson[3], J. Halekas[4], C. Mazelle[1], V. Génot[1]
[1]IRAP, University of Toulouse, CNRS, UPS, CNES, France
[2]LATMOS/IPSL, UVSQ Université Paris-Saclay, UPMC University Paris CNRS, France,
[3]LASP, University of Colorado, Boulder, USA,
[4]Department of Physics and Astronomy, University of Iowa, Iowa City, USA,

Introduction

This study focuses on characterising the dayside of the induced magnetosphere of Mars by studying the dominant pressure terms in the different plasma regimes found in this region. A correct characterisation is important in order to understand the structure and dynamics of the Martian magnetosphere, both the present one and the past. The thermal, dynamic, and magnetic pressure terms are estimated using almost 3 years of observations by the MAVEN spacecraft. As expected, the dominant terms are the solar wind dynamic pressure P_d, the thermal pressure in the magnetosheath $P_{th,m}$, the magnetic pressure in the magnetic pileup region (MPR) P_B, and the thermal pressure in the ionosphere $P_{th,i}$. The dayside of the induced magnetosphere of Mars is shown to be a very dynamic region and the pressure terms vary with more than one order of magnitude for the same radial distance from the planet. However, the pressure estimates show a clear separation between the ionosphere, the MPR, and the magnetosheath.

Observations and pressure estimations

The P_d and $P_{th,m}$ are estimated using ion density n_i, velocity v_i, and temperature T_i measurements from the Solar Wind Ion Analyzer (SWIA) [5]. The dynamic pressure is estimated using

$$P_d = n_i m_p v_i^2 \cos(SZA)^2 \tag{1}$$

where m_p is the proton mass and SZA is the solar zenith angle. The thermal pressure is estimated using

$$P_{th,s} = n_j k_B T_j \quad \text{where } s = i,m \ \ \& \ \ j = e,i, \tag{2}$$

and k_B is the Boltzmann constant. The P_B is estimated using magnetic field measurements from the magnetometer investigation (MAG) [3]. The magnetic pressure is estimated using

$$P_B = B^2/2\mu_0 \tag{3}$$

where μ_0 is the vacuum permeability. The $P_{th,i}$ is estimated using equation (2) and the electron density n_e and temperature T_e measurements from the Langmuir Probe and Waves (LPW) instrument [1].

To estimate the pressure terms we use all SWIA, MAG, and LPW measurements recorded within two cylinders, one smaller for the regions within the bow shock and one larger for the solar wind measurements. The smaller cylinder ranges from altitude 115 km (the closest point of approach) to 3000 km with a radius of 1019 km (0.3 Mars radii R_M, where 1 R_M = 3396.2 km) and the larger from 1000 km to 6000 km with a radius of 3057 km (0.9 R_M). The data sets include all data recorded from the Mars orbit insertion on September 21, 2014 until June 29, 2017. We have excluded measurements over larger crustal field regions, $|B_{crust}|$ > 25 nT at 400 km, detected by the Morschhauser crustal field model [6].

Results

Figure 1 shows the mean values of the estimated pressure terms for each 10 km bin. The different regions are clearly separated by the upper pressure balance boundary, where $P_{th,m} = P_B$, located at around 750 km (1.22 R_M) and the lower pressure balance boundary, where $P_B = P_{th,i}$, located at around 175 km (1.05 R_M). The ranges of the different pressure terms are listed in Table 1. The presented values are in general smaller than the values presented by earlier measurements from the MEX spacecraft, which showed mean values of 1.1 > P_d > 1.8, 0.3 > $P_{th,m}$ > 0.7, and 0.7 > P_B > 1.8 nPa [4]. The smaller P_d confirms the previous finding that the n_i and v_i proxy derived from MEX is overestimating both parameters when compared to the direct measurements performed by SWIA [2]. The $P_{th,m}$ agrees well with the estimates presented in this study. The P_B obtained from MEX data is also based on a proxy, obtained from measurements by the Mars Advanced Radar for Subsurface and Ionospheric Sounding (MARSIS) radar, which is a possible reason for the slight overestimation of P_B.

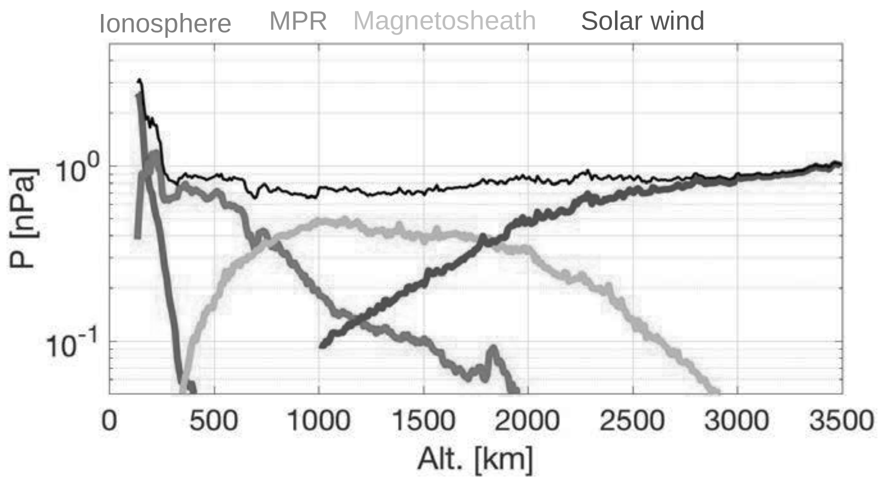

Figure 1: Average pressure, in nPa, estimated from almost 3 years of MAVEN measurements vs. altitude above the surface. The figure shows the thermal pressure of the ionosphere $P_{th,i}$ (blue), the magnetic pressure of the magnetic pileup region P_B (red), the thermal pressure of the magnetosheath $P_{th,m}$ (yellow), the solar wind dynamic pressure P_d (purple), and the total pressure P_{tot} (black) measured on the dayside of the magnetosphere for low SZA.

Region alt. [km]	Ionosphere < 175	MPR 175 - 750	Magnetosheath 750 - ~2000	Solar wind > ~2000
Pressure [nPa]	> 0.9	0.3 - 1.2	0.3 – 0.5	0.5-1

Table 1: The ranges of the estimated pressure terms, in nPa, for the respective regions.

The pressure boundaries do not correspond to the same altitudes as other boundaries such as the photoelectron boundary (PEB), the ion composition boundary (ICB), and the magnetic pileup boundary (MPB)/induced magnetosphere boundary (IMB). The PEB and the ICB is found within the MPR. The drop in electron flux associated with the MPB/IMB is usually also found within the MPR and only occasionally in the transition region between the MPR and the magnetosheath.

References

[1] Andersson, L., Ergun, R. E., Delory, G. T., Eriksson, A., Westfall, J., Reed, H., McCauly, J., Summers, D., and Meyers, D.: The Langmuir Probe and Waves (LPW) Instrument for MAVEN, Space Sci. Rev., 195, pp. 173–198, 2015.
[2] Budnik, E., Fedorov, A., and Barabash, S.: Solar wind parameters near Mars and Venus obtained by Mars Express and Venus Express missions. Comparison with simulations and MAVEN data, EPSC2017-948 poster, 2017.
[3] Connerney, J. E. P., Espley, J., Lawton, P., Murphy, S., Odom, J., Oliversen, R., and Sheppard, D.: The MAVEN magnetic field investigation, Space Sci. Rev., 195, pp. 257– 291, 2015.
[4] Dubinin, E., Modolo, R., Fraenz, M., Woch, J., Duru, F., Akalin, F., Gurnett, D., Lundin, R., Barabash, S., Plaut, J. J., and Picardi, G.: Structure and dynamics of the solar wind/ionosphere interface on Mars: MEX-ASPERA-3 and MEX-MARSIS observations, Geophys. Res. Lett., 35 (11), 2008.
[5] Halekas, J. S., Taylor, E. R., Dalton, G., Johnson, G., Curtis, D. W., McFadden, J. P., Mitchell, D. L., Lin, R. P., and Jakosky, B. M.: The solar wind ion analyzer for MAVEN, Space Sci. Rev., 195, pp. 125–151, 2013.
[6] Morschhauser, A., Lesur, V., and Grott, M.: A spherical harmonic model of the lithospheric magnetic field of Mars, J. Geophys. Res. Planets, 119, pp.1162-1188, 2014.

Modeling of energetic ions observations by MAVEN in the crustal field regions

A. Kotova[1*]; C. Mazelle[1], Y. Soobiah[2], Y. Ma[3], D. Mitchell[4], J. Halekas[5], J. Espley[2]
[1]IRAP, Université de Toulouse, CNRS, UPS, CNES, France
[2]NASA Goddard Space Flight Center, Greenbelt, Maryland, United States
[3]Institute of Geophysics and Planetary Physics, University of California, United States
[4]University of California, United States
[5]University of Iowa, United States

Abstract

During several passages of the Mars Atmosphere and Volatile EvolutioN (MAVEN) mission through low altitude crustal field regions its onboard instruments Solar Wind Ion Analyzer (SWIA) and Solar Wind Electron Analyzer (SWEA) had detected unexpected co-marsward directed ions and electrons of broad energy range, including relatively high energy ions of several keV. To understand the origin and driving mechanisms of these fluxes, the particle tracing code was applied to simulate the observations of MAVEN instruments using the backwards tracing approach. Time-dependent multispecies single-fluid MHD model of plasma environment around Mars was taken as a base for the particle tracing. Simulation concerns H+, O+ and O2+ ions. Here we would like to overview the data, that shows interesting keV-ion distribution, demonstrate the modelling technique and discuss the possible acceleration mechanism of those ions, their origin and probable ion energy dispersion in Martian crustal magnetic fields.

Effects of the Crustal Magnetic Fields and Changes in the IMF Orientation on the Magnetosphere of Mars

N. Romanelli[1*], R. Modolo[1], F. Leblanc[2], J-Y. Chaufray[1], S. Hess[3], D. Brain[4], J. Connerney[5], J. Halekas[6], J. McFadden[7], B. Jakosky[4].

[1] Laboratoire Atmosphères, Milieux et Observations Spatiales (LATMOS), IPSL, CNRS, UVSQ, UPMC, France

[2] LATMOS/IPSL, UPMC, Univ Paris06 Sorbonne Universités, UVSQ, CNRS, France.

[3] Office National d'Etudes et de Recherches Aérospatiales, France.

[4] Laboratory for Atmospheric and Space Physics, University of Colorado, USA.

[5] NASA Goddard Space Flight Center, USA.

[6] Department of Physics and Astronomy, University of Iowa, USA

[7] Space Sciences Laboratory, University of California, USA.

Introduction

The Mars Atmosphere and Volatile Evolution MissioN (MAVEN) is currently probing the very complex and dynamic Martian environment. Although the main structures resulting from the interaction between the solar wind (SW) and the induced magnetosphere of Mars can be described using a steady state picture, time-dependent physical processes play a key role modifying the response of this obstacle. These processes are the consequence of temporal variabilities in the internal and/or external electromagnetic fields and plasma properties. For instance, the rotation of the crustal magnetic fields (CF) constantly modifies the intrinsic magnetic field topology relative to the SW magnetized plasma flow. Moreover, changes in the interplanetary magnetic field (IMF) orientation are convected by the SW and also affect the structure of the magnetosphere [6].

Results

In this work we analyze magnetic field and plasma measurements provided by MAVEN [3] on 23 December 2014 between 06:00 UT and 14:20 UT. During this time interval the spacecraft sampled the Martian magnetosphere twice, with highly similar trajectories. MAVEN measurements suggest that the external conditions remained approximately constant when the spacecraft was inside the magnetosphere for the first time. In contrast, MAVEN observed changes in the IMF orientation before visiting the magnetosphere for the second time. To investigate the response of the Martian plasma environment to the rotation of the CF and the change of the background magnetic field orientation, we perform numerical simulations making use of the LatHyS three dimensional multispecies hybrid model [7,8]. These simulations include the rotation of the CF and use MAVEN observations to set the external SW conditions and the variation of the IMF. The simulation results are compared with MAVEN Magnetometer [1], Solar Wind Ion Analyzer [2] and Suprathermal and Thermal Ion Composition [5] observations obtained in the Martian magnetosphere and show a good agreement, as can be seen, for example, in Figure 1. Model results also show that the geometry of the bow shock is affected by the location of the strongest crustal magnetic field sources. In addition, we determine the timescales over which the Martian magnetosphere adapts to changes in the IMF orientation. In the particular case of the Martian magnetotail, we find that the external region adapts very quickly (∼ 8 seconds) and is capable of following the IMF rotation, after a small time delay. In contrast with this, the inner lobes follow the change in the IMF orientation in a smoother way (∼ 10 min) and with a much larger time delay. We also perform estimations of the total planetary proton and oxygen escape fluxes at different times during this event, shown in Figure 2. We find that the latter are not strongly affected by the observed changes in the IMF direction. However, we observe an appreciable anticorrelation (with some time delay) between the crustal magnetic field intensity at the dayside of Mars and magnitude O^+ ion loss rates, in agreement with results reported in previous studies [4].

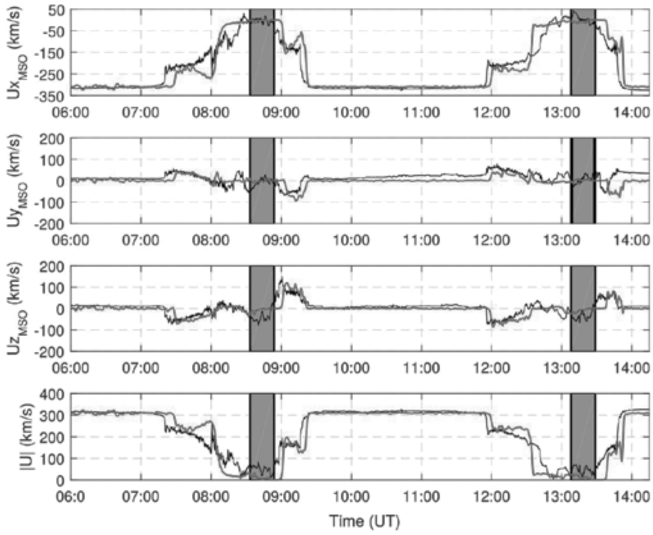

Figure 1: MAVEN Solar Wind Ion Analyzer plasma bulk velocity measurements as a function of time (in

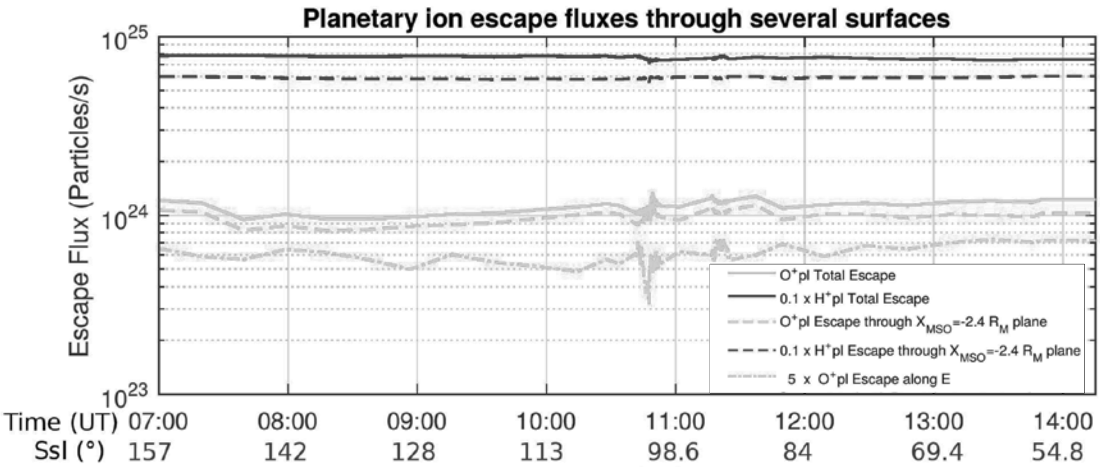

black) and LatHyS results projected along the spacecraft trajectory (in red).

Figure 2: LatHyS H^+ and O^+ escape fluxes through the simulation box (total), the plane XMSO =-2.4 RM (Martian radii) and the convective electric field as a function of time (The XMSO axis points from the center of Mars towards the Sun).

References

[1] Connerney, J. E. P., et al., (2015), Space Sci. Rev., 195, 1–35.
[2] Halekas, J. S., et al., (2015), Space. Sci. Rev., doi:10.1007/s11214-013-0029-z.
[3] Jakosky, B. M., et al. (2015), Space Sci. Rev., 195, 3–48.
[4] Ma, Y., et al. (2014), Geophys. Res. Lett., 41, 6563-6569, doi:10.1002/2014GL060785.
[5] McFadden, J., et al. (2015), Space Sci. Rev., 195, 199-256, doi:10.1007/s11214-015-0175-6.
[6] Modolo, R., G. M. Chanteur, and E. Dubinin (2012), Geophys. Res. Lett., 39, L01106.
[7] Modolo, R., et al. (2016), JGR, Space Phys., 121, 6378–6399.
[8] Modolo, R., et al. (2017), Planetary Space and Science, http://dx.doi.org/10.1016/j.pss.2017.02.015.

Acknoledgements

N.R. is supported by a CDD contract from Laboratoires d’excellence Exploration Spatiale des Environnements Planétaires (LABEX-ESEP ANR N° 572 2011-LABX-030)

Extracting hidden knowledge from data archives using machine learning and open data approaches for space weather effects investigation

R. Boumghar[1*]; O. Witasse[2], A. Donati[3]
[1]European Space Agency/ESOC, Germany
[2]European Space Agency/ESTEC, Netherlands
[3]European Space Agency/ESOC, Germany

Introduction

The development of scientific payloads to observe space weather take several years and involves an important number of scientists all over the world. Their work nurtured in years of training helped them building theories one after the other. Nowadays several space missions have flown or are still flying, acquiring a large amount of data to help scientists verify their hypothesis.

Too few projects involve data-driven approaches to create hypothesis directly from the data, permitting to find the humanly un-findable and sometimes un-thinkable. Human beings can generally build concepts with less than ten parameters while a data-driven algorithm can build models using more than a thousand of parameters.

New approaches

Machine learning and deep learning are part of artificial intelligence methods. They provide new tools for data-driven approaches to find, correlate, model, space weather. In the following figure, the blue curve is an automatically learnt model of the green curve which represents the thermal power consumption of Mars Express. Any discrepancy between the prediction and reality may be linked with external factors, factors not used during the training of the machine learning models, like space weather events.

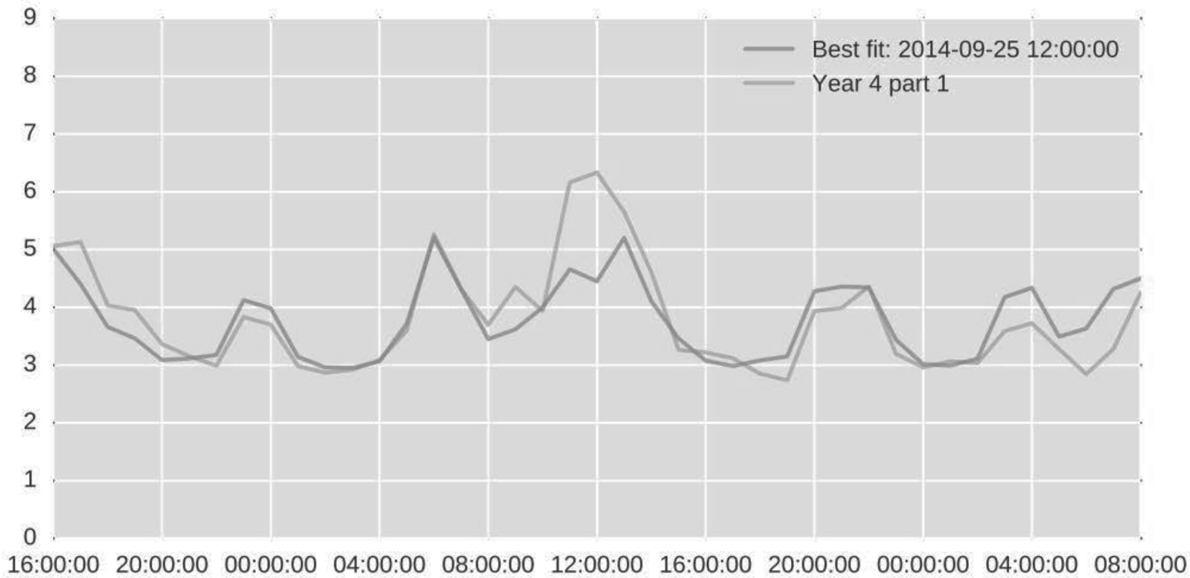

Thermal power consumption prediction, model build using about 400 parameters

In this paper, we show how data-driven approaches helped building the thermal subsystem power consumption model of the Mars Express mission, the estimation of the entry and exit from the radiation belt for the XMM-Newton and Integral missions. These examples offer potential benefits in increasing science capabilities by augmenting observation time or knowledge on available resources for operators.

We demonstrate the advantage of data-driven approaches. Having the prediction of behaviour of every subsystems on every spacecraft we can analyse It can extend the studies of space weather effects, that could be inferred from all the data of all the spacecraft in operations in the solar system.

The Dependences of the Structure and Properties of Martian Dayside Magnetosphere on Solar Zenith Angle and IMF Clock Angle as observed on MAVEN

V. Ermakov[1*]; *O. Vaisberg[2], S. Shuvalov[3], L. Zelenyi[4], J. Halekas[5], G. DiBraccio[6], E. Dubinin[7]*
[1]Space Research Institute of the Russian Academy of Sciences, Russia
[2]Space Research Institute of the Russian Academy of Sciences, Russia
[3]Space Research Institute of the Russian Academy of Sciences, Russia
[4]Space Research Institute of the Russian Academy of Sciences, Russia
[5]Department of Physics and Astronomy, University of Iowa, USA
[6]NASA Goddard Space Flight Center, USA
[7]Max-Planck-Institute for Solar System Research, Germany

Introduction

In contrast to the nightside magnetosphere of Mars, its dayside was not intensively studied because of its small thickness and low temporary resolution of plasma instruments on board Martian satellites prior to MAVEN spacecraft. Magnetosphere identified as a region between magnetosheath flow and the ionosphere is filled with planetary ions of intermediate energies in comparison to ion energies in surrounding regions. Despite small thickness of dayside magnetosphere, it is important region as the source of the magnetosphere and planetary ions on the night side.

Analysis

Using plasma and magnetic field measurements of STATIC and MAG instruments, respectively, we carried out an analysis of MAVEN crossings of this region in MSE coordinates derived from MAVEN measurements of interplanetary magnetic field (IMF) in the solar wind as described in [Halekas et al., 2017]. We used data from January 1, 2016 through April 1, 2016 in order to investigate dependence of magnetosphere properties on solar zenith angle (SZA) in the range from ~30° to ~80°

Magnetosphere boundaries locations as well as its thicknesses were calculated in dependence on SZA and IMF clock angle. Energy-time spectrograms of protons, O^+ and O_2^+, magnetic field to plasma energies ratios, magnetic barrier maximum location and magnitude, mass-loading and other properties of the magnetosphere are different for different IMF clock angles.

Discussion

The dependence of magnetosphere properties, especially mass-loading, on SZA was considered from the point of view of processes filling the dayside magnetosphere with planetary ions and leading to characteristic energy distribution. These processes include planetary ions pick-up by magnetic flux tubes convecting in the magnetosphere around the planet from the subsolar to terminator region and acceleration by the motional electric field of ionospheric, magnetospheric and exospheric ions.

References

[1] Halekas, J., Ruhunusiri, S., Harada, Y., Collinson, G., Mitchell, D., Mazelle, C., McFadden, J., Connerney, J., Espley, J., Eparvier, F., Luhmann, J., and Jakosky, B.: Structure, dynamics, and seasonal variability of the Mars-solar wind interaction: MAVEN Solar Wind Ion Analyzer in-flight performance and science results, Journal of Geophysical Research: Space Physics, Vol. 122, pp. 547-578, 2017.

A multiscale structure of the cross-tail CSs and its relation to the ion composition according to MAVEN observations in the Martian magnetotail

E. Grigorenko[1]; S. Shuvalov[1], H. Malova[2,1], L. Zelenyi[1].*
[1]Space Research Institute of RAS, Russia
[2]Scobeltsyn Nuclear Physics Institute of Moscow State University, Russia

Introduction

Multilayered (embedding) Current Sheets (CS) are often observed in the Earth's magnetotail [1]. Simulations based on quasi-adiabatic dynamics of different ion components showed that the observed multiscale structures can be reconstructed by taking into account the net electric currents carried by ions with different masses and, thus, with different gyroradii [2]. The last determines the spatial scales of the corresponding current layers. The embedding can be quantitatively described by the ratio of the magnetic field value at the edges of a thin embedded layer B_1 to the value of the magnetic field outside the CS B_0 [1]. For the Earth's magnetotail it was shown that there is a relation between the B_1/B_0 and the relative densities of heavy and light ion components [2].

The embedding CSs in the Martian magnetotail

In the Martian magnetotail the embedding feature is also often observed in the cross-tail CS formed by the draping of the IMF field lines [3]. The analysis of ~100 CS crossings by MAVEN spacecraft at $X_{MSO} < -1\ R_M$ (R_M is a radius of Mars) showed that in the Martian magnetotail the relation between the embedding characteristics and ion composition is similar to the one observed in the terrestrial CSs, and the spatial scales of the embedded layers are defined by the gyroradii of the current carrying ion component. This finding confirms that the quasi-equilibrium CS state is supported by universal mechanisms based on general principles of plasma kinetic.

References

[1] Petrukovich, A., Artemyev, A., Malova, H., Popov, V., Nakamura, R., Zelenyi, L.: Embedded current sheets in the Earth's magnetotail, J. Geophys. Res., Vol. 116, A00125, doi:10.1029/2010JA015749, 2011.
[2] Zelenyi, L., Malova, H., Popov, V., Delcourt, D., Ganushkina, N., Sharma, S.: "Matreshka" model of multilayered current sheet, Geophys. Res. Lett., Vol. 33, L05105, doi:10.1029/2005GL025117, 2006.
[3] Grigorenko, E., Shuvalov, S., Malova, H., Dubinin, E., Popov, V., Zelenyi, L., Espley, J., McFadden, J.: Imprints of quasi-adibatic ion dynamics on the current sheet structures observed in the Martian magnetotail by MAVEN, J. Geophys. Res., Vol. 122, doi:10.1002/2017JA024216, 2017.

The solar wind interaction with Mars: current systems and electromagnetic fields in the Martian ionosphere

S. A. Ledvina[1*]; *S. H. Brecht*[2]
[1]*Space Sciences Lab, University of California, USA*
[2]*Bay Area Research Corp. Orinda, USA*

Introduction

Understanding the solar wind/IMF interaction with the Martian atmosphere/ionosphere has been a long standing issue for the space physics community. The issue is such a challenge that it is a major focus of both the Mars Atmosphere and volatile Evolution Mission (MAVEN) and the Mars Express (MEX) missions. Complicating our understanding of the interaction is the presence of remnant crustal magnetic fields at Mars. These crustal fields make a significant modification to the interaction between the solar wind/IMF and the ionosphere of the planet.

To fully understand the Martian solar wind interaction, the currents systems around the planet and the crustal magnetic fields must be determined. The term current system means not just the total current, $J = c/4\pi$ (□x B), but the ion currents individually and collectively as well as the electron current. Because of diamagnetic effects, the paths of these currents need and probably will not be the same. Current systems map the path of the escaping ions as well as the sources of induced fields within the ionosphere. Therefore, along with the currents one must examine the local electromagnetic fields associated with these currents.

This leads to the following set of questions:

- What are the current patterns within the ionosphere and tail regions of Mars?
- Which current patterns lead to ion loss?
- What are the electromagnetic features associated with current patterns leading to ion loss.
- How do these currents and electromagnetic features change as Mars rotates throughout the day?
- Finally, are there current patterns that correspond to the jet stream found on the Earth (closed patterns)?

Approach

You We address these questions using hybrid (kinetic ion, fluid electron) simulations of the Martian solar wind interaction using the HALFSHEL hybrid code [cf. *Brecht et al.*, 2016, 2017; *Ledvina et al.,* 2017; and references therein]. The HALFSHEL code contains the following models:

- **A highly resolved photochemistry on high resolution spherical grid**.
- **Charge exchange**
- **A collisional model**.
- **A 3-D conductivity tensor model**.
- **A crustal magnetic field model from** *Purucker et al.* [2000].
- **A 3-D neutral atmosphere model with neutral winds courtesy of Dr. Stephen Bougher.**

The neutral atmosphere is the source of the photo-chemically driven ionosphere within the code. The neutral winds modify the ion-neutral drag as well as provide the initial velocity for newly created photo ionized ions.

From the simulations we extract the total current J, the individual species and total ion currents J_i and the electron currents J_e, as well as the electric and magnetic fields associated with them. An example of the O^+ tail currnets can be seen in figure 1. The results are examined and used to address the above listed questions.

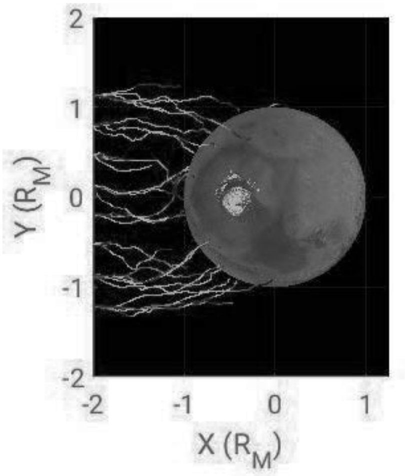

Figure 18 Martian O^+ tail currents

References

[1] Brecht, S. H., S. A. Ledvina, and S. W. Bougher, Ionospheric loss from Mars as predicted by hybrid particle simulations, J. Geophys. Res. Space Physics, 121, 10,190-10,208, 2016
[2] Brecht, S. H., S. A. Ledvina, and B. M. Jakosky, The role of the electron temperature on ion loss from Mars, J. Geophys. Res. Space Physics, 122, 8375-8390, 2017.
[3] Ledvina, S. A., S. H. Brecht, D. A. Brain, and B. M. Jakosky, Ion escape rates from Mars: Results from hybrid simulations compared to MAVEN observations, J. Geophys. Res. Space Physics, 122, 8391-8408, 2017
[4] Purucker, et al., An altitude normalized magnetic map of Mars and its interpretation, Geophys, Res. Lett., 27, 2449, 20

Effect of solar wind source variation events on planetary plasma environments

A. Opitz[1*]; *M. Dósa[2], A. Timár[1,2].*
[1]*Wigner RCP, Hungary*
[2]*Eötvös University, Hungary*

Introduction

Solar wind variations depend strongly on the solar source such as coronal holes, active regions and so forth. Their changes influence the temporal evolution of the solar wind structures such as CIRs or CMEs, which interact with the plasma environment of planets and comets.

Solar source variation events

We have performed a statistical search for solar wind source variation events through comparison of in situ solar wind plasma observations from multi-spacecraft (STEREO, SOHO, ACE, WIND, VEX and MEX). These changes in the solar source are responsible for solar wind spatial variability and temporal evolution on different scales.

Effects on planets and comets

The effects of these events on the plasma environment of planets and comets are very diverse depending on the characteristics of the planetary body. In this paper we compare a few examples, such as the effects on unmagnetized and magnetized bodies or planets with and without atmosphere.

Investigating space weather events at Mars with Mars Express housekeeping data

O. Witasse[1]*, R. F. Wimmer-Schweingruber[2], J. Guo[2], B. Sánchez–Cano[3], M. Lester[3], M. Denis[4], J. J. Plaut[5], D. Hassler[6]
[1] European Space Agency, ESTEC – Scientific Support Office, The Netherlands
[2] Institute of Experimental and Applied Physics, University of Kiel Germany,
[3] Radio and Space Plasma Physics Group, Department of Physics and Astronomy, University of Leicester, United Kingdom.
[4] European Space Agency, ESOC, Germany
[5] Jet Propulsion Laboratory, YSA
[6] Southwest Research Institute, Boulder, USA

Introduction

While space weather has been a growing field of research and applications over the last 15-20 years, "planetary space weather" is an emerging discipline [1]. To this end, scientists use plasma and field data from planetary missions. However, not all spacecraft provide relevant instrumentation. Nevertheless, some studies [2,3] have demonstrated that a spacecraft not equipped with dedicated sensors can act as a space weather monitor. Energetic particles impact detectors and subsystems on a spacecraft and their effects can be identified in selected housekeeping data sets. In this study, we test this idea with the Mars Express computer data.

1. Mars Express EDAC counter

High-energy particles which hit computer memory of a spacecraft can cause memory errors due to the charge deposited in the physical memory cells. Such errors are caught and corrected by the EDAC (Error Detection And Correction Code) algorithm. Once a correction is done, the relevant EDAC counter is incremented by 1. We studied the evolution of this housekeeping parameter on ESA's Mars Express spacecraft, and found that it successfully identifies some space weather events. The objective of this study is to assess the properties of space weather events that can be identified with this EDAC counter method.

2. The September 2017 event

Our test case is a recent and large space weather event which was detected at Mars around mid-September 2017: it consisted of a X-class solar flare, a fast coronal mass ejection (CME), and associated solar energetic particles (SEPs). Panel (A) of Figure 1 shows the evolution of the EDAC counter for the month of September. The change of slope occurs exactly during the space weather event. Panel (B) of Figure 1 displays the same counter but now with the addition of the cumulative count of the outer-scintillator sensor of the Mars Odyssey High-Energy Neutron Detector (HEND) instrument [4]. This sensor is sensitive to particle energies between 0.2 and 1.3 MeV. Our first conclusion is that the EDAC counter is a useful tool to detect some space weather events throughout the heliosphere.

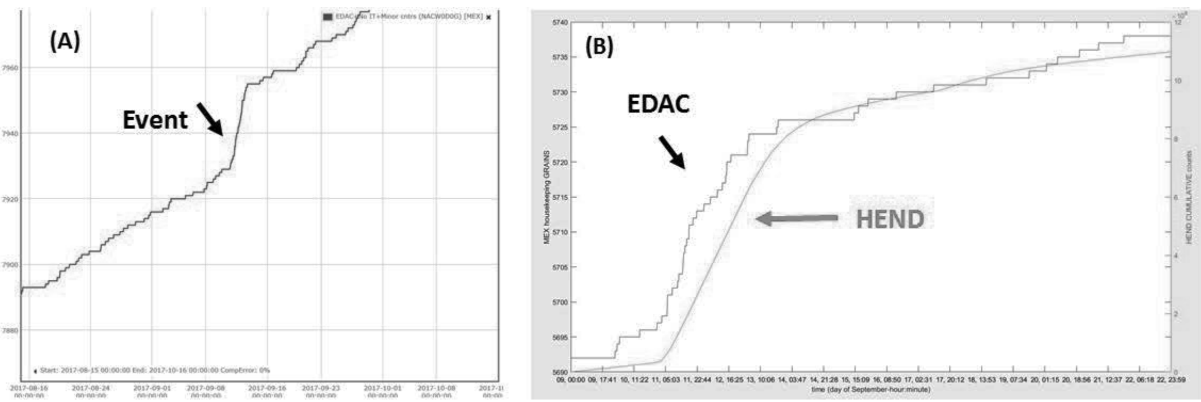

Figure 19: Panel (A): Evolution of the MEX EDAC counter in September 2017. The back arrow shows the time of the space weather event. Panel (B): A zoom on the space weather event. The EDAC counter (in black) is plotted together with the cumulative count of the HEND detector aboard Mars Odyssey (in pink).

3. Future work

The result of our assessment will be shown during this presentation, including calibration with HEND data and also with the Radiation Assessment Detector (RAD) data onboard NASA's MSL rover, Curiosity. We also study additional events to improve the statistics to demonstrate the validity of this method.

4. References

[1] Andre, N. et al., Planetary and Space Science,

[2] Hora, J. et al., The effects of cosmic rays and solar flares on the IRAC detectors: the first two years of in-flight operation, Proc. SPIE 6276, "High Energy, Optical, and Infrared Detectors for Astronomy II", 2006, eds. D. A. Dorn, A. D. Holland.

[3] Cheng, L. et al., Investigating Space Weather Events Impacting the Spitzer Space Telescope, AIAA 2014-1910

[4] Zeitlin et al., Mars Odyssey measurements of galactic cosmic rays and solar particles in Mars orbit, 2002–2008, SPACE WEATHER, VOL. 8, S00E06, doi:10.1029/2009SW000563, 2010

MESSENGER X-ray observations of electron precipitation events on the dayside surface of Mercury

S. T. Lindsay[*,1]; E. J. Bunce[1], S. M. Imber[1], A. Martindale[1], T. K. Yeoman[1]
[1]University of Leicester, UK

Introduction

Expanding upon previous reports describing electron-induced X-ray fluorescence events on the nightside surface of Mercury [1, 2], we describe the development of an algorithmic filter which reduces the contribution of fluorescence events driven by solar X-ray illumination. This has allowed tentative identification of analogous electron-induced X-ray fluorescence events taking place on the dayside. We discuss the distribution of these events in local time and latitude and the implications of these observations for particle motion in the planetary magnetosphere.

Method

Our analysis is based on data from the NASA/JHUAPL MESSENGER mission, which entered orbit about Mercury in March 2011 and operated until it impacted the planetary surface in April 2015. The X-Ray Spectrometer (XRS) onboard was a gas proportional counter-based X-ray fluorescence spectrometer, using three GPCs and applying the balanced filter method to achieve resolution of Al, Mg and Si fluorescence lines [3]. The XRS was paired with the Solar Assembly for X-rays (SAX), a Si PIN diode detector providing simultaneous observation of solar coronal X-ray emission (i.e. the presumed source for all surface X-ray fluorescence events).

Shortly after the beginning of MESSENGER's primary mission, X-ray fluorescence events were detected originating from the unlit surface of the planet where solar X-rays cannot be the source of fluorescent emission from the surface. Instead, these events are most likely driven by the precipitation of energetic particles, most likely electrons, from the magnetosphere to the surface [1]. When mapped in latitude-local time space, the locations of these particle-induced fluorescence events form clear organised regions reflecting the intersection of magnetospheric features, such as the open-closed field line boundary and magnetic equator, with the planetary surface [2].

Analysis of the distribution of these events on the dayside of the planet has been limited by our inability to distinguish particle-induced from solar-induced events. Our method avoids identifying individual fluorescence events as particle- or solar-induced, and instead filters an event catalogue which covers the whole mission, identifying event distributions as particle-induced with various levels of confidence dependent on the simultaneous solar X-ray spectrum. Thus, catalogues containing only events occurring where the solar X-ray spectrum is quiet are likely to contain proportionally more particle-induced fluorescence events than catalogues containing events occurring when levels of solar X-ray flux are high. Fluorescence in both Si and Ca was considered (these being rock-forming elements expected to be present broadly uniformly across the planetary surface), but solar and particle events were only separable in Ca fluorescence, which requires a higher energy to excite. Solar-induced Si fluorescence is present even when solar illumination is very low.

Results and discussion

The result () is a distribution of Ca fluorescence events in latitude and local time which exhibits a strong enhancement in particle-induced X-ray fluorescence centred at approximately local dawn and ~40°S. This enhancement appears at all levels of solar X-ray filtering which, along with the strong localisation, suggests that it is non-solar in origin. In addition, the nightside features previously observed and apparently associated with the open-closed field line boundary are still visible. No other significant organised enhancements were observed on the dayside of the planet.

Electrons within the magnetosphere moving from the nightside towards the dayside drift preferentially dawnward. Some precipitate at the nightside in latitudinal bands, while others may complete multiple drift orbits before being lost to the surface or at the magnetopause [4]. The detection of an intense area of electron precipitation at dawn suggests that a large fraction of these drifting electrons may be lost within a relatively small range of local times. The north-south asymmetry of this enhancement may be a result of the north-south asymmetry of the Mercury magnetic field, which results in a much larger loss cone in the southern hemisphere, although we note that the north-south asymmetry is less pronounced on the nightside of the planet.

Even if solar-induced events are not filtered out, the fraction of the total number of fluorescence events on the dayside occurring within the dawnward enhancement region is much larger than would be expected given isotropic illumination by a source such as the Sun. Therefore a significant fraction of fluorescence observed in the southern hemisphere can be expected to be electron-induced rather than solar-induced. It is important to understand and isolate these events, as knowledge of the illuminating spectrum is vital for the accurate analysis of X-ray fluorescence spectra. The impact on composition results returned from MESSENGER XRS is limited by the low spatial resolution of XRS data in the southern hemisphere.

Figures

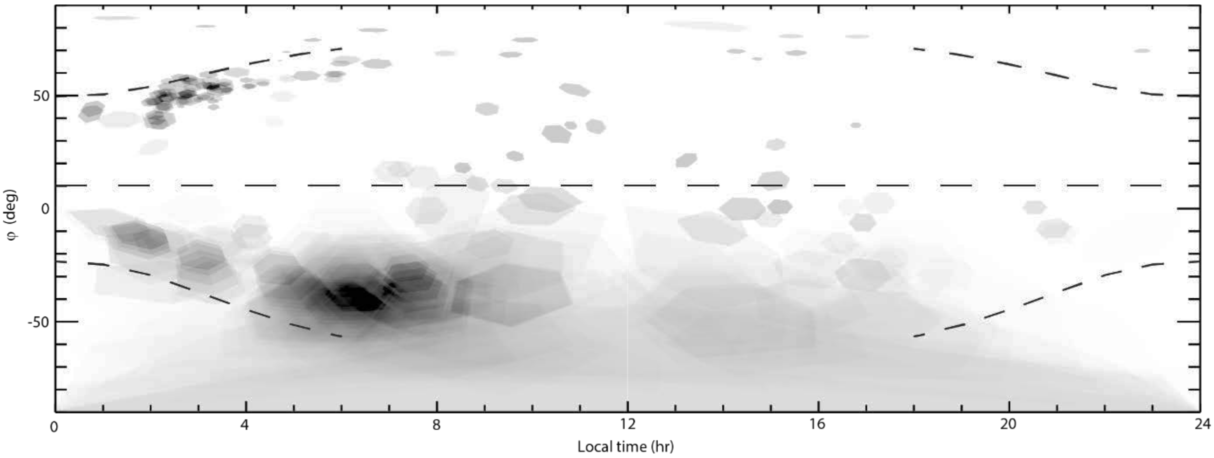

Figure 20: Distribution in local time and latitude of XRS footprints from records showing a identifiable fluorescence peak at the Ca-Kα fluorescence line; events where the concurrent SAX solar flux above the Ca K-edge was greater than 10s^{-1} are excluded. The dashed lines show the locations of the magnetic equator per Anderson et al.[5] and nightside open-closed field line boundary per Korth et al.[6]

References

1. Starr, R.D., et al., *MESSENGER detection of electron-induced X-ray fluorescence from Mercury's surface.* Journal of Geophysical Research, 2012. **117**: p. E00L02.
2. Lindsay, S.T., et al., *MESSENGER X-ray observations of magnetosphere-surface interaction on the nightside of Mercury.* Planetary and Space Science, 2016. **125**: p. 72-79.
3. Schlemm, C.E., et al., *The X-Ray spectrometer on the MESSENGER spacecraft.* Space Science Reviews, 2007. **131**: p. 393-415.
4. Baker, D.N., et al., *Energetic electron flux enhancements in Mercury's magnetosphere: An integrated view with multi-instrument observations from MESSENGER.* Geophysical Research Abstracts, 2015. **17**: p. 2517.
5. Anderson, B.J., et al., *The global magnetic field of Mercury from MESSENGER orbital observations.* Science, 2011. **333**: p. 1859-1862.
6. Korth, H., et al., *Modular model for Mercury's magnetospheric magnetic field confined within the average observed magnetopause.* Journal of Geophysical Research: Space Physics, 2015. **120**(6): p. 4503-4518.

Sodium pick-up ion observations in the solar wind upstream of Mercury

J. M. Jasinski[1,2,]*, J. A. Slavin[1], L. H. Regoli[1], J. M. Raines[1] and N. Murphy[2]
[1]Climate and Space Sciences and Engineering Dept., University of Michigan, USA.
[2]NASA Jet Propulsion Laboratory, USA.

Introduction

The pickup ion process is an important process that occurs when neutral particles are ionized and then "picked-up" by the local magnetic and electric fields of the solar wind. Pick-up ions are observed at many bodies, e.g. comets, moons of the Giant Planets, Mars and Venus [1,2,4]. Observations of pick-up ions are important as they allow to infer exospheric properties as well as loss processes from these bodies.

The MESSENGER spacecraft orbited Mercury in 2011-2015. Sodium ions were observed at Mercury's magnetosphere and dominate the planetary species [3]. Sodium is mostly observed in the magnetospheric cusp and plasma sheet, however they have also been observed in the magnetosheath.

Observations at Mercury with the MESSENGER spacecraft

We present the first observations of sodium pick-up ions upstream of Mercury's magnetosphere. The MESSENGER spacecraft's Fast Imaging Plasma Spectrometer observed multiple events of high sodium counts in the solar wind upstream of Mercury. The events display a shell velocity distribution, which is the characteristic signature of freshly picked up ions in the solar wind. From these observations we infer properties of Mercury's sodium exosphere and implications for the solar wind interaction with Mercury's magnetosphere.

References

[1] Coates, A. J., Ion pickup at comets, Advances in Space Research, Vol. 33, Issue 11, Pages 1977-1988, 2003.

[2] Cravens, T. E. et al., Pickup ions near Mars associated with escaping oxygen atoms, J. Geophys. Res., 107(A8), 2002.

[3] Raines, J. M., et al., Structure and dynamics of Mercury's magnetospheric cusp: MESSENGER measurements of protons and planetary ions, J. Geophys. Res. Space Physics, 119, 6587–6602, *2014.*

[4] Tokar, R. L., et al., Cassini detection of water-group pick-up ions in the Enceladus torus, Geophys. Res. Lett., 35, L14202, 2008.

Solar wind-magnetosphere interaction at Mercury during passage of coronal mass ejections

R. Jarvinen[1,2*], *M. Alho[1], E. Kallio[1], and T. I. Pulkkinen[1]*
[1]Aalto University, School of Electrical Engineering, Department of Electronics and Nanoengineering, Finland
[2]Finnish Meterorological Institute, Finland

Introduction

We analyze the interaction of the solar wind with the Hermean magnetic field including the formation of the bow shock, the magnetosheath and the magnetopause in a 3-dimensional global hybrid model. First we present the implementation of the numerical simulation model, where ions are treated as particles moving under the Lorentz force and electrons are a charge-neutralizing fluid. In the hybrid approach ion dynamics are self-consistently coupled with the propagation of the magnetic field by Faraday's law. The undisturbed solar wind flow is injected from the front wall of the simulation domain and the particles can reach the planetary surface, which is the inner boundary. Resistivity profiles of the planetary crust and core can be included as well. The incident solar wind can include, for example, conditions during stationary nominal and high-speed streams and solar wind transient conditions like interplanetary coronal mass ejections. In the analysis we concentrate on how the solar wind plasma gains access to different regions in Mercury's magnetosphere and its boundary layers.

Atmospheric escape at early Mars and constraints on the evolution of the Martian atmosphere

M. Scherf[1*]; S. Dyadechkin[1], U. Amerstorfer[1], H. Lammer[1], H. I. M. Lichtenegger[1], E. Kallio[2], M. Alho[2], R. Adam[3], M. L. Khodachenko[1], H. Groeller[4], F. Tian[5], L. Noack[6], C. Johnstone[7], M. Guedel7, L. Tu[7]
[1]Space Research Institute, Austrian Academy of Sciences, Austria
[2]Aalto University, School of Electrical Engineering, Department of Electronics and Nanoengineerung, Finland
[3]Institute of Physics, University of Graz, Austria
[4]Lunar and Planetary Laboratory, University of Arizona, USA
[5]Ministry of Education Key Laboratory for Earth System Modeling, Center for Earth System Science, Tsinghua University, China
[6]Freie Universität Berlin, Department of Earth Sciences, Germany
[7]Department of Astrophysics, University of Vienna, Austria

Introduction

It is assumed that the Martian atmosphere was much denser in the past then it is today. However, how and when the Martian atmosphere changed to the present time tenuous and dry atmosphere is still one of the fundamental science questions in Martian research. To gain a better understanding of this key question, we studied how the early Martian atmosphere responded to different EUV fluxes from the young Sun and how this influenced the loss of carbon and oxygen. In addition, we will also address the escape of argon over the planet's history.

Loss of oxygen and carbon

We study the escape of suprathermal oxygen and carbon from the martian atmosphere for four points in time in its history corresponding to 1, 3, 10, and 20 times the present solar EUV flux with a Monte-Carlo model. Different source reactions of hot oxygen and carbon atoms in the thermosphere and their changing importance with the EUV flux are discussed**.**

For the same EUV fluxes and solar wind parameters, we also investigate on how ionized atmospheric oxygen and carbon atoms are picked up by the solar wind convection electric field. Analysis was made by a 3D kinetic hybrid model which treats ions as particles and electrons as a massless charge neutralizing fluid. The hybrid simulation allows studying self-consistently the motion of ions in the Martian magnetosphere and together with the suprathermal escape rates from our Monte Carlo simulations we can testimate the total atmospheric escape rate during the Martian history.

Evolution of the Martian atmosphere

Finally, we discuss different magma ocean related and volcanic CO_2 outgassing scenarios and their interplay with thermal and non-thermal loss processes. Our results show that Mars could not have had a dense atmosphere at the end of the Noachian eon, since such an atmosphere would not have been able to escape until today. However, Mars could have had a dense atmosphere early on in the pre-Noachian eon.

An important insight into this early environment can also be gained by the strong isotopic fractionation of $^{36}Ar/^{38}Ar$ in the present-day Martian atmosphere, which suggests that a significant atmospheric amount should have been escaped in the early past. However, the fractionation of argon and other noble gases such as neon is strongly dependent on the environmental conditions, in particular on temperature and altitude of the exobase, which is in turn highly sensitive to the EUV flux of the early Sun.

Acknowledgement

The authors acknowledge the support of the FWF NFN project Pathways to "Habitability: From Disks to Active Stars, Planets and Life", in particular its related sub-projects S11604-N16, S11606-N16 and S11607-N16.

Dependence of O^+ escape rates from Venus on the solar wind and the solar activity

K. Masunaga[1*]; Y. Futaana[1], M. Persson[1], Z. J. Rong[2,3], S. Barabash[1], T. L. Zhang[4], and A. Fedorov[5]
[1]Swedish institute of Space Physics, Sweden,
[2]Key Laboratory of Earth and Planetary Physics, Institute of Geology and Geophysics, Chinese Academy of Sciences, China
[3]Space Research Institute, Austrian Academy of Science, Austria
[4]IRAP, France

Abstract

The ion escape from Venus is one of the important topics in order to understand the history of Venus' atmosphere. Past observations show that the ion escape is controlled by the solar wind and solar radiation [e.g., 1]. There are several studies investigating the dependence of the ion escape rates regarding particular solar events [e.g. 2, 3]. For these studies, several upstream parameters of the solar wind and solar radiation change in the same time. Thus, it is still unclear what upstream parameter controls the escape rates, and to what degree. In this study, we investigate dependences of O^+ escape rates (with energies more than 10 eV) from Venus both on the solar wind and the solar activity by using the whole dataset of the Ion Mass Analyser and the magnetometer on Venus Express (2006-2014). We separated the dataset into 8 cases depending on the solar wind's dynamic pressure, the magnitude of the motional electric field, and the solar activity based on the F10.7 index. We find that O^+ ions mostly escape from the induced magnetosphere of Venus regardless the upstream conditions. A contribution of the O^+ escape from Venus magnetosheath is small, with fractions ranging 6-25 % of the total escape rates. We also find that the Venusward fluxes of O^+ in the tail region increase in the solar maximum period. The largest escape rates are observed during the solar minimum with a large motional electric field magnitude. We conclude that the influence of the motional electric field to enhance the O^+ escape rates is slightly larger than that of the dynamic pressure. On the other hand, these two influences are overwhelmed by the increase of the return flow to Venus, which is dominantly controlled by the solar activity. Therefore, the net flux of the escaping O^+ is smaller in the solar minimum than that in the solar maximum.

References

[1] Futaana, Y., et al., Space Sci. Rev., 212: 1453, 2017
[2] Luhmann, J. G., et al., J. Geophys. Res., 112, E04S10, 2007
[3] Edberg, N. J. T., et al., J. Geophys. Res., 116, A09308, 2011

2-Dimensional Model of the Martian Exosphere Applied to HST Observations

D. Bhattacharyya[1*]; M. Mayyasi[1], J. T. Clarke[1], J. Y. Chaufray[2], S. Stone[3], R. V. Yelle[3], J. L. Bertaux[2], M. S. Chaffin[4], N. M. Schneider[4], H. Gröller[2], M. Benna[5], P. Mahaffy[5].
[1]Center for Space Physics, Boston University, USA
[2]LATMOS, France
[3]Lunar and Planetary Laboratory, University of Arizona, USA.
[4]LASP, University of Colorado, USA
[5]GSFC, USA

Introduction

The Martian hydrogen corona is highly dynamic [1], [2], [3]. Most of the earlier models have considered a 1 - dimensional density structure with spherical symmetry for simulating the Lyman α emissions from the Martian hydrogen exosphere [2], [3], [4]. However, modelling and observations have shown that the 3 – dimensional density structure of the hydrogen exosphere at Mars is most likely non-uniform and non-isothermal, especially at lower altitudes [5], [6], [7], [8]. We have developed a 2-D model to simulate the non-uniform structure of the Martian hydrogen exosphere based on parameters constrained from MAVEN observations and will apply it to currently ongoing Hubble Space Telescope (HST) observations of Mars at Lyman α (121.6 nm). This study will allow us to understand the effects of using a 1-D model vs a 2-D model in constraining the present-day escape rate of hydrogen from Mars, which is directly tied to the escape of water.

2-Dimensional Model of the Martian Exosphere

The temperature variations with solar longitude (season) and local time in the Martian atmosphere at altitudes where the exobase is located (~200 km), have been constrained from MAVEN observations. Figure 1 shows the variation in temperature with local time as observed by MAVEN. The hydrogen exobase density variation with local time is based on a mathematical formulation derived by Hodges and Johnson [9]. The only free parameters in the model are the densities of thermal and superthermal hydrogen at the exobase at solar zenith angle, SZA = 0°. The density profile for the background CO_2 is derived assuming hydrostatic equilibrium. For hydrogen, a simple diffusion model is assumed below the exobase, while above it the density profile is derived using a modified Chamberlain theory [10] to account for changes in density not only with altitude, but also with solar zenith angle (SZA) variations.

Since the resonantly scattered Lyman α emission in the hydrogen exosphere of Mars is optically thick, a radiative transfer model is required to derive physical properties of this species. We have developed a radiative transfer model that takes into account the variations in temperature and density with altitude as well as solar zenith angle.

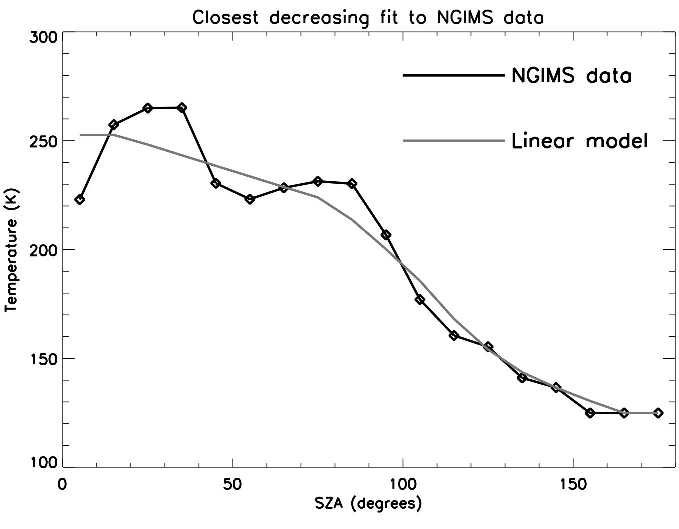

Figure 1: Variation of exobase temperature with solar zenith angle at Mars observed by NGIMS on board MAVEN. As can be seen in the figure above, there is a significant difference in temperature of the order of ~100 K between the dayside and night side of Mars.

Scientific Analysis

The 2-dimensional radiative transfer model of the Martian exosphere is used to analyse HST observations of the Martian exosphere (31st Dec. 2017 – 10th Feb. 2018). These observations of Mars in Lyman α were conducted when Mars was close to aphelion and solar activity was approaching minimum. The results will allow us to better understand the 3-dimensional structure of the thermal atoms present in the exosphere of Mars. The superthermal population density of H atoms have been speculated to be low when Mars is close to aphelion [3], [7], however not much is known about the characteristics of this population. Due to Mars' low gravity and large atmospheric scale height in comparison to Earth and Venus, the two populations are mixed well at Mars, even at higher altitudes. Therefore, the observations close to aphelion and under low solar activity conditions will allow us to study the effects of using a 1-D vs a 2-D model of the exosphere in order to constrain the thermal escape rate of hydrogen. With the 2-D model we will have much more accurate numbers for the global escape flux. An accurate estimate is crucial towards establishing the water escape timeline from Mars.

References

[1] Clarke, J. T., Bertaux, J. L., Gladstone, G. R., Quemerais, E., Wilson, J. K., and Bhattacharyya, D.: A rapid decrease of the hydrogen corona of Mars, Geophys. Res. Lett., Vol. 41, pp. 8013-8020, 2014.
[2] Chaffin, M. S., Chaufray, J. Y., Stewart, I., Montmessin, M., Schneider, N. M., and Bertaux, J. L.; Unexpected variability of Martian hydrogen escape, Geophys. Res. Lett., 41, pp. 314-320, 2014.
[3] Bhattacharyya, D., Clarke, J. T., Bertaux, J. L., Chaufray, J. Y., and Mayyasi, M.; A strong seasonal dependence in the Martian hydrogen exosphere, Geophys. Res. Lett., Vol. 42, pp. 8678-8685, 2015.
[4] Chaufray, J. Y., Bertaux, J. L., Leblanc, F., and Quemerais, E.; Observation of the hydrogen corona with SPICAM on Mars Express, Icarus, Vo. 195, pp. 598-613, 2008.
[5] Chaufray, J. Y., Gonzalez-Galindo, F., Forget, F., Lopez-Valverde, M. A., Leblanc, F., Modolo, R., and Hess, S.; Variability of the hydrogen in the Martian upper atmosphere as simulated by a 3D atmosphere-exosphere coupling, Icarus, Vol. 245, pp. 282-294, 2015.
[6] Holmström, M.; Asymmetries in Mars' exosphere. Implications for X-Ray and ENA imaging, Sp. Sci. Rev., Vol. 126, pp. 435-445, 2006.
[7] Bhattacharyya, D., Clarke, J. T., Bertaux, J. L., Chaufray, J. Y., and Mayyasi, M.; Analysis and modelling of remote observations of the Martian hydrogen exosphere, Icarus, Vol. 281, pp. 264-280, 2017.
[8] Chaffin, M. S., Chaufray, J. Y., Deighan, J., Schneider, N. M., McClintock, W. E., Stewart, A. I. F., Thiemann, E., Clarke, J. T., Holsclaw, G. M., Jain, S. K., Crismani, M. M., Stiepen, A., Montmessin, F., Eparvier, F. G., Chamberlain, P. C., and Jakosky, B. M.; Three-dimensional structure in the Mars H corona revealed by IUVS on MAVEN, Geophys. Res. Lett., Vol. 42, pp. 9001-9008, 2015.
[9] Hodges, R. R., and Johnson, F. S.; Lateral transport in planetary atmospheres, J. Geophys. Res., Vol. 73, pp. 7307, 1968.
[10] Vidal-Madjar, A., and Bertaux, J. L., A calculated hydrogen distribution in the exosphere, Planet Sp. Sci., Vol. 20, pp. 1147-1162, 1972.

Modeling deuterium from surface to space to understand Mars atmospheric evolution

E. Cangi[1,2*]; M. Chaffin[1], J. Deighan[1], A.I.F. Stewart[1], N. Schneider[1,2]
[1]Laboratory for Atmospheric and Space Physics, Boulder, Colorado, USA
[2]University of Colorado – Boulder, Department of Astrophysical and Planetary Sciences, USA

Introduction

A wealth of evidence from the surface and atmosphere of Mars indicates that it was once a much wetter world [1, 9]; today, it is known that much of this water has been lost over time, either via escape to space or movement into the interior. Water, as well as other hydrogen-containing species like H_2, can appear in "deuterated forms", where one or more of the hydrogen atoms are replaced by deuterium. When water vapor in the Martian atmosphere is photodissociated, hydrogen, deuterium, and oxygen are freed and can escape the atmosphere. Because deuterium is twice as massive as hydrogen, it is less likely to escape compared to hydrogen. This leads to an overall enrichment of deuterium on Mars as compared to Earth [10]. Knowing the current Martian D/H ratio, as well as the escape rates of both deuterium and hydrogen, makes it possible to estimate how much atmosphere Mars has lost and, by extension, how much water it has lost [2]. This is key information in the discussion of atmospheric evolution and planetary habitability.

Investigating the effects of the D/H ratio and high-altitude water on hydrogen escape

Using a 1D photochemical and transport model, Chaffin et al. [3] recently demonstrated that a discrepancy between theory and observation of hydrogen escape could be resolved by seasonal injections of high-altitude water vapor, which was detected by the Mars Express SPICAM instrument [6]. In this work, we extend the model created by Chaffin et al. to include deuterium chemistry, and study its effect on hydrogen escape in terms of the high-altitude water explanation, which has not been explored in past models (e.g. [10]).

The model used by Chaffin et al. [3] tracks the concentrations and distributions of neutral chemical species in the Martian atmosphere in response to seasonal injections of high-altitude water. Each simulation tracks the response to a variety of water densities (in ppm) injected at different altitudes (increments of 20 km). Additionally, the model uses data from each simulation to quantify the outgoing hydrogen flux over time as a function of the elevated water parcel. In this work, we have updated the model to include deuterium chemistry for comparison to the results without deuterium chemistry. Preliminary results for the concentrations and distributions of select key species are shown in Figure 1. Additional results for hydrogen and deuterium outgoing flux are currently being quantified and analysed.

Future Work

While there have been many studies concerning the D/H ratio on Mars and its globally averaged or locally specified values, no single study has explored the effect of the many ways the D/H ratio varies on atmospheric escape. As a result, the role of deuterium in escape has not been thoroughly quantified. This work will be extended in the future via the following steps to form a more holistic picture of the effect of the D/H ratio on Martian atmospheric escape.

- Include other types of atmospheric escape (currently, only Jeans escape is accounted for).
- Constrain assumptions about the D/H ratio using data from the NASA Mars Atmosphere and Volatile EvolutioN (MAVEN) mission and the ESA's ExoMars Trace Gas Orbiter (TGO).
- Aggregate results and information from multiple studies to account for changes in the D/H ratio due to altitude [2], season [7], geographical location [7, 9, 4], and obliquity [5, 8]; study the effect of these variations on the outgoing flux of hydrogen and deuterium.
- Use the results for outgoing flux to explore a variety of potential early Mars scenarios.

References

[1] VR Baker, RG Strom, VC Gulick, JS Kargel, Goro Komatsu, and VS Kale. Ancient oceans, ice sheets and the hydrological cycle on mars. *Nature*, 352(6336):589, 1991.

[2] JL Bertaux and F Montmessin. Isotopic fractionation through water vapor condensation: The Deuteropause, a cold trap for deuterium in the atmosphere of Mars. *Journal of*

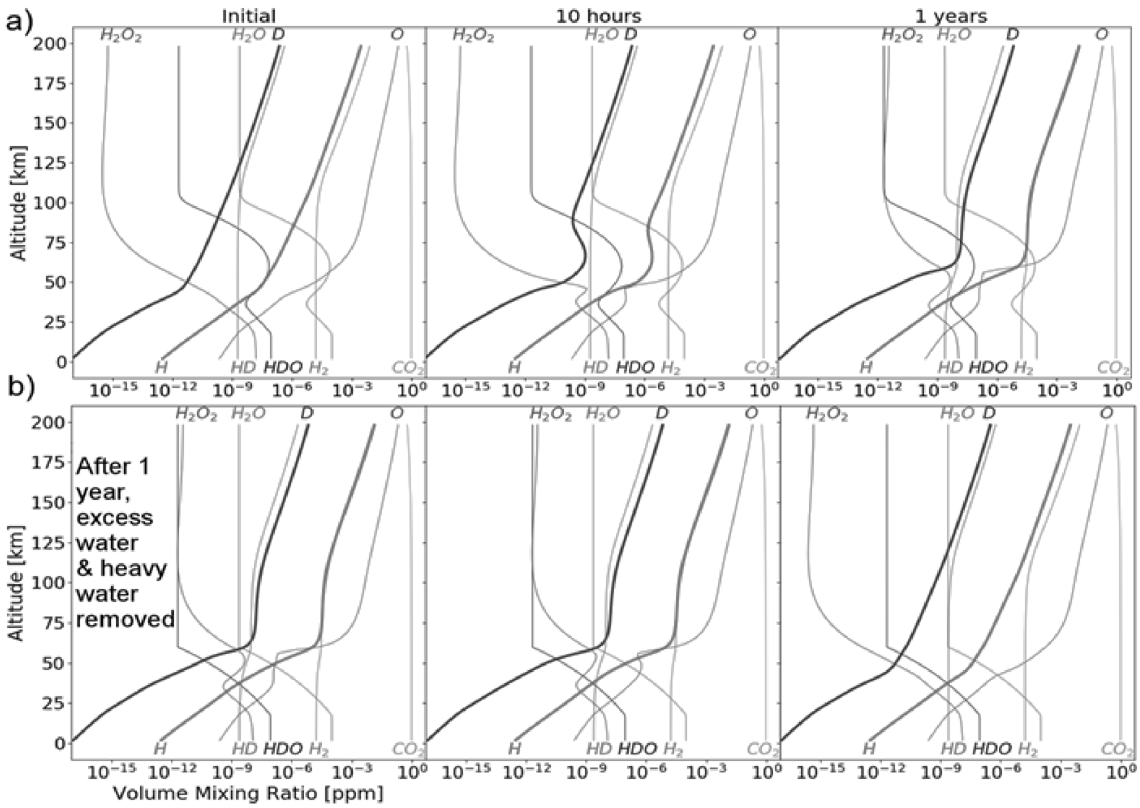

Figure 1: Atmospheric response of select key species over time to a) addition of excess water/heavy water at 60 km and b) removal of the enhanced water profiles. After introduction of elevated water, H and D mixing ratios are enhanced, leading to elevated escape.

Geophysical Research-Planets, 106(E12):32879{32884, 2001. doi:10.1029/2000JE001358.

[3] M. S. Chaffin, J. Deighan, N. M. Schneider, and A. I. F. Stewart. Elevated atmospheric escape of atomic hydrogen from Mars induced by high-altitude water. *Nature Geoscience*, (January):1{6, 2017. doi:10.1038/ngeo2887.

[4] Vladimir A. Krasnopolsky. On the hydrogen escape from Mars: Comments to Variability of the hydrogen in the martian upper atmosphere as simulated by a 3D atmosphere-exosphere coupling by J.Y. Chaufray et al. (2015, Icarus 245, 282294). *Icarus*, 281:262{263, jan 2017. doi:10.1016/J.ICARUS.2016.09.002.

[5] J. Laskar, A.C.M. Correia, M. Gastineau, F. Joutel, B. Levrard, and P. Robutel. Long term evolution and chaotic diffusion of the insolation quantities of Mars. *Icarus*, 170(2): 343{364, aug 2004. doi:10.1016/J.ICARUS.2004.04.005.

[6] L. Maltagliati, F. Montmessin, O. Korablev, A. Fedorova, F. Forget, A. Määttänen, F. Lefèvre, and J. L. Bertaux. Annual survey of water vapor vertical distribution and wateraerosol coupling in the martian atmosphere observed by SPICAM/MEx solar occultations. *Icarus*, 223(2):942{962, 2013. doi:10.1016/j.icarus.2012.12.012.

[7] F. Montmessin, T. Fouchet, and F. Forget. Modeling the annual cycle of HDO in the Martian atmosphere. *Journal of Geophysical Research E: Planets*, 110(3):1{16, 2005. doi:10.1029/2004JE002357.

[8] Martin Turbet, François Forget, James W. Head, and Robin Wordsworth. 3D modelling of the climatic impact of outflow channel formation events on early Mars. *Icarus*, 288:10{36, may 2017. doi:10.1016/j.icarus.2017.01.024.

[9] G. L. Villanueva, M. J. Mumma, R. E. Novak, H. U. Kaufl, P. Hartogh, T. Encrenaz, A. Tokunaga, A. Khayat, and M. D. Smith. Strong water isotopic anomalies in the martian atmosphere: Probing current and ancient reservoirs. *Science*, 348(6231):218{221, 2015. doi:10.1126/science.aaa3630.

[10] Yuk L. Yung, Jun Shan Wen, Joseph P. Pinto, Mark Allen, Kathryn K. Pierce, and Suzanne Paulson. HDO in the Martian atmosphere: Implications for the abundance of crustal water. *Icarus*, 76(1):146{159, 1988. doi:10.1016/0019-1035 (88)90147-9.

Modeling of Ion and Photochemical Losses to Space over the Martian History

C. F. Dong[1*], Y. Lee[2], Y. J. Ma[3], S. W. Bougher[4], J. G. Luhmann[5], S. M. Curry[5], G. Toth[4], A. F. Nagy[4], D. A. Brain[6], and B. M. Jakosky[6]
[1]Department of Astrophysical Sciences, Princeton University, USA,
[2]NASA Goddard Space Flight Center, USA
[3]Institute of Geophysics and Planetary Physics, University of California, USA
[4]Climate and Space Sciences and Engineering, University of Michigan, USA
[5]Space Sciences Laboratory, University of California, USA
[6]Laboratory for Atmospheric and Space Physics, University of Colorado, USA

Introduction

Mars may have had a thicker atmosphere and liquid water on its surface between 3.5 and 4 billion years ago. However, today's Red Planet has dry and cold surface environments and a small surface pressure (~6 mbar) mainly resulting from the thin and cold atmosphere. So one of the most important questions is: where did all of the atmosphere and liquid water go? One of the MAVEN's primary objectives is to quantify the atmospheric escape to space over time [e.g., 1,2]. In order to understand the effect of atmospheric losses to space on the long-term evolution of the Martian atmosphere (e.g., loss of water) and its climate change over its history, the well-validated 3-D state-of-the-art numerical tools are essential to study both the ion and photochemical escape back to 4 billion years ago.

Method

In this study, we adopted the one-way coupled framework (Figure 1, left panel) that has been employed to study the ion and photochemical losses at the current epoch [3,4]. We adopted the 3-D Mars thermosphere (i.e., neutral temperatures T_n, neutral densities [O], [CO_2], and photoionization frequencies IO, ICO_2) from the Mars Global Ionosphere Thermosphere Model (M-GITM) [5] and the hot atomic oxygen density, [Ohot], from the Mars exosphere Monte Carlo model Adaptive Mesh Particle Simulator (M-AMPS) [3]. These neutral profiles are one-way coupled with the 3-D BATS-R-US Mars multi-fluid MHD model [6]. The M-AMPS hot oxygen corona and the associated photochemical loss rate were calculated based on the thermospheric/ionospheric background from M-GITM. The historical solar radiation and solar wind parameters were adopted from Ref. [7]. We started the simulation at the current epoch based on the autumnal equinox solar cycle moderate conditions.

Results

Figure 1 (right panel) presents the calculated ion (solid lines) and photochemical (dashed line) escape rates by using this one-way coupled framework (Figure 1, left panel) over the Martian history. In Figure 1 (right panel), the O^+ ion loss dominates over heavy ion species (O_2^+ and CO_2^+) at early Mars and the corresponding O^+ ion escape rate is much higher than the current value. Although the photochemical escape is the dominant loss mechanism at current Mars, the total ion escape rate is much higher than the photochemical escape rate at early Mars.

In summary, this study informs our understanding of the long-term evolution of the Martian climate due to atmospheric losses to space, and has implications for analogous change on exoplanets. Thus, it offers fresh insights concerning the habitability of early Mars as well as the increasing number of exoplanets discovered yearly.

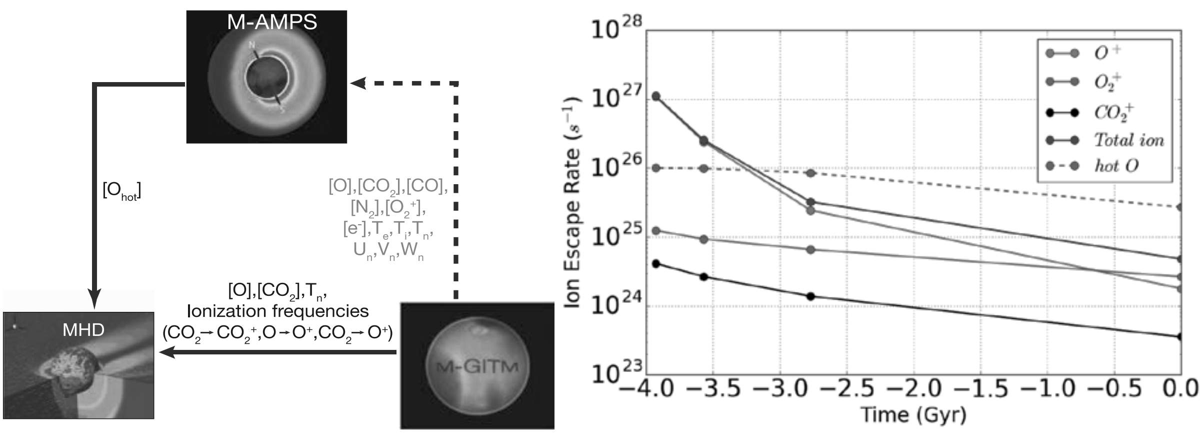

Figure 21: Left: A sketch of a one-way coupling approach between M-GITM, M-AMPS, and MHD [4]. The notation Tn denotes neutral atmosphere temperatures, and [O], [CO2], and [Ohot] are the neutral O, CO2, and hot atomic oxygen number densities, respectively. Right: Calculated ion and photochemical escape rates over the Martian history.

References

[1] Jakosky B. M. et al. (2015) SSRev **195**, 3.
[2] Brain D. A. et al. (2015) GRL **42**, 9142.
[3] Lee Y. et al. (2015) JGR **120**, 1880.
[4] Dong C. F. et al. (2015) JGR **120**, 7857.
[5] Bougher S. W. et al. (2015) JGR **120**, 311.
[6] Najib D. et al. (2014) JGR **116**, A05204.
[7] Boesswetter A. et al. (2010) PSS **58**, 2031.

A parametric study of Enceladus plumes based on DSMC calculations for retrieving the outgassing parameters as measured by Cassini instruments

A. Mahieux[1,2*]; *D. B. Goldstein[1], P. Varghese[1], L. M. Trafton[1]*
[1]The University of Texas at Austin, Austin, USA
[2]Belgian Institute for Space Aeronomy, Belgium

Introduction

Various instruments on board the CASSINI spacecraft – ISS, INMS, CDA, UVS, observed two-phased water outgassing originating from five crevasses located near the Enceladus South pole [1], where the surface temperature also was recorded to be larger than at other places on this icy moon of Saturn [2]. The geysers have been inferred to be mainly composed of water molecules and water ice particles, and extend hundreds of kilometres above the surface. Various authors tried to explain their origin, from near-surface explosion of boiling liquid water [1], clathrate decomposition [3] or evaporation from a underground salty ocean [4].
From these observations, studies have tried to constrain the outgassing flow rate from the observed geysers, for example [5-7], together with the flow characteristics, such as its temperature and speed.

DSMC model

In this work [8], we present results from a set of single geyser DSMC simulations of water vapour and ice grains expanding into vacuum, from which we parametrized the geysers' characteristics at an altitude of 10 km above the ground once the flow has becomes collisionless, i.e. considering the two-phased number density, velocity, kinetic and rotational temperatures distributions. DSMC simulations are computationally expensive, with a computation time larger than 48 hours for a single resolved geyser calculation. However, our parametrizations presented in this work can be used to quickly and robustly reconstruct the plume characteristics at 10 km, that is in a few milliseconds, considering variations of the outgassing flow characteristics at the vent, such as the vent radius, the mass density flow, the water molecule/water ice particle mass ratio, the water molecule and water ice speed, the vent exit opening angle, the water ice particle radius and the flow temperature. These parametrizations can then be used to calculate the flow properties at altitudes larger than 10 km, using a computationally cheap free-molecular code, since the flow is non-collisional at these altitudes.

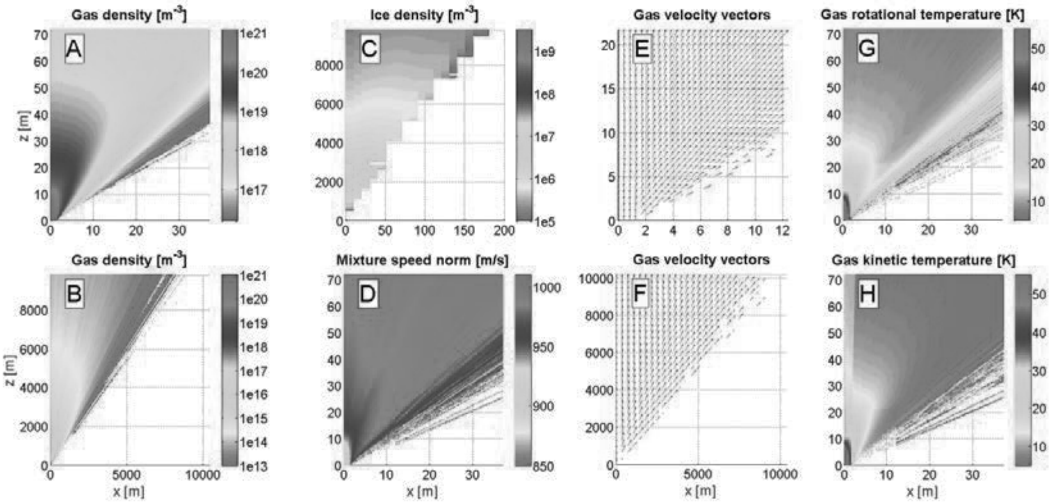

Figure 22: Example of DSMC plume simulation. Panel A: H_2O molecule number density close to the vent. Panel B: H_2O molecule number density for the whole domain. Panel C: Ice particle number density for the whole domain. Panel D: Speed of water molecule and ice particle mixture. Panels E and F: Velocity vectors close to the vent (Panel E) and for the whole domain (Panel F). Panels G and H: H_2O rotational and kinetic temperature close to the vent.
We modelled the near-field of the outgassing geysers using the PLANET DSMC code [9], see , from the surface of Enceladus up to an altitude of 10 km from the centre of the vent. A DSMC approach is suitable for the simulation of this problem since it can correctly reproduce all the different states that the flow is undergoing while expanding into vacuum, from a high density and collisional configuration at the surface to free-molecular and collisionless at high altitude.

We extract the DSMC fields at an altitude of 10 km, see , and modelled the radial profiles of the quantities of interest using functional forms, i.e. the water molecule and ice particle number densities, vertical and horizontal velocity components, and the rotational and kinetic temperatures.

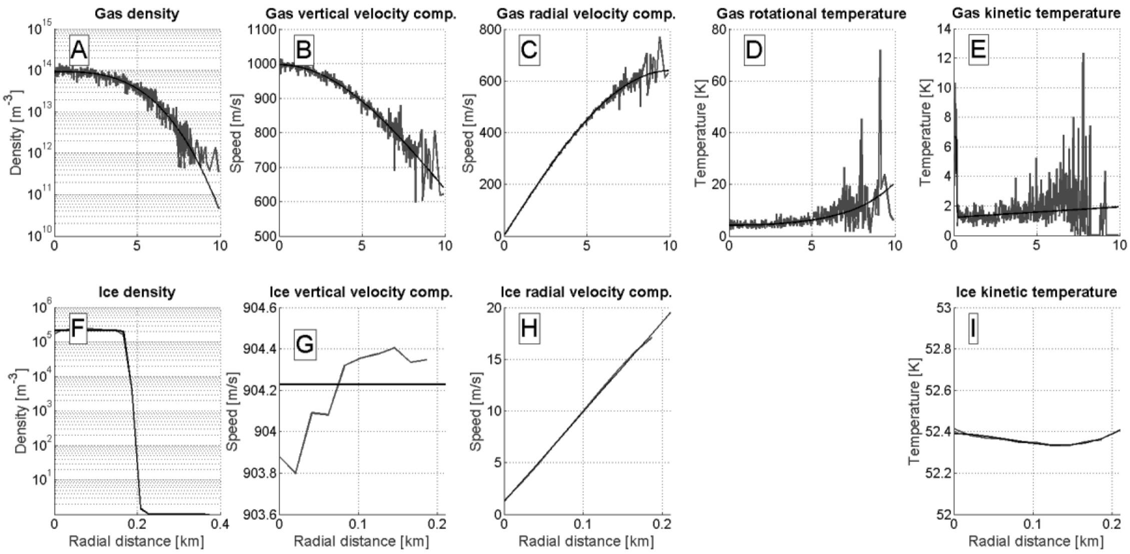

Figure 23: Number density (Panels A and F), vertical component of the velocity (Panels B and G), radial component of the velocity (Panels C and H), rotational temperature (Panel D), and kinetic temperature (Panels E and I) of water molecules (Panels A to E) and ice particles (Panels F to I) radial profiles at an altitude of 10 km for the DSMC simulation of a default case. The blue curves are the DSMC results while the black curves are the best fits using the functional forms.

Parametrization of the Radial Profiles

We varied the vent parameters about a nominal or default case. To do so, we ran more than a hundred DSMC simulations for different vent parameters configurations, and we studied how the variation of these parameters influence the flow at 10 km, and parametrized the functional forms to account for these variations. We finally compared the parametrized radial profiles with DSMC simulations while varying more than one vent parameter, i.e. checking the linear independence of the input parameters.

References

[1] Porco, C.C., et al., *Cassini observes the active south pole of Enceladus.* Science, 2006. **311**(80): p. 1393–1401.

[2] Spencer, J.R., et al., *Cassini encounters Enceladus: background and the discovery of a south polar hot spot.* Science, 2006. **311**: p. 1401–1405.

[3] Kieffer, S.W., et al., *A Clathrate Reservoir Hypothesis for Enceladus' South Polar Plume.* Science, 2006. **314**(5806): p. 1764-1766.

[4] Porco, C., et al., *How the geysers, tidal stresses, and thermal emission across the south polar terrain of Enceladus are related.* The Astronomical Journal, 2014. **148**(45).

[5] Hansen, C.J., et al., *Enceladus' Water Vapor Plume.* Science, 2006. **311**(5766): p. 1422-1425.

[6] Burger, M.H., et al., *Understanding the escape of water from Enceladus.* J. Geophys. Res., 2007. **112**(A06219).

[7] Yeoh, S.K., et al., *Constraining the Enceladus plume using numerical simulation and Cassini data.* Icarus, 2017. **281**: p. 357-378.

[8] Mahieux, A., et al., *Parametric study of water vapor and water ice particles plumes based on DSMC calculations: Application to the Enceladus geysers.* Icarus, 2018. **Submitted**.

[9] Yeoh, S.K., et al., *On understanding the physics of the Enceladus south polar plume via numerical simulation.* Icarus, 2015. **253**: p. 205-222.

The terrestrial paleo-magnetosphere during the late Hadean and Archean: Implications on the evolution of the terrestrial atmosphere

M. Scherf[1*], *M. Khodachenko[1,2], H. Lammer[1], I. Alexeev[2], L. Spross[3], C. Johnstone[4], M. Guedel[4], M. Blokhina[2], E. Belenkaya[2], J. Tarduno[5], H. Lichtenegger[1], Y. Kulikov[6], L. Tu[4]*
[1]Space Research Institute, Austrian Academy of Sciences, Austria
[2]Skobeltsyn Institute of Nuclear Physics, Moscow State University, Russia
[3]Institute of Physics, University of Graz, Austria
[4]Institute of Astrophysics, University of Vienna, Austria
[5]Department of Earth and Environmental Sciences, University of Rochester, USA
[6]Polar Geophysical Institute, Russian Academy of Sciences, Russian Federation

Introduction

The present-day terrestrial atmosphere, as dominated by the volatile elements nitrogen and oxygen, is providing a habitable environment for a diverse range of life forms. However, simulations of the terrestrial paleo-magnetosphere as well as of the solar wind induced atmospheric ion-pickup escape ~4 Gyr ago (see e.g. [1]) are indicating that during the harsh conditions of the Hadean and early Archean eons a nitrogen dominated atmosphere would not have been able to survive, but would have been eroded within a few million years due to the high EUV flux and the strong solar wind of the early Sun [2][3]. In addition, these results are suggesting that the present-day nitrogen-dominated atmosphere has its origin during later stages of the geological history of the Earth, whereas for the late Hadean and early Archean, CO2 can be considered as the dominating atmospheric constituent. However, the small $^{14}N/^{15}N$ isotope disequilibrium between internal and surface reservoirs at the Earth [4] is indicating that some atmospheric escape of nitrogen should have taken place in the past.

The terrestrial paleo-magnetosphere and the evolution of the terrestrial atmosphere

Atmospheric escape, as well as the overall historical composition of the atmosphere, is strongly coupled to the shape of the paleo-magnetosphere and to its interplay with the varying solar activity factors. Thus, we will present simulations of the terrestrial paleo-magnetosphere during the late Hadean and Archean eons and its influence on the evolution of the terrestrial nitrogen atmosphere. This also includes an estimation of nitrogen lost to space based on the observed terrestrial 14N/15N fractionation. Our results support the idea that the nitrogen dominated atmosphere started to build up during the Archean eon and slowly evolved from a low-pressure atmosphere via outgassing of N2 into the present-day habitable environment. Important environmental conditions for this evolution and its interconnections will be discussed within this presentation. This also includes a potential solution for the before mentioned $^{14}N/^{15}N$ disequilibrium.

Acknowledgement

The authors acknowledge the support of the FWF NFN project Pathways to “Habitability: From Disks to Active Stars, Planets and Life”, in particular its related sub-projects S11604-N16, S11606-N16 and S11607-N16. This publication is supported by the Austrian Science Fund (FWF) and the 550 US NSF (EAR1015269 to JAT).

References

[1] Lichtenegger, H., Lammer, H., Griessmeier, J.-M., Kulikov, Y., von Paris, P., Hausleitner, W., Krauss, S., Rauer, H.: Aeronomical evidence for higher CO_2 levels during Earth’s Hadean epoch, Icarus, 210, 1-7, 2010.
[2] Tu, L., Johnstone, C., Guedel, M., Lammer, H., The Extreme Ultraviolet and X-Ray Sun in Time: High-Energy Evolutionary Tracks of a Solar-Like Star, Astron. Astrophys, 577, L3, 2015.
[3] Johnstone, C., Guedel, M., Brott, I., Lueftinger, T., Stellar winds on the main-sequence II. The evolution of rotation and winds, Astron. Astrophys., 577, A28, 2015.
[4] Cartigny, P., Marty, B., Nitrogen isotopes and mantle geodynamics: the mergence of life and the atmosphere-crust-mantle connection, Elements, 9, 359-366, 2013.

O^+ escape at Earth during the magnetic storm on September 4th – 10th, 2017

A. Schillings[1,2*]; H. Nilsson[1], R. Slapak[3], P. Wintoft[4], M. Yamauchi[1], M. Wik[4], I. Dandouras[5]
[1]Swedish Institute of Space Physics, Sweden,
[2]Division of Space Technology, Luleå University of Technology, Sweden
[3]EISCAT Scientific Association, Sweden
[4]Swedish Institute of Space Physics, Sweden
[5]IRAP, Université de Toulouse, CNRS, UPS, CNES, France

Introduction

Solar flares are considered as proxies of the young Sun billions of years ago [1] because it was more active. Extreme solar flare as X-flare associated with coronal mass ejections (CME) irradiate the Earth's upper atmosphere. Furthermore, interplanetary coronal mass ejections (ICMEs) associated with magnetic clouds – subsets of CMEs ejecta – or post-shock/sheath regions produce intense geomagnetic storms ($Kp > 7$ and $Dst < -100$ nT) [2]. The intense geomagnetic storm initiated by an ICME leads to O^+ escape. Therefore, a better understanding of the O^+ escape during intense storms provides knowledge on the evolution of our atmosphere in the past.

During these extreme events, the O^+ at high altitude are heated through different processes like wave interactions [3] or accelerated by centrifugal force [4]. When the energized O^+ have sufficient velocity and evade Earth's gravity, they escape into the solar wind through the plasma mantle or cusp. Despite several studies have already estimated the O^+ outflow in different magnetospheric regions and for disturbed geomagnetic conditions [5], [6], the O^+ outflow/escape has not been related directly to the solar driver producing the storm. Thus, in case of the September 4th to 10th, 2017 we studied how long is the response time between the observation of the solar driver and the O^+ outflow and consequently how much O^+ escape the magnetosphere in association with the storm.

Data and method

The O^+ data we used, come from the CODIF instrument onboard the Cluster spacecraft 4 [7]. The CODIF instrument uses a time-of-flight section which enables it to resolve ion species namely He^+, He^{2+}, H^+ and O^+. The O^+ escape rate was estimated on 7th - 8th of September 2017, when Cluster passed through the open magnetic field line regions; the polar cap, the cusp and the plasma mantle. We identified these regions with the O^+ and H^+ energy spectrograms, by looking at the magnetic field data taken from the fluxgate magnetometer [8] and plotting the Cluster orbit. The orbit that gives the position of the spacecraft together with the energy spectrograms defined the time period in the interesting magnetospheric region where we estimated the O^+ flux. Afterward, we looked at the velocity components to identify O^+ outflow. To identify the solar driver, we analysed solar wind data from the DSCOVR satellite (delivered by NOAA SWPC). Moreover, Dst and Kp indices were used to distinguish the storm phases and establish the timing of the storm.

Results

Multiple X-type flares and Earth-directed CMEs were observed during 4th – 10th September 2017. The Bz IMF component, solar wind velocity and density show ICME signatures on the 7th of September early in the morning and late in the evening. On 7th around 23:30 UT, O^+ and H^+ energy spectrograms showed Cluster in the polar cap and cusp where a clear signature of the storm was visible. The storm signature led to an equatorward motion of the cusp described by Newell et al. [9], [10]. Moreover, in the polar cap after the storm signature, a relative enhancement of 1 order of magnitude in the O^+ flux is observed compared to the O^+ flux in the polar cap before the storm signature. This enhancement confirms the trend observed by [11] and an increase of the O+ outflow with increased geomagnetic activity [12].

Discussion

Geomagnetic storms are primarily driven by the negative turning of the upstream Bz and high solar wind speed. Late on September 7th an ICME initiated a geomagnetic storm that reached $Dst = -140$ nT. The ICME may be linked to a CME occurring at the Sun around noon on September 6th. As a consequence, the O^+ outflow increased with higher geomagnetic activity (Dst, Kp indices). This higher activity was observed with the compression effect of the magnetosphere and the equatorward moving cusp in the Northern Hemisphere on 7th, which also corresponds to a sudden Dst drop around the same time. With the Dst index, we distinguished the storm phases and luckily Cluster was in the polar cap and cusp during the main phase. This time fits with the 1 order of magnitude enhancement observed in the O^+ outflow. Similar observations were made in the Southern Hemisphere where Cluster was in the plasma mantle during the recovery phase. However, the O^+ flux (we were not able to prove that it was outflow) during this phase is already lower than in the beginning of the storm and no clear enhancement were visible between the different plasma mantle – polar cap encounters.

Conclusion

We estimated the O^+ outflow in the polar cap and plasma mantle in the Northern and the Southern Hemisphere respectively between September 7th and 8th, 2017. Our results show 1 order of magnitude enhancement in the polar cap for higher geomagnetic activity and consequently tell us how the atmospheric composition is, in the long term, affected by intense magnetic storms. Tentatively, Earth is losing more atmosphere during storms, while there are indications that Mars does not [13]. Therefore, a question is remaining regarding how does the Earth's magnetic field protects the atmosphere from O^+ escape?

References

[8] Balogh A., C. M. Carr, M. H. Acuna, M. W. Dunlop, T. J. Beek, P. Brown, K.-H. Forna{\c c}on, E. Georgescu, K.-H. Glassmeier, J. Harris, G. Musmann, T. Oddy and K. Schwingenschuh, "The Cluster Magnetic Field Investigation: overview of in-flight performance and initial results," *Ann. Geophys,* vol. 19, pp. 1207-1217, 10 2001.

[7] Escoubet C. P., M. Fehringer and M. Goldstein, "IntroductionThe Cluster mission," *Ann. Geophys,* vol. 19, pp. 1197-1200, 10 2001.

[5] Haaland S., A. Eriksson, M. André, L. Maes, L. Baddeley, A. Barakat, R. Chappell, V. Eccles, C. Johnsen, B. Lybekk, K. Li, A. Pedersen, R. Schunk and D. Welling, "Estimation of cold plasma outflow during geomagnetic storms," *J. Geoph. Res. (Space Physics),* vol. 120, p. 10, 12 2015.

[2] Huttunen K. E. J. and H. E. J. Koskinen, "Importance of post-shock streams and sheath region as drivers of intense magnetospheric storms and high-latitude activity," *Ann. Geophys,* vol. 22, pp. 1729-1738, 2004.

[6] Kistler L. M., C. G. Mouikis, X. Cao, H. Frey, B. Klecker, I. Dandouras, A. Korth, M. F. Marcucci, R. Lundin, M. McCarthy, R. Friedel and E. Lucek, "Ion composition and pressure changes in storm time and nonstorm substorms in the vicinity of the near-Earth neutral line," *J. Geoph. Res. (Space Physics),* vol. 111, p. A11222, 11 2006.

[1] Krauss S., B. Fichtinger, H. Lammer, W. Hausleitner, Y. N. Kulikov, I. I. Ribas, V. I. Shematovich, D. Bisikalo, H. I. M. Lichtenegger, T. V. Zaqarashvili, M. L. Khodachenko and A. Hanslmeier, "Solar flares as proxy for the young Sun: satellite observed thermosphere response to an X17.2 flare of Earth's upper atmosphere," *Ann. Geophys,* vol. 30, pp. 1129-1141, 8 2012.

[9] Newell P. T. and C.-I. Meng, "Ionospheric projections of magnetospheric regions under low and high solar wind pressure conditions," *J. Geophys. Res. (Space Physics),* vol. 99, pp. 273-286, 1 1994.

[10] Newell P. T., C.-I. Meng, D. G. Sibeck and R. Lepping, "Some low-altitude cusp dependencies on the interplanetary magnetic field," *J. Geophys. Res. (Space Physics),* vol. 94, pp. 8921-8927, 7 1989.

[4] Nilsson H., I. A. Barghouthi, R. Slapak, A. I. Eriksson and M. André, "Hot and cold ion outflow: Spatial distribution of ion heating," *J. Geophys. Res. (Space Physics),* vol. 117, p. A11201, 11 2012.

[13] Ramstad R., S. Barabash, Y. Futaana, H. Nilsson and M. Holmström, "Global Mars-solar wind coupling and ion escape," *J. Geophys. R.: Space Physics,* vol. 122, pp. 8051-8062, 2017.

[11] Schillings A., H. Nilsson, R. Slapak, M. Yamauchi and L.-G. Westerberg, "Relative outflow enhancements during major geomagnetic storms -- Cluster observations," *Ann. Geophys,* vol. 35, pp. 1341-1352, 2017.

[12] Slapak R., A. Schillings, H. Nilsson, M. Yamauchi, L.-G. Westerberg and I. Dandouras, "Atmospheric loss from the dayside open polar region and its dependence on geomagnetic activity: implications for atmospheric escape on evolutionary timescales," *Ann. Geophys,* vol. 35, pp. 721-731, 4 2017.

[3] Slapak R., H. Nilsson, M. Waara, M. André, G. Stenberg and I. A. Barghouthi, "O^+ heating associated with strong wave activity in the high altitude cusp and mantle," *Ann. Geophys,* vol. 29, pp. 931-944, 5 2011.

A concept for permanent stations on Phobos and Deimos: Study of the Mars space environment

E. Sefton-Nash[1]*, O. Witasse[1], G. Thébault[1], B. Segret[2], D. Koschny[1], B. Foing[1], B. Sánchez–Cano[3], A. Cardesin-Moinelo[4], F. Cipriani[1].
[1] European Space Agency, ESTEC (European Space Research and Technology Centre), The Netherlands
[2]C2ERES, Paris Sciences Lettres, Observatoire de Paris, France.
[3]Radio and Space Plasma Physics Group, Department of Physics and Astronomy, University of Leicester, United Kingdom.
[4]European Space Agency, ESAC (European Space Astronomy Centre), Spain.

Introduction

The surfaces of the martian moons, Phobos and Deimos [1] may offer a stable environment for long-term operation of platforms. However, a broad assessment of the potential scientific, strategic and operational opportunities of platforms on either moon have not been conducted. A mission including such platforms could serve several purposes: (a) as a positioning system, (b) data relay stations for Mars surface assets or for interplanetary missions, (c) monitoring of Mars surface and atmospheric conditions, (d) scientific investigations of Mars and its moons, or (e) investigation for in-situ resources exploitation and precursory human or robotic based station. We show here a preliminary mission concept, with some applications in the study of the Mars space environment.

Platform concept

In our study we consider a concept comprising two permanent installations, with continuous power potentially supplied by a combination of radioisotope thermoelectric generators, batteries and solar panels. A full trade is not yet available between possible scientific and strategic objectives and location on the moon's surfaces, however it is clear that polar vs non-polar positions on the two tidally-locked bodies would offer unique advantages and drawbacks. Communications with Earth, between stations and with other spacecraft could conceivably be via typical Ka- or X-band links, UHF links or even optical laser subsystems.

Study of the Space Environment

Depending on the science payload, study of the space environment by a mission based on this concept could address science questions in a number of research domains:

- Monitoring of the solar system radiation environment: galactic cosmic rays, solar wind, solar photons (X-Ray, EUV), magnetic field.
- Monitoring martian atmospheric and ionospheric phenomena, using: high sensitivity visible and UV imagers or spectrometers; and radio-occultation between the two moons, or between one moon and a Mars-orbiting spacecraft. To demonstrate high frequency and extensive geographic coverage of possible occultation observations, we plot the sub-tangent point latitude on Mars of Phobos-Mars-Deimos occultations throughout the year 2030 (Figure 1).
- Study of solar wind interaction with the moon's surfaces or of their neutral and ionized tori [2,3,4].

Payload Opportunities

Payload instruments and instrument packages that could be part of such platforms that are specific to plasma/aeronomy, as well as other science objectives, could include:

- Radio science via communication links and the inclusion of an ultra-stable oscillator, for input to reference frames, geodesy, and for occultation observations; Phobos-Mars-Deimos, or moon-Mars-spacecraft.
- Wide and narrow FOV imagers for Mars monitoring observations. For atmospheric monitoring, filters could be included for water ice and CO_2 clouds, ozone, etc..
- High sensitivity imagers or spectrometers for observations of night-time auroras (visible, UV), meteor showers (visible) and possible electrostatic discharges (e.g. resulting from dust storms) [5, 6].
- Fabry-Perot interferometer, for investigation of martian wind speeds at different pressure levels.
- Plasma package for solar wind and cosmic ray monitoring.

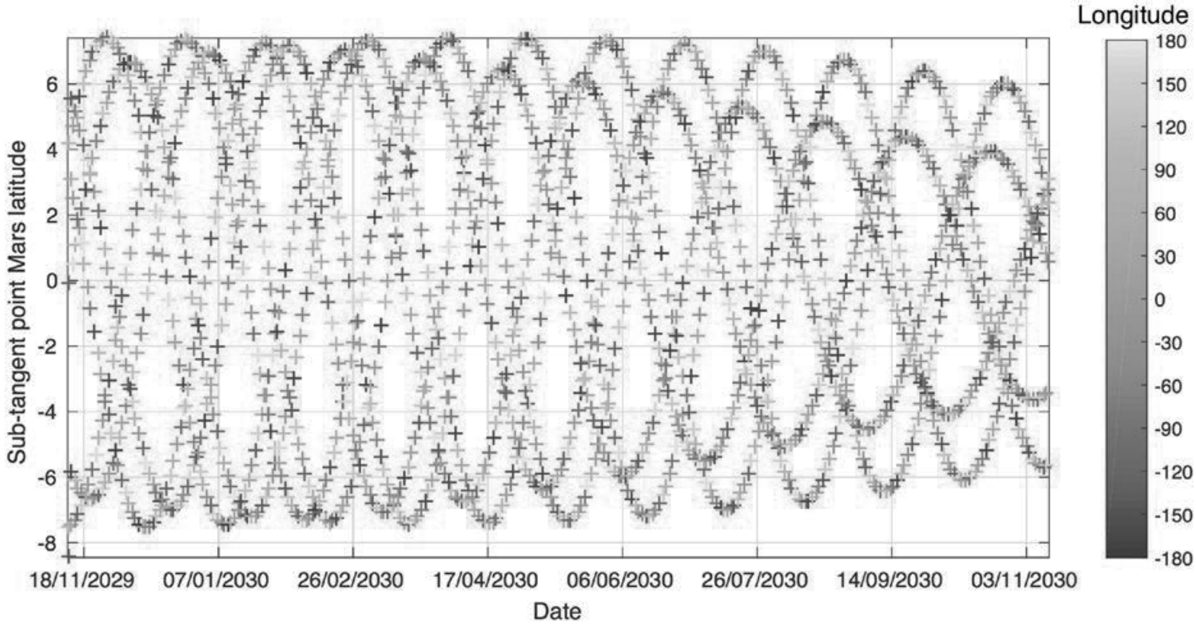

Figure 1: Illustration of coverage of possible atmospheric and ionospheric sounding: Sub-tangent point latitude (colourised by sub-tangent point longitude) on Mars of Phobos-Mars-Deimos occultations throughout 2030.

Strategic Questions

In order to assess the potential science return and strategic value of this concept, we assert that a number of key lines of questioning should be pursued to fully elucidate any constraints that are inherent to the geometry of Phobos and Deimos' shape and orbits. Specifically:

- What visibility to Earth over Phobos/Deimos' surface would be available for down/up-link to Earth?
- What visibility exists between Phobos and Deimos for a potential radio/laser link between the two for ranging?
- What is the range of illumination conditions that exist on the moon's surfaces, and how would this affect power generation and the thermal environment? This would include self-shadowing effects.
- What visibility to the surface of Mars exists, e.g. to communicate with landers, and what is the distribution of visibility from equator to poles and over season?
- How would one optimise the position of a moon-based platform based on its operational and scientific requirements using the geometric information that is available?

Such questions can be addressed using available tools such as NAIF's SPICE [7] or DOCKS, developed at Paris Observatory's Space Centre [8] combined with shape models [e.g. 9]. As we proceed to develop the scientific and strategic case for this concept, and explore the geometric constraints, we are hopeful the results will encourage discussion in the community as well as feedback on the concept.

References

[1] Witasse O. et al. (2014), Mars Express investigations of Phobos and Deimos, Planetary and Space Science, 102, p. 18-34. **[2]** Poppe, A. R. et al. (2016) The Phobos neutral and ionized torus, Journal of Geophysical Research: Planets 121 (5) p. 770-783. **[3]** Cipriani, F. et al. (2011), A model of interaction of Phobos' surface with the martian environment, Icarus 212 (2) p. 643-648. **[4]** Futaana, Y. et al (2010), Backscattered solar wind protons by Phobos, J. of Geophys. Res. 115 (A10), A10213. **[5]** Delory, G. T., et al. (2006), Oxidant Enhancement in Martian Dust Devils and Storms: Storm Electric Fields and Electron Dissociative Attachment, Astrobiology 6 (3), p.451–462. **[6]** Farrell, W. M. et al. (2004), Electric and magnetic signatures of dust devils from the 2000–2001 MATADOR desert tests, J. of Geophys. Res. 109, E03004. **[7]** NASA's Navigation and Ancillary Information Facility (NAIF) and SPICE (Spacecraft, Planet, Instrument, C-matrix, Events'): https://naif.jpl.nasa.gov/naif/index.html **[8]** Segret, B. et al. (2017), DOCKS at Paris Observatory's Space Center, Open Source CubeSat Workshop, ESOC. **[9]** Willner, K. et al. (2014), Phobos' shape and topography models, Planetary and Space Science 102, p. 51-59.

The Mars Express/ASPERA-3 and Venus Express/ASPERA-4 Solar Wind Databases

M. Holmström[1*]; R. Ramstad[1], S. Barabash[1], Y. Futaana[1], X.-D. Wang[1]
[1]Swedish Institute of Space Physics, Sweden

Introduction

The upstream solar wind environments at Mars and Venus are often thought to influence, or be the major drivers of many processes in the planets' upper atmospheres and induced magnetospheres. To facilitate studies of such processes and general heliophysics, the PI-institute of the ASPERA-3 and ASPERA-4 plasma particles packages aboard Mars Express and Venus Express has developed a database of official solar wind moments (density, velocity, temperature) to be publicly available and archived. We present the methods used to develop these moments, including the results of intercalibrations with other missions (ACE, WIND, STEREO and MAVEN) and the first solar wind statistics collected at Mars over a full solar cycle.

Method

Moments are generated in five steps:
1. Identify IMA scans outside the bow shock, including an additional safety margin.
2. Exclude all data outside the solar wind direction and when the sun-direction is in a shadowed part of the field-of-view.
3. Subtract background counts (assuming no signal below 100 eV in the solar wind to get noise profile). Negligates contamination noise during SEP events.
4. Fit Gaussian curves to the mass-spectra to separate H^+, He^{++} and "ghost" H^+ signals.
5. Integrate distribution to find n_{sw} , v_{sw} . Fit Maxwell to find T_{sw} .

Status and availability:

Mars.
The Mars Express/ASPERA-3 solar wind database is available in two versions, one (SCAN) based on individual 192 second scans of the instrument and the other (ORB) based on counts integrated over the available inbound/outbound segments before/after crossing bow shock safety margin. Calibration against upstream monitors (ACE/WIND/STEREO) is completed(see Figure 2 for an example comparison) and intercalibration with NASA's more recently arrived MAVEN mission is in progress. A copy of the database can currently be retrieved by request to the ASPERA-3 PI Mats Holmström (matsh@irf.se) and will be publically available from ESA's Planetary Science Archive (PSA) in the near future.

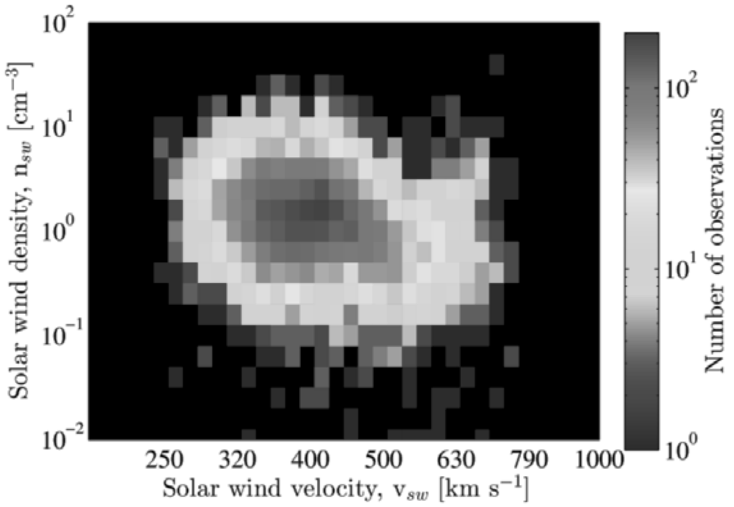

Figure 1: Solar wind density-velocity distribution at Mars based on all included solar wind data collected by ASPERA-3/IMA data and using the ORB version of the database. The mean density and velocity here is 2 cm^{-3} , 400 km/s respectively.

Venus.
The Venus Express/ASPERA-4 solar wind database is under development and set to be finalized and published to PSA in the near future. Contact ASPERA-4 PI Yoshifumi Futaana for inquires (futaana@irf.se).

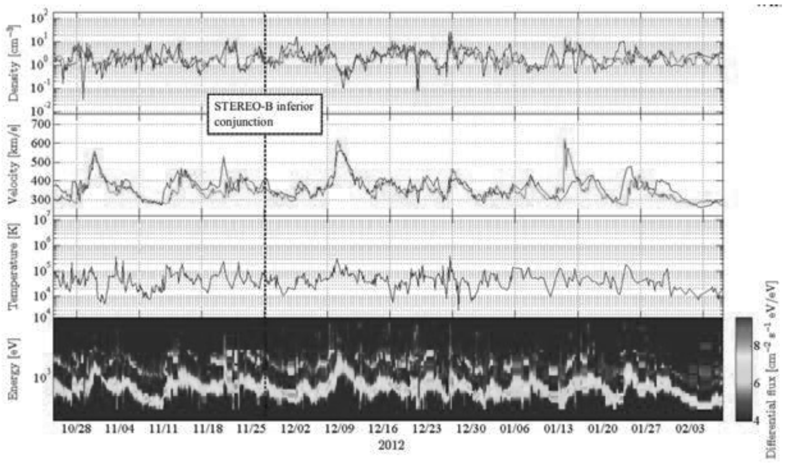

Figure 2: Comparison with 1 AU solar wind monitors. Example ASPERA-3/IMA solar wind moments (black) and spectra, plotted with STEREO-B/PLASTIC moments that are time-shifted and intensity adjusted to Mars angular position and radial distancefrom the Sun (red).

References

[1] Andrews, D.J., et al. (2016), JGR.
[2] Behar, E., et al. (2016), A&A.
[3] Edberg, N.J.T., et al. (2016), JGR.
[4] Ramstad, R., et al. (2015), JGR.
[5] Hall, B.E.S. et al. (2016), JGR.
[6] Ramstad, R., et al. (2016) JGR.

ESCAPE (European SpaceCraft for the study of Atmospheric Particle Escape): a planetary mission to Earth, proposed to ESA in response to the M5-call

I. Dandouras[1*]; M. Yamauchi[2], H. Rème[1], J. De Keyser[3], O. Marghitu[4], A. Fazakerley[5], B. Grison[6], L. Kistler[7], A. Milillo[8], R. Nakamura[9], N. Paschalidis[10], A. Paschalis[11], J.-L. Pinçon[12], T. Sakanoi[13], M. Wieser[2], P. Wurz[14], I. Yoshikawa[15], I. Häggström[16], M. Liemohn[17], F. Tian[18], and I. Daglis[11]

[1]IRAP, Université de Toulouse, CNRS, UPS, CNES, France
[2]Swedish Institute of Space Physics, Sweden
[3]Royal Belgian Institute for Space Aeronomy, Belgium
[4]Institute for Space Sciences, Romania
[5]UCL/MSSL, UK
[6]Institute of Atmospheric Physics, The Czech Academy of Sciences, Czech Republic
[7]University of New Hampshire, USA
[8]INAF/Istituto di Astrofisica e Planetologia Spaziali, Italy
[9]Institut für Weltraumforschung, Austria
[10]NASA Goddard Space Flight Center, USA
[11]National and Kapodistrian University of Athens, Greece
[12]Laboratoire de Physique et Chimie de l'Environnement et de l'Espace, France
[13]Tohoku University, Japan
[14]University of Bern, Physikalisches Institut, Switzerland
[15]University of Tokyo, Japan
[16]EISCAT Headquarters, Sweden
[17]University of Michigan, USA
[18]Tsinghua University, China

Introduction

ESCAPE is a mission proposed to ESA in response to the M5 call that will quantitatively estimate the amount of escaping particles of the major atmospheric components (nitrogen and oxygen), as neutral and ionised species, escaping from the Earth as a magnetised planet. The spatial distribution and temporal variability of the flux of these species and their isotopic composition will be for the first time systematically investigated in an extended altitude range, from the exobase/upper ionosphere (500 km altitude) up to the magnetosphere.

The goal is to understand the importance of each escape mechanism (thermal or non-thermal), its dependence on solar and geomagnetic activity, in order to infer the history of the Earth's atmosphere over a long (geological scale) time period. Since the solar EUV and solar wind conditions during solar maximum at present are comparable to the solar minimum conditions 1–2 billion years ago, the escaping amount and the isotope and N/O ratios should be obtained as a function of external forcing (solar and geomagnetic conditions) to allow a scaling of the escape rates to the past. The results will be used as a reference to understand the atmospheric/ionospheric evolution of magnetised planets or exoplanets, which is essential for habitability.

Proposed mission

To achieve this goal an Earth orbiting spacecraft is proposed, equipped with a suite of instruments developed and supplied by an international consortium. These instruments will detect the upper atmosphere and magnetosphere escaping populations by a combination of in-situ measurements and of remote-sensing observations. The measurements will cover ions and neutrals over a broad energy range and with a high mass resolution.

The spacecraft will be on a high-inclination (> 80°) orbit, with perigee and apogee at ~500 km 33000 km altitudes respectively, to cover the polar cap, inner magnetosphere, exosphere, and topside ionosphere at all local times. It will be slowly spinning, for the in-situ measurements, and equipped with a despun platform for the remote sensing optical observations.

The ESCAPE mission proposal successfully passed the first technical and programmatic screening by ESA and is now in the scientific assessment phase.

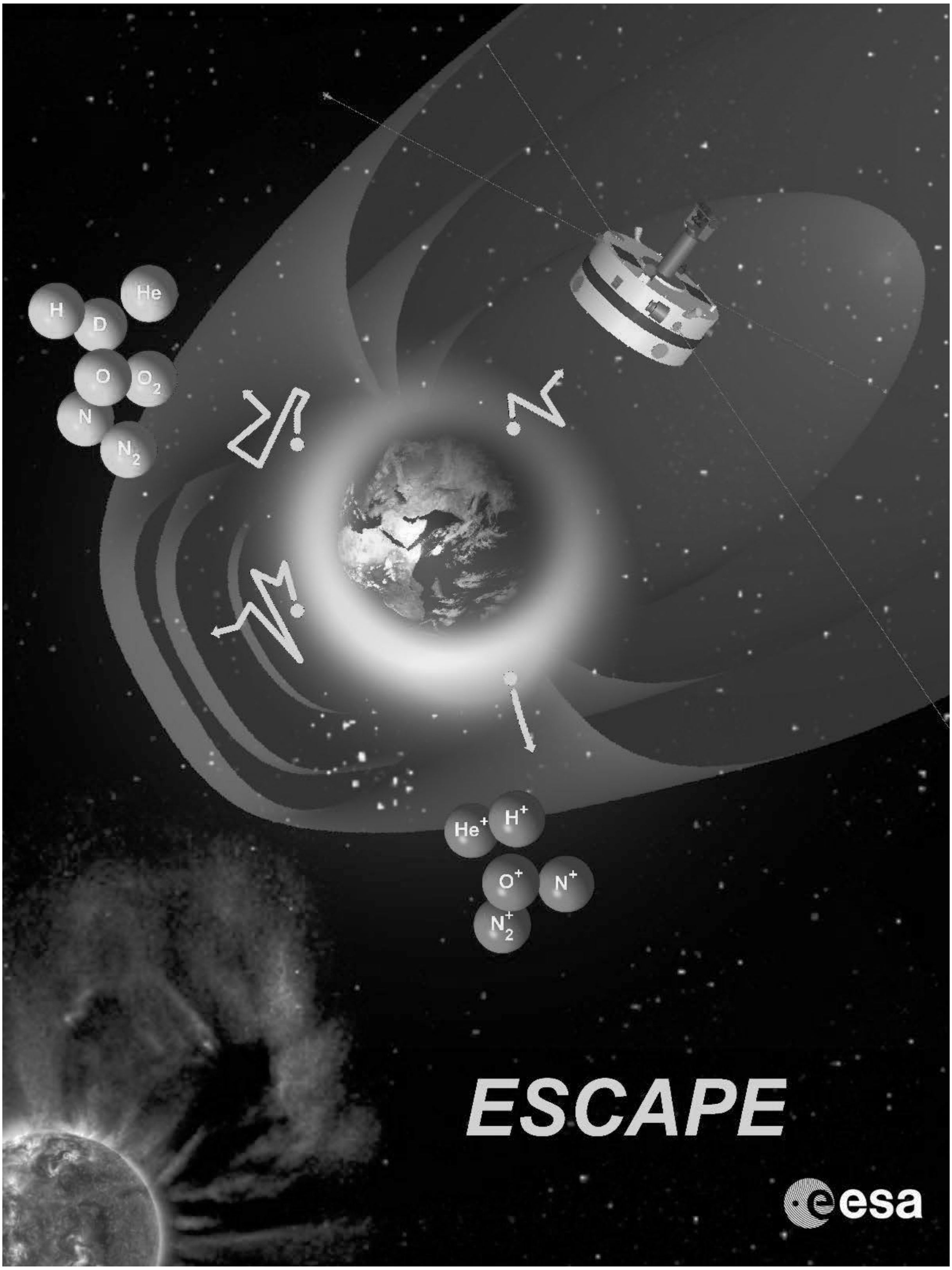

Figure 1: The ESCAPE (European SpaceCraft for the study of Atmospheric Particle Escape) mission proposed to ESA.

Solar SENTINEL: a satellite constellation mission concept for early forecasting of Coronal Mass Ejections

J. Rodrigues[1,2*]; E. Scott[2], A. Roberts[2], I. Hernandez Arroyo[2,3], Y. Jagessur[2], C. Bennett[2], M. Deligny[2], M. Retana[2], J. McNeil[2], I. Perez de Bartolome[2]
[1]University of Cambridge, United Kingdom
[2]University of Bristol, United Kingdom
[3]Skolkovo Institute of Science and Technology, Russia

Introduction

In 1859, Richard Carrington recorded observations of a large Coronal Mass Ejection (CME) which hit the Earth. A similar event today would cause more than $2 trillion in damage to telecoms, GPS, finance and transportation systems [1]. Recent literature claims there is a 12% chance of Earth being hit by a "superstorm" in the next ten years [2], with a Carrington-class event having narrowly missed the Earth in 2012 [1]. Observations from vantage points away from the Sun-Earth line have the potential to provide warnings before the active region of the Sun rotates towards the Sun-Earth line. The proposed mission will provide for the first time persistent 3D maps of the equatorial solar surface, allowing accurate and timely forecasts of CMEs many days in advance of current capabilities.

Mission scope

The mission requirements were defined by Airbus Defence and Space and are outlined in Table 1. The mission budget was to be minimised and the use of a European launcher was preferred.

	Requirement		Requirement
1	IMF measurements and white light images shall be downloaded at least once every day.	6	Tolerates single-point failures at system and sub-system level.
2	White light images should cover area at least ±45 degrees from the Sun's equator.	7	Magnetic field dynamic range: +/- 200 nT.
3	Launch by 2022; operational within 5 years.	8	Min. radiation tolerance: 100 krad per year.
4	Minimum lifetime of 10 years post-launch.	9	Sensor shall have a 1024 x 1024 CCD.
5	Maximum mass equivalent to two Ariane 5 payloads.	10	Telemetry data rate of 10 kbps to be downloaded every day.

Table 1: Mission requirements.

Mission analysis

The Solar SENTINEL mission will feature a constellation of four satellites in a circular heliocentric orbit, at 1 AU from the Sun as shown in Figure 1. Two satellites will orbit in Lagrange points L_4 and L_5. Two more satellites operate in non-Lagrangian positions termed L_{4b} and L_{5b}. The STEREO missions proved that satellites at 180 degrees from each other can monitor the entire solar equator. With a constellation of four, we meet this objective while still ensuring system-level redundancy as per Requirement 6.

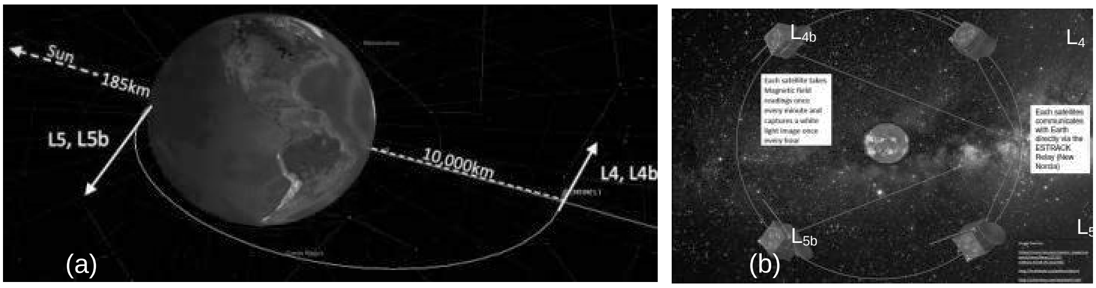

Figure 1: Parking and escape orbits in STK (a) and SENTINEL constellation once operational (b).

A single Ariane 5 launcher solution was chosen for the four satellites to reduce launch costs. A geocentric parking orbit with a perigee of 185 km, and an apogee of 10,000 km was selected through a trade-off study. A 400 N hypergolic Apogee Engine is used for the phasing orbits due to its high specific impulse and storage stability. The ΔV budget for each satellite accounted for the 15% margin in agreement with ESA's Cosmic Vision Philosophy, as well as End-of-Life considerations (ΔVL_4 = 4.5 km/s, ΔVL_5 = 2.9 km/s, ΔVL_{4b} = 5.4 km/s, ΔVL_{5b} = 3.7 km/s). A separate propulsion system was designed for attitude and orbit control (AOCS). Full 3 axis stability is provided through use of 8 canted hydrazine 20 N thrusters, with position and orientation determined by Sun Sensors and Star Trackers.

Sub-systems

Payloads

A trade-off study considering CCD sensors and magnetometers used in previous missions was undertaken. Missions included in this study included Ulysses, SOHO, WIND, STEREO, DSCOVR, Solar Orbiter, Cassini and Double Star. Power Mass Volume constraints as well as dynamic ranges, resolution and field-of-view were used to help with the selection. The EUVI CCD Imager (STEREO) and the Double Star Magnetometer (Double Star) were selected. To tolerate single point failures, the Solar SENTINEL satellites will carry two of each. A Magnetic Cleanliness Program (MCP) was developed to reduce magnetic interference.

Power and thermal control

The power requirements are highly variable throughout the mission life. To support this, the power system comprises of a 2.4 m^2 body mounted Ga-As solar array, 140Ah rechargeable Li-Ion battery unit, and a Power Control and Distribution Unit. Gallium Arsenide technology was chosen due to its high efficiency and resistance to radiation. A Maximum Peak Power Tracking architecture is chosen to regulate the power generated by the solar array using a fully regulated 28V bus. Multi-layered insulation, heat patches and heat pipes are used to ensure components remain within operational temperatures.

Communications and data handling

Data imputed to the on-board computer is modulated to either the X-band for the payload data or S-band for telemetry during transfer. These are then amplified and sent to a 35m ESTRAK antenna. The controls are received through one of two low-gain helix antennas (LGA). The high-gain antenna (HGA) is a horn fed Cassegrain antenna in carbon and Al-honeycomb for high efficiency and low mass.

Configuration

The final configuration selected is shown in Figure 2. The satellites are stacked in order of decreasing mass and have a total mass of 5.4 tonnes. The magnetometers are mounted on a telescopic boom. The main load bearing structure houses the apogee fire tanks and features a bench for the CCD imagers. This stacked configuration meets all the Ariane 5 load and natural frequency requirements.

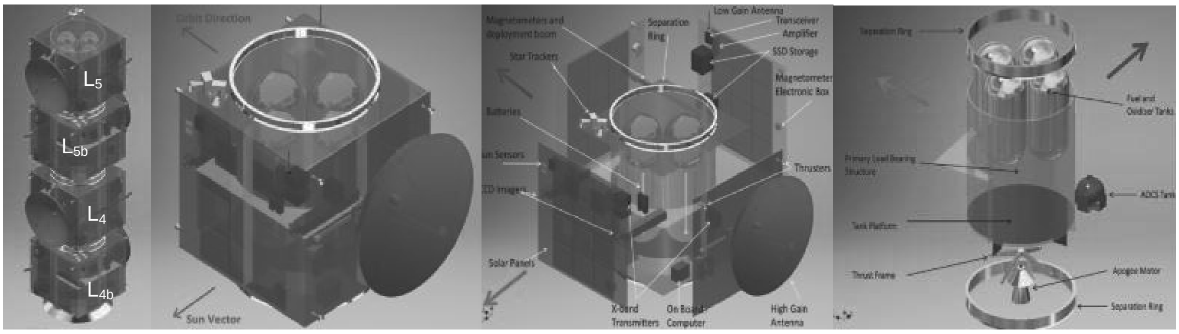

Figure 2: stacked launch configuration (a); isotropic (b) and exploded view of (c) satellite and (d) core cylinder.

Conclusions

The Solar SENTINEL mission will help further the understanding of the conditions that create CMEs. Persistent monitoring of solar activity, with single-point failure redundancy at both the system and sub-system level, presented a number of design challenges. Trade studies, parametric investigations, and detailed analyses within each sub-system were performed. A constellation of four satellites was chosen with their dry masses ranging between 382 – 413 kg and a peak power requirement of 912 W. These will orbit the Sun at L_4 and L_5 positions, as well as their mirror positions, termed L_{4b} and L_{5b}. An Ariane 5 will launch the four stacked satellites in a single launch. The satellites feature two CCD sensors for capturing white light images, as well as two magnetometers for measuring the IMF. Data can be downloaded every day to the European Space Agency antenna network. In its current state, the Solar SENTINEL mission meets all requirements for a 2022 launch at an estimated cost of €120m.

References

[1] Liu, Y. D., et al., Observations of an extreme storm in interplanetary space caused by successive coronal mass ejections, Nature Communications, Vol. 5, 3481, 2014.

[2] Riley, P., On the probability of occurrence of extreme space weather events, Space Weather, Vol. 10, 10, 2012